

Stem cell models of adipogenesis

Modulating temperature to promote MSC-derived beige adipocytes

by Hilda Anaid Lugo Leija, MSc.

Thesis submitted to the University of Nottingham for the degree of

Doctor in Philosophy, May 2020.

Table of Contents

Table of Contents i
List of Tables vii
List of Figures viii
List of Appendix Figures xii
Abstract 13
Declaration 17
Acknowledgements 18
Abbreviations xxi
Chapter 1. Introduction 1
1.1 Structure and function of adipose tissue 3
1.1.1 White Adipose Tissue (WAT) 3
1.1.1.1 Molecular signature in white adipocytes 7
1.1.2 Brown Adipose Tissue (BAT) 9
1.1.2.1 Molecular signature in brown adipocytes 9
1.1.3 Beige Adipose Tissue (bAT) 12
1.1.3.1 Molecular signature in beige/brite adipocytes 12
1.2 Mesenchymal stem cells (MSCs) 14
1.2.1 Adipogenic differentiation 14
1.2.1.1 White adipocytes from progenitor cells (MSCs) 17
1.2.1.2 Brown adipocytes from progenitor cells (MSCs) 17
1.2.1.3 beige adipocytes from progenitor cells (MSCs) 18
1.3 Adipose-derived stem cells (ADSCs) 18
1.4 Cellular models of white, brown and brite differentiation 19
1.4.1 MSCs cell lines 19
1.4.1.1 D1 cell line 19
1.4.2 Pre-adipocyte cell lines 20
1.4.3 Immortalized cell lines from human BAT 20
1.4.4 Primary cultures of human AT 21
1.4.4.1 Primary cultures derived from human WAT 21

1.4.4.2 Primary cultures derived from human BAT 22
1.4.5 Primary cultures of adult MSCs. 22
1.4.5.1 Adult bone marrow MSCs 22
1.4.5.2 Fetal bone marrow MSCs (fBM-MSCs) 23
1.4.5.3 Fetal Muscle-derived MSCs 23
1.4.5.4 Umbilical Cord Blood (UCB) MSCs 23
1.4.6 human pluripotent stem cells (hPSC) 24
1.5 Adipogenic medium 25
1.5.1 Insulin 25
1.5.2 Dexamethasone (Dex) 26
1.5.3 Rosiglitazone (Rosi) 26
1.5.4 IBMX 27
1.5.5 Triiodothyonine (T3) 27
1.5.6 Other growth factors 28
1.5.7 Cold stimuli for brown activation 29
1.5.7.1 Cold exposure *in vivo* 29
1.5.7.1.1 Cold exposure in humans 29
1.5.7.1.2 Cold exposure in animals 31
1.5.7.2 Cold exposure *in vitro* 31
1.5.7.2.1 Transient Receptor Potential channels (TRPs) 32
Aims 35
Chapter 2. Methods 38
2.1 Chemicals and Reagents 39
2.2 Cell culture 39
2.2.1 mMSCs D1 culture 39
2.2.2 Passaging of mMSCs 40
2.2.3 Gelatine coated plates and coverslips 40
2.2.4 mMSCs adipogenic differentiation 40
2.2.5 Cryopreservation of mMSCs 41
2.3 Human umbilical cord tissue (hUCT) 41
2.3.1 Background of the hUCT 41
2.3.2 hUCT isolation 44
2.3.3 Mycoplasma test 47

2.3.4 hUCT-MSCs culture 47
2.3.5 Passaging of hUCT-MSCs 47
2.3.6 Proliferative potential 48
2.3.7 hUCT-MSC adipogenic differentiation 48
2.3.8 hUCT-MSCs osteogenic differentiation 49
2.3.9 Cryopreservation of hUCT-MSCs 49
2.4 Live assays and staining 50
2.4.1 Metabolic activity 50
2.4.2 Seahorse Assay 50
2.4.3 Mitochondrial staining and quantification 52
2.4.4 Calcium staining and quantification 53
2.5 Fixation of cells for subsequent staining 53
2.5.1 Oil Red O (ORO) imaging and quantification 54
2.5.2 Hoechst staining and quantification 54
2.5.3 Immunocytochemistry 55
2.6 Molecular Biology 57
2.6.1 Harvesting mouse tissue for RNA extraction 57
2.6.2 Harvesting cells for RNA extraction 58
2.6.3 RNA extraction 58
2.6.3.1 RNA quantification 58
2.6.4 Reverse (RT) - Polymerase Chain Reaction (PCR) 59
2.6.5 Primer optimisation and validation 59
2.6.5.1 Primer design 59
2.6.5.2 Primer validation 60
2.6.5.2.1 PCR 60
2.6.5.2.2 Electrophoresis 61
2.6.5.2.3 Gel extraction (DNA) 61
2.6.5.2.4 DNA quantification 61
2.6.5.2.5 Standard curves of each gene done by quantitative Real-Time PCR (qPCR) 61
2.6.6 qPCR 64
2.6.6.1 mMSCs qPCR 64
2.6.6.1.1 Fast SYBR green protocol 64

2.6.6.1.2 TaqMan protocol 64
2.6.6.2 hUCT-MSC qPCR 65
2.6.7 geNorm 65
2.6.7.1 mMSCs geNorm 66
2.6.7.2 hUCT-MSCs geNorm 66
2.7 Imaging and image analysis 67
2.7.1 Brightfield and fluorescent images 67
2.7.2 Super-resolution imaging in structured illumination mode 67
2.7.3 Morphometric and stereological analysis 68
2.7.4 Densitometric analysis of UCP1 positive area 69
2.8 Statistical analysis 70
Chapter 3. Low temperature exposure induces browning of bone marrow stem cell derived adipocytes *in vitro* 71
3.1 Main Findings 72
3.2 Introduction 73
3.3 Methods 76
3.4 Results 77
3.4.1 Mouse Mesenchymal stem cells (mMSCs) achieve an adipogenic phenotype and express both UCP1 and leptin. 77
3.4.2 Enhanced adipogenesis and morphological changes shows signs of browning in hypothermic conditions. 79
3.4.3 Temperature-related changes in differentiated mMSC-derived adipocytes: increased UCP1 protein expression and leptin translocation to the nucleus 82
3.4.4 Lower temperature conditions affect PGC-1α expression, the bioenergetic status and reduce coupling efficiency of MSC-derived adipocytes. 89
3.4.5 Mouse MSC-derived adipocytes exhibit characteristics of white, beige and brown adipocytes at protein and mRNA level. 93
3.4.6 Ca+ levels 99
3.5 Discussion 100
3.5.1 Adipogenic phenotype and expression of UCP1 and leptin in mouse Mesenchymal Stem Cells (mMSCs) 100
3.5.2 Browning phenotype and increase of adipogenesis in cold temperature conditions 101

3.5.3 Lower temperature conditions affect the bioenergetics profile and mitochondria frequency of adipocytes derived from mMSCs. 101

3.5.4 White, beige and brown features shown by MSC-derived adipocytes at mRNA level 102

3.5.5 Cold-induced brown phenotype and UCP1 expression in MSC-derived adipocytes are retained after rewarming..... 104

Chapter 4. MSC derived-adipocytes differentiated under hypothermic conditions exhibit a brown phenotype after warm acclimatisation..... 106

4.1 Main findings 107

4.2 Introduction 108

4.3 Methods 110

4.4 Results 112

4.4.1 Cold-induced adipocytes retain brown-like cellular and morphological features when returned to a normothermic environment..... 112

4.4.2 Cold-induced adipocytes maintain brown-like marker expression when returned to 37°C for 21 days..... 119

4.4.3 Metabolic function of cold-induced adipocytes is modified when returned to a thermoneutral environment..... 127

4.5 Discussion 129

4.5.1 The bioenergetics benefits are retained..... 129

4.5.2 The induced brown-like phenotype is not fully reversible 131

4.5.3 Beige-brown marker expression 131

4.5.4 Temperature sensing channels 134

Chapter 5. Isolation and media optimisation of hUCT MSCs 136

5.1 Main findings 137

5.2 Introduction 138

5.3 Methods 141

5.4 Results 143

5.4.1 Media evaluation for hUCT MSCs expansion 143

5.4.2 Immunofluorescence characterization of hUCT-MSCs 149

5.4.3 Adipogenic medium evaluation for hUCT MSCs 152

5.4.4 Osteogenic evaluation of hUCT MSCs 157

5.5 Discussion 159

5.5.1 Explant culture versus enzymatic isolation 159

5.5.2 Human Platelet lysate (hPL) medium provides the best growth…… 160
5.5.3 Adipogenic differentiation medium differs from growth medium…. 161
5.5.4 MSCs potential and membrane markers 162
Chapter 6. Cold temperature exposure of hUCTs MSCs from healthy and diabetic backgrounds 164
6.1 Main findings 165
6.2 Introduction 166
6.3 Methods 169
6.4 Results 170
6.4.1 Metabolic activity and lipid content 170
6.4.2 Gene expression at hypothermal and normal culture conditions… 178
6.4.3 Molecular signature overview 182
6.4.4 UCP1 protein expression is enhanced in healthy cells at hypothermal conditions 184
6.5 Discussion 187
6.5.1 Obesity and GD evidence in early development 187
6.5.2 hUCT-MSCs potentiality towards adipogenesis 187
6.5.3 Adipogenic response of GD MSCs 188
6.5.4 Adipogenic response of healthy MSCs 190
6.5.5 Heterogeneity of the hUCT-MSCs 191
6.5.6 hUCT-MSCs as a therapeutic option 192
Chapter 7. Final conclusions 194
7.1 MSC-derived adipocytes 196
7.2 Brown features maintenance 198
7.3 MSC human isolation 200
7.4 Browning of healthy and GD hUCT-MSCs 202
7.5 Final remarks 204
References 208
Appendix 230
Equipment 231
Reagents 232

List of Tables

Table 1.1. Characteristics of white, beige and brown adipocytes..... 10

Table 2.1. Information from the umbilical cord tissues collected. All tissues collected were from male babies..... 42

Table 2.2 List of antibodies used for immunocytochemistry..... 56

Table 2.3. Primer design conditions..... 59

Table 2.4. PCR recipes. 60

Table 2.5. List of primers used for gene expression analysis..... 63

Table 5.1. Cell number according to MSC medium used from different passages and doubling time (DT) calculation..... 145

List of Figures

Figure 1.1. Distribution of (A) white and (B) brown adipose tissue depots in (B) adult human, (C) infant and in (D) mouse. 8
Figure 1.2. Differentiation into skeletal muscle, white, beige or brown adipocytes. 16
Figure 2.1.Graphical representation of the hUCT-MSC isolation. Detailed description can be found in Chapter 2.3.12, p. 48. 47
Figure 2.2.Example of the densitometric analysis of MitoTracker positive area. 53
Figure 2.3. mouse tissue: eWAT (yellow), iWAT (orange), iBAT (brown) and muscle (red). 57
Figure 2.4. Example of the morphometric and stereological analysis. 68
Figure 2.5. Example of the densitometric analysis of UCP1 positive area. 69
Figure 3.1. mMSCs differentiated adipocytes show uncoupling protein (UCP)1 and leptin expression. 79
Figure 3.2. Cellular response of mMSCs exposed to 9-day adipogenic differentiation under standard or hypothermal conditions. 81
Figure 3.3. Temperature-related changes in differentiating mMSCs. 84
Figure 3.4. Image from a confocal z-stack with orthogonal views of leptin (purple) localization in mMSCs differentiated adipocytes at 32°C. 85
Figure 3.5. Temperature-related changes in differentiating mouse primary bone marrow (BM) mesenchymal stem cells (MSC) derived and human adipose-derived cells (hADSCs). 87

Figure 3.6. Morphological changes in cells transferred from 32 to 37°C and UCP1 expression. 89
Figure 3.7. PGC-1**α** immunoexpression, mitochondrial localization and bioenergetics measurement during mMSCs differentiation under different temperature conditions. 91
Figure 3.8. CD137 and TMEM26 immunodetection in undifferentiated mMSCs at 37°C. 93
Figure 3.9.Expression of beige and brown markers in mMSCs-derived adipocytes differentiated at 32°C. 94
Figure 3.10.Leptin nuclear localization in UCP1^{+} mesenchymal stem cell-derived adipocytes differentiated at 32°C. 95
Figure 3.11. Real-time PCR analysis of gene expression during mMSCs differentiation under different temperature conditions. 98
Figure 3.12. Real-time PCR analysis of Leptin and Leptin 98
Figure 3.13. Temperature-related changes in differentiated mouse MSCs stained with Fluo-4. 99
Figure 4.1. Schematic diagram of MSCs adipogenesis treatments. 111
Figure 4.2. Effect of culture temperature on the abundance of mitochondria and uncoupling protein (UCP)1. 114
Figure 4.3. Cellular and morphological response of adipogenic MSCs differentiated under normal, Transfer and hypothermic conditions at 14, 21 and 28 days. 116
Figure 4.4. Oil Red O (ORO) staining of mMSCs differentiated under adipogenic treatment in normal, transferred and hypothermic conditions. 118
Figure 4.5. The effect of incubation temperature on gene expression patterns as determined by hierarchical clustering (HCA) and principal component analysis (PCA). 122

Figure 4.6. Changes in gene expression between normal, Transfer and hypothermic treatments of adipogenic MSC cultures at day 14, 21 and 28. 122
Figure 4.7. Changes in gene expression between normal, Transfer and hypothermic treatments of adipogenic MSC cultures at day 14, 21 and 28. 123
Figure 4.8. Gene expression comparison of thermotransient receptor potential ion channels at same time-points by real time PCR. 125
Figure 4.9. Zoom image of Figure 4.8D Transfer. Live staining showing calcium staining in Transfer cells at day 28. 126
Figure 4.10. Effect of incubation temperature on the bioenergetics status of adipogenic MSC cultures after 28 days. 128
Figure 5.1. Picture of the first half of the hUCT before processing for explants. Each piece was cut in four 10 mm pieces. 142
Figure 5.2. Picture of the second half of the hUCT after the mincing process and before the collagenase step. 142
Figure 5.3. Doubling time of hUCT-MSCs cultured in medium three. 147
Figure 5.4. hUCT MSC-like isolated with the collagenase method without filtration from donor 851 in medium one, two and three. ... 148
Figure 5.5. hUCT-MSCs stained individually for CD73, CD90 and CD105. 150
Figure 5.6 hUCT-MSCs co-stained for CD73 with CD105 and CD90 with CD105. 151
Figure 5.7. Adipogenic differentiation of hUCT-MSC. 152
Figure 5.8. Evaluation of adipogenic differentiation with three different growth media and two adipogenic differentiation medium in hUCT MSC-like. 154

Figure 5.9. Oil Red O staining and quantification of hUCT MSC-like passage 1 grown in medium three. 156
Figure 5.10. Alizarin red staining and quantification of hUCT MSC. 158
Figure 6.1. Schematic diagram of hUCT-MSCs adipogenesis treatments. 171
Figure 6.2.Cellular and morphological response of adipogenic hMSCs differentiated under normal and hypothermic conditions at 28 days. 174
Figure 6.3. Oil Red O staining of healthy and gestational diabetic hUCT MSC-like passage 1 at day 28. 175
Figure 6.4. Oil Red O staining of healthy and gestational diabetic hUCT MSC-like passage 2 or 3 at day 28. 176
Figure 6.5. Expression levels of common adipogenic markers: Adiponectin, PPARγ, Glut4, Leptin and Insulin receptor at day 28. . 180
Figure 6.6. Expression level of brown adipogenic markers: PRDM16, PGC1α, CIDEA, DIO2, FGF21, and *β3-AR* at day 28. 182
Figure 6.7. The effect of incubation temperature on gene expression patterns as determined by hierarchical clustering (HCA) and principal component analysis (PCA). 184
Figure 6.8. Effect of culture temperature on the abundance of uncoupling protein (UCP)1 in hUCT-MSCs at 28 days. 186
Figure 7.1. Cold temperature exposure induces browning of MSC-derived adipocytes. 198
Figure 7.2. Cold induced browning of MSC-derived adipocytes is not fully reversible after return to normal culture conditions. 199
Figure 7.3. hUCT-MSC isolation and characterization. 201
Figure 7.4. hUCT MSCs-derived adipocytes are able to differentiate under normal and hypothermal culture conditions. 203

List of Appendix Figures

Appendix Figure 1. Metabolic activity (Presto Blue) standard curve in mMSCs D1 undifferentiated (control) and differentiated (adipogenic). 230

Abstract

Since the discovery of brown adipose tissue (BAT), emerging strategies to promote its activation and recruitment have been examined due to the thermogenic capacity of BAT, which makes it an encouraging approach to regulate obesity and related diseases. Uncoupling protein 1 (*UCP1*) is a specific protein located in the inner mitochondria of brown adipocytes, when activated, uncouples substrate oxidation from ATP production by dissipating energy in the form of heat. Beige adipocytes have been recently discovered and are cells which possess the morphological and biochemical characteristics of brown adipocytes, including *UCP1*. It has been previously reported that human BAT expresses beige cell-selective genes instead of classical brown markers which underline the importance of understanding beige adipogenic differentiation, induction and maintenance. All adipocytes share a mesodermal origin. Mesenchymal stem cells (MSCs) are able to differentiate into a variety of lineages, including adipocytes. To date, the most potent stimulus to activate *UCP1* in BAT is cold exposure. However, whether cells sense temperature and differentiate into brown and beige lineages is not fully understood. The aim of this thesis is to obtain a better understanding on how low temperature affects the differentiation of MSCs into white, beige and brown adipocytes and if these traits acquired are maintained after being switched to normal culture conditions (37°C). Additionally, cold exposure evaluation during adipogenic differentiation of human MSCs derived from cord tissue taken from diabetic and healthy pregnancies at term were examined.

Cold temperature (32°C) was investigated for its potential to activate browning in adipocytes. Here, MSCs differentiated under normal culture conditions showed a dual leptin and *UCP1* protein expression in the majority of differentiated cells. Hypothermic conditions applied while the MSCs were under adipogenic differentiation promoted a brown/beige morphological and molecular signature. These changes were accompanied with enhanced *UCP1* protein abundance, uncoupled respiration and metabolic adaptation. Hypothermic differentiated cells showed a marked translocation of leptin into adipocyte nuclei, which indicates a potential role for leptin in the browning process. These results indicated that MSCs could be driven to form beige like adipocytes by differentiating them in a cold environment.

To further investigate whether these MSC-derived adipocytes could adapt overtime and retain their brown/beige traits, brown-like cells produced under hypothermic conditions were transferred to normal culture conditions. MSCs differentiated at 32°C and then rewarmed maintained an intermediate brown/beige phenotype and gene profile with *UCP1* protein expression found after 21 days of warm acclimation (37°C). Additionally, these cells showed an intermediate mitochondrial respiration level, lipolysis, fatty acid oxidation, glycolysis rate and intracellular calcium expression, suggesting a shared mechanism of calcium mediated *UCP1*-independent thermogenesis. Moreover, these cells stored lipids and produce heat when stimulated. Altogether these results highlight the plasticity of MSCs to generate and preserve *de novo* beige adipocytes.

Several isolation and culture methods were then tested in order to establish optimal conditions for human umbilical cord tissue MSCs (hUCT-MSCs) isolation, growth and differentiation. For hUCT-MSCs isolation, an enzymatic method using collagenase B (0.4 U/ml per cm) was used. After testing different culture mediums, it was found that DMEM low glucose,1% L-glutamine, 1% penicillin/streptomycin and 10% human platelet lysate was the best growth medium for these cells, while for adipogenic differentiation the best suitable medium was DMEM F12, 1% penicillin/streptomycin and 10% foetal bovine serum supplemented with 1 μM dexamethasone, 500 μM isobutyl-methylxanthine, 1 μM rosiglitazone and 10 μg/ml insulin.

Finally, the hypothermic differentiation model of adipogenesis was tested in hUCT-MSCs from gestational diabetic and healthy backgrounds. A decreased metabolic activity was found in diabetic cells at lower temperature. Healthy cells showed less adipogenic potential at hypothermic conditions, however no difference in lipid content was found between temperatures and different metabolic backgrounds. Using these hUCT-MSCs models, upregulation of *AdipoQ*, *PPARγ, Glut4* mRNA and *UCP1* protein expression in MSCs-adipocytes derived from healthy cells was detected while diabetic adipocytes displayed increased *β3-AR* and *PPARγ* and decreased *PRDM16* mRNA at normal culture conditions. *β3-AR* was identified as the only upregulated gene in diabetic cells differentiated under hypothermic conditions. These results indicate *β3-AR* as a potential signalling pathway for functional evaluation in recruiting stored fat and energy expenditure in human adipocyte differentiation.

In conclusion, results presented here suggest that MSCs differentiated under hypothermic conditions could provide a source of thermogenic beige adipocytes which can preserve induced molecular and metabolic features. Maintenance of these properties suggest a mechanism of differentiation memory particularly when combined with browning stimulus in order to activate energy expenditure in obese populations. Cold temperature (32°C) as an adipogenic differentiation strategy in MSCs represents a potential approach to understand beige and brown adipogenesis. Overall these results highlight MSCs as an available cell source to model the differentiation and maintenance of functional beige adipocytes.

Keywords: *adipocyte, MSCs, browning, UCP1, cold temperature, energy expenditure, obesity*.

Declaration

I hereby declare that this thesis has been composed by myself and has not been submitted for any other degree previously. Acknowledgements of specific procedures not performed by myself are stated; otherwise, the work described is my own.

Date: 17/05/2020

Hilda Anaid Lugo Leija

Acknowledgements

First, I would like to thank my supervisors Dr. Virginie Sottile and Professor Michael Symonds for trusting me to carry out this project and for giving me a place in their groups. Their support and encouragement made these four years an enjoyable experience. I am indebted and grateful to Dr. Ksenija Velickovic, for her constant support, guidance and teaching during my project, I could not have asked for a better "partner in lab" and friend. I am thankful to Dr. Robert Markus for his help and advice in the confocal.

I would like to acknowledge my sponsor CONACyT for funding me and giving me the opportunity to carry out my PhD.

A big thank you to all the past and present members of the V lab and the division of child health, obstetrics and gynaecology. A special thanks to Nigel, Pete, Ian, Mark for keeping me sane, the laughs, coffees and donuts.

Quiero agradecer a mi madre, por todos los cirios prendidos, sus oraciones, pero sobretodo por las largas platicas cuando no tenía inspiración para continuar escribiendo. Gracias por ponerme estas alas y enseñarme a nunca darme por vencida. A mi padre, que con su arduo trabajo me ha demostrado lo lejos que puedes llegar. Gracias a mi hermanito, por todo su amor y admiración. Gracias a mi familia, por consentirnos con tanta comida, reuniones y cariños. Estoy muy agradecida a todos mis amigos por sus palabras de aliento y apoyo incondicional, especialmente a Dorita, María y Daniela. Gracias a nuestra familia española.

Finalmente, gracias infinitas Adrian, este logro no sería posible sin ti.

To ADAM

"What I love about science is that as you learn, you don't really get answers. You just get better questions."

— John Green.

Abbreviations

<	less than
>	greater than
β-AR	beta adrenergic receptors
a.u.	arbitrary fluorescent units
AdipoQ	adiponectin
ADSCs	adipose-derived stem cells
Agt	angiotensinogen
AR	alizarin red
asWAT	anterior subcutaneous white adipose tissue
AT	adipose tissue
ATP	adenosine triphosphate
B2M	beta-2-Microglobulin
BAT	brown adipose tissue
BM	bone marrow
BMI	body max index
BMP	bone morphogenetic protein
C/EBPβ	CCAAT-enhancer binding protein β
Ca^{2+}	calcium ion
cAMP	cyclic adenosine monophosphate
cBAT	cervical brown adipose tissue
cDNA	complementary DNA
CIDEA	cell death-inducing DFFA-like effector A
CITED1	cbp/p300-interacting transactivator with Glu/Asp-rich carboxy-terminal domain 1
CO_2	carbon dioxide
COX2	cyclooxygenase 2
COX8b	cytochrome C Oxidase Subunit VIIIb
Ct	cycle threshold
dex	dexamethasone
DIO2	deiodinase iodothyronine type II
DMEM	Dulbecco's modified eagle's medium
DMSO	dimethyl sulfoxide

DNA	deoxyribonucleic acid
DT	doubling time
ECAR	extracellular acidification rate
EDF3	ethylene response DNA binding factor 3
EEF2	elongation factor 2
EGF	epidermal growth factor
EPSTI1	epithelial stromal interaction 1
etOH	ethanol
EVA1	epithelial V-like antigen 1
FABP4	fatty acid-binding protein 4
FBS	fetal bovine serum
FCCP	carbonyl cyanide-4-(trifluoromethoxy)phenylhydrazone
FCS	fetal calf serum
FFA	free fatty acids
FGF	fibroblast growth factor
FGF21	fibroblast growth factor 21
G3PDH	glyceraldehyde 3-phosphate dehydrogenase
GD	gestational diabetic
GLUT4	Glucose transporter type 4
GMP	good manufacturing practice
HCA	hierarchical clustering analysis
hESCs	human Embryonic Stem cells
hiPSCs	human induced Pluripotent Stem cells
hPL	human platelet lysate
HS	human serum
HSBP7	heat shock protein family B (small) member 7
iBAT	interscapular brown adipose tissue
IBMX	3-Isobutyl-1-methylxanthine
IGF-1	insulin-like growth factor-1
iWAT	inguinal white adipose tissue
LDs	lipid droplets
LHX8	LIM homeobox protein 8
LPL	lipoprotein lipase
LY6A	lymphocyte antigen 6 complex, locus A
M	stability value

MFD	maximum Feret's Diameter
MPCs	mesenchymal Progenitor Cells
mRNA	messenger RNA
MSCs	mesenchymal stem cells
mWAT	mesenteric white adipose tissue
MYF	myogenic Factor
NE	norepinephrine
NEAA	non-essential amino acids
NRTC	non-reverse transcriptase control
NTC	non-template control
OCR	oxygen consumption rate
ORO	oil red o
P/S	penicillin/streptomycin
P2RX5	P2X purinoreceptor 5
PAT2	proton-coupled amino acid transporter 2
PBS	phosphate buffered saline
PBT	PBS + 0.1% Tween20
PCA	principal component analysis
PCR	polymerase chain reaction
PDGFR	platelet-derived growth factor receptor
PDK4	pyruvate dehydrogenase lipoamide kinase isozyme 4
PET	positron emission tomography
PFA	paraformaldehyde
PGC1α	peroxisome proliferator-activated receptor (*PPARγ*) coactivator-1α
pgWAT	perigonadal white adipose tissue
PKA	protein kinase A
PPAR	peroxisome proliferator-activator receptor
PRDM16	PR domain zinc finger protein 16
PREF1	preadipocyte factor
qPCR	quantitative PCR
RelQ	relative quantities
Res	resistin
RIP140	receptor-interacting protein 140
RNA	ribonucleic acid

rosi	rosiglitazone
RPLP0	ribosomal protein lateral stalk subunit P0
RT	room temperature
RT-PCR	reverse transcriptase PCR
rWAT	retroperitoneal white adipose tissue
sBAT	subscapular brown adipose tissue
SEM	standard error of the mean
SERCA2	sarcoendoplasmic Ca^{2+} ATPase
sHOX2	short stature homeobox 2
SM	standard medium
SNS	sympathetic nervous system
sWAT	subcutaneous white adipose tissue
T3	triiodothyronine
TBP	TATA sequence binding protein
TBX1	T-Box Transcription Factor 1
TCF21	transcription factor 21
TG	triglycerides
TMEM26	transmembrane protein 26
Transfer	cells cultured at 32°C for 7 days and then transferred to 37°C
TRPV	thermotransient receptor potential ion channel subfamily V
TZD	thiazolidinedione
UCP1	uncoupling protein 1
UCT	umbilical cord tissue
vWAT	visceral white adipose tissue
WAT	white adipose tissue
WP	well plate
WT1	Wilms tumour 1
ZIC1	zinc finger protein of the cerebellum 1

Chapter 1. Introduction

According to the world obesity federation (WOF), obesity is defined as an irregular or excess of fat accumulation which presents a risk to health. Obesity has been already catalogued as a chronic disease. Overweight and obesity are two major risk factors for a variety of chronic diseases such as diabetes, cardiovascular diseases and cancer[1,2].

Fat, also known as adipose tissue (AT), is composed by adipocytes, and is one of the organs regulating and coordinating energy homeostasis in the human body. There are two main types of AT, white and brown. White adipose tissue (WAT) is principally involved in the storage and mobilization of energy in the form of triglycerides (TG). WAT is distributed throughout the body in subcutaneous regions, being the principal type of AT found in adult humans. On the other hand, brown adipose tissue (BAT) regulates body temperature, generating heat by consuming stored energy. This consumption is stimulated during cold or diet-induced thermogenesis[3]. BAT its located in the paravertebral, supraclavicular and periadrenal regions in adult humans[4].

Adipocytes derive from multipotent mesenchymal stem cells (MSCs), which have the capacity to differentiate into a restricted set of cell types including myocytes, chondrocytes, osteocytes and adipocytes[5–7]. Recently some adipocytes have been described as "brite", as they possess shared characteristics with BAT such as a positive correlation with metabolic health and thermogenesis[8]. The characterization of MSCs to adipose formation represents an important step towards identifying better treatments to target obesity related pathologies. This project investigates the molecular and cellular processes involved in the commitment of MSCs into the brown adipocyte lineage using cold exposure during their differentiation. Understanding the mechanisms regulating the formation of the diverse types of AT, especially beige

adipocytes, will open new therapeutic avenues for the management of adipose tissue-related diseases through the regulation of endogenous progenitor populations.

1.1 Structure and function of adipose tissue

The adipose organ is located in several parts of the body, playing an important role in the regulation of energy homeostasis and carries out multiple fundamental endocrine functions[9]. It is mainly composed of adipocytes surrounded by fibroblasts, adipocyte precursors, endothelial cells, nerves and immune cells[10]. WAT is composed by white adipocytes which are characterised for containing an extensive unilocular lipid droplet. Its main role is the storage of excess energy in form of triglycerides (TG)[11]. On the contrary, BAT, is mainly involved in thermogenesis. BAT is composed by brown adipocytes harbouring multiloculated adipocytes that contain larger amount of mitochondria, providing them its characteristic brown colour[12].

1.1.1 White Adipose Tissue (WAT)

WAT is a dynamic endocrine organ that controls different activities, such as insulin sensitivity, lipid metabolism and satiety[13]. Also, it is the principal type of adipose tissue found in adult humans and is distributed throughout the body in subcutaneous regions, there are two main types: visceral WAT (vWAT) and subcutaneous WAT (sWAT). vWAT, or abdominal fat, is found around organs (e.g., stomach, liver, intestines, and kidneys) offering protective padding. Depending on the location, vWAT is sub-divided into mesenteric, retroperitoneal,

perigonadal and omental adipose tissue. The largest vWAT depots are the perigonadal, mesenteric, and retroperitoneal. sWAT is distributed under the skin and inside the abdominal cavity and provides protection from heat or cold. In humans, sWAT is located around the hips, thighs, and buttocks, in the cranial, facial and abdominal depots[14,15] (Figure 1.1A). sWAT role is to serve as heat insulation and protection against mechanical damage[14,15] while vWAT purpose is to protect organs[16]. One example of sWAT is inguinal WAT (iWAT), which can be found anterior to the higher site of the hind limbs and beneath the skin in mice (Figure 1.1.D). The largest sWAT in mice are the anterior, interscapular and posterior inguinal (Figure 1.1.D)[4,13,17]. In human, obese women show a higher accumulation of sWAT leading to a pear-shaped body form while in men vWAT accumulates more in an apple-shape, both fat accumulation are associated with a lower and higher metabolic risk, respectively[18]. Furthermore, it has been described that adipocytes from sWAT are bigger in men than in women, but this effect shrinks in obese people[19]. Regarding the subcutaneous and visceral WAT it has been seen a variability in their cellular and molecular biology properties, which suggest an heterogeneity within fat depots[20–22]. Several studies suggest that these depots should be studied as "separate mini organs"[23] with heterogeneous adipocyte populations from different cell precursors[16].

Additional to large WAT depots, there are minor depots broadly located thought the body. Dermal adipose tissue (dWAT) consist of mature, unilocular white adipocytes which are in contact with skin appendages and hair follicles (HF) in human and mice[24]. In mice, dWAT forms a continuous layer separated from sWAT by the panniculus carnosus[24]. On the other hand, humans lack this specific layer but the

fascia superficiallis delimits two defined skin adipose compartments: the superficial areolar and deep lamellar layers[25,26]. These two layers have different cellular distribution and metabolic activity[27,28]. HF cycling occurs parallel with dWAT size variation[29–31], dWAT expansion involves proliferation of adipocyte precursors which have defined by the expression of the cellular surface markers CD34, CD29 and Sca1[32,33]. The cross-regulation between epithelial and adipose cell lineages during HF and dWAT expansion provides an example of functional association[25]. Moreover, it has been suggested that dWAT plays a key role in wound repair[25], however the specific role of adipocytes is not yet fully understood but it could be related to two adipokines, leptin[34–36] and adiponectin[37–39] which have been involved in re-epithelialisation and re-vascularization, respectively.

Another WAT depot can be located around the joints. Some examples of joint adipose tissue are located in the hip and knee joints, its function is to mitigate and decrease friction between neighbouring skeletal structures[40]. Interestingly, knee joint is conserved in extreme starvation which suggest its main role is biomechanical instead of energy storage[25]. However, in diseased joints, adipocytes secrete higher levels of IL-6 cytokine and adipokines, including adiponectin and leptin which are thought to function as paracrine drivers of joint inflammation[41–43].

Cardiovascular adipose tissue is divided in two: epicardial and pericardial WAT (eWAT and pWAT, respectively)[44]. eWAT is situated amongst the myocardium and the visceral layer of the pericardium and shields 80% of the heart's outer area and is especially important in normal heart physiology and in other cardiovascular diseases[45] (Figure 1.1A). Epicardial adipocytes resemble white adipocytes however, these adipocytes express high levels of uncoupling protein 1 (UCP1)[46],

suggesting that they actively produce heat and supply the heart with thermal protection, besides mechanical cushioning[25]. Furthermore, eWAT produces high levels of free fatty acids that function as a supplementary local energy source[45], as well as to secrete pro and anti-inflammatory cytokines that can signal the adjacent heart muscle and other arteries[47,48]. pWAT is located anterior to the eWAT between visceral and parietal epicardial and might modulate coronary arteries. It has been previously suggested that pWAT should be considered as perivascular fat (pVAT)[44]. pVAT is located around the aorta, common carotid and brachiocephalic arteries[49]. In rodents, aortic perivascular fat is composed of BAT and WAT, with BAT being the predominant tissue in thoracic over abdominal aorta. However, the function and implication of pVAT in vascular biology remains to be elucidated[49].

One of the most studied adipose depots is the bone marrow adipose tissue (bmAT). Bone marrow contains specialised adipocytes with brown and white characteristics[50]. Additionally, bmAT harbours progenitor populations such as mesenchymal stem cells which have the potential to differentiate into adipocytes, chondrocytes and osteocytes among other lineages[51]. These cells can be identified by the cell surface markers $CD45^-$, $CD31^-$, $Sca1^+$, $CD24^+$[32]. bmAT might function as an endocrine organ and control hematopoiesis[52], it has been shown to increase in young women with prolonged calorie restriction when compared to control patients and healthier individuals[53]. Moreover, bmAT also increases in elder and obese individuals, as well as in growth hormone deficiency[51,54]. A study in mice suggests that adiponectin secreted by bmAT acts as a depot-specific response when the body experience caloric limitations, regulating skeletal muscle during energy restriction[55]. Interestingly, an

experiment in rodents showed a 70% decrease in bmAT when they were exposed to cold temperatures, it is believed this loss is mediated via lipolysis[56]. Furthermore, it has been suggested that adipocytes in long bones stimulate hematopoietic stem cells maintenance and regeneration and it is probably mediated by a stem cell factor further to be investigated[57].

1.1.1.1 Molecular signature in white adipocytes

White adipocytes are the most common type of adipocytes and their principal function is to store fuel and release adipokines such as leptin and adiponectin for the regulation of the systemic energy homeostasis[17]. White adipocytes are characterised for having one large lipid droplet, low mitochondria density, positive correlation with insulin resistance, and nearly undetectable expression of uncoupling protein 1 (*UCP1*)[4,17]. In addition, adiponectin (*AdipoQ*), resistin (*Res*), *LPL*, *TCF21* and *G3PDH*, have been reported to be WAT specific markers[4,58] (See Table 1.1).

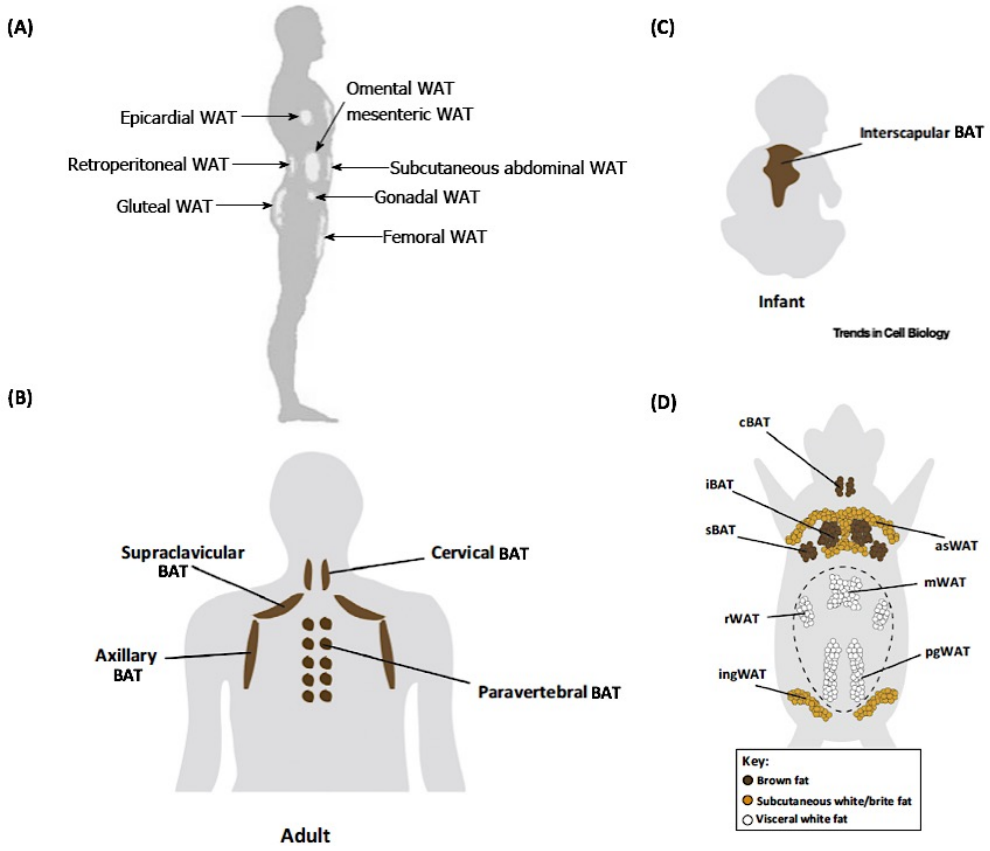


Figure 1.1. Distribution of (A) white and (B) brown adipose tissue depots in (B) adult human, (C) infant and in (D) mouse.

A: White fat - Subcutaneous (abdominal, femoral and gluteal), visceral (epicardial, gonadal, mesenteric, omental and retroperitoneal). B: Brown fat (supraclavicular, cervical, axillary and paravertebral), C: Brown fat (interscapular). D: Brown fat - iBAT, interscapular BAT; sBAT, subscapular BAT; cBAT, cervical BAT; subcutaneous white fat - asWAT, anterior subcutaneous WAT; iWAT, inguinal WAT; visceral white fat - mWAT, mesenteric WAT; rWAT, retroperitoneal WAT; pgWAT, perigonadal WAT. The peritoneum is represented by a dotted line. Image adapted from: Park 2014 and Sanchez-Gurmaches et al 2016[4,17].

1.1.2 Brown Adipose Tissue (BAT)

BAT is known to dissipate energy in the form of heat, regulating non-shivering thermogenesis, which suggests that this adipose tissue could have a natural anti-obesity role. There are two main regions in which brown fat is usually distributed, in the upper back region (interscapular) and around the kidney (perirenal). BAT can also be found around interscapular BAT (iBAT), axillary, paravertebral and perirenal sites. Although it was believed that BAT was restricted to the newborn and early childhood stages, it was proved by positron emission tomography (PET) that BAT is present in adult humans at certain anatomical sites such as cervical, supraclavicular, paravertebral, pericardial and some mediastinal and mesenteric areas (Figure 1.1.B and C). The largest depots in mice are in the interscapular, sub-scapular, and cervical regions (Figure 1.1.D) [4,17].

1.1.2.1 Molecular signature in brown adipocytes

Brown adipocytes possess many features that distinguish them from white adipocytes, including numerous small lipid droplets, high mitochondrial density, negative correlation with insulin resistance, and positive *UCP1* expression. *UCP1* is located in the inner mitochondria membrane, when active its function is to uncouple the mitochondrial respiratory chain from ATP production to dissipate heat. *UCP1* is activated in response to cold exposure and adrenergic stimuli[17]. Furthermore, BAT is clustered in highly vascularised regions, which allows BAT to dissipate the generated heat throughout the body blood vessels [4,17]. Additionally to *UCP1*, *Zic1*, *Eva1*, *Pdk4*, *Edf3*, and *Hsbp7* have been reported to be BAT specific markers[4,58] (See Table 1.1).

Table 1.1. Characteristics of white, beige and brown adipocytes.

	White	Beige	Brown
Location	Inguinal (subcutaneous), mesenteric, retroperitoneal, perigonadal, omental (visceral)	WAT depots (prominent in inguinal)	Interscapular, cervical, axillary, paravertebral and perirenal.
Morphology	Unilocular/large lipid droplet	Unilocular large/multiple small lipid droplets	Multilocular/small lipid droplets
Function	Storage of energy as triglycerides	Adaptive thermogenesis	Heat production
Mitochondria	(+)	Upon stimulation (+++)	(+++)
UCP1	Nearly undetectable	Upon stimulation (+++)	(+++)
Pre-adipocyte Markers	WT1	Ebf2	CD137*
Adipocyte Markers	Lep RetN Agt	TBX1 CITED1 Shox2 CD137 TMEM26 Pat2* P2RX5*	Lhx8 Zic1 Eva1 Pdk4
Shared brown and brite Markers	/	UCP1 DIO2 CIDEA PGC-1α PPARα Cox7α1 Cox8b Prdm16 Ebf2 Epsti1	
Shared pre-adipocyte Markers	Pdgfra LY6A CD34		

		Pref1 CD29	
Shared Markers		AdipoQ FABP4 PPARγ C/EBPIIB	
Adrenergic receptors α and β	β3 (++), α2(+)	β3	β3 (+++)
Activators	High fat diet	Cold, thiazolidinediones, natriuretic peptide, FGF21, irisin, catecholamines, β –adrenergic receptor agonists	Cold, thiazolidinediones, thyroid hormone, FGF21, BMP7, BMP8b, natriuretic peptide.

Preadipocyte factor (PREF1; also known as DLK1) is a common marker for adipocytes. Wilms tumour 1 (WT1) is a specific marker of visceral white adipocyte progenitors in the mesothelium. Beige selective markers include T-box 1 (TBX1), Cbp/p300-interacting transactivator with Glu/Asp-rich carboxy-terminal domain 1 (CITED1), short stature homeobox 2 (sHOX2). CD137. Transmembrane protein 26 (TMEM26). Proton-coupled amino acid transporter 2 (Pat2) and P2X purinoreceptor 5 (P2RX5). CD29 (also known as integrin β1). AdipoQ, adiponectin. C1Q and collagen domain containing: Agt, angiotensinogen; C/EBPIIB, CCAAT/enhancer-binding protein-IIβ; CIDEA, cell death-inducing DFFA-like effector A; Cox, cytochrome c oxidase; DIO2, deiodinase iodothyronine type II; Fabp4, fatty acid-binding protein 4; Lep, leptin; LY6A, lymphocyte antigen 6 complex, locus A; PDGFR, platelet-derived growth factor receptor; PPAR, peroxisome proliferator-activator receptor; PRDM16, PR domain zinc finger protein 16. Brown selective markers include LIM homeobox protein 8 (Lhx8), zinc finger protein of the cerebellum 1 (Zic1), epithelial V-like antigen 1 (Eva1; also known as MPZL2), pyruvate dehydrogenase kinase 4 (PDK4) and epithelial stromal interaction 1 (Epsti1). RetN, resistin; UCP1, uncoupling protein 1. *Cell surface markers. Table 1 was extracted and modified from Park 2014; Jong et al 2015; Wang et al 2016[4,58,59].

1.1.3 Beige Adipose Tissue (bAT)

Brite or beige adipocytes are located through WAT and it is reported these cells can be activated by cold exposure and/or β-adrenergic stimulation, preventing weight gain in the absence of brown adipose tissue[60]. There are two hypotheses describing how beige or brite adipocytes appear to have a common origin with white adipocytes, one of them is through trans-differentiation from white to brown stimulated by adrenergic stimulation[61] and the second one is by sharing same early progenitors[62].

It is generally accepted that these cells generate heat to help to maintain body temperature as well as brown adipocytes, however when beige adipocytes are not activated their appearance is characteristically similar to white adipocytes[4,17]. Brite adipocytes that exist in WAT, could be found specially in iWAT (Figure 1.1.D).

1.1.3.1 Molecular signature in beige/brite adipocytes

Brite adipocytes possess some features similar to brown adipocytes, such as multiple lipid droplets, medium mitochondria density, negative correlation with insulin resistance, and positive *UCP1* expression upon stimulation. PRD1-BF1-RIZ1 homologous domain-containing 16 (*PRDM16*) and the transcription co-factors peroxisome proliferator-activated receptor (*PPARγ*) coactivator-1α (*PGC1α*), *PPARα/γ* and CCAAT-enhancer binding protein β (*C/EBPβ*) are the complex involved in the differentiation into brown or brown-in-white (beige/brite) adipocytes[63,64].

Several thermoregulatory genes like *UCP1*, Cell Death-Inducing DFFA-Like Effector A (*CIDEA*) or Cytochrome C Oxidase Subunit VIIIb (*Cox8b*) have been used to assess `beiging´ of white adipocytes. Additionally,

numerous markers such as, *TBX1*, *TMEM26*, *CD137*, *FGF21*, *P2RX5*, *Pat2*, *Car4*, and *CITED1*, have been reported to be exclusive for beige adipocytes[4,58–60]. There have been disagreements with some of these beige markers. It has been reported *TBX1*, *CD137* and *TMEM26* are specific of britening[65] but in other publications these genes have not been acknowledged in response to hypothermal conditions or β-adrenergic stimulation[66], nevertheless *TBX1* has been reported to be upregulated by cold stimulation[67]. Garcia et al, described for possible interconversion from white to beige can use any of the thermoregulatory genes with *TMEM26* as exception, it was also pointed out upon adrenergic stimulation *CIDEA* and *Car4* should be avoided due their low change, and *CITED1* is not reliable due to its lost capacity to discriminate between brown and beige adipocytes. To evaluate the change from whitening to beiging, *UCP1*, *CIDEA*, and *COX8b* can be used. For this purpose, the top beige markers in murine studies are *FGF21*, *P2RX5*, *Pat2* and *Car4*[60] (See Table 1.1).

1.2 Mesenchymal stem cells (MSCs)

MSCs have been investigated for their potency to form mesodermal lineages such as osteoblasts, adipocytes, chondrocytes and myocytes[6,7] MSCs can be isolated from bone marrow (BM) aspirates, skeletal muscle, connective tissue, adipose tissue (AT), umbilical cord blood (UCB) and cord tissue (UCT), foetal blood and liver, human trabecular bones and periosteum. MSCs can be identified with several markers as CD29, CD44, CD73, CD90, CD105 and primitive Stro-1[5]. MSCs can be differentiated *in vitro* and have been shown to be regulated by key transcription factors, for adipose tissue formation the PPARγ, for osteogenic differentiation is Runx2/Cbfa1, Sox9 for chondrocyte formation and MyoD for skeletal muscle[68].

1.2.1 Adipogenic differentiation

Due to their plasticity, it has been suggested that MSCs could be targeted to switch in to the brown adipogenic lineage to help control energy homeostasis and combat metabolic diseases to the dysfunction and excess of white adipose tissue, such as obesity and diabetes type 2[69]. Some studies have demonstrated that an increment in BAT and its thermogenic activity could counteract obesity by increasing body energy expenditure[64]. Members of the transforming growth factor-β (TGF- β), the bone morphogenetic protein (BMP) family, the fibroblast growth factor (FGF) family, the wingless (Wnt), hedgehog families, and others developmental signalling molecules are implicated in the differentiation of MSCs to adipogenic development (Figure 1.2). It has been demonstrated that BMP7 helps as a potent inductive signal for brown adipogenic differentiation[70,71]. Likewise, BMP8b is secreted by

brown and beige adipocytes enhancing thermogenesis and promoting browning[72,73], while BMP2 and BMP4 have a role in white adipogenesis[74]. FGF16, 19 and 21 are also needed in brown adipogenesis[75]. On the other hand, Wnt signalling inhibit fat formation and enhances myogenesis or osteogenesis in MSCs[75]. Lastly, the hedgehog gene has been identified as a determinant factor between brown and white adipogenesis[75]. Subpopulations of adipogenic progenitors have been identified in brown, white and skeletal muscle. These cells are referred to as Sca-1$^+$ progenitor cells, (ScaPCs) and display Sca-1$^+$, CD45$^-$, and Mac1$^-$ markers[76].

It has been demonstrated that white and brown adipocytes follow different routes from MSCs to adipocyte but in both cell types *PPAR*γ is the main regulator of differentiation (Figure 1.2)[77].

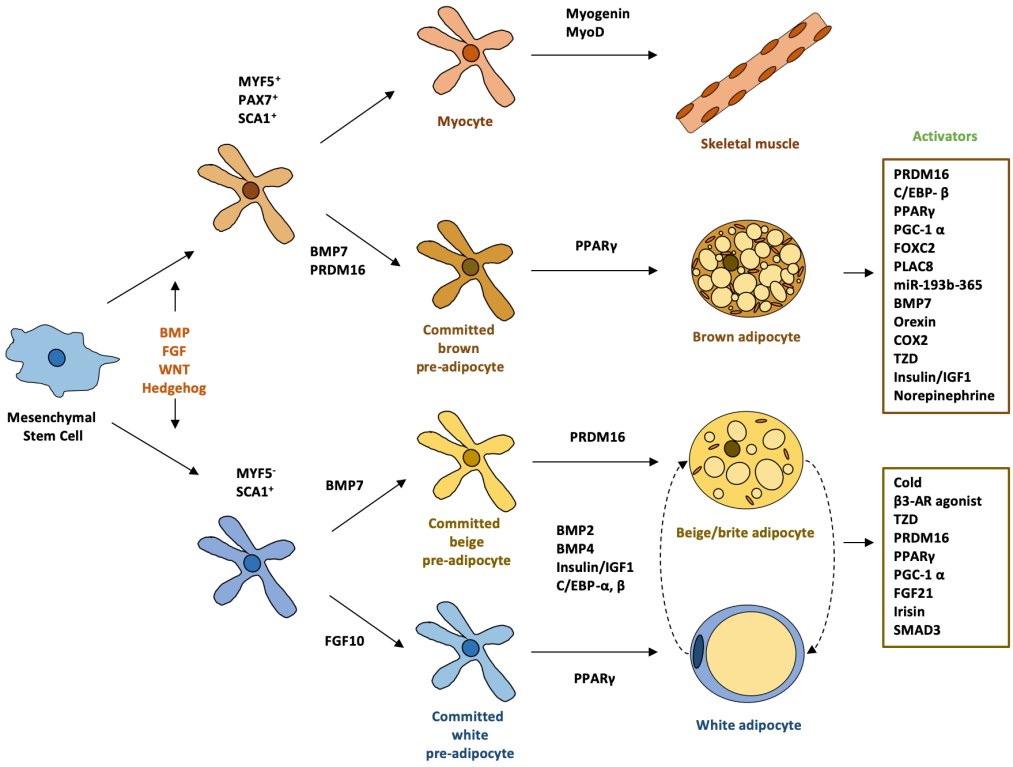


Figure 1.2. Differentiation into skeletal muscle, white, beige or brown adipocytes. Studies had demonstrated that brown cells share a progenitor cell (Myf5^{+}, Pax7^{+} and Sca1^{+}) with skeletal muscle. The Myf5^{+}, Pax7^{+} and Sca1^{+} precursor cells are induced by peroxisome proliferator-activated receptor γ (PPARγ) and CCAAT/enhancer-binding proteins (C/EBPs) in cooperation with the transcriptional co-regulator PR domain- containing 16 (PRDM16) and peroxisome proliferator activated receptor gamma coactivator 1 alpha (PGC-1α) to transform into brown adipocytes. Agents that can promote brown adipogenic differentiation include norepinephrine, insulin/IGF1, thiazolidinedione (TZD), cyclooxygenase 2 (Cox2), orexin, bone morphogenetic protein 7 (BMP7) and others. At the molecular level, a number of transcriptional/post-transcriptional regulators have been shown to specify or enhance brown phenotype, such as FOXC2, Plac8 and miR-193b-365. On the other hand, Myf5^{+}, Pax7^{+} and Sca1^{+} precursor cells are regulated by Myogenin and MyoD to transform into skeletal muscle. The Myf5^{-} and Sca1^{-} cells are induced by BMP2, BMP4, insulin/IGF1, C/EBPs and PPARγ to transform into white adipocytes. White adipocytes can also be transformed to beige/brite adipocytes, by cold exposure, β-adrenergic receptor, FGF21 (fibroblast growth factor 21), PGC-1α, TZD, SMAD3, Irisin, PPARγ, PRDM16. Image modified from Townsend & Tseng 2012 and Park 2014[4,75].

1.2.1.1 White adipocytes from progenitor cells (MSCs)

The C/EBP transcription factor has been described as one of the main regulators of white adipogenic differentiation. The early induction of C/EBPβ and δ leads to the activation of C/EBPα and *PPARγ*. Once adipogenesis induction has started, cAMP is phosphorylated and induces the expression of C/EBPβ. At the early stage of adipogenic differentiation, mitogen activated protein (MAP) kinase and GSK3β phosphorylate C/EBPβ, two monomers of C/EBPβ are induced after C/EBPβ phosphorylation, and a DNA binding domain appears. Pre-adipocytes enter the cell cycle due to the binding of C/EBPβ to DNA, showing that C/EBPβ plays an important role in mitotic clonal expansion. Finally, C/EBPβ and DNA binding activates C/EBPα and *PPARγ* which turns into a positive feedback maintained until adipocyte maturation[4,77].

PPARγ is known for controlling key genes involved in adipogenic functions, such as lipid transport and metabolism, insulin signalling and adipokine production. Thiazolidinediones (TDZs) are synthetic *PPARγ* agonists, their function is to enhance insulin resistance and decrease blood glucose levels in patients with diabetes type 2[77].

1.2.1.2 Brown adipocytes from progenitor cells (MSCs)

Brown adipogenesis during development has been linked to a positive *Myf5* progenitor cell (Figure 1.2)[17]. The transforming growth factor β-family proteins control browning, as well as BMP7 and myostatin[70,71]. Brown adipogenesis could be suppressed by Wnt signalling[4]. C/EBPβ and the transcriptional *PRDM16* are the key factors inducing the expression of *PPARγ* and *PGC-1α* needed for brown adipogenic differentiation[63]. *PGC-1α* couples with *PPARγ* to regulate mitochondrial biogenesis and oxidative metabolism[78]. Additionally,

C/EBPβ has been investigated to be the main factor of *UCP1* expression and the thermogenic activity, while its upregulation in white adipocytes promotes browning[4].

1.2.1.3 beige adipocytes from progenitor cells (MSCs)

Beige adipogenesis has been detected in classical WAT depots[79,80]. As mentioned before, these adipocytes possess many brown characteristics, but they do not express myocyte enriched genes (Figure 1.2)[80]. This suggests that beige adipocytes have a distinct origin from a non-Myf5 cell lineage. *In vivo,* beige cells have positive *UCP1* detection upon cold or β-adrenergic stimulation[80]. In mice, it has been investigated that these beige depots play a more important role than iBAT for losing weight after cold or β-adrenergic stimulation[81]. The interconversion of white into active beige adipocytes could be an encouraging approach to increase energy expenditure. Lastly, it has been described that the molecular signature of brown human depots are more similar to brite fat depots from mice[65].

1.3 Adipose-derived stem cells (ADSCs)

Adipose-derived stem cells (ADSCs) are found in the stromal vascular fraction (SVF) of adipose tissue and display similar characteristics to adult bone marrow-derived MSCs[82,83]. Their easy availability and purification make them an accessible source. ADSCs could be isolated and differentiated into mature adipocytes. Furthermore, ADSCs are a comparable source between primary pre-adipocytes *in vivo* and pre-adipocytes cell lines. Adipose-derived stromal cells express the following surface markers: $CD31^-$, $CD34^+$, $CD45^-$, $CD90^+$, $CD105^-$, $CD146^-$, and represent between 70 and 90% of the total $CD45^-$ adipose

cells. Adipose committed pre-adipocytes express specific surface markers that include $CD34^{+}/CD31^{-}$ and are negative for CD105 expression, allowing a selective purification by flow cytometry cell sorting[83].

1.4 Cellular models of white, brown and brite differentiation

1.4.1 MSCs cell lines

1.4.1.1 D1 cell line

The murine bone marrow-derived D1 MSC cell line was first isolated by Diduch et al., and has been proven to differentiate *in vitro* into osteocytes, chondrocytes, adipocytes and myocytes; to form *in vivo* a bone-like structure and some adipogenesis in diffusion chambers[68,84,85]. *PPARγ*, *Runx2* and *Sox2* are highly expressed in D1 cells[86]. *PPARγ* is key regulator for adipocyte differentiation[87] while *Runx2* is needed for osteoblast differentiation[88] and *Sox2* is vital for self-renewal and proliferation of osteoblast precursors[89]. This means, D1 cell line possess the ability to differentiate into adipocytes and/or osteocytes[86]. The D1 cell line has shown osteogenic characteristics, involving production of type I collagen, high alkaline phosphatase activity and expression of osteocalcin mRNA[84]. It has been shown that D1 cell line requires dexamethasone (Dex) to differentiate into the adipogenic lineage expressing a fat specific gene called 422 (*aP2*), which is expressed during adipogenic differentiation of pluripotent mesenchymal cells, otherwise it will differentiate mostly into osteoblasts[85]. The addition of a *PPARγ* agonist, rosiglitazone (Rosi), induces adipogenic differentiation of D1 cells increasing triglyceride production and reducing the length of the differentiation process from

2 to 3 week to 6 to 7 days[90]. Together, Dex and Rosi, induce the commitment of a stem cell into the adipogenic lineage giving rise to functional adipocytes by activation of *C/EBPα* and *PPARγ*[91]. Due to the characteristic of the D1 cell line to express *PPARγ* and to differentiate in a short period of time, it has been proposed to be a suitable model to investigate adipogenic potential and explore browning and 'britening' with different pro and anti-adipogenic agents.

Recently, the D1 cell line has been used as a model of browning using cold exposure[92] or caffeine addition[93] during the adipogenic differentiation treatment.

1.4.2 Pre-adipocyte cell lines

The most used pre-adipocyte lines are the 3T3-F442A and 3T3-L1, from the Swiss 3T3 cell line. These lines have the advantage of indefinite passages and homogeneous cellular population which offers a reliable source of white adipogenesis study[94]. These cell lines have showed multilocular fat droplets and brite characteristics[69]. Another cell line is Ob17, derived from epididimal fat pads of obese adult mice. These cells present a later pre-adipogenic stage in white adipogenesis[83,94]. Additionally, the D12 cell line, has been immortalized from mouse iWAT, this cell line can differentiate into brown adipocytes and retain brown characteristics such as UCP1 expression upon certain stimulation (β-adrenergic agonist)[65].

1.4.3 Immortalized cell lines from human BAT

Only one cell line derived from human BAT has been described. The PAZ6 cell line was derived from the SVF of human infant BAT and then

immortalized through infection with SV40 large T antigen[95]. The PAZ6 cell line has been investigated as an adipogenic line which expresses low levels of *UCP1* and forms multilocular adipocytes after 2 weeks of differentiation treatment. TZD treatments induce the expression of several adipocyte markers (*aP2, LPL, β3-AR, HLS*) and *UCP2*, which is an isoform of *UCP1* expressed in white adipocytes. This could indicate that PAZ6 cell line might possess a mixed brown/brite phenotype[8,62]. Recently, a protocol has been described to establish immortalized human brown and white preadipocytes from human neck fat biopsies[96].

1.4.4 Primary cultures of human AT

Primary cultures from human adipose tissues have been widely used to investigate white and brown adipogenesis being considered the closest model for *in vivo* differentiation.

1.4.4.1 Primary cultures derived from human WAT

Adipose derived stem cells (ADSCs) and pre- and mature adipocytes from the liposuction aspirate fluid (LAF) have been isolated and characterized[82]. 48 hrs overexpression of *PGC-1α,* in 13 days *in vitro* adipogenic treatment mature white adipocytes (sWAT) isolated surgically from human, induced the expression of *UCP1* and other hallmarks described in brown adipogenesis[97].

ADSCs have been investigated for their potential to exhibit *UCP1* mRNA expression and multiloculated cells after one week in adipogenic culture conditions. It was reported that these cells lost the *UCP1* expression and presented unilocular lipid droplets after being cultured for two weeks[98], suggesting a possible switch from browning/beigeing to whitening[99].

1.4.4.2 Primary cultures derived from human BAT

Some reports have described the isolation and use of primary BAT cells from supraclavicular fat to study brown adipogenic differentiation[100-102]. A recent primary BAT culture derived from human foetal interscapular tissue was developed for the first time. This model displays an ability to differentiate towards mature classical brown adipocytes and represents an opportunity to study *in vivo* adipogenesis in humans[103].

1.4.5 Primary cultures of adult MSCs.

As mentioned above, another potential human source to investigate brown and white adipogenesis are MSCs. These cells are present is several tissues throughout the body. Sources from adult and foetal bone marrow, umbilical cord blood (UCB) and muscle have been investigated towards adipogenesis[62].

1.4.5.1 Adult bone marrow MSCs

MSCs derived from bone marrow (BM) have the multipotentiality to differentiate into adipocytes, osteocytes and chondrocytes[7]. BM-MSCs have been investigated towards their potentiality to differentiate into distinct adipocytes types, such as white, beige and brown. It has been suggested that BM-MSCs overexpress *PGC-1α*[104], paired with these observations it was observed an increased expression in several brown markers such as, *PPARα*, *PPARγ* and *C/EBPβ* [104]. These cells also showed a higher expression of genes regulating electron transport chain, cellular respiration, the Krebs cycle and fatty acid β-oxidation. Moreover, *PGC-1α* expressing cells displayed a decreased expression in white markers with higher mitochondrial content, *UCP1* mRNA and

protein expression and oxygen consumption levels[105,106]. These observations suggest that *PGC-1α* is an important regulator of beige and brown adipogenic differentiation and metabolic activation[106].

1.4.5.2 Fetal bone marrow MSCs (fBM-MSCs)

fBM-MSCs have only been used once so far to evaluate the ability to differentiate towards adipocytes. This investigation showed that fBM-MSCs have the potentiality to go towards white or brown adipocytes according to the donor background. *UCP1*, *PGC-1α*, *PRDM16* and *RIP140* were the genes selected to evaluate browning in undifferentiated cells, however no expression could be observed, concluding that fBM-MSCs could be used as a heterogeneous population for white and brown models of adipogenesis. Importantly, Morganstein and colleagues identified a novel estrogen related receptor α (ERRα) pathway involved in to control of *UCP1* expression[107].

1.4.5.3 Fetal Muscle-derived MSCs

As described before, brown adipocytes have a common progenitor with myocytes (Figure 1.2). Crisan and colleagues described that cells isolated from muscle expressing the surface marker CD34 have the ability to differentiate to brown adipocytes with a high level of *UCP1* expression and uncoupled respiration. However, after several passages these cells lose their potentiality towards browning which suggest a shift from brown to white adipogenic phenotype[108].

1.4.5.4 Umbilical Cord Blood (UCB) MSCs

UCB MSCs have been recently analysed for its potentiality towards whitening and browning, showing these cells are not an appropriate stem cell type to be differentiated into white and brown adipocytes due to their little capacity to differentiate into adipocytes[109]. Isolation and

characterisation of MSCs from umbilical cord tissue (UCT) have been reported[110–114], however the brown adipogenesis potential of UCT has not been reported yet[115,116].

1.4.6 human pluripotent stem cells (hPSC)

hPSCs have been recently used with the aim of detecting key factors and pathways for white and brown adipogenic differentiation[117,118]. The first study that investigated these cells used Mesenchymal Progenitor Cells (MPCs) derived from human Embryonic Stem cells (hESc) and human induced Pluripotent Stem cells (hiPSCs). The MPCs were transduced with several single factors to evaluate each factor potential. Cells transfected with *PPARγ2* alone were able to differentiate into white adipocytes while cells with a combination of *PPARγ2* and C/EBPβ and/or *PRDM16* gave rise to brown adipocytes. White derived MPCs adipocytes expressed insulin sensitivity and similar properties to primary adipocytes while brown derived MPCs adipocytes showed mitochondrial activity, *UCP1* and *PGC-1α* expression[117]. The second study used a mix of different molecules, a TGFβ-inhibitor SB431542 in combination with ascorbic acid and EGF, to promote hiPSCs brown/beige differentiation at a similar level of brown adipocytes located in human depots. These brown progenitor cells expressed a pool of brown markers, *UCP1*, *Pax3*, *CIDEA*, *DIO2*, *Zic1* and *CD137*. These results emphasize the importance of TGFβ pathway in brown adipogenesis[118].

1.5 Adipogenic medium

A large number of adipogenic differentiation protocols use standard Dulbecco's modified Eagle's medium (DMEM) supplemented with 10% of fetal bovine serum (FBS). There are several modulators used for whitening and browning, mostly they have been identified and characterised in mouse models *in vitro* and *in vivo*[71,76]. Generally, three components are used in adipogenic induction medium for bone marrow MSCs, those are insulin, dexamethasone (Dex), and 3-Isobutyl-1-methylxanthine (IBMX)[119].

1.5.1 Insulin

In WAT insulin stimulates glucose uptake, an important physiological process that is insulin mediated in which glucose transporter 4 (GLUT4) is translocated to the plasma membrane to facilitate an elevation entry of glucose[120] for adipogenic synthesis of triglycerides[121].

Insulin and insulin like growth factor 1 (IGF-1) stimulate multiples intracellular pathways that triggers adipogenic induction and maturation via the activation of an intracellular signalling cascade including insulin receptor (INSR), insulin receptor substrate (INS) proteins, phosphatidyl inositol 3-kinase (PI3K) and protein kinase B (AKT)[122,123]. MSCs express INSR-A, a splice variant of INSR, linked to cell proliferation and less-differentiated cells[123]. AKT phosphorylates and regulate numerous transcription factors involving adipogenesis such as the forkhead box O (FOXO) and the mammalian target of rapamycin (mTOR) which lead to the activation of PPARγ, therefore adipogenic differentiation[124].

1.5.2 Dexamethasone (Dex)

Dex is a synthetic anti-inflammatory steroid compound ligand for glucocorticoid receptor (GR) that activates osteogenic and adipogenic differentiation in a cell-, time-, and concentration-dependent manner. High and extended exposure of Dex, produce a larger number of adipocytes *in vitro* suppressing osteogenic differentiation[91,125,126].

Dex accelerate adipogenic differentiation by directly promoting the expression of several transcription factors C/EBPα, β and δ, KLF5 and 9 and PPARγ in the early stage of differentiation[127]. The main role of Dex is to bind GR and enhance adipogenic genes through the activation of C/EBPβ by H3K27 acetyltransferase CBP. It has been reported that Dex alone can induce adipogenic differentiation in certain bone marrow derived cell lines[85,128] or Dex and insulin in stromal cells[129].

1.5.3 Rosiglitazone (Rosi)

Rosi is a *PPARγ* agonist, these types of components are not only beneficial to people under diabetic conditions but also are widely used to accelerate adipogenic differentiation of pre-adipocytes or progenitor cells with the ability to differentiate into adipocytes *in vitro*. Rosi binds to *PPARγ,* incrementing the capacity of the cells to be stimulated to insulin, it also increases the amount of differentiation of cells[90,91,130]. It has also been reported that brown adipocytes exposed 24 hrs to Rosi showed *UCP1* gene expression, increased basal respiration rate and lipoprotein lipase (LPL) activity. It has been implied that Rosi could induce the thermogenic mechanism from lipoproteins[131].

1.5.4 IBMX

IBMX is a nonselective phosphodiesterase inhibitor, increasing intracellular cAMP and protein kinase A (PKA). Activation of *PPARγ* is regulated by PKA signalling pathway. Furthermore, IBMX and Dex induce C/EBPβ and δ, which have been described above. *PPARγ* agonists, thiazolidineldiones or glitazones, are used for diabetes treatment, and are also known for enhance adipogenesis *in vitro*. For example, rosiglitazone binds to PPARγ, and stimulate adipocytes uptake of insulin[119]. IBMX and Dex induce *PPARγ,* enhancing adipogenic differentiation in the presence of *PPARγ* agonists like, rosiglitazone[69,91,126].

1.5.5 Triiodothyonine (T3)

Thyroid hormone (TH) effects are regulated by T3, which mediates gene expression through binding to the nuclear receptors, TRα and β[132], leading to the activation of both the PI3K[133] and the MAPK pathway[134]. Activation of PI3K induces the phosphorylation and activation of AKT/protein kinase B and phosphorylation of mTOR[135] which drives to an increase of certain genes, some of them involves hypoxia-inducible factor (HIF-1α), calcineurin inhibitor (ZAKI-4α)[135,136], *GPD*, *ME*, *PEPCK*, *S14*, *FAS*, *Glut4* and *LPL*, among others[132,137]. T3 is a regulator of adipogenic differentiation and mechanism related, lipogenesis, lipolysis, gluconeogenesis and glycolysis both *in vivo* and *in vitro*[137] by controlling PPARs[137].

Deiodinases D1, D2 and D3 control the availability of T3[132]. D3 is stimulated by serum and mitogens during proliferation of preadipocytes whereas D2 deiodinase (*DIO2*) is associated to the

differentiation program of adipocytes, throughout C/EBPs, increasing the adrenergic response and rising T3 in BAT[132] for thermogenesis and lipolysis[137]. Moreover, T3 increases the adrenergic stimulation of *UCP1*[137,138] and in thermoneutrality, T3 is also required for *UCP1* mRNA expression and stability, this response is mediated by TRβ1 isoform[132]. The role of TH during the proliferative stage of brown adipocytes is to impede bFGF and aFGF mitogenic effect, suggesting an important role of T3 during proliferation[137].

Finally, the function of T3 is equally transcriptional and stabilising the mRNA, plus it is synergic with the function of insulin[137].

1.5.6 Other growth factors

There are several factors that have been described in order to enhance white or brown adipogenic differentiation. BMPs are known for producing more of an effect not only in osteogenesis, but also on adipogenesis and angiogenesis. BMP7 has been investigated for promoting brown adipogenesis by inducting of *PRDM16* and *PGC-1α,* increasing *UCP1* expression, *PPARγ,* C/EBPs and mitochondria biogenesis[71,74,119]. Ascorbic acid is normally used in osteogenic differentiation but has also been reported to increase the accumulation of lipid droplets[139]. FGF-2 has showed to increase cellular proliferation and induce PPARγ expression[140,141]. CL-31623 is a β-adrenergic receptor *(β3-AR*) agonist that has been investigated *in vivo* an *in vitro*[142,143]. An increased *UCP1* expression in brown but not in white adipogenic cultures was detected after CL-31623 treatment[142]. Rats that were treated with this compound produce multilocular adipocytes

in WAT with *UCP1* positive expression[143]. Both studies suggest that *β3-AR* agonists could induce browning *in vivo* but not *in vitro*.

1.5.7 Cold stimuli for brown activation

Shivering is initiated by exposure to cold, a normal involuntary response to maintain body temperature in adults and other mammals[138]. Although it is a rapid way to initiate heat production is less efficient than heat produced through mitochondrial uncoupling in BAT[132]. In addition to BAT, beige adipocytes located in WAT can activate *UCP1*, this activation is followed by cold exposure in response to the β-adrenergic stimulation[144]. When the demand for heat increases in the cold, heat is generated. Thermogenesis is activated by cold *in vivo* due to the activation of the sympathetic nervous system (SNS) through the norepinephrine (NE) liberated from the nerve endings onto brown and beige adipocytes[137,138,144]. NE binds to the β-AR activating adenylate cyclase which rise cAMP, then lipolysis is activated and free fatty acids (FFA) are increased leading to *UCP1* activation[137,144,145]. It has been described that some adipocytes located in WAT *in vivo* and white adipocytes *in vitro* possess a temperature sensitive, β-AR-independent and cell-autonomous program, capable to respond to cold stimulus activating thermogenesis and upregulating brown genes[144].

1.5.7.1 Cold exposure *in vivo*

1.5.7.1.1 Cold exposure in humans

Targeting BAT in humans has been a recent research focus as it is believed that the recruitment of BAT could counterbalance obesity and

the metabolic diseases developed. Several human studies evaluating cold acclimation and BAT increased activation have been done.

One of the first studies done was performed by Davis[146], male subjects were exposed to cold temperature which resulted in elevated heat production. This study did not state which tissue was responsible and at that time it was unsure if humans could possess enough amount of active BAT[146]. Similar studies starting with 2.5 hrs to ten days cold acclimation, reported no sex differences in BAT presence and activation, nevertheless it was suggested that a variable indoor environment with recurrent cold exposure could be an suitable approach to increase energy expenditure[147] without changes in food intake[148]. Another study also reported increased BAT activity in most healthy subjects when exposed to cold, and interestingly a negative correlation between body max index (BMI) plus percentage of body fat with BAT was found as lower BAT activity was detected on obese subjects[149], nevertheless it has been reported that ten days cold acclimation in obese subjects can recruit BAT[150]. Furthermore, Blondin and colleagues demonstrated that daily cold exposure for four weeks in males increases the volume of metabolically active BAT, its oxidative capacity, hence its contribution to cold-induced thermogenesis[151]. They have also shown that acute cold exposure in healthy lean men leads to glucose uptake closely related with BAT metabolic activation. It appears that glucose utilisation is greater in muscle than in BAT during cold exposure[152] however after four weeks of cold acclimation there is a reduction in muscle thermogenesis and a shift to BAT activation[153]. These studies indicate that cold acclimation could result in an increase in energy expenditure which might lead to prevent

weight gain or help reduce weight in obese people. However, the maintenance of BAT activation is still being investigated.

1.5.7.1.2 Cold exposure in animals

Several studies have been done evaluating different mammals, the most studied are mice, rats, guinea pigs, among others. The aim of most of these studies is to elucidate the molecular, protein, hormones and bioenergetics impact of cold response in different types of AT. Rosenwald et al, reported beige adipogenesis induction from cold stimulated mice, these traits were reverted to a white status accompanied with a decrease of brown selective genes within six weeks of warm acclimatisation, nonetheless these brite cells have the capacity to revert into brite adipocytes on additional cold stimulation[67]. Gene expression of WAT and BAT of mice after of cold exposure has been extensively evaluated, the main genes involved in thermogenesis are normally upregulated, *UCP1*, *PGC-1α* and C/EBPβ but also several other pathways have been identified, such as cytochrome P450, apolipoprotein[154], SERCA2a (sarcoendoplasmic Ca^{2+} ATPase)[155], β3-AR[79], also improvement in glucose tolerance and enhanced insulin sensitivity have been detected[156].

1.5.7.2 Cold exposure *in vitro*

In vitro adipogenic differentiation has been also evaluated, browning of 3T3-F442A adipocytes kept up to 10 days in cold exposure was found to be reversible by *UCP1* decrease to base line once the temperature was changed to normal conditions (37°C)[144]. Furthermore, Altshuler-Keylin and colleagues showed that beige to white adipocyte transition occurred by loss of multilocular lipids and *UCP1* expression in 15 to 20 days once a β-AR agonist is removed[157]. In contrast, brown adipocytes are capable of maintaining their multilocular morphology

for one month on the same culture conditions[157]. These results demonstrate a distinct mechanism from beige to brown adipocytes of *UCP1* maintenance after the main stimulus is removed which could be explained by mitochondrial biogenesis and mitophagy of brown and beige adipocytes, respectively[157,158].

Cold exposure has been proved to enhance *in vitro* differentiation of bone marrow MSC into a beige/brown status. It was previously demonstrated that after one week of warm adaptation, beige adipocytes differentiated under cold culture conditions (32°C) were still showing increased *UCP1* protein[92], however molecular mechanisms underlying beige adipocyte phenotype maintenance after rewarming are poorly understood.

1.5.7.2.1 Transient Receptor Potential channels (TRPs)

The thermotransient receptor potential (TRP) channels, are the most characterised molecular sensors for temperature in cells, adipocytes being one of them[159]. These channels respond to certain stimuli such as: PIP2, Ca^{2+}, temperature, osmotic pressure, cyclic nucleotides, phosphorylation potential among others[160]. It is know that adipocytes express the transient receptor potential cation channel subfamily V members (TRPV) 1, 2 and 4[159,161]. Among these three, TRPV1 and TRPV4 have been reported to inhibit adipogenic differentiation[162]. However, their modulation with temperature exposure has been described as follows. TRPV1/TRPV4 double-knockout mice adipocytes isolated from the stromal-vascular adipose depots, are able to respond to 4 h of cold temperature exposure (31°C) and increase UCP1 mRNA expression. These results suggests that temperature sensing mechanism could be independent of TRPV1 and TRPV4[144]. Although the role of Ca^{2+} is not well known, recent reports have demonstrated

that beige adipocytes possess an independent-UCP1 mechanism involving the sarco-endoplasmic reticulum Ca^{2+}-ATPase 2b (SERCA2b) which can generate heat[163]. Overall these results could indicate that TRPs activation thought Ca^{2+} might be linked to adipogenic browning. However, further experiments are needed in order to determine whether TRPV1 inhibition reduces the browning response induced by hypothermal culture conditions and if other TRPV family members are involved in mediating the temperature response.

TRPV2, is known to be a Ca^{2+}permeable channel sensitive to temperature and to be a critical player for thermogenic function on primary mouse brown adipocytes[164]. However, its evaluation during temperature exposure has not been previously described. Sun and colleagues showed TRPV2 activation by mechanical force, their results concluded that TRPV2 negatively regulates browning differentiation both *in vivo* and *in vitro*[164,165].

Additionally, to temperature stimuli, TRP agonist have been also been reported when stimulating browning in adipocytes. TRPV1 and the transient receptor potential cation channel subfamily A member 1 (TRPA1) activation in 3T3-L1 adipocytes has been shown with the alkamide *trans*-pellitorine by suppressing lipid accumulation[166].

Furthermore, the transient receptor potential cation channel subfamily M member 8 (TRPM8) is functionally present in mouse brown adipocytes. Menthol, a TRPM8 agonist, has been used to promote browning. Ma and colleagues showed that induction of brown adipocytes promotes UCP1 upregulation and is associated with protein kinase A phosporylation[167]. Moreover, primary mice white adipocytes have also been reported to exhibit a high TRPM8 mRNA

after menthol stimulation increasing thermogenic genes, which suggest TRPM8 could be involved in WAT browning[168]. Human white adipocytes has also been activated by menthol and icilin treatment, these cells showed UCP1 expression, mitochondrial activation, glucose uptake and heat production induced by TRPM8[169].

The TRP involvement in temperature exposed-adipocytes needs to be additionally explored in order to characterise their function in a cell-autonomous manner. Further questions are still unknown. Are these TRP channels cell type specific? Is Adrβ3 linked to the TRP thermogenic function? Are other TRP members compensating when one of them is inhibited?

Aims

This project aims to establish a stem cell-based model of adipogenic differentiation and *in vitro* suitable conditions to enable the comparative study of pathways involved in the regulation, kinetics and expression profile of white, brown and beige adipogenesis.

Using mesenchymal stem cells as adipogenic progenitors from mice and human, this project will analyse the process of adipogenic differentiation through 4 experimental aims:

Establish and validate an in-vitro model of adipogenesis using stem cells

This first objective will involve the establishment and validation of and *in vitro* model of adipogenesis using a mouse mesenchymal stem cell line, in order to optimise the conditions towards adipogenic differentiation: white, beige/brown. The properties of stem cell-derived adipocytes will be analysed and compared to the molecular signatures associated with primary white, brown and beige adipose tissue.

Hypothesis: mMSCs are able to differentiate into beige adipocytes under hypothermal culture conditions (32°C).

Evaluate the cellular response and resulting gene expression changes upon exposure to pro/anti-adipogenic regulators including candidate pathways activator/inhibitor and environmental stimuli

The second objective of this investigation will be to assess the effect of different pro- and anti- adipogenic *in vitro* regulators and environmental stimuli such as T3 and cold exposure, on the activation of brown adipogenic markers in the stablished *in vitro* MSC model. The effect of cold and warm *in vitro* differentiation conditions will be evaluated in order to maintain the beige/brown characteristics in the MSC-derived adipocytes.

Hypothesis: cold mMSCs derived adipocytes are able to maintain beige like properties after 21 days of being transferred to normal culture conditions (37°C).

Isolation and characterisation of human umbilical cord tissue MSCs

The third objective of this research is to isolate and characterise primary MSCs derived from healthy and gestational diabetes conditions, for this purpose umbilical cord tissue will be used. This part will involve testing different isolation protocols, growth and adipogenic differentiation media in order to provide the best conditions for both states.

Hypothesis: Isolation of hMSCs from UCT is feasible through an enzymatic method. Furthermore, hMSCS from UCT are able to differentiate into adipocytes.

Use the established *in vitro* conditions to evaluate the adipogenic response of stem cells isolated from different physiological states and evaluate the effect on the nature of the adipogenic response.

The last objective or the project will involve testing the *in vitro* established conditions of adipogenesis to compare the adipogenic response of primary MSCs from umbilical cord tissue originating from healthy and gestational diabetic donors, with the aim of identifying whether these browning responses can be achieved and/or are affected.

Hypothesis: hUCT-MSCs from gestational diabetic (GD) background will display a higher adipogenic potential at normal culture conditions (37°C) than healthy cells, while at hypothermal conditions (32°C) GD cells will be impaired to differentiate towards adipogenic lineage whereas healthy cells will be able to show beige like properties.

Chapter 2. Methods

2.1 Chemicals and Reagents

All commonly used solution stocks were prepared and autoclaved. Generally used plastic ware was purchased from Thermo Fisher Scientific (UK) unless otherwise stated.

A list of equipment and reagents can be found in the Appendix (p. 226).

Mouse bone marrow mesenchymal stem cells (mMSCs) D1 was kindly provided by Dr. Virginie Sottile, cell line was obtained from ATCC (CRL-12424). The human adipose-derived stem cells (hADSCs) were kindly provided by Dr. James Law (ThermoFisher UK, Cat. No R7788-115) and primary mouse BM-derived stem cells were isolated and provided by Dr. Zubair Nizamudeen.

Human umbilical cord tissue (hUCT) was purchased from the Anthony Nolan institute, all hUCT were from male babies, background of the donors was chosen as healthy and gestational diabetes, a table with the specifications of each hUCT can be found in Chapter 2.3.1, p. 46.

2.2 Cell culture

All cells were kept at either 37°C or 32°C, 95% humidity and 5% CO_2. Cell culture experiments were performed in a type II Biological Safety Cabinet.

2.2.1 mMSCs D1 culture

mMSCs D1 cell line (mMSCs) was cultured using DMEM low-glucose, 1% of L-Glutamine (200mM), 1% of non-essential amino acids (100X - NEAA), 1% of penicillin/streptomycin (10,000 U/ml - P/S) and 10% fetal

bovine serum (FBS) (referred to as standard medium -SM-). Medium was changed every 2 to 3 days depending upon seeding density and confluency.

2.2.2 Passaging of mMSCs

mMSCs were passaged when confluency reached 70 - 80%. The cells were washed with sterile PBS and treated with 500 µl of 0.05% trypsin/EDTA per T25 flask for up to 3 minutes. Trypsinised cells were then diluted in SM and transferred to a new cell culture flask at a ratio of 1:4 to 1:8 to seed the next cultures. Medium was renewed every 2 to 3 days as needed.

2.2.3 Gelatine coated plates and coverslips

A solution of 0.1% gelatine with 1% of P/S was prepared in sterile distilled water and filtered before its use. 24 well plates were prepared with or without sterile glass coverslips (1.5H; 170±5µm; 18 x 18 mm; Scientific Laboratory Supplies or Zeiss), wells were coated with 500 µl of gelatine for 15 min at room temperature, gelatine was aspirated before cells were seeded.

2.2.4 mMSCs adipogenic differentiation

Adipogenic differentiation was done by seeding 80,000 cells/well in a 24-well plate and 2,000,000 cells in T25, adipogenic treatment was started at a confluency of 80% and stimulated by supplementing SM with 10 µg/mL insulin, 1 µM rosiglitazone, 1 µM dexamethasone and 100 µM 3-isobutyl-1-methylxanthine (IBMX), length of the treatment varied as indicated. Triiodothyronine (T3) was added in combination to

the adipogenic differentiation medium as indicated. Cells were differentiated in parallel at 37°C and 32°C thermal conditions as indicated.

2.2.5 Cryopreservation of mMSCs

mMSCs were trypsinised, collected in SM and centrifuged for 5 minutes at 200g. After aspirating the supernatant, the pellet was resuspended in a 1:1 solution of FBS and ice-cold freezing mix (60% SM, 20% FBS and 20% dimethyl sulfoxide (DMSO)) and transferred to a cryovial. Cells were kept up to 72 hrs at -80°C, for long term storage cells were transferred to liquid nitrogen. For cell reanimation, cryovials were quickly thawed and transferred to a tube containing 4 ml of SM. Cells were then centrifuged for 5 minutes at 200g, the pellet was resuspended in 5 ml of SM and transferred to a flask according to frozen ratio.

2.3 Human umbilical cord tissue (hUCT)

2.3.1 Background of the hUCT

hUCT were ordered with certain specifications. Unfortunately, due the poor number of UCT from diabetic background, all GD tissues received by the Anthony Nolan were collected. Exclusion criteria for the tissues collected included infectious diseases. Demographic information, including maternal and paternal ethnicity were obtained. Data on birth weight was also recorded. Table 2.1 shows detailed background of all hUCT received.

Table 2.1. Information from the umbilical cord tissues collected. All tissues collected were from male babies.

Sample N°	Maternal ethnicity	Paternal ethnicity	Baby weight (gr)	Date/Time collection	Date isolation	Description	Final status
9221218152851	White British	European	2595	22.03.2018 12:05	23.03.2018	Healthy	Cultured
9221218166248	UK	UK	-	09.09.2018 03:10	10.09.2018	Healthy	Discarded (Virology)
9221218166272	UK/Ireland	UK	3260	09.09.2018 10:20	10.09.2018	Gestational diabetic + Maternal history	Cultured
9221218167837	Mixed white	Mixed white	3775	27.10.2018 21:48	29.10.2018	Gestational diabetic	Discarded (no cells)
922121816852	Eastern Europe	Eastern Europe	3410	28.10.2018 06:28	29.10.2018	Healthy	Discarded (no cells)
9221219172794	Southern & other European (White)	Southern & other European (White)	3555	13.02.2019 14:17	14.02.2019	Healthy	Cultured

9221219172767	South Asian	South Asian	3590	13.02.2019 06:35	14.02.2019	Gestational diabetic	Cultured
9221219167481	South Asian	South Asian	2555	13.02.2019 06:30	14.02.2019	Gestational diabetic	Discarded (Virology)
9221219172828	UK/Ireland	African Caribbean & African (black)	3950	14.02.2019 12:23	15.02.2019	Healthy	Cultured
9221219173823	UK/Ireland	UK/Ireland	3220	12.03.2019	13.03.2019	Gestational diabetic	Cultured

2.3.2 hUCT isolation

Optimization of the isolation method was done with one hUCT (#851) collected from the Anthony Nolan centre, 24 cm long approximately, tissue was cut in half.

First half of the hUCT was processed with the explant method. Tissue was washed three times in PBS, followed with 70% etOH for 30 seconds, and finally washed with PBS again to remove any etOH residuals, both ends of the cord were cut. Cord tissue was carefully cut in explants of 10 mm pieces with incisions in the inner matrix, 12 explants were obtained and each one was put in a well from a 6-well plate, four explants were placed per 6-well plate, to be treated with different growing MSC medium. Medium was changed every two days, explants were removed until cells reached 80% confluency[170].

Second half of the hUCT was treated with an enzymatic method, tissue was intensely washed with PBS containing 1% P/S, then tissue was minced and digested at a ratio of 4 mL of collagenase Type B (0.4 U/mL) per cm of minced tissue for 2 hours at 37 °C with intermittent intense agitation every 15 min. Afterwards, tissue was neutralised with DMEM low-glucose containing 1% P/S and filtered through a 70 µM cell strainer. To obtain the pellet, the filtered tissue was centrifuged at 2,000 rpm for 5 minutes and the pellet was resuspended in 10 mL of 2% FBS in DMEM low-glucose followed by another centrifugation at the same conditions[170]. Finally, each pellet was resuspended in 5 mL of three different standard medium and seed in a three different T25 culture flask. Medium was changed every two days.

A variation of the enzymatic method had to be improvised due to the thickness of the digested hUCT and its inability to be filtered. After the neutralisation step with DMEM, the tissue was immediately seeded into three T75 flasks and each flask was fed with its corresponding media (see Chapter 2.3.4 hUCT-MSC culture, p. 48). Medium was changed every 2-3 days, without removing the remaining undigested tissue from the flasks. A graphical representation of the hUCT isolation optimisation can be seen in Figure 2.1.

After the isolation process was optimised the subsequent hUCT were isolated with the enzymatic method without the centrifugation step described above.

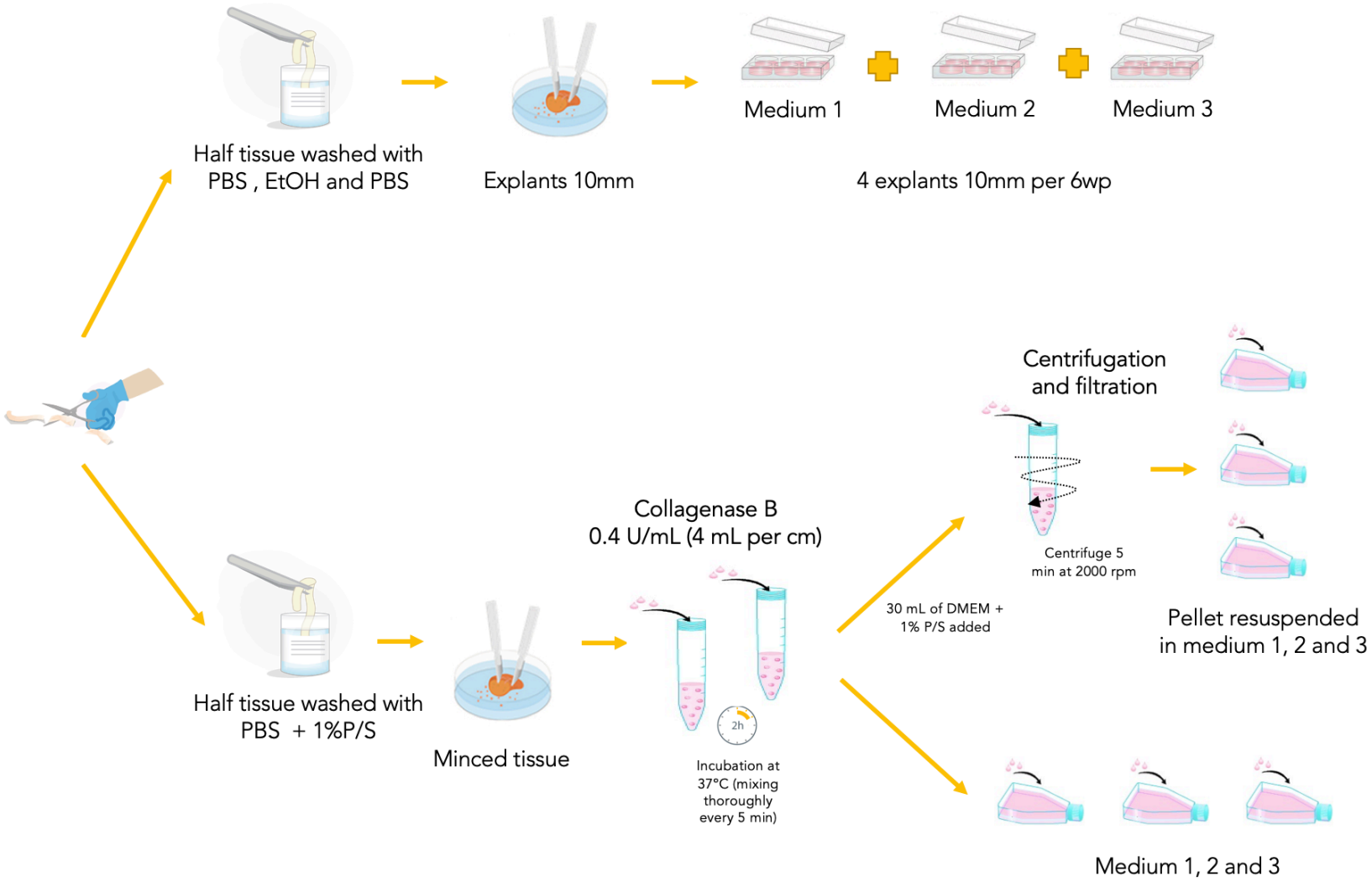

Half tissue washed with
PBS , EtOH and PBS
Explants 10mm
Medium 1
Medium 2
Medium 3
4 explants 10mm per 6wp
Half tissue washed with
PBS + 1%P/S
Minced tissue
Collagenase B
0.4 U/mL (4 mL per cm)
2h
Incubation at
37°C (mixing
thoroughly
every 5 min)
30 mL of DMEM +
1% P/S added
Centrifugation
and filtration
Centrifuge 5
min at 2000 rpm
Pellet resuspended
in medium 1, 2 and 3
Medium 1, 2 and 3

Figure 2.1.Graphical representation of the hUCT-MSC isolation. Detailed description can be found in Chapter 2.3.2, p. 44.

2.3.3 Mycoplasma test

When cells reached around 70% confluency, 500 µl of medium was extracted of each donor sample cells' flask and tested for mycoplasma contamination. EZ-PCR™ Mycoplasma Detection Kit was used following the manufacturer's protocol (EZ-PCR™ Mycoplasma Detection Kit Instructions for Use). Each sample was run with its appropriate positive and negative (sterile water) controls.

2.3.4 hUCT-MSCs culture

Three different MSC media were evaluated in order to determine which one provided a heathy status and rapid growing time on hUCT-MSC cells. Medium number one, two and three had the following compounds; medium 1: DMEM F12 + 10% FBS + 1% P/S[171]; medium 2: DMEM low glucose + 10% FBS + 1% P/S[114]; medium 3: DMEM low glucose + 1% L-glutamine + 1% P/S + 10% human platelet lysate (hPL)[172].

After the media optimisation was done the subsequent hUCT-MSCs were cultured in medium number three described above.

2.3.5 Passaging of hUCT-MSCs

hUCT-MSCs were passaged when confluency reached 80 to 90%. The cells were washed with sterile PBS and treated with 500 µl of 0.05% trypsin/EDTA per T25 flask for up to 5 minutes. Trypsinised cells were

then diluted in the indicated medium and centrifuged for 5 minutes at 200g, the pellet was resuspended in the indicated medium and transferred to a new cell culture flask at a ratio of 1:4 to 1:8 to seed the next cultures. Medium was renewed every 2 to 3 days as needed.

After the media optimisation, the subsequent hUCT-MSCs were passaged in medium number three described in Chapter 2.3.4 hUCT-MSCs culture, p. 48.

2.3.6 Proliferative potential

During the passaging of hUCT-MSCs, cells were counted using a hemocytometer and population doubling (PD) was obtained for each passage according to the formula: PD= log2 (Nf/Ni), where Ni is the initial cell number and Nf is the harvested cell number. The population double time (DT) was obtained according to the formula: DT= T/PD where T is the time for each passage (https://www.doubling-time.com/compute.php).

2.3.7 hUCT-MSC adipogenic differentiation

To continue with the medium optimization, adipogenic differentiation was set up with cells grew in each medium. Two different adipogenic cocktails were tested. Medium A contained their corresponding growth medium supplemented with: 10 µg/mL insulin, 1 µM rosiglitazone, 500 µM IBMX and 1 µM dexamethasone[114], and medium B which had two steps: the induction medium, in which cells were fed for the first three days with their growth medium supplemented with: 10 µg/mL insulin, 1 µM rosiglitazone, 500 µM IBMX and 1 µM dexamethasone, followed by a four days feeding step of maintenance

medium with growth medium supplemented with: 10 μg/mL insulin. Cells were differentiated for 28 days, and medium was changed every 2 or 3 days[173].

After the media optimisation was done the subsequent hUCT-MSCs were differentiated in medium number one described in Chapter 2.3.4 hUCT-MSCs culture, p. 48, supplemented with: 10 μg/mL insulin, 1 μM rosiglitazone, 500 μM IBMX and 1 μM dexamethasone[114].

2.3.8 hUCT-MSCs osteogenic differentiation

For the osteogenic differentiation cells were seeded in 24 well plates and started until 50% confluency was reached. Osteogenic medium was supplemented with DMEM F12 + 10% FBS + 1% P/S[171], 10 mM β-glycerophosphate, 50 μM ascorbic acid, 100 nM dexamethasone[111,174]. Cells were differentiated for 28 days, and medium was changed every 2 or 3 days.

2.3.9 Cryopreservation of hUCT-MSCs

The procedure was similar to the cryopreservation procedure described for the mMSCs (Chapter 2.2.5 Cryopreservation of mMSCs, p. 44); however, FBS was replaced for hPL, instead.

2.4 Live assays and staining

2.4.1 Metabolic activity

Presto Blue was used to measure either cell viability or metabolic activity at the last day of each treatment. Human or mouse MSCs were seeded in 24-well plates, and differentiated in parallel at 32°C and 37°C. At the end of experiment, medium was replaced with 500 µL of a working solution of 10% v/v Presto Blue stock solution, then cells were transferred back to the incubator at 32°C or 37°C. After 45 min incubation triplicates of 100 µL were taken from every well and transferred to a 96-well plate. The fluorescent signal was measured with a multimode microplate reader (Tecan Infinite 200 PRO) using an excitation wavelength of 560 nm and an emission wavelength of 590 nm. The measured fluorescent signal was expressed as arbitrary fluorescent units (AU). For every measurement, the background signal of the solution was determined and subtracted as described before[175]. A standard curve was done, metabolic activity was measured every 10 min for 90 min to select the best incubation time (Appendix, p. 225).

2.4.2 Seahorse Assay.

mMSCs were seeded into the XFe96 Microplates to measure the OCR, an indicator of mitochondrial respiration, and the ECAR, an indicator of glycolysis. Prior to the start of the Seahorse XF Cell Mito Stress Test Assay, cells differentiated at either 37 or 32°C were washed 3 times and incubated in XF-Basal Medium supplemented with 10 mM glucose, 1mM sodium pyruvate, and 2mM L-glutamine. OCR and ECAR readings were taken over time under basal conditions and after the

addition of mitochondrial inhibitors (1.5 or 2.5 μM oligomycin, 0.8 or 0.5μM FCCP and 1μM rotenone/antimycin for treatments described in Chapter 3 or 4, respectively) at 37°C and 32°C. OCR and ECAR were determined using the Seahorse Wave 2.4 XF-96 software and the data obtained for each condition were normalized to the cell number per well and expressed as the OCR in pmol/min/10^4 cells. Measures of mitochondrial respiration (basal respiration, ATP-linked respiration, proton leak, maximal and reserve capacity) were derived by the sequential addition of oligomycin, FCCP and rotenone/antimycin. First, the basal respiration rate was calculated by subtracting the residual OCR determined after the addition of rotenone. ATP-linked respiration was determined from the difference between basal OCR and OCR following oligomycin addition. The difference in OCR between rotenone and oligomycin represented the amount of oxygen consumed due to proton leak respiration. Maximal OCR was determined by subtracting the OCR after rotenone addition from the OCR induced by FCCP. Lastly, the mitochondrial reserve capacity was calculated by subtracting basal respiration from maximal reserve capacity.

ECAR was measured simultaneously with OCR using the same conditions as described previously[176] and glycolytic rate was determined by monitoring extracellular pH induced by the change in lactate. Similar to OCR, basal ECAR refers to the ECAR measured before injection of rotenone. To determine the influence of low temperature on oxidative phosphorylation and glycolysis, basal OCR was plotted against basal ECAR. Finally, coupling efficiency, an indicator of the proportion of respiratory activity used to make ATP,

was determined by calculating the percentage of OCR immediately following the oligomycin treatment with the final baseline value.

2.4.3 Mitochondrial staining and quantification

Mouse or human MSCs were cultured as indicated in coverslips, MitoTracker Orange CM-H_2 TMRos or MitoTracker Deep Red (100 nM, Molecular Probes) together with Hoechst 33258 (20 μg/mL, Invitrogen) and Bodipy 493/503 (10μM, Molecular Probes) staining was performed according to the manufacturer's protocol and applied to cells in culture at 37°C and 32°C for 45 minutes. After two medium wash, coverslips were fixed for 15 min with ice-cold 4% paraformaldehyde (PFA), mounted on microscopic slides with FluoroGel mounting medium (GeneTex, USA) and assessed with a Zeiss fluorescence microscope. Mitochondria numbers were evaluated using 15 randomly selected images per condition of three biological replicates. Relative fluorescence intensity was measured applying identical instrument settings. Moreover, relative fluorescence intensity was measured with ImageJ software creating a macro, shortly maximum entropy threshold was applied in all pictures followed by a gaussian blur and an un-sharp mask, same conditions were applied to all pictures. An example of the analysis is shown in Figure 2.2.

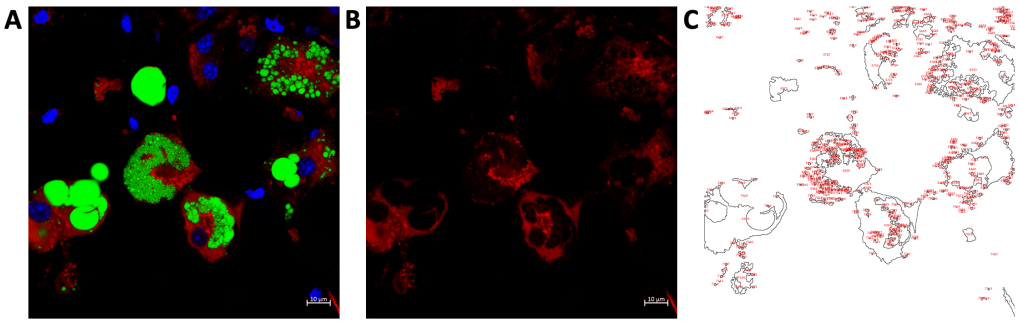


Figure 2.2.Example of the densitometric analysis of MitoTracker positive area. (A) shows fluorescent image taken of mMSCs at day 14 of differentiation at 32°C, MitoTracker Orange CM-H_2 TMRos (red), Hoechst 33258 (nuclei – blue) and Bodipy 493/503 (LDs – green), (B) red channel (MitoTracker), (C) image showing analysis done in ImageJ. Scale bar 10 μm.

2.4.4 Calcium staining and quantification

Live cells were stained for 60 min with Fluo-4 Direct™ (Invitrogen) according to manufacturer's instructions. Shortly, a final volume of 1X Fluo-4 Direct™ calcium reagent was added to the well of each treatment and then plates were incubated at 37°C or 32°C. Fluorescent measurements were done in triplicates using an excitation wavelength of 494 nm and an emission wavelength of 516 nm in a multimode microplate reader (Tecan Infinite 200 PRO, Tecan, Switzerland). After the calcium response was measured, fluorescent and brightfield images were taken using identical settings with a Nikon eclipse TS2 microscope coupled to a Nikon D3300 camera.

2.5 Fixation of cells for subsequent staining

At the end of each treatment, medium was removed of each well, cells were washed once with 500 μl PBS, fixed with 500 μl of 4% ice-cold paraformaldehyde (PFA) per well (24 WP), incubated for 15 min at RT

and subsequently washed twice with PBS. Cells were stored at 4°C in PBS until staining.

2.5.1 Oil Red O (ORO) imaging and quantification

For ORO staining, cells fixed with 4% PFA were subsequently stained with 60% working solution of ORO for 10 min, cells were rinsed twice with water, washed for 1 min with 60% isopropanol and if indicated subsequently stained with haematoxylin. The staining was quantified by extracting ORO staining with 100% isopropanol and measuring absorbance in triplicates at 510 nm with a multimode microplate reader (Tecan Infinite 200 PRO). For every measurement, the background signal of the blank (isopropanol) was determined and subtracted. The measured absorbance signal was expressed as arbitrary absorbance units (AU).

2.5.2 Hoechst staining and quantification

Fixed cells were stained using 500 µL of a working solution of 20 µg/mL Hoechst in 50mM Hepes buffer, pH 7.0 and incubated for 30 min at room temperature. Hoechst working solution was removed and washed twice with Hepes buffer, pH 7.0 for 2 min to remove any non-bound dye. To extract Hoechst 500 µL of denatured ethanol was added to each well and incubated for 5 min at room temperature, shaking the plate every minute. Then, triplicates of 100 µL were taken from every well and transferred to a 96-well plate. The fluorescent signal was measured with a multimode microplate reader (Tecan Infinite 200 PRO) using an excitation wavelength of 360 nm and an emission wavelength of 460 nm. The measured fluorescent signal was expressed as arbitrary

fluorescent units (AU). For every measurement, the background signal of the blank (ethanol) was determined and subtracted[177].

2.5.3 Immunocytochemistry

Cells seeded on coverslips were differentiated as indicated and fixed with 4% PFA, washed twice with PBS and if necessary permeabilised for 30 min using 0.1% Triton X-100 (Sigma) in PBS, followed by three 5 min PBS washes. Coverslips were blocked using 10% normal goat serum or fetal bovine serum in PBS (depending on secondary antibody host) for 60 min at room temperature. Samples were then incubated in the appropriate primary antibody for 90 min and washed three times in PBT (PBS + 0.1% Tween20 – Sigma) before the incubation with the appropriate fluorophore-conjugated secondary antibodies) together with Hoechst 33258 (20 μg/mL, Invitrogen) and Bodipy 493/503 (10μM, Molecular Probes) for 60 min at room temperature in the dark. After three to five washes in PBT, samples were then dried and mounted with FluoroGel mounting medium (GeneTex, USA) and examined with Zeiss Elyra PS.1 microscope. If biotinylated secondary antibodies (VectorLabs) were used, signal was visualized with 3,3′-diaminobenzidine (DAB) as the chromo- gen (VectorLabs), samples were mounted on slides using DPX and examined with a Nikon microscope.

All antibodies used in this study are presented in Table 2.2.

Table 2.2 List of antibodies used for immunocytochemistry.

Primary antibody	**Host**	**Source**	**Dilution**
Anti-UCP1	Rabbit	Abcam (ab10983)	1:500
Anti-UCP1	Goat	Novus Biologicals (NB100-2828ss)	1:100
Anti-Ob	Rabbit	Santa Cruz (sc-843)	1:100
Anti-CD137	Rabbit	Abcam (ab203391)	1:100
Anti-TMEM26	Rabbit	Novus Biologicals (NBP2-27334ss)	1:100
Anti-TRPV1	Rabbit	ThermoFisher Scientific (PA1-29421)	1:100
CD73	Rabbit	Abcam (ab175396)	1:100
CD90	Rabbit	Abcam (ab133350)	1:100
CD105	Mouse	Abcam (ab11414)	1:100
Secondary antibody	**Host**	**Source**	**Dilution**
Anti-rabbit IgG Alexa 488	Goat	ThermoFisher Scientific (A11008)	1:1000
Anti-mouse IgG Alexa 488	Goat	ThermoFisher Scientific (A11001)	1:500
Anti-goat IgG Alexa 488	Donkey	Abcam (ab150129)	1:1000
Anti-rabbit IgG Alexa 594	Goat	ThermoFisher Scientific (R37117)	1:500
Anti-rabbit IgG Alexa 633	Goat	ThermoFisher Scientific (A21070)	1:500
Anti-goat IgG Alexa 647	Goat	ThermoFisher Scientific (A21244)	1:500
Anti-goat IgG Alexa 647	Donkey	ThermoFisher Scientific (A21447)	1:500
HRP Anti-Rabbit IgG	Goat	Vector Laboratories (PI-100)	1:300

2.6 Molecular Biology

2.6.1 Harvesting mouse tissue for RNA extraction

Mouse tissue was collected from different depots, iBAT, eWAT, sWAT, muscle and liver. Tissue was carefully isolated and washed twice with sterile PBS, minced and collected into an Eppendorf tube with 500 µl of TRI® Reagent, approximately 50 mg of tissue were collected per depot. Figure 2.3 shows isolated tissue depots.

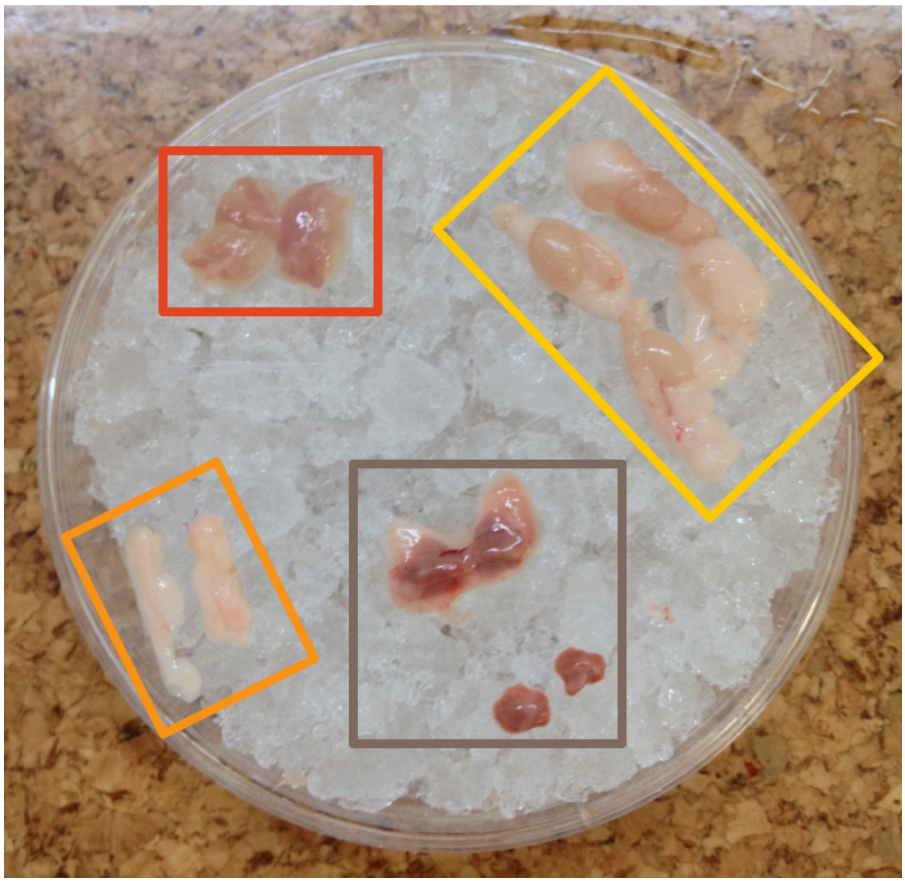


Figure 2.3. mouse tissue: eWAT (yellow), iWAT (orange), iBAT (brown) and muscle (red).

2.6.2 Harvesting cells for RNA extraction

At the end of each treatment, medium was aspirated and washed once with PBS. Cells were then harvested by adding 500 µl of TRI ® Reagent per T25 flask using a cell scraper, cells were collected in an Eppendorf tube and frozen immediately in dry ice. Cells were kept at -80°C until RNA extraction was done.

2.6.3 RNA extraction

Cells and tissue kept at -80°C in TRI ® Reagent were then thawed at room temperature. Then, 70 µl and 120 µl of chloroform for cells and tissue was added, respectively, per 500 µl of TRI® Reagent. Samples were vortexed for 2 minutes and incubated at room temperature for 10 minutes, then samples were centrifuged at 12000g for 15 minutes at 4°C. The supernatant part (top transparent layer) was retrieved into a new tube, a 1:1 volume of 70% etOH was added to the supernatant retrieved and mixed properly. Next, the mixture was transferred to a pink tube and centrifuged at 10000g for 1 minutes at 4°C. The flow throw was discarded. RNA extraction was then continued following instructions starting from #6 on the RNeasy® micro Handbook p. 21-22.

2.6.3.1 RNA quantification

The RNA was quantified by spectrophotometry based on the OD260 nm using the nanodrop ND-1000 spectrophotometer (Nanodrop Technologies). A260/280 ratio around 2 and 2.0-2.2 ratio for A260/230 were accepted.

2.6.4 Reverse (RT) - Polymerase Chain Reaction (PCR)

According to the total RNA quantified from mouse MSCs, WAT, BAT and liver tissue samples. RNA was normalized to 0.5 or 1 µg/µl. For RT-PCR the High-Capacity RNA-to-cDNA™ Kit (Applied Biosystems) was used following manufacturer's instructions. Detail methods can be found in the ThermoFisher Scientific web.

The reactions were set up in a thermal cycler (Touchgene gradient, Scientific Laboratories Supplies). With the following steps: an initial step of 1 hour at 37°C and a final step of 5 minutes at 95°C followed by 8°C on hold. For each set of experiments, two NRTC (non-reverse transcriptase control) and two NTC (non-template control) were used.

2.6.5 Primer optimisation and validation

2.6.5.1 Primer design

Specific primers were designed using Primer3 (https://primer3.org). for each gene its cDNA sequence showing only exons was obtained from Ensembl (https://www.ensembl.org/index.html). The product size of each primer set was set in between 90-200 base pairs. Primer-BLAST (https://www.ncbi.nlm.nih.gov/tools/primer-blast/) was used to verify the specificity of the primer pair. The general primer picking conditions of each primer set are shown in table 2.3. All designed primers were purchased from Eurofins MWG Operon (Ebersberg, Germany).

Table 2.3. Primer design conditions.

	Minimum	**Optimal**	**Maximum**
Size	18	20	24
Tm	57	60	62
GC%	45	50	60

2.6.5.2 Primer validation

All primer sets were diluted with DNase free water according to the information sheet provided by Eurofins to 100 pmol/µl. The optimisation process was followed by testing the primers with their respective tissue for specificity expression.

2.6.5.2.1 PCR

PCR was performed in a reaction volume of 20 µl with 40 cycles of amplification. The reactions were set up in a thermal cycler (Touchgene gradient, Scientific Laboratories Supplies). With the following steps: an initial denaturation step for 30 seconds at 94°C; a cycle consisted of a denaturation step for 30 seconds at 94°C, followed by 30 seconds at an annealing temperature of 60°C and an extension step at 68°C for 60 seconds; and a final step of 5 minutes at 68°C followed by 8°C on hold. All primers were diluted at a ratio of 1:40 to start, according to primer dimers or band strength primers were then diluted 1:80 and PCR recipe was adjusted (Table 2.4, positive/negative 1 or 2). PCR was performed with each set of primers, according to their specificity cDNA from mouse WAT, BAT or liver was used. Two positive (cDNA) and one negative (SDW instead of cDNA) reactions per gene were performed. The amplified products were analysed by agarose gel electrophoresis (Chapter 2.6.5.2.2).

Table 2.4. PCR recipes.

	Positive		**Negative**	
	1	**2**	**1**	**2**
DNase free water	-	5 µl	2 µl	8 µl
Sample (RNA)	2 µl	3 µl	-	-
One Taq master mix	10 µl	10 µl	10 µl	10 µl
Primer up	4 µl	1 µl	4 µl	1 µl
Primer down	4 µl	1 µl	4 µl	1 µl

2.6.5.2.2 Electrophoresis

Agarose was mixed with 1X TAE buffer (Tris-Acetate-EDTA) to give 2% of gel required. The suspension was heated in a microwave oven to dissolve the agarose. Ethidium-bromide was added at a concentration 4 ng/ml. after pouring the melted agarose into a gel-casting tray with comb, the gel was allowed to settle for 20 minutes. 20 µl of the PCR samples were loaded onto the gel. Gels were run from 90-120 V for about 35 minutes with a BioRad Power Pac 300. The PCR products on the gel were visualised using the Luminescent Image analyser Fuji LAS-3000 (FIjufilm) and band sizes were estimated using the Quick-load DNA ladder- 100bp (BioLabs, New England).

2.6.5.2.3 Gel extraction (DNA)

After performing the PCR, the DNA fragments of interest were cut out from an agarose gel and extracted using the Qiagen gel extraction kit following the manufacturer's instructions (Quick-Start Protocol can be found in the Qiagen page).

2.6.5.2.4 DNA quantification

DNA purity and concentration were quantified by spectrophotometry based on the OD260 nm using the nanodrop ND-1000 spectrophotometer (Nanodrop Technologies). A260/280 ratio around 1.8-2 and 2.0-2.2 ratio for A260/230 were accepted.

2.6.5.2.5 Standard curves of each gene done by quantitative Real-Time PCR (qPCR)

To test efficiency of each set of primer a standard curve was prepared using the DNA extracted per gene starting from 1ng/µl DNA to 0.01 fl/µl using 0.1 mg/ml of tRNA water. Standards were run in duplicates to calculate the coefficient of variation within each experiment.

A master mix was done for each gene: 5 µl of Fast SYBR™ green master mix, 1 µl forward primer, 1 µl reverse primer and 1 µl DNase free water; a total of 8 µl per well. 2 µl of each standard concentration were added at the end in each well. For each PCR plate (MicroAmp® Fast 96-well reaction plate, 0.1 ml, Applied Biosystems) duplicates of two NRTC, two NTC, and one negative (water instead of cDNA) were done. Once prepared, PCR plates were sealed using optical adhesive covers (Applied Biosystems) and centrifuged for 2 minutes in a mini plate spinner (Labnet).

The reactions were set up in a thermal cycler Step One Plus (Real-Time PCR system and v.2.2 software, Applied Biosystems) selecting fast mode and SYBR™ green reagents with the following steps: an initial activation step for 20 seconds at 95°C; a cycle consisted of a denaturation step for 3 seconds at 95°C, followed by 30 seconds at an annealing/extension temperature of 60°C; the melt curve was done from 65-95°C, increasing 0.5°C every 5 seconds.

Newly designed primers used in this study are listed in Table 2.5.

Table 2.5. List of primers used for gene expression analysis.

Target gene	**Primers sequence**	**Dil.**	**Eff%.**	**R^2**
Adiponectin				
Forward	AACTTGTGCAGGTTGGATGGC	1:40	101.07	1
Reverse	TTCTCTCCCTTCTCTCCAGGA			
CD137				
Forward	CGTGCAGAACTCCTGTGATAAC	1:80	105.99	0.99
Reverse	GTCCACCTATGCTGGAGAAGG			
CIDEA				
Forward	TGACATTCATGGGATTGCAGAC	1:80	84.58	0.99
Reverse	GGCCAGTTGTGATGACTAAGAC			
CITED1				
Forward	AACCTTGGAGTGAAGGATCGC	1:80	99.42	1
Reverse	GTAGGAGAGCCTATTGGAGATGT			
FABP4				
Forward	TGGAAGCTTGTCTCCAGTGA	1:40	99.40	0.99
Reverse	AATCCCCATTTACGCTGATG			
LHX8				
Forward	AAGAGGCAGCTGTCCACG	1:80	99.57	1
Reverse	GAAGCTGGTCCGAGCTCTTT			
PPARγ				
Forward	GCCGAGTCTGTGGGGATAAA	1:80	98.69	0.99
Reverse	GTGAGACATCCCCACAGCAA			
RIP140				
Forward	TCCCCGACACGAAAAAGAAAG	1:40	97.01	1
Reverse	ACATCCATTCAAAAGCCCAGG			
Reference genes				
RPLP0				
Forward	CTGGAGAAACTGCTGCCTCA	1:80	97.42	1
Reverse	AGTGTTCTGAGCTGGCACA			
TBP				
Forward	CCTTGTACCCTTCACCAATGAC	1:40	146.28	0.96
Reverse	ACAGCCAAGATTCACGGTAGA			
B2M				
Forward	CCCTGGTCTTTCTGG	1:80	103.86	0.99
Reverse	TGTTCGGCTTCCCAT			

2.6.6 qPCR

2.6.6.1 mMSCs qPCR

qPCR was performed using either Fast SYBR™ Green Taq polymerase master mix or TaqMan universal master mix with murine-specific oligonucleotide primers (Eurofins) or FAM-MGB TaqMan probes.

2.6.6.1.1 Fast SYBR green protocol

When possible, standard curves were run at the same time than samples from the different set of experiments. Same master mix and qPCR protocol was followed as described in Chapter 2.6.5.2.5 (p. 70)

2.6.6.1.2 TaqMan protocol

According to the limit detection of the designed primers (>35 cycles), TaqMan probes were chosen for the following genes*: UCP1, PRDM16, ATP2a2, COX8b, P2RX5, DIO2, TRPV1, TRPV2* and *TRPV4* (Thermoscientific TaqMan Gene Expression assays; assay: Mm00494069_m1, Mm00712556_m1, Mm01201431_m1; and BioRad TaqMan Gene Expression assays; assay, qMmuCIP0034367, qRnoCIP0024301, qMmuCEP0052679, qMmuCIP0031313, qMmuCIP0035343 and qMmuCIP0032629, respectively).

A master mix was done for each gene: 5 µl of iTaq™ Universal Probes Supermix, 0.5 µl Taqprobe, 2.5 µl water; a total of 8 µl per well. 2 µl of sample were added at the end in each well. For each plate run (MicroAmp® Fast 96-well reaction plate, 0.1 ml, Applied Biosystems) duplicates of two NRTC, two NTC, and one negative (water instead of cDNA) were done. Once prepared, PCR plates were sealed using optical adhesive covers (Applied Biosystems) and centrifuged for 2 minutes in a mini plate spinner (Labnet).

The reactions were set up in a thermal cycler Step One Plus (Real-Time PCR system and v.2.2 software, Applied Biosystems) selecting fast mode and TaqMan reagents with the following steps: an initial activation step for 2 minutes at 95°C; a cycle consisted of a denaturation step for 5 seconds at 95°C, followed by 30 seconds at an annealing/extension temperature of 60°C; the melt curve was done from 65-95°C, increasing 0.5°C every 5 seconds.

2.6.6.2 hUCT-MSC qPCR

For human MSCs total RNA from MSCs samples was extracted and normalized to 1 µg/µl and reverse transcribed to cDNA as previously described (Chapter 2.6.4 RT-PCR, p. 66). TaqMan probes were chosen for the following genes: *Actβ*, Adiponectin, *PPARγ, β3-AR; Glut4, FGF21, InsR, Lep, PGC1α, PRDM16, DIO2, CIDEA, RetN* (BioRad TaqMan Gene Expression assays; assay, qHsaCEP0036280, qHsaCEP0054708, qHsaCEP0051687, qHsaCEP0055256, qHsaCEP0054748, qHsaCIP0032896, qHsaCIP0031043, qHsaCIP0031310, qHsaCIP0026151, qHsaCEP0052327, qHsaCEP0055819, qHsaCEP0024748, qHsaCEP0050303, respectively) and *UCP1* (Thermoscientific TaqMan Gene Expression assay: Hs00222453_m1).

qPCR reactions and program were similar to the one described above (Chapter 2.6.6.1.2 TaqMan protocol, p. 73).

2.6.7 geNorm

To analyse gene expression the best reference genes in each set of experiments were selected by geNorm using Microsoft Excel. First, geometric mean is calculated and pairwise variation of each gene was

compared to all other genes analysed, a stability value (M) was then calculated and the two most stable genes were selected (lower M value). Raw Ct values of the gene of interest were converted to relative quantities (Rel Q) using the following formula:

$$Rel\ Q = 2^{(min\ value - Ct\ value)}$$

where 2 means 100% efficiency of the gene of interest.

The relative gene expression of the gene of interest was normalised using Rel Q against the geometric mean of the selected reference genes. The formula described above takes different PCR efficiencies into account by substituting 2 accordingly.

2.6.7.1 mMSCs geNorm

Gene expression was determined using geNorm normalization algorithm against two selected reference genes out of three: *TBP* (TATA sequence binding protein), *B2M* (Beta-2-Microglobulin) or acidic ribosomal protein subunit P0 (*RPLP0*), (*TBP* and *RPLP0* stability value M=0.47 and *B2M* and *RPLP0* stability value M=0.36 for Chapter 3 and 4, respectively).

2.6.7.2 hUCT-MSCs geNorm

Gene expression was determined using geNorm normalization algorithm against two selected reference genes (stability value M=0.25) elongation factor 2 (*EEF2*) (qHsaCIP0028057) and acidic ribosomal protein subunit P0 (*RPLP0*) (qHsaCEP0041375).

2.7 Imaging and image analysis

2.7.1 Brightfield and fluorescent images

Brightfield images were taken using a Nikon eclipse TS100. As indicated fluorescent images were taken using Nikon eclipse 90i fluorescent microscope, a micropublisher 5.0 RTV digital camera and Volocity software version 5.2.0, Improvision Ltd. All images were taken using same settings and conditions.

2.7.2 Super-resolution imaging in structured illumination mode

For super-resolution imaging, cells mounted with CitiFluor (CF3) medium (Agarscientific, UK) were imaged using a Zeiss Elyra PS.1 microscope, in structured illumination mode (SIM), with the following settings: objective Plan- Apochromat 63 x /1.4 Oil DIC M27, filter set LBF −405/633, cmos camera exposure time 20 ms. Three imaging tracks were set up in fast frame mode, which alternates the excitation lasers (solid state 405, 488 nm and 633 nm, at 1, 1.2 and 4.5% laser power settings, respectively). In the fast frame mode, images from the three channels were acquired almost simultaneously with an exposure time difference of 20 ms between the blue, red and green channel. Image processing and channel alignment was done using the manufacturer's software (https://www.zeiss.com/microscopy/int/products/microscope-software/zenlite.html).

2.7.3 Morphometric and stereological analysis

The percentage of differentiated cells was estimated by dividing the total number of differentiated cells by the total number of all cells, using randomly selected micrographs per condition (three biological replicates) at a final magnification of 400. The same images taken for Mitochondrial staining, using only the green channel (Bodipy 493/503 staining), were used to evaluate Maximum Feret's Diameter (MFD), the longest distance between any two points of the object. Ferret's diameter is generally used in optical microscopy to measure the size of irregularly shaped particles[178]. In order to analyse lipid droplets (LDs) distribution, LDs in fifteen micrographs per group were measured. For all calculations and measurements, ImageJ software was used. Images displaying only LDs were transformed to 8-bit, then colour threshold was adjusted to black and white, next watershed was applied to separate LDs reaching each other, finally LDs were then measured. An example of the analysis is shown in Figure 2.4.

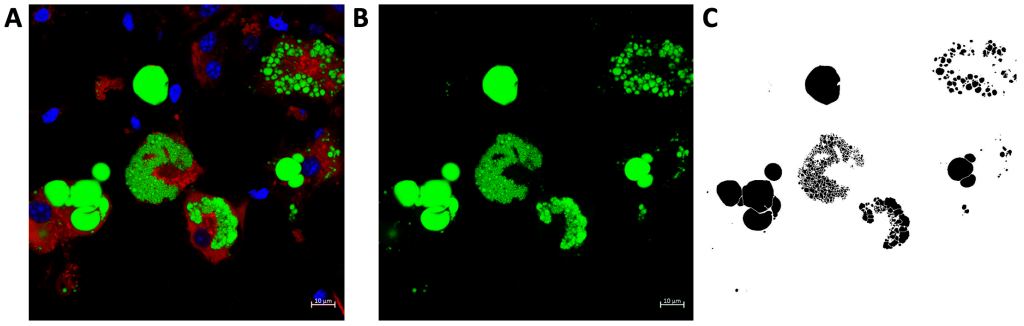


Figure 2.4. Example of the morphometric and stereological analysis.
(A) shows fluorescent image taken of mMSCs at day 14 of differentiation at 32°C, MitoTracker Orange CM-H_2 TMRos (red), Hoechst 33258 (nuclei – blue) and Bodipy 493/503 (LDs – green), (B) green channel (Bodipy 493/503 staining), (C) image show analysis performed in ImageJ. Scale bar 10 μm.

2.7.4 Densitometric analysis of UCP1 positive area

Twelve to fifteen fields per condition (three biological replicates) were randomly selected at either x400 or x630 magnification and the UCP1 positive areas were calculated using the processing software ImageJ. The images were converted to HSB stack with saturation settings for MinThreshold and MaxThreshold to segment UCP1 positive areas. The percentage of area within the threshold range was measured. When indicated a macro used in ImageJ software was created, maximum entropy threshold was applied in all pictures followed by a gaussian blur and an un-sharp mask, same processing conditions were applied to all pictures. An example of the analysis is shown in Figure 2.5.

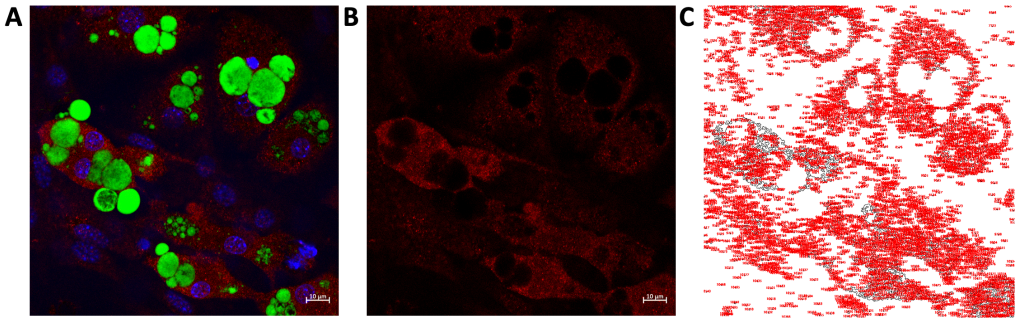


Figure 2.5. Example of the densitometric analysis of UCP1 positive area.
(A) shows fluorescent image taken of mMSCs at day 14 of differentiation at 37°C, UCP1 (red), Hoechst 33258 (nuclei – blue) and Bodipy 493/503 (LDs – green), (B) red channel (goat anti rabbit - Alexa Fluor 633), (C) image show analysis performed in ImageJ. Scale bar 10 μm.

2.8 Statistical analysis

All data were evaluated and interpreted graphically using Graph Pad Prism 7 Software (https://www.graphpad.com). For data that was normally distributed t-test was used. To evaluate the statistical significance in two groups comparison, in gene expression analysis data, the nonparametric Mann Whitney test was used. For three or more groups evaluation, the nonparametric Kruskal-Wallis test with multiple comparison was done with uncorrected Dunn's test to evaluate the statistical significance between groups. Statistical significance was accepted at $p<0.05$, with *$p<0.05$; **$p<0.01$; ***$p<0.001$. Errors bars plotted on graphs are presented as the mean ± SEM. n= 3 or 4 individual experiments. For principal component analysis, ClusVis (https://biit.cs.ut.ee/clustvis/) was used.

.

Chapter 3. Low temperature exposure induces browning of bone marrow stem cell derived adipocytes *in vitro*

3.1 Main Findings

- mMSC derived adipocytes show both leptin and UCP1protein expression at normal culture conditions.
- mMSC derived adipocytes display leptin nuclei translocation when exposed to cold temperature.
- mMSC generate adipocytes that have a specific phenotype with a prevalence of beige/brown molecular characteristics.
- cold differentiated adipocytes show an increased bioenergetics response.

3.2 Introduction

Traditionally, two types of adipose tissue are recognized in mammals: white adipose tissue (WAT) and brown adipose tissue (BAT)[145]. Both types are specialized to store energy in the form of lipids, whilst BAT has capacity to dissipate energy in the form of heat, thereby contributing to thermogenesis in mammals[179,180]. Heat production in BAT is mediated by a unique uncoupling protein 1 (*UCP)1* which stimulates proton conductance across the mitochondrial membrane to uncouple respiration from adenosine triphosphate (ATP) synthesis[145]. A third type of adipocytes has been recently discovered. Beige adipocytes resemble brown adipocytes due to multilocular lipids droplets, high mitochondrial density and *UCP1* expression[158] and can be activated through cold exposure or β-adrenergic stimulation[181].

The most potent physiological stimulus to activate *UCP1* is cold exposure, which has been shown to promote the appearance of *UCP1* both *in vivo* and *in vitro*[144,149]. It is unclear, however, whether this thermal response could have a comparable impact on the regulation of stem cell differentiation into adipocytes. The importance of thermal stimulation in determining the composition of fat is emphasized from the fact that brown-like adipocytes can also appear at anatomical sites corresponding to WAT[99,143] to form recruitable 'beige' adipocytes[80,182]. Unlike classic BAT, beige cells express much lower amounts of *UCP1*[65], but after cold stimulation or treatment with β-adrenergic receptor agonists, they resemble classic BAT and *UCP1* is upregulated[65,183]. Moreover, when fully stimulated, beige adipocytes undergo *UCP1*-mediated respiration[65], but their molecular and developmental characteristics are different from brown adipocytes. For example, in

addition to *UCP1*, beige cells express a subset of specific markers such as *CD137*, *TMEM26*, *CITED1* and *P2RX5*, which is also recognised as an adipogenic regulator[58–60,65,66,184,185].

Critically, all adipocytes are mesenchymal in origin[4]. Mesenchymal stem cells (MSCs) are present in a wide range of tissues, and used as a cellular model to study differentiation towards a variety of lineages[186].

Bone Marrow (BM) derived MSCs are characterised by their potential to differentiate into several cell types, including osteoblasts, chondroblasts, adipocytes and myocytes[6]. Recently, more complex roles have been attributed to BM adipocytes, not only as a passive fat depot, but also as cells actively participating in BM lipid metabolism and osteogenesis, with features described as a mix of both WAT and BAT characteristics. However, detailed characterization of BM-derived mMSCs and the mechanism enabling them to develop into brown, beige or white adipocytes have not previously been examined. MSCs have recently been proposed to provide a source of thermogenic cells that could ultimately be used to treat obesity and/or diabetes. An important step towards this goal is to establish the optimal conditions for inducing brown and/or white-to-brown adipogenesis from MSCs and to test our hypothesis regarding the effects of different temperature conditions on adipogenic differentiation *in vitro*. It is known that BM adipocytes secrete and express high levels of adiponectin and leptin, raised leptin is one marker of adipocyte differentiation. Accordingly, the potential of BM-derived mouse MSCs to undergo browning and the extent to which this can be modulated by the temperature at which the cells are incubated during differentiation was evaluated, together with its potential impact on brown/beige markers and leptin expression.

The present chapter investigates the principal molecular and cellular processes driving the commitment of mouse MSCs into the brown adipocyte lineage. Low temperature was observed to stimulate browning in mMSCs adipogenic cultures, increase adipocyte number and, upregulate adipogenic and thermogenic factors. Cold-exposed differentiated cells showed a clear cytoplasmic remodelling, illustrated by both an increase in mitochondria content and a build-up in small multilocular lipid droplets (LDs). Finally, brown-adipogenic characteristics were confirmed by the detection of the beige and brown cell-specific molecular markers *TMEM26*, *CD137* and *P2RX5*, as well as *FABP4*, *UCP1*, *LHX8*, *COX8b* and *RIP140*. These results show that mMSCs generate adipocytes that have a specific phenotype with a prevalence of beige/brown characteristics and display temperature-responsiveness, with upregulation of beige and brown markers, increased bioenergetics response, accompanied by morphological changes in line with BAT features, indicating that MSCs provide a source of thermogenic adipocytes which can be used to model BAT-based approaches to treat metabolic diseases.

The work for this chapter was performed in collaboration with Ksenija Velickovic (K.V.) PhD. K.V. and H.A.L.L., carried out all cellular experiments, optimisation of ORO, mitochondria and calcium staining. K.V. preformed all immunostainings and seahorse analysis. H.A.L.L. carried out the design and optimisation of the primers used for the study and molecular analysis. Interpretation of results, final review and discussion of the study was done by all authors cited here: DOI:10.1038/s41598-018-23267-9.

K.V. and H.A.L.L. performed all cell culture, metabolic activity, ORO and lipid quantification. K.V. performed all immunofluorescence, MitoTracker staining, confocal microscopy, image analysis and seahorse measurements and analysis. H.A.L.L optimised Mitotracker, Bodipy and Hoechst staining, designed and validate all primers, performed RNA extraction, RT-PCR, qPCR, molecular analysis, calcium images and transferred cells.

3.3 Methods

mMSCs D1 (BM-derived mouse MSCs) were differentiated as described in Chapter 2.2.4 mMSC adipogenic differentiation, p. 40. Adipocytes were differentiated for 11 days at 37°C and 32°C culture conditions. At the end of the treatment metabolic activity, morphologic, lipid content, molecular signature; *UCP1, TMEM26, CD137*, leptin and TRPVs protein expression as well as bioenergetic capacity was analysed as described in Chapter 2.4.1, p. 50; 2.4.3, p. 52; 2.5.1, p. 54; 2.5.3, p. 55. BM-derived mouse MSCs will be referred as mMSCs.

3.4 Results

3.4.1 Mouse Mesenchymal stem cells (mMSCs) achieve an adipogenic phenotype and express both UCP1 and leptin.

In order to examine the time course of mMSC differentiation, cells were treated with adipogenic medium at 37°C. By day 9, cells were clearly distinguishable from untreated cells maintained in standard medium, as confirmed by oil red O (ORO) staining (Fig. 3.1A). To further characterize the adipogenic response, *UCP1* and leptin immunostaining was performed. Both markers were observed to be expressed in the majority of differentiated cells (Fig. 3.1B). *UCP1* was found only after adipogenic treatment, while leptin was observed in both control and adipogenic conditions (Fig. 3.3A and C).

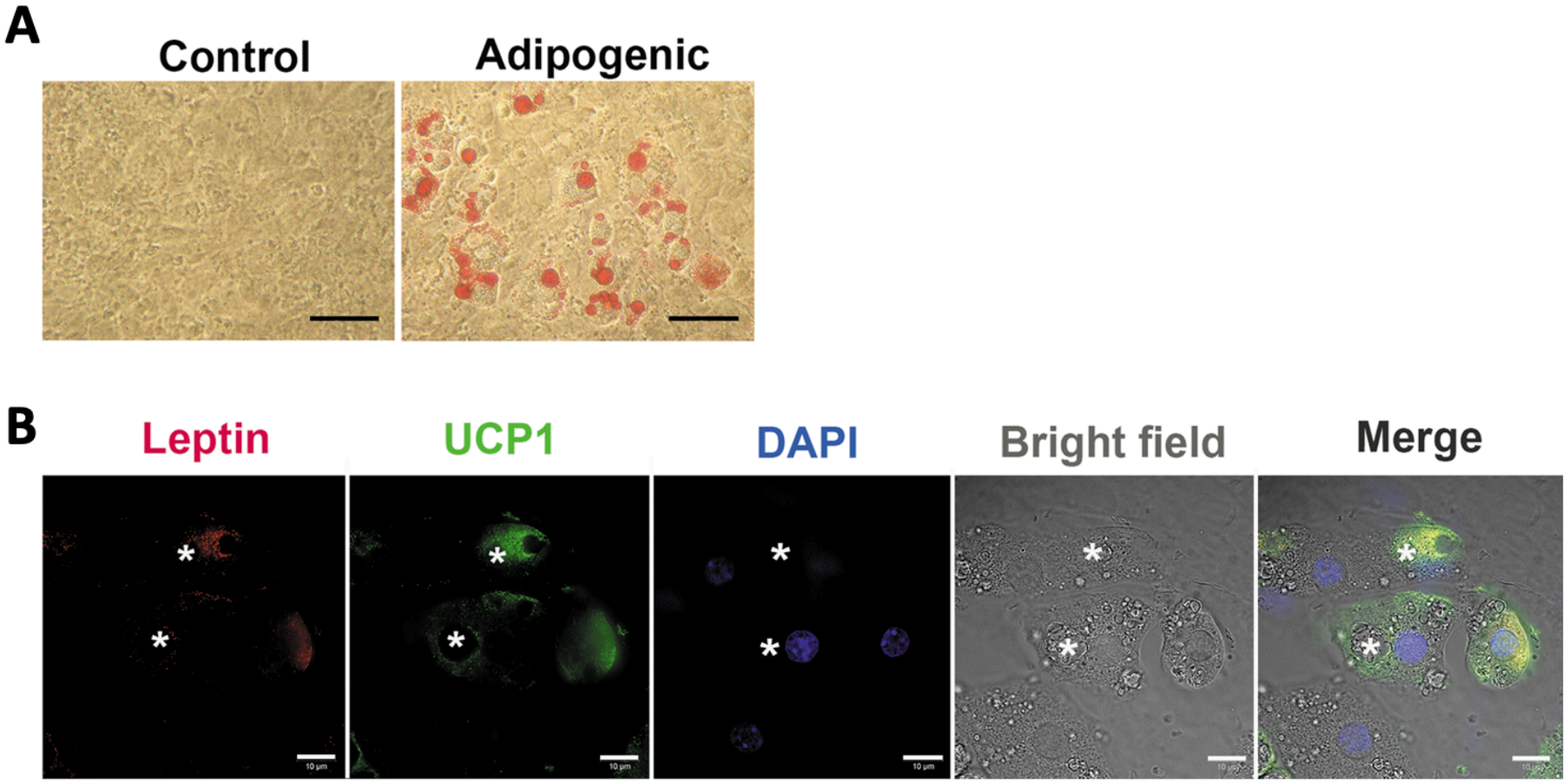

A
Control
Adipogenic
B
Leptin
UCP1
DAPI
Bright field
Merge

Figure 3.1. mMSCs differentiated adipocytes show uncoupling protein (UCP)1 and leptin expression.

(a) mMSCs acquired an adipogenic phenotype confirmed by ORO staining. Scale bars: 50 μm. (b) Super-resolved structured illumination microscope image showing presence of leptin^{+}/UCP1^{+} cells in adipocytes-treated mMSC cultures analysed by immunofluorescence. Leptin (red) and *UCP1* (green) were found to be co-expressed in differentiated cells (asterisks highlight LDs), with DAPI nuclear counterstain (blue). Scale bars: 10 μm. n = 3 individual experiments. Panel A performed by Hilda Anaid Lugo Leija; panel B performed by Dr. Ksenija Velickovic.

3.4.2 Enhanced adipogenesis and morphological changes shows signs of browning in hypothermic conditions.

In order to investigate the influence of temperature on *UCP1* expression in our model, cells were either maintained at 37°C (standard temperature) or 32°C (lower temperature) and subjected to adipogenic treatment. Using the Presto Blue assay, no deleterious effect was noticed in adipocytes differentiated at 32°C and metabolic activity was increased (Fig. 3.2A and B). Cells were then subjected to ORO staining to further evaluate adipogenic differentiation. A large perinuclear LDs were observed in the cytoplasm of adipocytes differentiated at 37°C, compared with numerous, smaller LDs located further away from the nucleus in adipocytes differentiated at 32°C (Fig. 3.2C). Morphometric analysis of LD diameter confirmed the prevalence of larger LDs in adipocytes differentiated at 37°C (Fig. 3.2D), which was accompanied by a lower total lipid content (Fig. 3.2E) and fewer differentiated cells (Fig. 3.2F). Taken together these results show increased metabolic activity, cellular differentiation and lipid content when incubated at a cooler temperature.

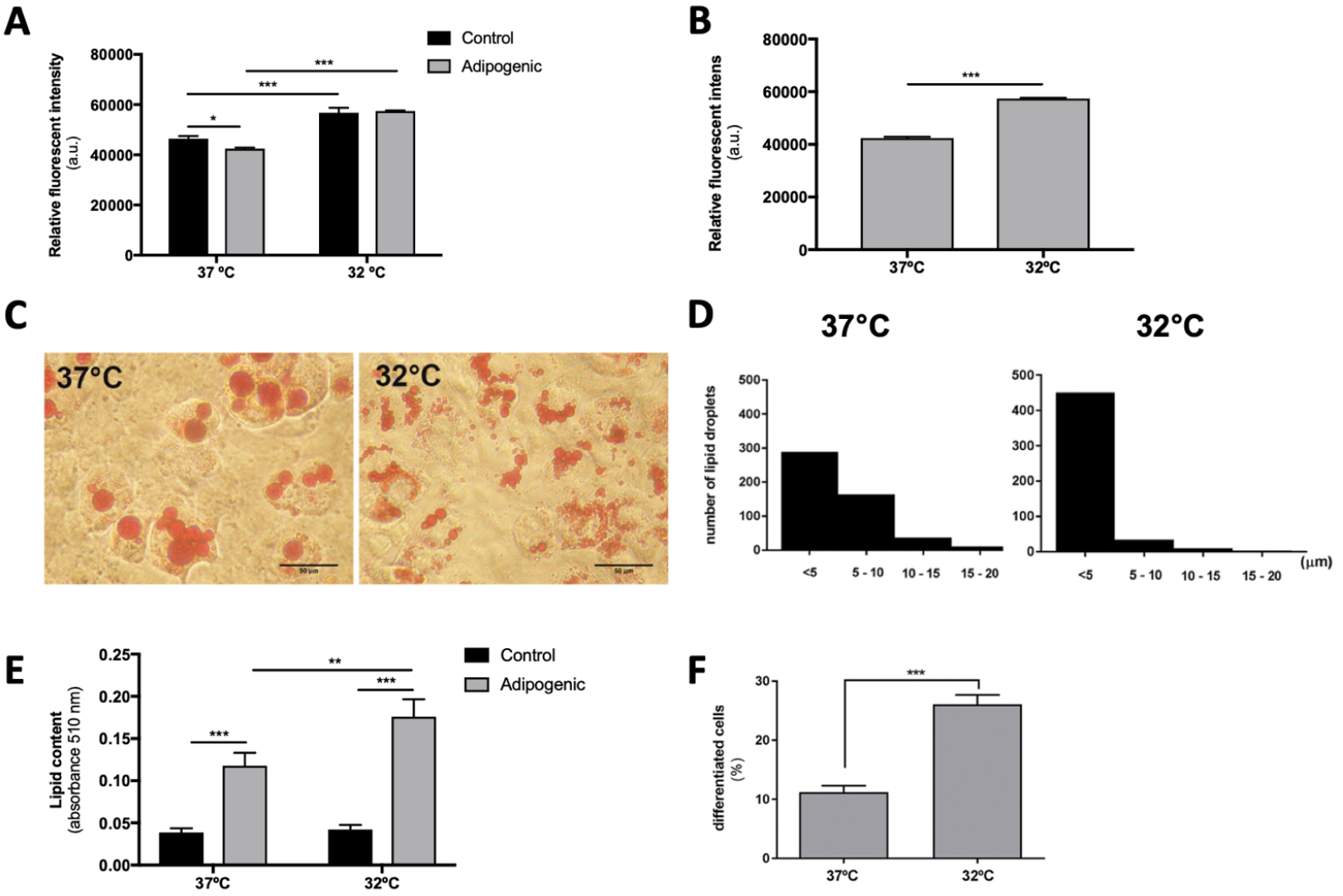

A
Control
Adipogenic
Relative fluorescent intensity (a.u.)
80000
60000
40000
20000
0
*
***
***
37 °C
32 °C
B
Relative fluorescent intens (a.u.)
80000
60000
40000
20000
0
***
37°C
32°C
C
37°C
32°C
D
37°C
32°C
number of lipid droplets
500
400
300
200
100
0
<5
5 - 10
10 - 15
15 - 20
(µm)
E
Control
Adipogenic
Lipid content (absorbance 510 nm)
0.25
0.20
0.15
0.10
0.05
0.00
**
***
***
37°C
32°C
F
differentiated cells (%)
30
20
10
0
***
37°C
32°C

Figure 3.2. Cellular response of mMSCs exposed to 9-day adipogenic differentiation under standard or hypothermal conditions.

(a and b) Metabolic activity measured in adipogenic treated cultures maintained at 32 and 37°C. (c) ORO staining of cells after 9 days of differentiation at 32°C and 37°C, and (d) changes in LDs size distribution (mean diameter). Scale bars, 20 μm. (e) Changes in lipid content per well in cells differentiated at 32 and 37°C. *** Comparison of the same treatments at different temperature. Statistical significance was set at $p<0.05$. (f) Proportion of lipid-containing cells after differentiation at 32°C and 37°C. Measurements (d and f) were done on 50 randomly selected micrographs per condition (n = 3 individual experiments). Data are shown as mean ± SEM. Statistical significance was set at $p<0.05$. Panels A, B, C & E performed by Hilda Anaid Lugo Leija; D & F performed by Dr. Ksenija Velickovic.

3.4.3 Temperature-related changes in differentiated mMSC-derived adipocytes: increased UCP1 protein expression and leptin translocation to the nucleus.

Next, the effect of temperature on *UCP1* and leptin was analysed (Fig. 3.3), and although *UCP1* was observed in most differentiated adipocytes, exposure to a lower temperature strongly enhanced *UCP1* abundance (Fig. 3.3A and B). Similarly, leptin was expressed in both adipogenic groups but surprisingly, unlike adipocytes differentiated at 37°C where leptin was localized in the cytoplasm, whereas in adipocytes differentiated at 32°C leptin was found to be localized in the nucleus (Fig. 3.3C and D). This difference was confirmed by immunofluorescence detection using confocal microscopy imaging of serial sections with a thickness less than 1 μm (Fig. 3.4). The same morphological changes related to LD size and their distribution were observed in primary mouse BM-derived adipocytes as well as in human adipose-derived stem cells (hADSCs) (Fig. 3.5). Furthermore, in both cell types *UCP1* protein expression was increased (Fig. 3.5A) in adipocytes differentiated at 32°C and leptin was observed to be localized in the nucleus (Fig. 3.5B).

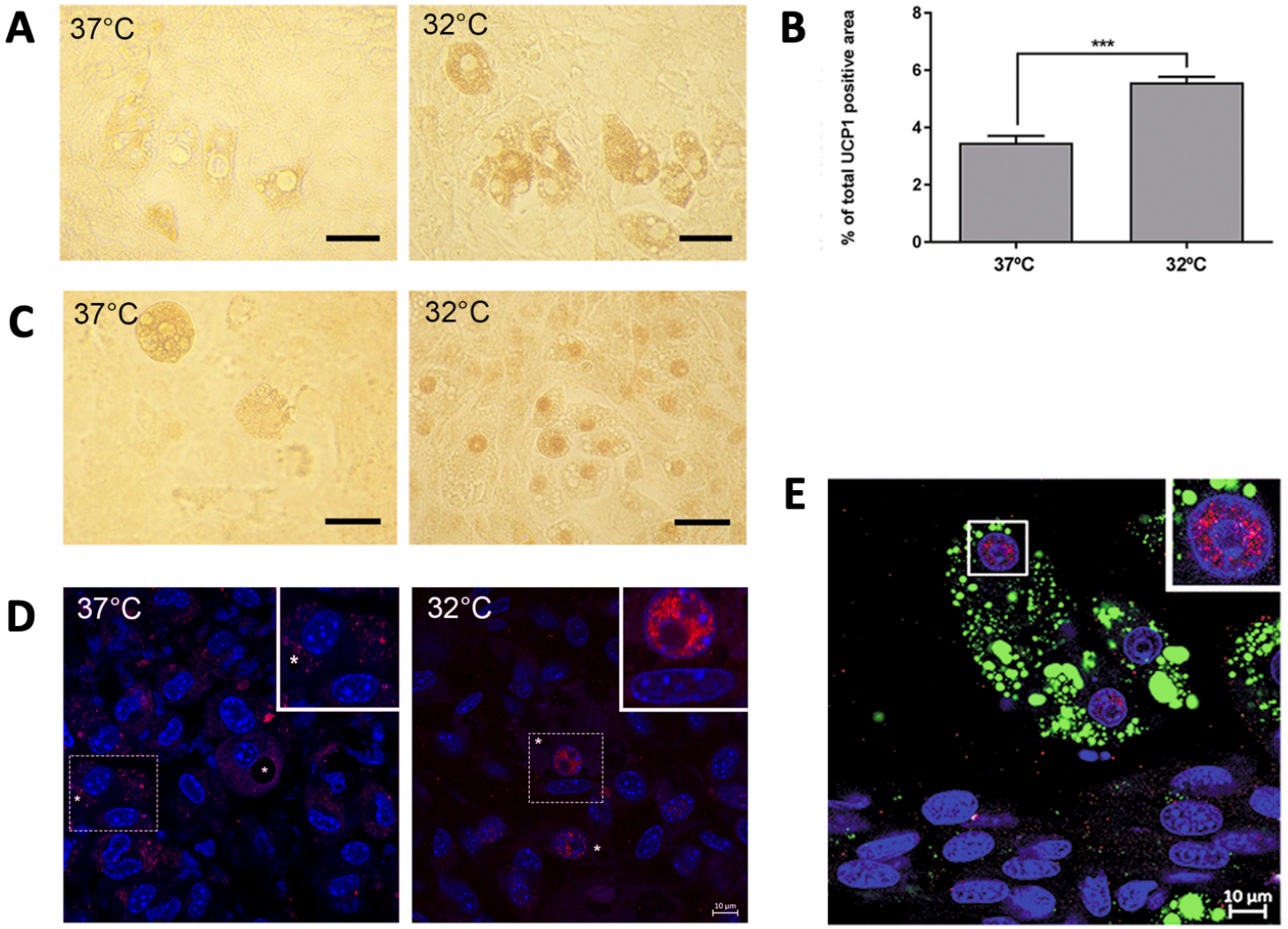

A
37°C
32°C
B
% of total UCP1 positive area
***
8
6
4
2
0
37°C
32°C
C
37°C
32°C
D
37°C
32°C
10 µm
E
10 µm

Figure 3.3. Temperature-related changes in differentiating mMSCs.

(a) Detection of uncoupling protein (UCP)1 protein expression in adipocytes differentiated at 37 vs 32°C visualized with 3, 3′-diaminobenzidine (DAB) as the chromogen. Scale bar: 20μm. (b) Image quantification of UCP1-positive cell area. Data represent the mean ± SEM. Statistical significance was set at $p<0.05$. (c) Leptin immunodetection in adipogenic cells in cultures differentiated in 37 vs 32°C visualized with 3, 3′-diaminobenzidine (DAB) as the chromogen. Scale bar: 20μm. (d) Fluorescence image of leptin (red) cytoplasmic localization in adipocytes differentiated in 37°C (left image) and leptin nuclear localization in adipocytes differentiated at 32°C (right image). DAPI was used to identify nuclei (blue) and asterisks indicate LDs. Image inserts show enlarged view of adipocytes in boxed areas. Scale bar: 10 μm. (e) Representative fluorescence image of leptin nuclear localization (red) in adipocytes differentiated at 32°C. DAPI was used to identify nuclei (blue) and BODIPY was used to identify LDs (green). Insert shows enlarged view of nucleus in boxed area. Scale bar: 10μm. n = 3 individual experiments. Performed by Dr. Ksenija Velickovic. Differentiation performed equally by Hilda Anaid Lugo Leija and Dr. Ksenija Velickovic; immunocytochemistry, quantification and imaging performed by Dr. Ksenija Velickovic.

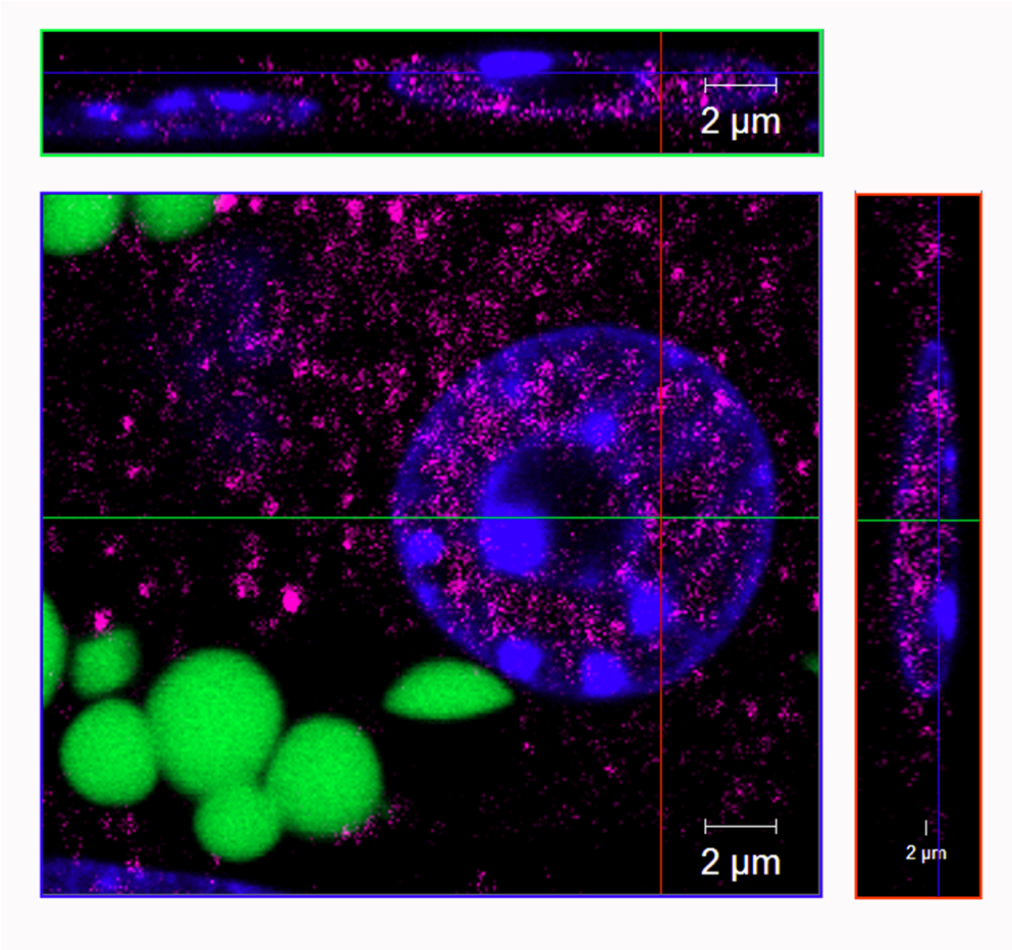


Figure 3.4. Image from a confocal z-stack with orthogonal views of leptin (purple) localization in mMSCs differentiated adipocytes at 32°C.
DAPI was used to identify nuclei (blue) and BODIPY was used to identify LDs (green). Scale bar: 2 µm. Performed by Dr. Ksenija Velickovic.

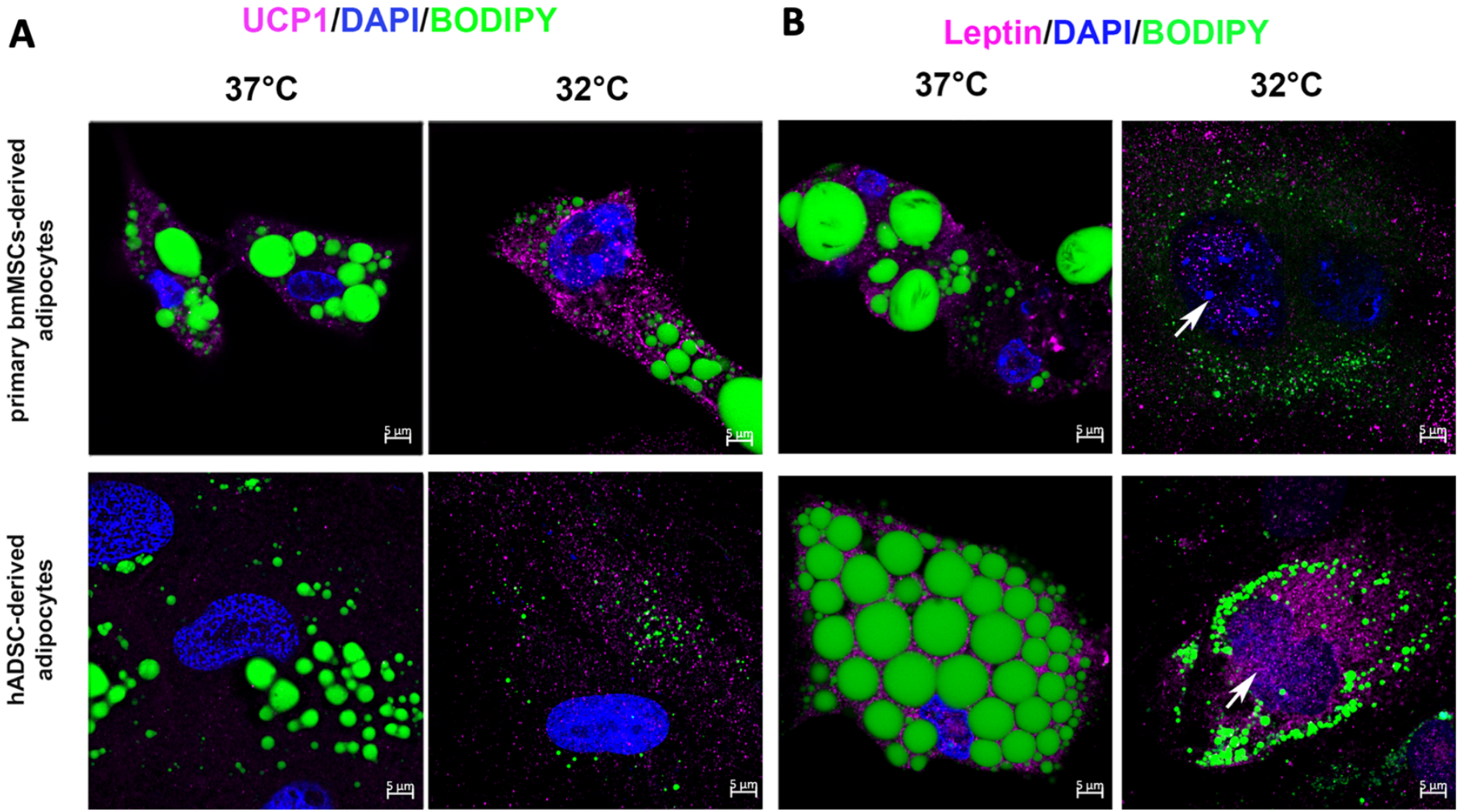

A
UCP1/DAPI/BODIPY
37°C
32°C
B
Leptin/DAPI/BODIPY
37°C
32°C
primary bmMSCs-derived adipocytes
hADSC-derived adipocytes
5 μm

Figure 3.5. Temperature-related changes in differentiating mouse primary bone marrow (BM) mesenchymal stem cells (MSC) derived and human adipose-derived cells (hADSCs).

Detection of (a) *UCP1* and (b) leptin (purple) protein expression in adipocytes differentiated at 37 vs 32°C. DAPI was used to identify nuclei (blue) and BODIPY was used to identify LDs (green). Arrows indicate leptin nuclear localization in cells differentiated at 32°C. Scale bar: 5 μm. n = 3 individual experiments. Performed by Dr. Ksenija Velickovic.

To determine whether this adipogenic phenotype acquired at 32°C may be reversible as found *in vivo*, cells differentiated at 32°C were subsequently transferred to standard culture conditions (37°C). These cells exhibited a morphology more similar to cells differentiated solely at 37°C than that of cells differentiated at 32°C (Fig. 3.6). Morphological changes were accompanied with changes in *UCP1* and leptin expression (Fig. 3.6B, C and D).As can be seen from (Fig. 3.6), cells transferred from 32°C to 37°C showed a pattern of *UCP1* expression similar to that of cells differentiated at 32°C, as well as positive leptin reaction in nuclei, showing that the hypothermic cells retained their cold phenotype after rewarming (Fig. 3.6D). Additionally, cells transferred from 37 to 32°C showed the same pattern of *UCP1* thermotransient receptor potential ion channel subfamily V (*TRPV)1* expression as cells differentiated at 32°C (Fig. 3.6E).

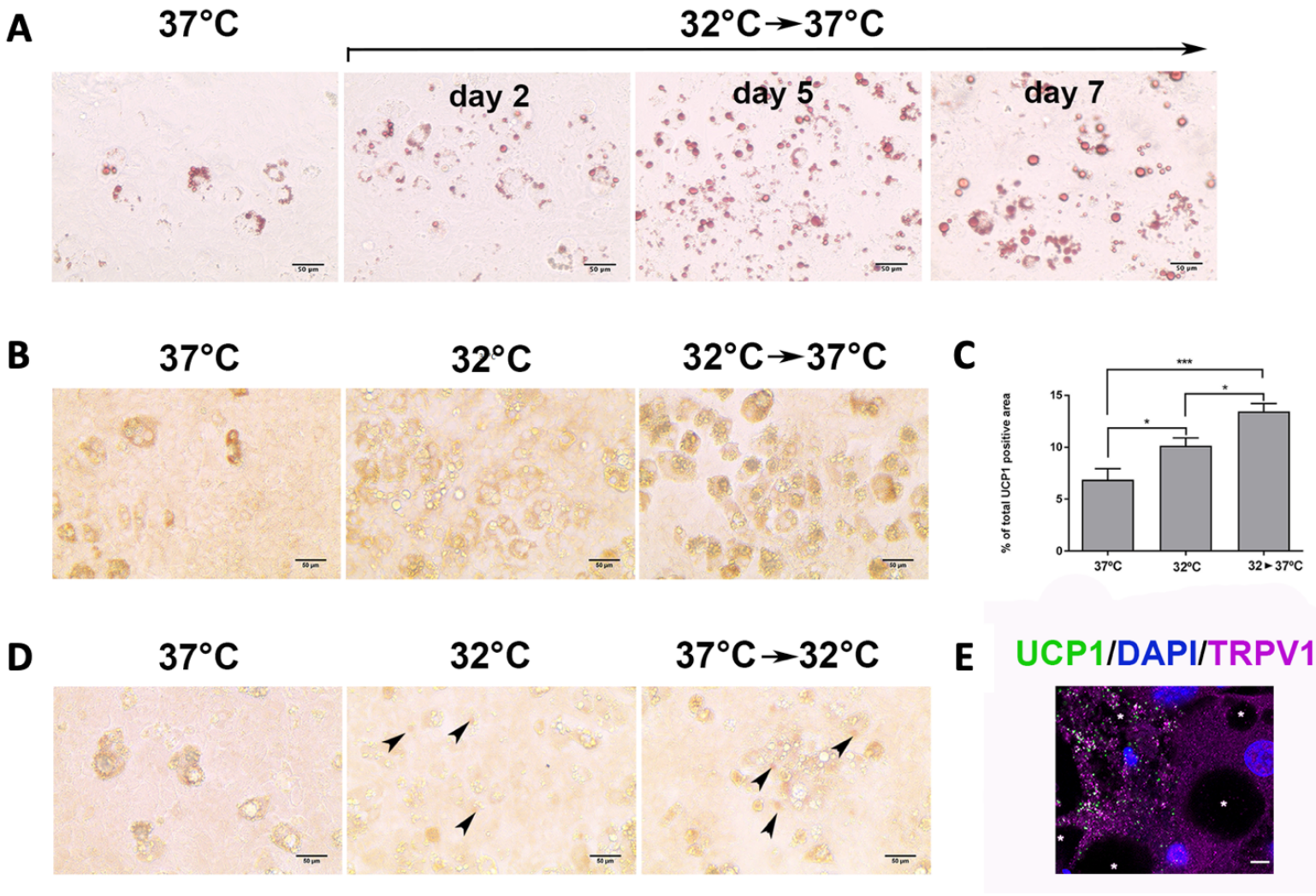

A
37°C
32°C→37°C
day 2
day 5
day 7
B
37°C
32°C
32°C→37°C
C
% of total UCP1 positive area
37°C
32°C
32►37°C
D
37°C
32°C
37°C→32°C
E
UCP1/DAPI/TRPV1

Figure 3.6. Morphological changes in cells transferred from 32 to 37°C and UCP1 expression.

(a) mMSCs were differentiated at 32°C for seven days, transferred to 37°C for the next seven days and stained with ORO. During this period, cells achieved intermediate phenotype with large LDs and enhanced differentiation. (b) Morphological changes are accompanied by variation in UCP1 protein expression. Higher level of UCP1 expression could be seen in groups differentiated at 32°C and transferred to 37°C. (c) Image quantification of UCP1-positive cell area. Data represent the mean ± SEM. Statistical significance was set at $p<0.05$. (d) Leptin expression in adipocyte nuclei in groups differentiated at 32°C and transferred to 37°C. Scale bars: 50 μm. (e) Representative image showing double staining of TRPV1 (purple) and UCP1 (green) protein expression in adipocytes transferred from 32 to 37°C. DAPI was used to identify nuclei (blue) and asterisks indicate LDs. Scale bar: 5 μm. Images representative of 3 individual experiments. *$p<0.05$, **$p<0.01$, ***$p<0.001$. Differentiation and ORO performed by Hilda Anaid Lugo Leija; immunocytochemistry and quantification performed by Dr. Ksenija Velickovic.

3.4.4 Lower temperature conditions affect PGC-1α expression, the bioenergetic status and reduce coupling efficiency of MSC-derived adipocytes.

The dynamic process of adipocyte differentiation in both WAT and BAT is accompanied by changes in the mitochondrial number (mitochondrial biogenesis), shape and localization, and is under the control of several transcription factors including *PGC-1α*, a *PPARγ* coactivator and main regulator of mitochondrial biogenesis and oxidative phosphorylation[187,188]. *PGC-1α* immunostaining (Fig. 3.7A), and mitochondrial staining performed using MitoTracker Orange (Fig. 3.7B), revealed that cells differentiated at 32°C exhibited strong nuclear *PGC-1α* signal compared to the cytoplasmic staining observed in cells differentiated at 37°C. MitoTracker relative fluorescence

intensity was slightly increased in adipocytes differentiated at 32°C compared with 37°C, although statistical significance was not reached (Fig. 3.7C). However, MitoTracker relative fluorescence intensity measured around LDs (Fig. 3.7D) was significantly enhanced in adipocytes differentiated at 32°C, which confirmed that at lower temperature mitochondria were more frequently observed adjacent to the LDs compared with mitochondria in cells differentiated at 37°C.

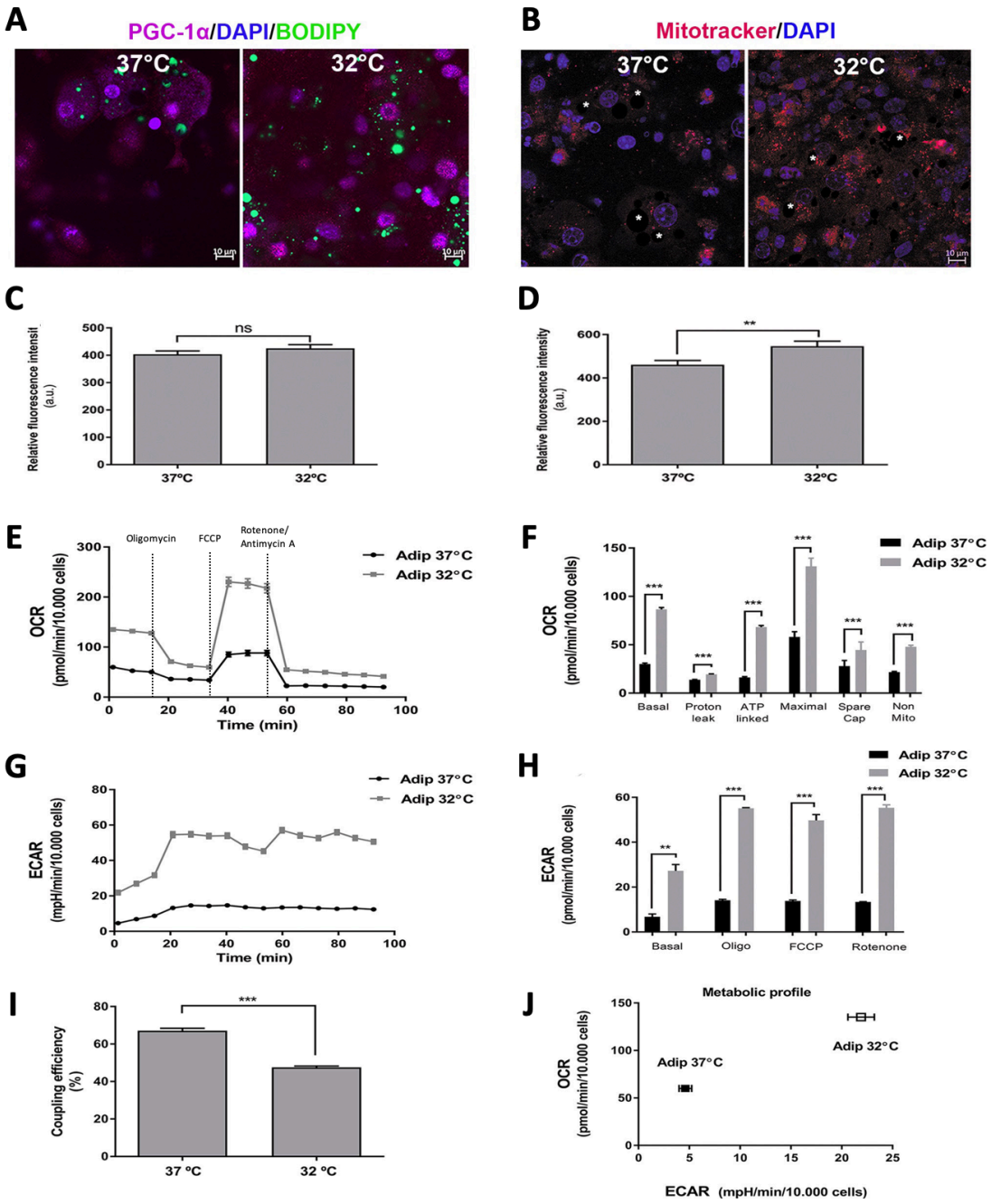


Figure 3.7. PGC-1α immunoexpression, mitochondrial localization and bioenergetics measurement during mMSCs differentiation under different temperature conditions. (a) Fluorescence image of PGC-1α (purple) in adipocytes differentiated at 37 °C and 32 °C. DAPI was used to identify nuclei (blue) and BODIPY was used to identify LDs (green). (b) mMSC-derived adipocytes stained with MitoTracker Orange CM-H2 TRos (red) and DAPI nuclear counterstain (blue). Asterisks indicate LDs. Scale bar: 10 μm. (c) Relative fluorescence intensity of MitoTracker staining was determined at randomly selected images, measuring relative fluorescence intensity on whole image (d) Relative fluorescence intensity of MitoTracker staining was determined at randomly selected ROI around LDs, at distance of 3 μm from LD's membrane. Data represent the mean ± SEM. Statistical significance was set at $p < 0.05$. (e) OCR following differentiation of adipocytes at 37 and 32 °C, respectively. (f) Six parameters of mitochondrial function calculated from the bioenergetics profile (basal respiration, proton leak, ATP-linked respiration, maximal capacity, spare capacity and non-mitochondrial respiration). Data represent the mean ± SEM. Statistical significance was set at $p < 0.05$. (g) ECAR following differentiation of adipocytes at 37 and 32 °C, respectively. (h) Quantitative ECAR analysis of adipocytes differentiated at 37 and 32 °C, respectively following treatments with mitochondrial inhibitors. (i) Coupling efficiency indicating the proportion of respiratory activity used for ATP synthesis. Bars represent mean ± SEM. Statistical significance was set at $p < 0.05$. (j) The metabolic profile for both adipogenic groups was determined by plotting ECAR to OCR. Bars represent mean ± SEM. Statistical significance was set at $p < 0.05$. $n = 6$ individual experiments. Performed by Dr. Ksenija Velickovic.

The bioenergetic status of cells was then investigated using a Seahorse XF96 flux analyser (Chapter 2.4.2 Seahorse assay, p. 50). OCR and ECAR readings were taken over time under basal conditions and after the addition of mitochondrial inhibitors (1.5 μM oligomycin, 0.8 μM FCCP and 1μM rotenone/antimycin). The overall respiratory responses (Fig. 3.7E) were calculated for the six key regulators of mitochondrial function. Adipocytes differentiated at 32°C had a markedly higher mitochondrial respiration under basal conditions and following oligomycin treatment (Fig. 3.7F), which results in chemically-induced uncoupling. Furthermore, ATP-linked oxygen consumption rate (OCR), maximal OCR, reserve capacity and non-mitochondrial OCR were all increased in adipocytes differentiated at 32°C (Fig. 3.7F) and coupling efficiency (Fig. 3.7I), an indicator of the proportion of respiratory activity used for ATP synthesis, was reduced.

Simultaneously with the OCR detection, the extracellular acidification rate (ECAR) (Fig. 3.7G and 3.7H) was raised in cells differentiated at 32°C. Following oligomycin treatment, when mitochondrial ATP synthesis is blocked, both adipocyte cultures were able to upregulate glycolysis to meet the demand for ATP. The ECAR response also increased more during carbonyl cyanide 4-(trifluoromethoxy) phenylhydrazone (FCCP) and rotenone/antimycin treatment in adipocytes differentiated at a low temperature (Fig. 3.7H). Plotting basal ECAR against OCR (Fig. 3.7J) summarised the effect of temperature which, when reduced, led to an increase not only in glycolysis, but also in oxidative phosphorylation, indicating more metabolically active cells.

3.4.5 Mouse MSC-derived adipocytes exhibit characteristics of white, beige and brown adipocytes at protein and mRNA level.

To determine whether our new model could generate adipocytes that exhibit the main features of beige cells, immunofluorescence detection (Chapter 2.5.3. p.55) was performed for *CD137* and *TMEM26* in undifferentiated mMSCs at 37°C (Fig. 3.8) and was found to be positive, with co-localisation on the cell membrane.

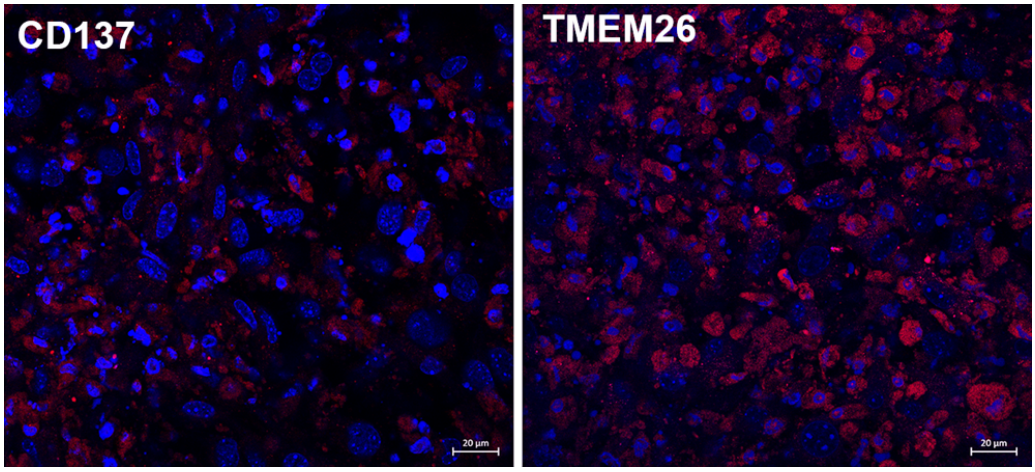


Figure 3.8. CD137 and TMEM26 immunodetection in undifferentiated mMSCs at 37°C. Fluorescence image of beige precursor markers showing cell membrane expression. DAPI was used to identify nuclei (blue). Scale bars: 20 µm. Images representative of 3 individual experiments. Differentiation equally performed by Hilda Anaid Lugo Leija and Dr. Ksenija Velickovic; immunocytochemistry performed by Dr. Ksenija Velickovic.

Co-staining for *CD137* and *UCP1* showed that most of the adipocytes differentiated at 32°C were positive for both (Fig. 3.9). Nuclear leptin localization in *UCP1*-expressing cells was further confirmed using immunofluorescence and confocal microscopy (Fig. 3.10). Additionally, this confirmed leptin and *UCP1* co-expression in adipocytes

differentiated at both 37 and 32°C, with nuclear translocation of leptin only observed in the later.

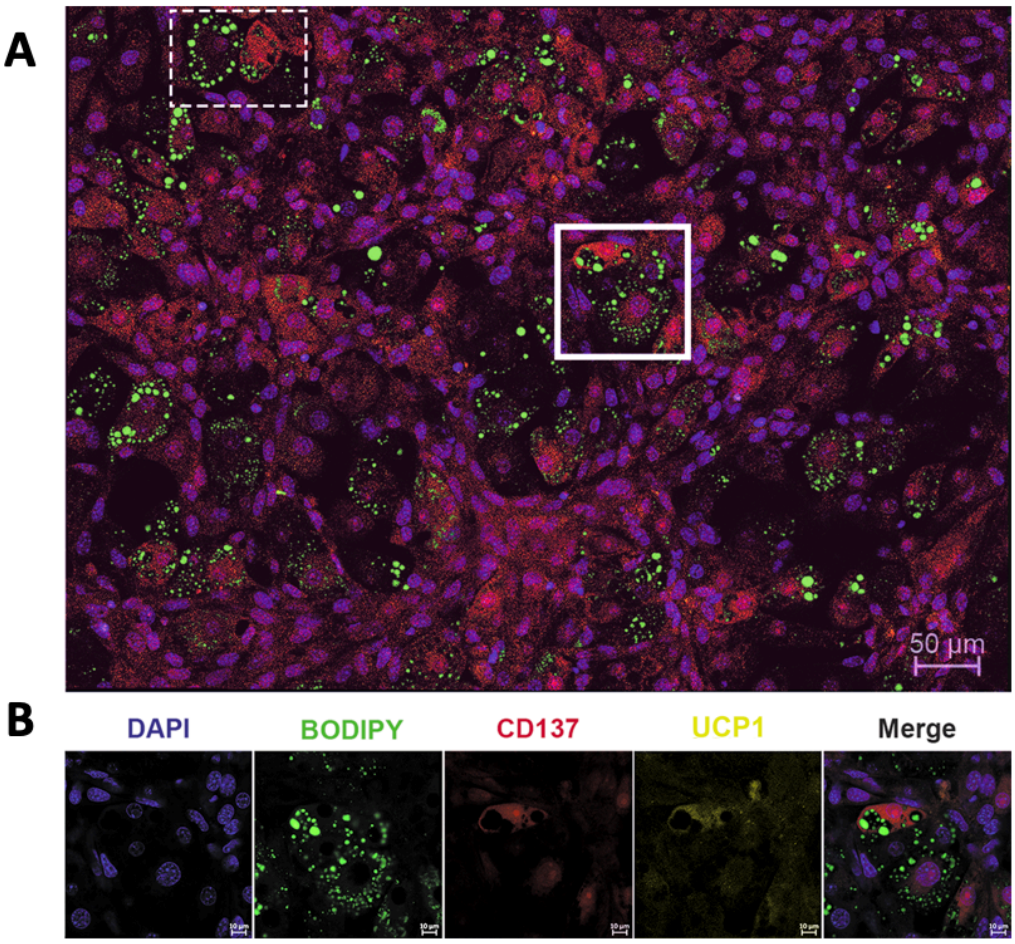


Figure 3.9.Expression of beige and brown markers in mMSCs-derived adipocytes differentiated at 32°C.

(a) Representative image showing the prevalence of beige cell-specific marker *CD137* (red), multilocular phenotype and uncoupling protein (UCP)1 expression (yellow). DAPI was used to identify nuclei (blue) and BODIPY was used to identify LDs (green). The dashed square highlights difference in staining between two adjacent adipocytes. Scale bar: 50 µm. (b) Enlarged view of the square area, with individual and merged images showing adipocytes positive for both beige selective markers, *CD137* (red) and brown cell-specific marker, *UCP1* (yellow). Scale bars: 10µm. n = 3 individual experiments. Differentiation equally performed by Hilda Anaid Lugo Leija and and Dr. Ksenija Velickovic; immunocytochemistry and imaging performed by Dr. Ksenija Velickovic.

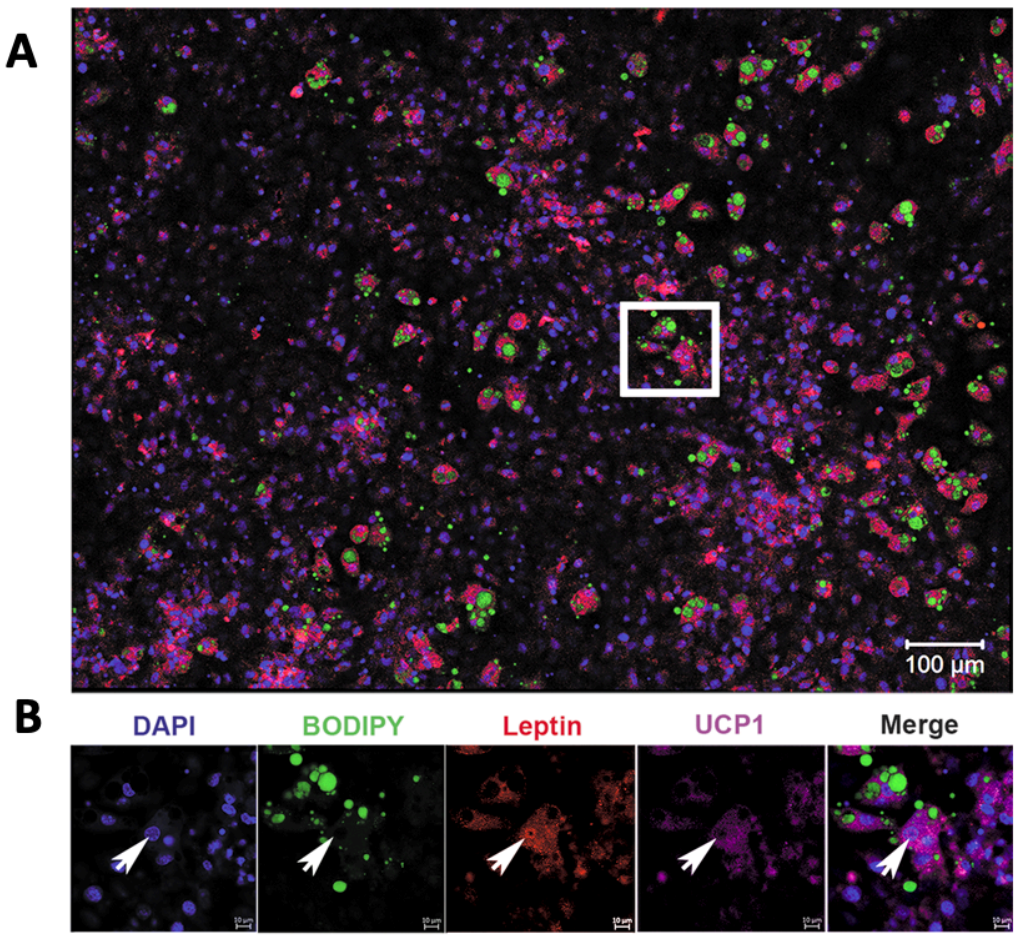


Figure 3.10.Leptin nuclear localization in UCP1^{+} mesenchymal stem cell-derived adipocytes differentiated at 32°C.

(a) Representative image showing double staining for leptin (red) and uncoupling protein (UCP)1 (purple). DAPI was used to identify nuclei (blue) and BODIPY was used to identify LDs (green). Scale bar: 100 µm. (b) Enlarged view of the square area, with individual and merged images showing adipocytes nuclei positive for leptin (red) and positive for UCP1 (purple). Arrows indicate nucleus positive for leptin and UCP1 cytoplasmic expression in the same cell differentiated at 32°C Scale bar: 10µm. n = 3 individual experiments. Differentiation equally performed by Hilda Anaid Lugo Leija and Dr. Ksenija Velickovic; immunocytochemistry and imaging performed by Dr. Ksenija Velickovic.

For the gene expression analysis (Chapter 2.6 Molecular Biology, p. 57) RNA was normalized to 0.5 µg/µl to perform real-time PCR (Fig. 3.11) and, whilst *PPARγ* gene expression was detected in all samples, the expression of other general adipogenic markers, such as *AdipoQ* and *FABP4*, was found only in adipogenic-treated cultures. In addition, cells differentiated at 32°C showed increased expression for each of these genes (Fig. 3.11A) when compared to its respective control. Furthermore, leptin and leptin receptor expression were confirmed in all experimental groups (Fig.3.12). Similarly, beige-selective genes *CITED1*, *CD137* and *P2RX5* were expressed in all samples, and upregulated during differentiation at 32°C when compared to its control (Fig. 3.711B). Notably, adipocyte differentiation at 32°C promoted the upregulation of brown-selective genes, including *UCP1*, *LHX8*, *COXb8* and *RIP140*, but decreased the expression of *CIDEA* (Fig. 3.11C) when compared to its control. Furthermore, expression of the *TRPV*1, 2 and 4 was detected in BM-derived adipocytes differentiated at 37 and 32°C, respectively. However, cells differentiated at 32°C significantly increased the expression of *TRPV1*, when compared to adipocytes differentiated at 37°C showing its involvement in mediating temperature-sensing mechanism (Fig. 3.11D). Moreover, immunofluorescent staining confirms *TRPV1*/*UCP1* co-expression in adipocytes differentiated at 32°C and 37°C, with enhanced *TRPV1* immunoexpression in cells differentiated at 32°C (Fig. 3.11E and 3.11F).

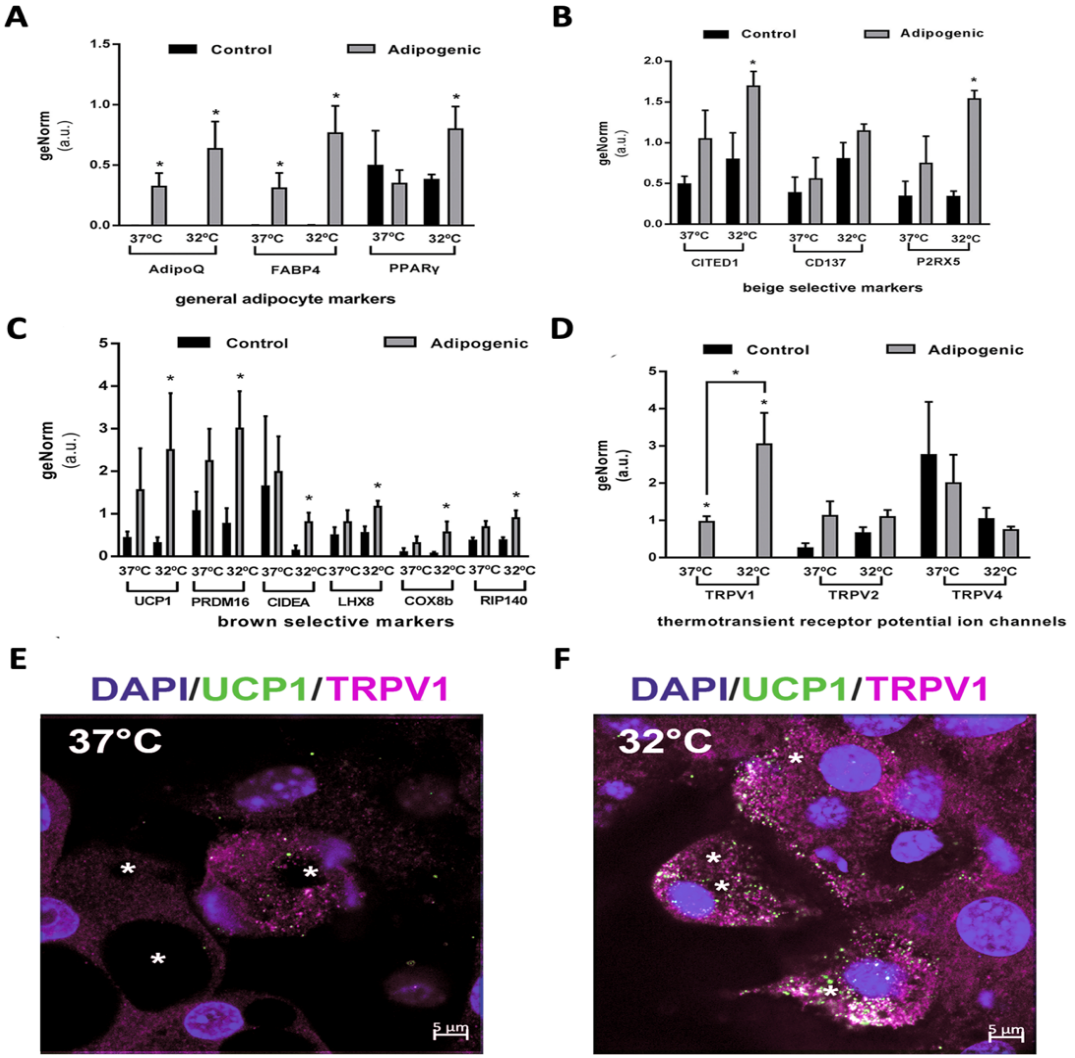

A
Control
Adipogenic
geNorm (a.u.)
37°C
32°C
AdipoQ
FABP4
PPARγ
general adipocyte markers
B
CITED1
CD137
P2RX5
beige selective markers
C
UCP1
PRDM16
CIDEA
LHX8
COX8b
RIP140
brown selective markers
D
TRPV1
TRPV2
TRPV4
thermotransient receptor potential ion channels
E
DAPI/UCP1/TRPV1
37°C
5 µm
F
32°C

Figure 3.11. Real-time PCR analysis of gene expression during mMSCs differentiation under different temperature conditions.

(a) Expression levels of general adipocytes markers: AdipoQ, FABP4 and PPARγ. Data represent the mean ± SEM of three replicas. Statistical significance was set at $p<0.05$. (b) Expression levels of beige lineage markers: CITED1, CD137 and P2RX5. Data represent the mean ± SEM of three replicas. Statistical significance was set at $p<0.05$. (c) Expression levels of brown lineage markers: UCP1, PRDM16, CIDEA, LHX8, COX8b and RIP140. Data represent the mean ± SEM of three replicas. Statistical significance was set at $p<0.05$. (d) Expression levels of TRPV1, TRPV2 and TRPV4. Data represent the mean ± SEM of three replicas. Statistical significance was set at $p<0.05$. (e and f) Representative images showing double staining of TRPV1 (purple) and UCP1 (green) protein expression in adipocytes differentiated at 37 (e) and 32°C (f) DAPI was used to identify nuclei (blue) and asterisks present LDs. Scale bars: 5μm. n = 3 individual experiments. Panels A - D performed by Hilda Anaid Lugo Leija; panels E & F performed by Dr. Ksenija Velickovic.

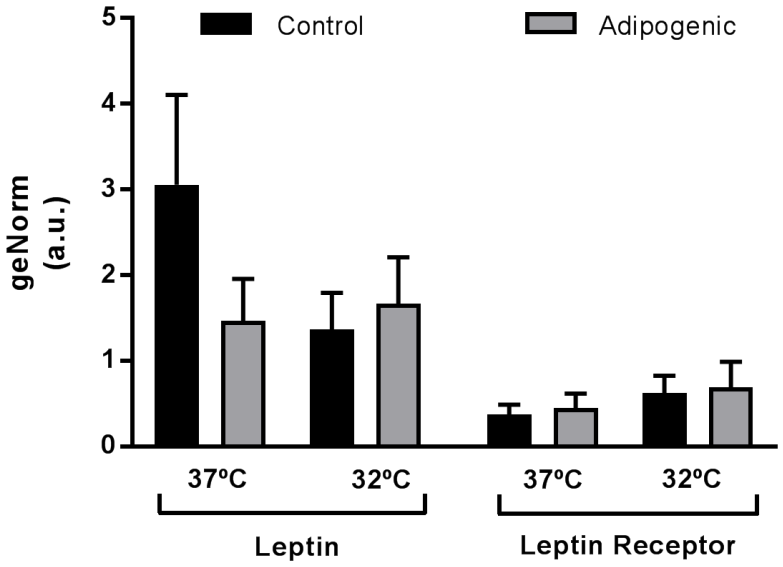


Figure 3.12. Real-time PCR analysis of Leptin and Leptin Receptor gene expression during mMSCs differentiation under different temperature conditions at day 9. Data represent the mean ± SEM of three replicates. Statistical significance was set at $p<0.05$. Performed by Hilda Anaid Lugo Leija.

3.4.6 Ca+ levels

Since *TRPV1* is Ca^{2+}-permeable cation channel and its activation leads to calcium influx, cells were stained with Fluo-4, a Ca^{2+}-sensitive dye. While signal for intracellular calcium was not detected in the majority of cells differentiated at 37°C, more cells differentiated at 32°C showed high cytoplasmic Fluo-4 signal, consistent with *TRPV1* activation in cells differentiated under low temperature conditions (Fig. 3.13).

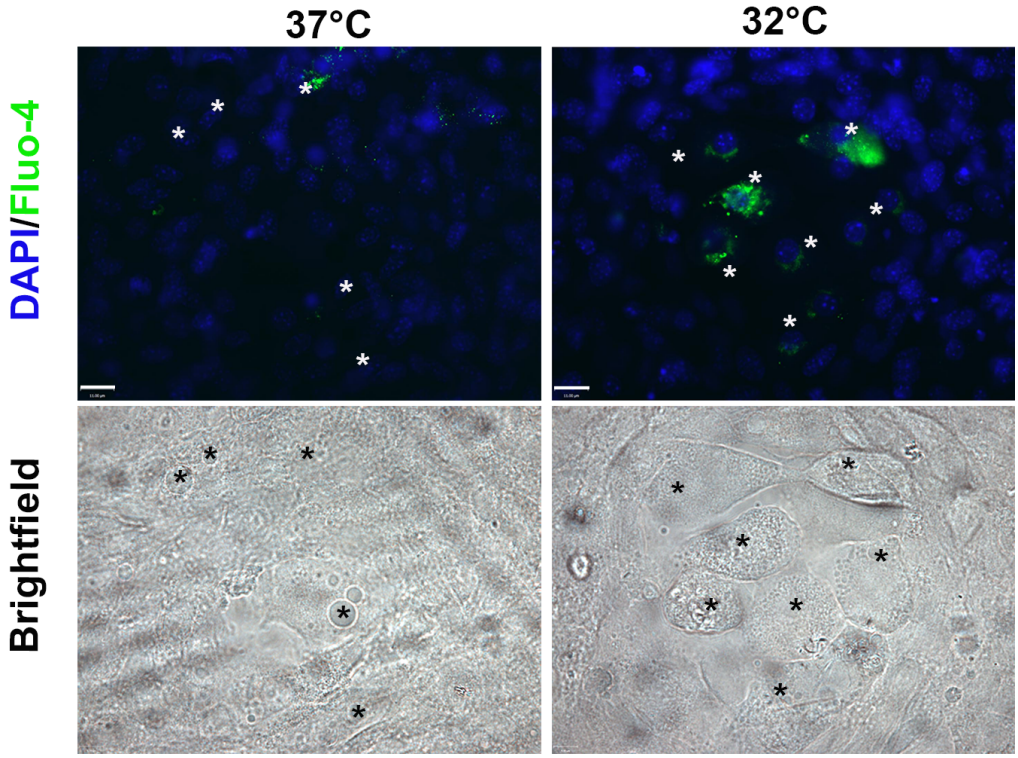


Figure 3.13. Temperature-related changes in differentiated mouse MSCs stained with Fluo-4.

Detection of Ca2+ (green) in adipocytes differentiated at 37 vs 32°C after 9 days. DAPI was used to identify nuclei (blue). Stars indicate LDs-laden adipocytes. Scale bar: 10 µm. Performed by Hilda Anaid Lugo Leija.

3.5 Discussion

3.5.1 Adipogenic phenotype and expression of UCP1 and leptin in mouse Mesenchymal Stem Cells (mMSCs)

Differentiation of mMSCs showed cells were able to successfully differentiate into adipocytes as previously reported[86]. In order to assess if our cells were able to differentiate into brown and white like adipocytes, leptin and *UCP1* immuno-expression was performed at the end of the adipogenic treatment at 37°C. Adipose tissue secretes leptin, this protein has been found in WAT and rat's brown adipose tissue at birth[189]. The nuclear presence of steroid and thyroid hormones is well documented[190], and as adipocytes express the leptin receptor, it is possible that the leptin-leptin receptor complex enters adipocyte nuclei as recently observed in cancer cells[191]. Thus, the nuclear localisation and possible regulatory role of leptin in adipocytes could be linked to existing literature in other cellular models, including myoblasts[192] suggesting a possible new regulatory role for leptin, a hypothesis consistent with its reported stimulatory effect on fatty acid oxidation[192]. It has also been reported the expression of leptin by adipocytes differentiated from primary bone marrow culture[193] but the co-expression of leptin and UCP1 has only been reported in unilocular adipocytes *in vivo*[194], suggesting the role of leptin is related to cell morphology, hence to thermogenesis activity[194]. *UCP1*/leptin dual expression phenotype, shown here, could indicate their functional diversity and potential to develop into both white and brown like adipocytes. Leptin nuclear function might influence in the control of adipocyte fate during development and differentiation process in addition to its role in appetite control[195].

3.5.2 Browning phenotype and increase of adipogenesis in cold temperature conditions

Low temperature exposure is one of the most important physiological stimulators of cellular energy metabolism[187], especially for BAT, and, *in vivo*, is known to increase proliferation, differentiation, *UCP1* activity[145] and the browning of beige adipocytes[61,144]. Here, increased metabolic activity determined by Presto blue assay and Seahorse XF96 analysis was accompanied with raised adipogenesis and changes in intracellular lipid content, as determined by calculating number of differentiated cells and the ORO assay in both treatments, respectively. Adipocytes differentiated at normal culture conditions showed lower frequency of differentiated cells and bigger lipid droplets compared with adipocytes under cold conditions. Both the lipid content and the proportion of differentiated cells were raised under low temperature conditions, followed by the appearance of numerous, small lipid droplets located in the cytoplasm further away from the nucleus, one of the most relevant morphological signs of browning[4,75].

3.5.3 Lower temperature conditions affect the bioenergetics profile and mitochondria frequency of adipocytes derived from mMSCs.

A key structural aspect of adipogenesis and the browning process is mitochondrial biogenesis[145] when mitochondria are remodelled, changing shape and size, increasing in number and cristae formation[196]. Even thought, mitochondria observed in adipocytes differentiated at 37°C were less frequent, relative fluorescence intensity quantification did not reveal any differences when compared

to 32°C. The main observation in adipogenic differentiation at 32°C were the size of lipid droplets which appear smaller and more numerous compared to adipocytes differentiated at 37°C, suggesting the enhancement of mitochondrial fatty acid oxidation in cold temperature. This was supported by the proximity of mitochondria and lipid droplets observed in this study, suggesting a modified distribution to optimise substrate supply.

It is known that adipogenic differentiation promotes a transition from glycolytic metabolism to oxidative phosphorylation[197], and an enhanced glycolytic rate has typically been interpreted as a consequence of reduced efficiency of ATP formation[176]. Here we found enhancement of two ATP-producing metabolic pathways, thus clearly indicating high energy demands of cells differentiated at 32°C. Furthermore, the metabolic profile, *UCP1* activation, increased lipid content and reduced coupling efficiency suggest raised fatty acid oxidation and lipogenesis. These two processes have already been reported to act in parallel. Simultaneous induction of specific genes involved in fatty acid oxidation and synthesis in brown, beige and white adipocytes occurs, enabling a continuous cycle of triglycerides hydrolysis and resynthesis[198]. These processes require large amounts of ATP and could, at least partly, be a further cause of increased metabolic activity as observed in our study.

3.5.4 White, beige and brown features shown by MSC-derived adipocytes at mRNA level

Hypothermic differentiated adipocytes displayed an increased expression of beige cell markers i.e. *UCP1*, *CITED1*, *COX8b* and

P2RX5[58] when compared to their control, unfortunately such increase was not shown to be significant when it was compared to adipocytes differentiated at 37ºC. Only *CD137* marker was detected in both control and adipogenic cells and it could be an indication of mMSCs' commitment to an adipogenic beige lineage[4]. Additionally, double-staining showed adipocyte differentiation at a low temperature promoted the appearance of *CD137/UCP1*-positive cells. Gene expression was analysed in order to assess the transcriptional regulation of adipocytes differentiated from our cell model. Adipocyte cultures differentiated from mMSCs expressed several white, brown and beige fat markers, with a prevalent molecular signature of beige adipocytes in both the non-differentiated and differentiated state. *P2RX5* is a beige adipogenic marker and its expression has been shown to increase in BAT and subcutaneous WAT in mice in response to chronic cold exposure[66]. On the other hand, *COX8b* has been described as a distinctive marker of WAT `browning´[60]. Upregulation of these genes, *COX8b*, *UCP1*, *P2RX5*, *CITED1* and *CD137* could suggest a transition from white to beige/brown adipocytes when differentiated at hypothermic conditions which was not achieved at a warmer temperature (37ºC). Unfortunately, some inconsistencies and limitations of the temperature effect were found with *UCP1* gene detection, it is recognised that mRNA is not the principal determinant of protein quantity and function[199]. Increased *TRPV1* expression suggested that cold exposure is able to affect adipogenic differentiation directly in cell-autonomous manner, activating a thermogenic program independently from of the central nervous system. These findings extend the observations accordingly to one previous report showing that 3T3-F442A adipocytes can directly sense

temperature to activate thermogenesis[144]. Interestingly, *TRPV1* was recently identified as a novel regulator of leptin resistance in mice[200].

3.5.5 Cold-induced brown phenotype and UCP1 expression in MSC-derived adipocytes are retained after rewarming.

In order to corroborate *UCP1* positive expression in cells differentiated under cold culture conditions, *UCP1* expression by immunocytochemistry was performed and quantified. For the adipogenic differentiation treatments, results showed that mMSCs can express higher amount of *UCP1* protein immunoexpression. This *UCP1* increase together with mitochondria redistribution after adipogenic induction at hypothermic conditions, highlights two hallmarks of brown adipogenesis[4,75,107]. It is known that *UCP1* is necessary to activate thermogenesis on brown adipocytes[199] therefore, to evaluate if *UCP1* activation could be retained after re-warming, adipocyte derived-mMSCs differentiated under cold conditions were transferred to normal culture conditions, it was shown the *UCP1* retaining capacity of this model after 7 days of re-acclimation, this could be explained by the ability of the cells to "remember", it has been shown endothelial cells in culture have a "memory" capacity when these cells were induced to high glucose stress[201], however morphological changes in lipid droplets size could be spotted once cells where transferred, giving a mixture in characteristics resembling white adipocytes with *UCP1* expression.

The results presented here are the answer to one specific hypothesis, namely whether mMSCs are capable to differentiate into beige adipocytes under hypothermal culture conditions (32°C). In summary, results showed that mMSCs were able to successfully differentiate into adipocytes with leptin and *UCP1* co-expression. MSC-derived adipocytes differentiated under hypothermal conditions exhibited an intermediate beige and brown phenotype showing small lipid droplets and mitochondria remodelling with increased metabolic activity, differentiated cells and lipid content. Notwithstanding adipocytes differentiated at hypothermic conditions did not achieve a significant increase in beigeing/browning gene expression when compared with their warmer counterpart, these results show the importance of cold exposure during adipogenesis by increasing certain browning traits which are not achieved at normothermic culture conditions, such as increased bioenergetics. Gene expression also confirmed a defined beigeing/browning molecular signature of cold differentiated mMSCs by the upregulation of *COX8b*, *UCP1*, *P2RX5*, *CITED1* accompanied with increased *TRPV1* expression and immuno-expression of *CD137* when compared to their controls. Finally, MSC-derived adipocytes differentiated in standard culture conditions under hypothermal conditions also exhibited a mixed phenotype with both characteristics of cells differentiated at 32°C and at 37°C. They retained leptin and high *UCP1* signal while holding larger lipid droplets as an adaptive response. These intermediate characteristics indicate that MSC-differentiated cells exhibit phenotypic plasticity and suggest a possible cellular memory of previous environmental conditions.

Chapter 4. MSC derived-adipocytes differentiated under hypothermic conditions exhibit a brown phenotype after warm acclimatisation

4.1 Main findings

- Transfer MSC-derived adipocytes maintained their multilocular morphology and exhibit an intermediate brown/beige gene expression profile.
- UCP1 protein expression in Transfer adipocytes remained similar to that found in cells kept at 32°C.
- Transfer MSC-derived adipocytes are able to remain metabolically active after up to 3 weeks of acclimatisation.
- An intermediate profile in Transfer cells could suggest a shared mechanism of calcium mediated UCP1-independent thermogenesis.

4.2 Introduction

White and brown adipocytes have different origins and functions[10]. White adipocytes, which provide energy storage in the form of triglycerides, are characterised by single large lipid droplets and few mitochondria. By contrast, brown adipocytes are multilocular and contain several small lipid droplets and many mitochondria, that promote energy expenditure through heat production[10,132,138,202]. The defining characteristic of brown adipocytes is the presence of the mitochondrial uncoupling protein 1 (*UCP1*), which when stimulated enables the free flow of protons across the inner mitochondrial membrane without phosphorylating ADP[138,203]. Consequently, the potential thermogenic capacity of brown fat is up to 300 times greater than all other tissues[145]. In addition to brown and white adipocytes, beige adipocytes have recently been reported to display a similar morphology to white cells in the basal state, but can be stimulated by cold exposure to acquire an activated brown-like morphology with significant *UCP1* expression[4,92,144,147]. The extent to which a temperature induced stimulation of beige fat can be maintained upon return to a warm environment has not been widely studied. *In vivo* it appears that beige adipocytes from cold-stimulated mice revert to white fat within six weeks of warm acclimatisation[67]. Similarly, *in vitro* browning during adipogenic differentiation, mediated by maintaining the adipocytes at 27-33°C for 10 days is not maintained after the temperature was restored to 37°C[144]. Once established, however, brown adipocytes can maintain their multilocular morphology for one month in the same culture conditions[157]. This longer term adaptation appears to be mediated by a different mechanism from that initially promoting the appearance of *UCP1* and could include adaptations in

the rate of biogenesis[157] and mitophagy[204]. Mesenchymal stem cells (MSCs) are progenitors found in the bone marrow which have the potential to differentiate into several cell types[4,7], including adipocytes[4,102,205–208]. Cold exposure has been shown to enhance the *in vitro* differentiation of MSCs into *UCP1*-expressing adipocytes[92], but the extent to which this phenotype can be retained after return to normothermic conditions (i.e. 37°C) is not known.

This chapter continues with the evaluation of the stability and the acquired cellular features using the *in vitro* model of MSC differentiation under hypothermic conditions described in Chapter 3. Results described here demonstrate that these differentiated cells maintained some brown-like features and an intermediate thermogenic phenotype over 3 weeks of subsequent culture under a temperature of 37°C. Here, cells transferred from 32 to 37°C were found to maintain their multilocular morphology and to exhibit an intermediate gene expression profile, with both brown-like and white adipocyte characteristics, which declined after being returned to 37°C incubation for 21 days. *UCP1* protein expression, however, remained similar to that found in cells maintained at 32°C. Metabolic profile analysis indicated that the bioenergetic status of cells initially differentiated at 32°C adapted post-transfer to 37°C, showing an increase in mitochondrial respiration and glycolysis. The ability of the transferred cells to respond under stress conditions (e.g. FCCP treatment) demonstrated higher functional capacity of enzymes involved in electron transport chain and capability to supply substrate to the mitochondria. Overall, MSC-derived adipocytes incubated at 32°C were able to remain metabolically active and retain brown-like features after up to 3 weeks of acclimatisation at 37°C, indicating these

phenotypic characteristics acquired in response to environmental conditions are not fully reversible.

4.3 Methods

To continue with the analysis on the stability of the browning traits induced by hypothermic conditions, mMSCs D1 were exposed to different culture environments (Fig. 4.1), cells were differentiated during 7 days at 32ºC and then transferred to standard culture conditions (37ºC – referred as Transfer). Parallel cells were differentiated at 37ºC and 32ºC to compare metabolic, morphologic, molecular signature, UCP1 protein expression and bioenergetic capacity of the transferred cells for an endpoint of 14, 21 and 28 days under adipogenic differentiation treatment, methods are described in Chapter 2.4.1, p. 50; 2.4.3, p. 52; 2.5.1, p. 54; 2.5.3, p. 55. Adipogenic differentiation experiments were done with the adipogenic medium described in Chapter 2.2.4, p. 40. Supplemented with 1 nM of T3 (Sigma Aldrich, UK).

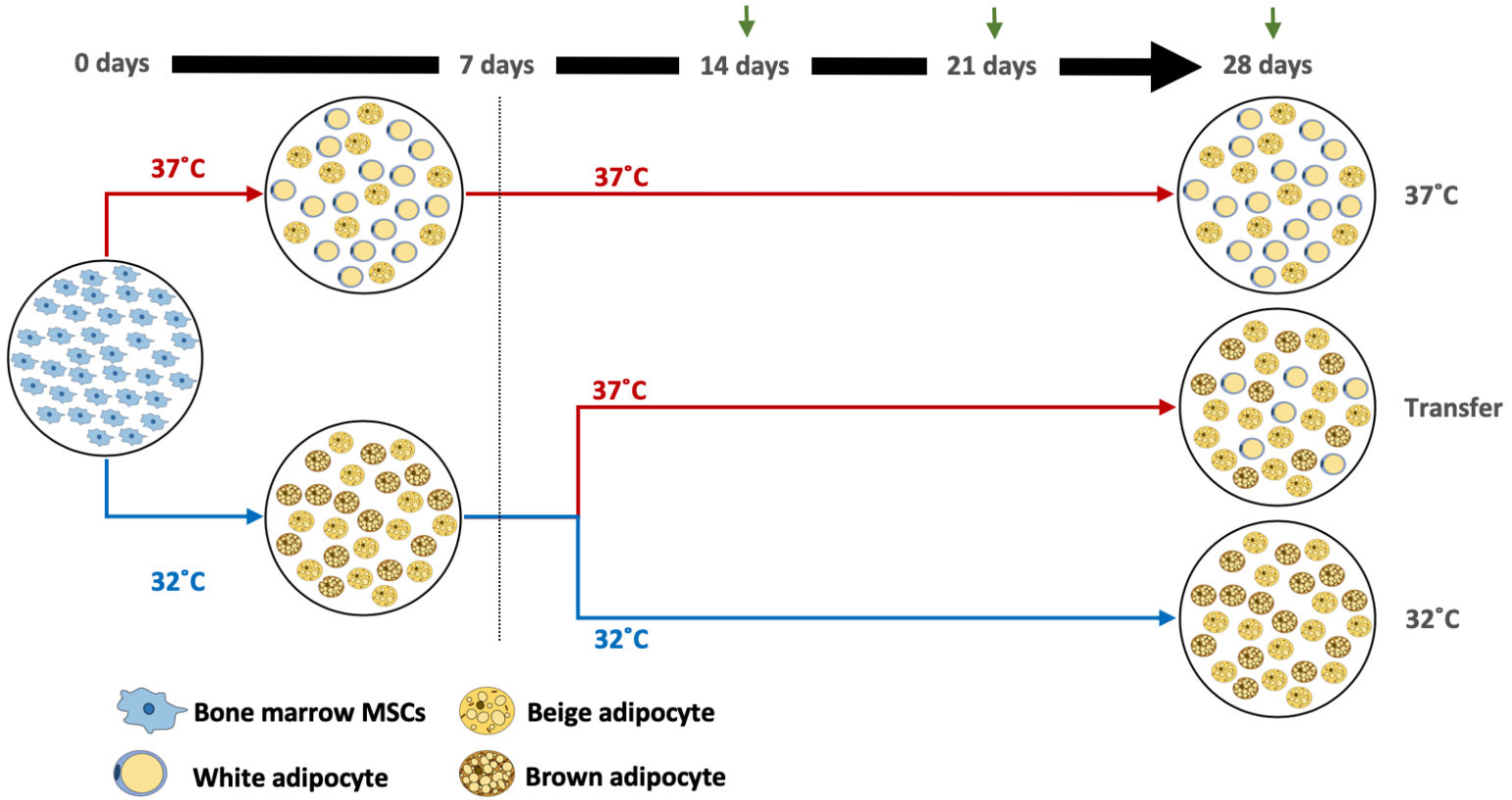


Figure 4.1. Schematic diagram of MSCs adipogenesis treatments.

MSCs were cultured in adipogenic medium at 37°C or 32°C for 7 days, and then either maintained at this temperature or transferred to 37°C. Green arrows indicate samples' timepoints at 14, 21 or 28 days.

4.4 Results

4.4.1 Cold-induced adipocytes retain brown-like cellular and morphological features when returned to a normothermic environment

At the end of each timepoint, mitochondria abundance and *UCP1* protein expression were measured by quantifying the relative fluorescence of the MitoTracker Deep Red (100 nM, Molecular Probes) staining and *UCP1* immunofluorescence intensity, respectively. When compared to normothermic control cultures, cells transferred from 32 to 37°C showed similar expression of *UCP1* protein and morphological features associated with hypothermal conditions, such as multilocular lipid droplets and increased mitochondria number which was maintained until day 21 (Fig. 4. 2).

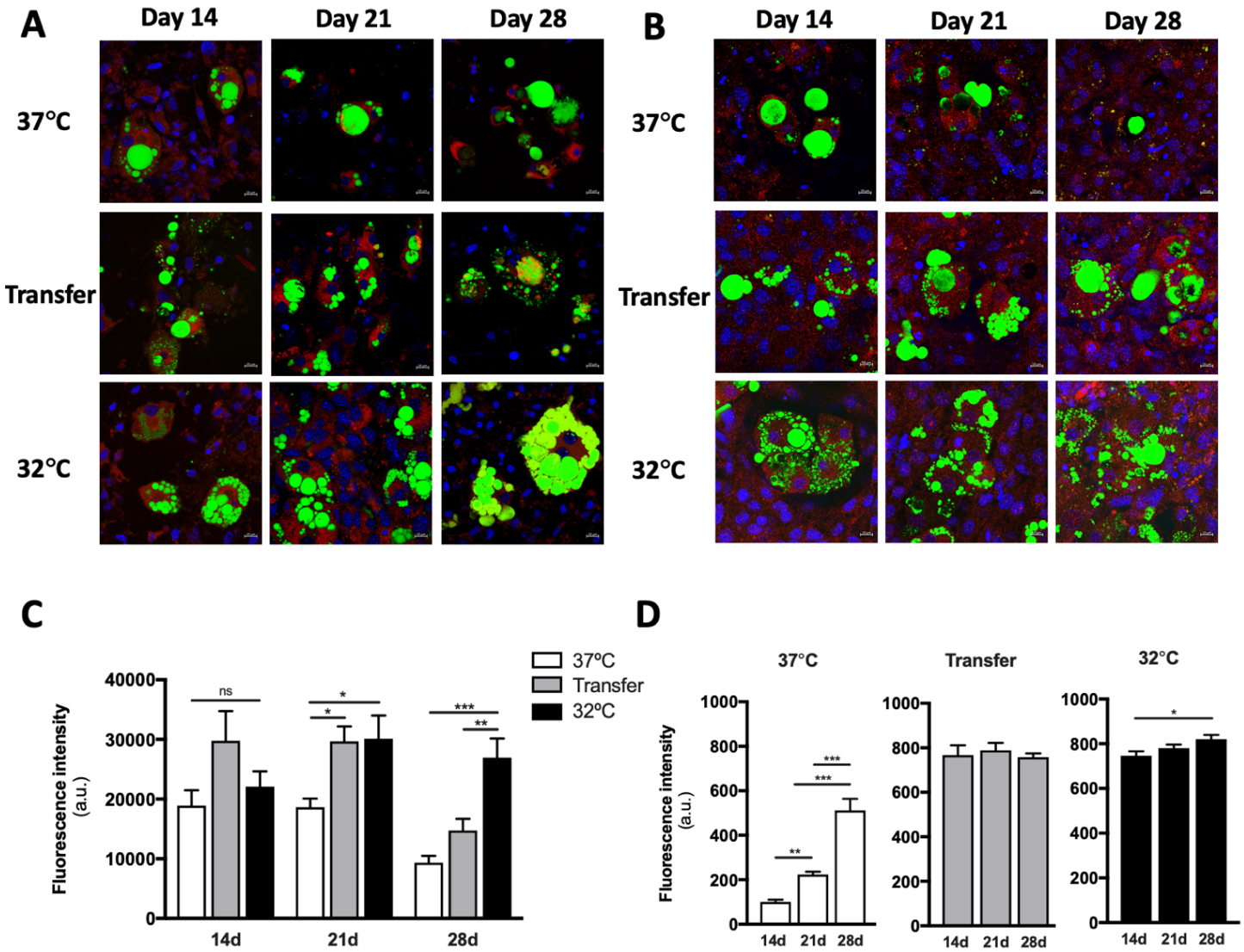

A
Day 14
Day 21
Day 28
37°C
Transfer
32°C
B
Day 14
Day 21
Day 28
37°C
Transfer
32°C
C
37°C
Transfer
32°C
Fluorescence intensity (a.u.)
40000
30000
20000
10000
0
ns
*
*
***
**
14d
21d
28d
D
37°C
Transfer
32°C
Fluorescence intensity (a.u.)
1000
800
600
400
200
0
**
***
***
*
14d
21d
28d

Figure 4.2. Effect of culture temperature on the abundance of mitochondria and uncoupling protein (UCP)1.
Representative images of (A) MitoTracker staining and (B) UCP1 shown in red, with Hoechst 33258 nuclear counterstain in blue, and Bodipy in green. Scale bar = 10 μM. Relative fluorescence intensity of (C) MitoTracker and (D) UCP1 staining as measured in 15 randomly selected micrographs of 3 independent experiments. *p<0.05, **p<0.01, ***p<0.001.

In order to study the metabolic behaviour of the Transfer cells, Presto Blue assay was done at 14, 21 and 28 days of adipogenic culture. Compared to normothermic controls, metabolic activity was significantly increased in cells maintained at 32°C, but not in cells subsequently transferred back to 37°C (Fig. 4.3A). Next, cells were stained with ORO staining for further assessment. In contrast with metabolic activity, lipid content increased with time in cells that were maintained at 32°C and in those subsequently transferred to 37°C (Fig. 4.3B). Same trend could be observed when the percentage of differentiated cells was analysed (Fig. 4.3C) as well as with the shift detected in lipid droplets size (Fig. 4.3D). The changes in lipid content were reflected by differences in cell morphologies, as MSCs differentiated at 37°C contained large perinuclear lipid droplets consistent with a white phenotype, while those differentiated at 32°C were mostly multilocular with smaller lipid droplets on days 14 and 21, and then exhibited larger lipid vacuoles by day 28. Cells transferred from 32 to 37°C displayed an intermediate phenotype with mixed uni- and multilocular cells, which became more unilocular by 28 days, however some adipocytes were able to maintain multilocularity (Fig. 4.4), which could suggest an intermediary phenotype.

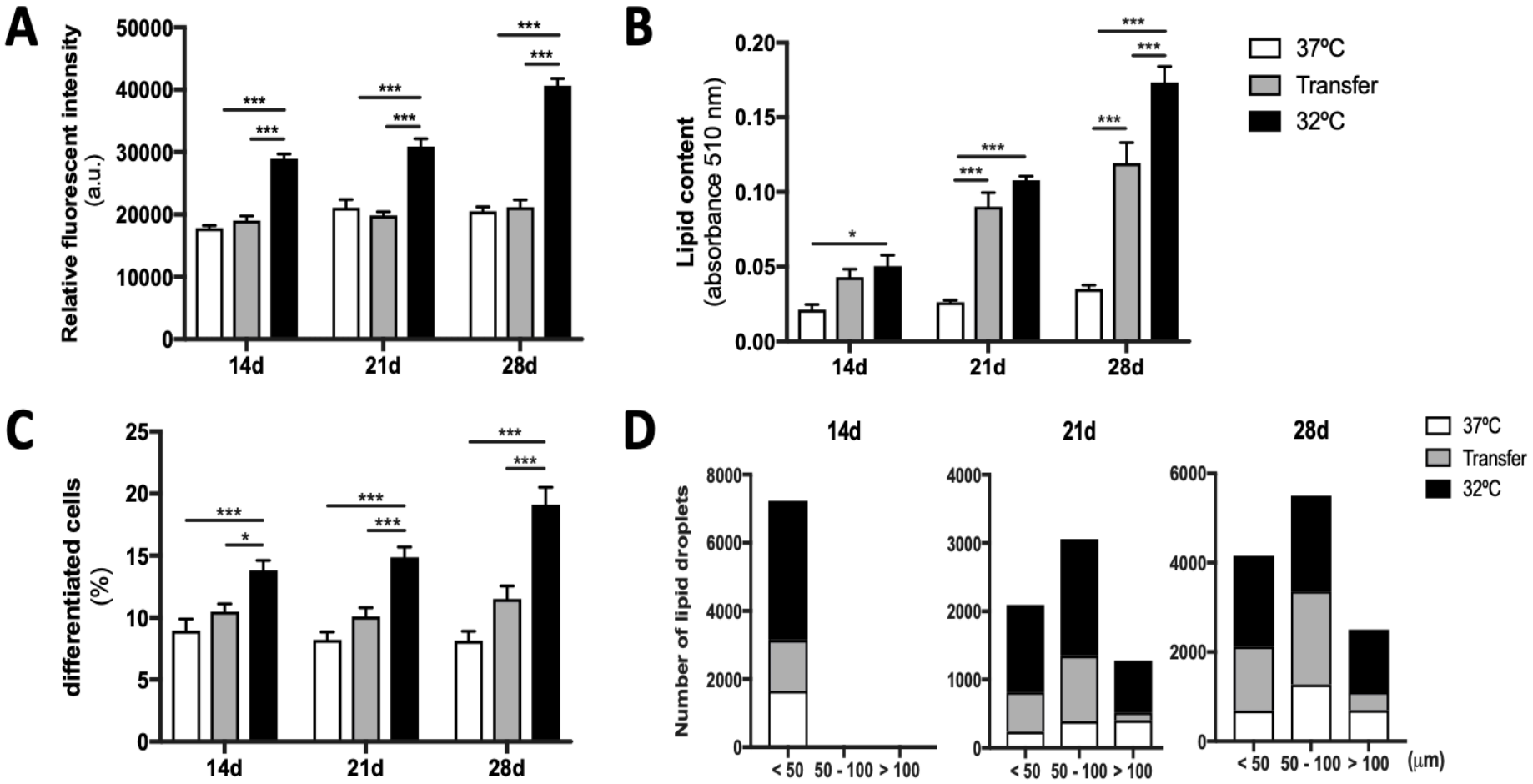

A
Relative fluorescent intensity
(a.u.)
50000
40000
30000
20000
10000
0
14d
21d
28d
B
Lipid content
(absorbance 510 nm)
0.20
0.15
0.10
0.05
0.00
37ºC
Transfer
32ºC
C
differentiated cells
(%)
25
20
15
10
5
0
D
Number of lipid droplets
8000
6000
4000
2000
1000
3000
< 50
50 - 100
> 100
(μm)

Figure 4.3. Cellular and morphological response of adipogenic MSCs differentiated under normal, Transfer and hypothermic conditions at 14, 21 and 28 days.
(A) Metabolic activity measurements in adipogenic cultures. (B) Lipid content measured by Oil Red O staining in adipogenic cultures. (C) Proportion of differentiated cells containing lipid droplets and (D) lipid droplet size measured for each condition and time-points, lipid droplets >50 μm were not detected on day 14. Data are shown as mean ± SEM. *p<0.05, **p<0.01, ***p<0.001.

.

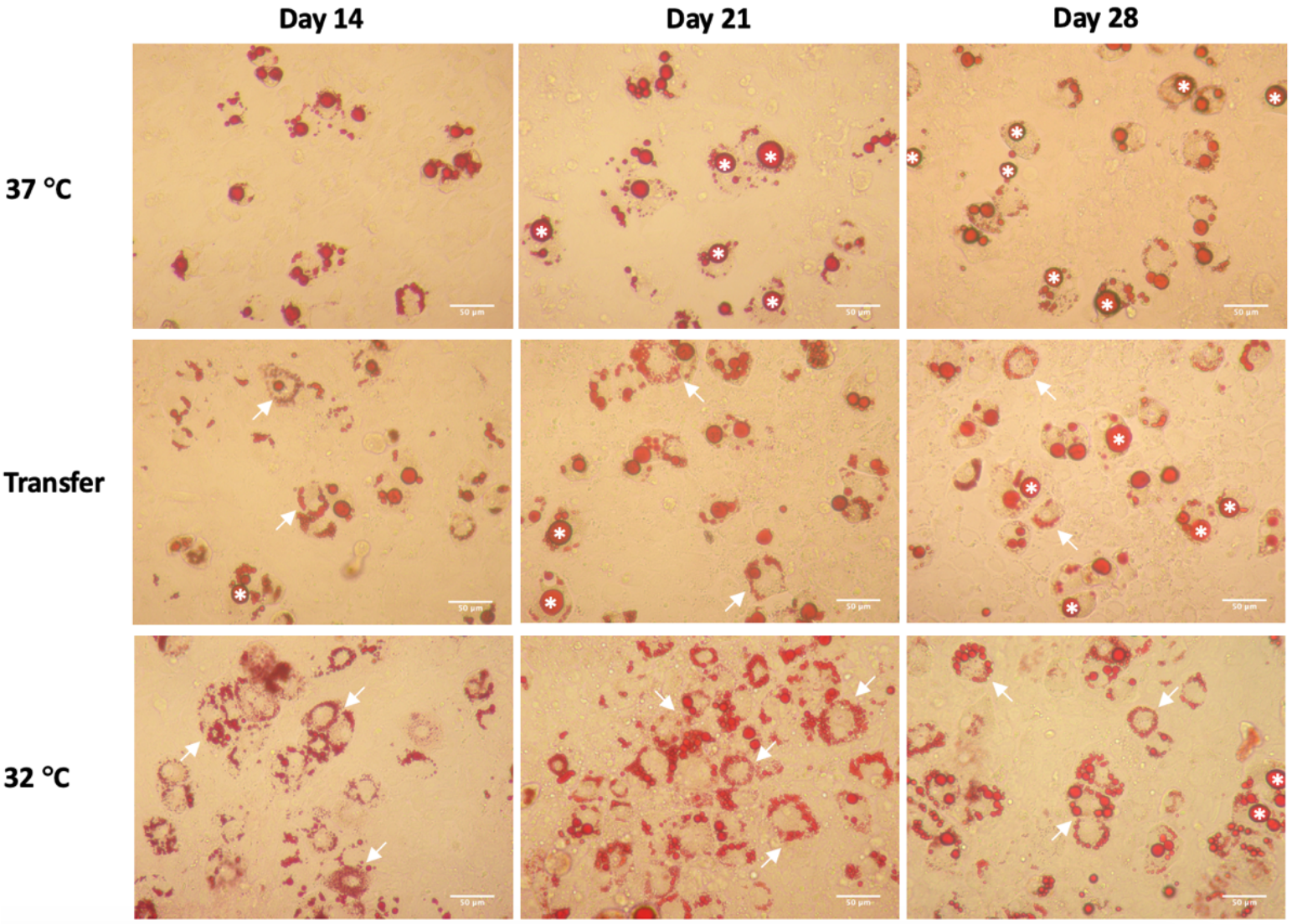

Day 14
Day 21
Day 28
37 °C
Transfer
32 °C

Figure 4.4. Oil Red O (ORO) staining of mMSCs differentiated under adipogenic treatment in normal, transferred and hypothermic conditions.
Representative images of ORO at day 14, 21 and 28 of differentiation treatment. Arrows indicate multilocular cells and asterisks indicates cells with one single lipid droplet.

4.4.2 Cold-induced adipocytes maintain brown-like marker expression when returned to 37°C for 21 days

In order to analyse gene expression and the effect of the temperature on the Transfer cells against normal and hypothermic adipocytes, RNA was normalized to 1 µg/µl and real-time PCR was performed (2.6 Molecular Biology, p. 57). Gene expression changes showed that while hypothermal conditions induced enhanced expression of adipogenic markers *AdipoQ*, *FABP4* and *PPARγ*, expression in Transfer cells was not significantly different from cells differentiated at 37°C (Fig. 4.5A). When evaluating brown markers, expression levels were higher in the hypothermal 32°C condition over the time-course, compared to MSC cells differentiated under normal conditions, and Transfer cells showed a dynamic pattern, with significantly higher UCP1 signal at day 14 and 21 which progressively decreased at later time-points, while *CIDEA* and *PRDM16* expression were maintained over the time-course. Expression of 2 other brown markers, *COX8b* and *LHX8*, also increased in Transfer cells compared to normal 37°C cultures, in a pattern comparable to that seen in hypothermal cultures (Fig. 4.5B). Three brown and beige markers were also evaluated: *DIO2*, *P2RX5* and *CITED* mRNA, but no significant changes for these markers were detected (Fig. 4.6). To evaluate adipocyte's response to T3 in Transfer cells via adrenoreceptors and calcium regulation, *β3-AR* and SERCA2 were also evaluated. Transfer cells showed an increased *β3-AR* mRNA by day 14 and 21 compared to 32°C differentiated adipocytes, and an intermediate mRNA SERCA2 expression (Fig.4.7).

To have a better understanding of the overall gene expression analysis, hierarchical clustering analysis (HCA) and principal component

analysis (PCA) of the common, beige and brown adipogenic expressed genes were performed. For HCA, datasets were grouped per gene, and then presented across the 3 time-points in order to show variation overtime. By day 28, HCA revealed that Transfer adipocytes exhibited an intermediate molecular signature, between that of normothermic and hypothermic culture conditions (Fig. 4.5C). When samples were analysed PCA adipogenic cells differentiated under normal 37°C culture conditions showed a more defined cluster at later time-points exhibiting homogeneity in gene expression, while Transfer cells overlapped with both 37°C samples and 32°C groups (Fig. 4.5D).

Both analyses confirmed MSC Transfer adipocytes exhibited an activated transitional state, showing MSC are able to differentiate under hypothermal condition culture and maintain brown gene expression after 21 days of being transferred to 37°C.

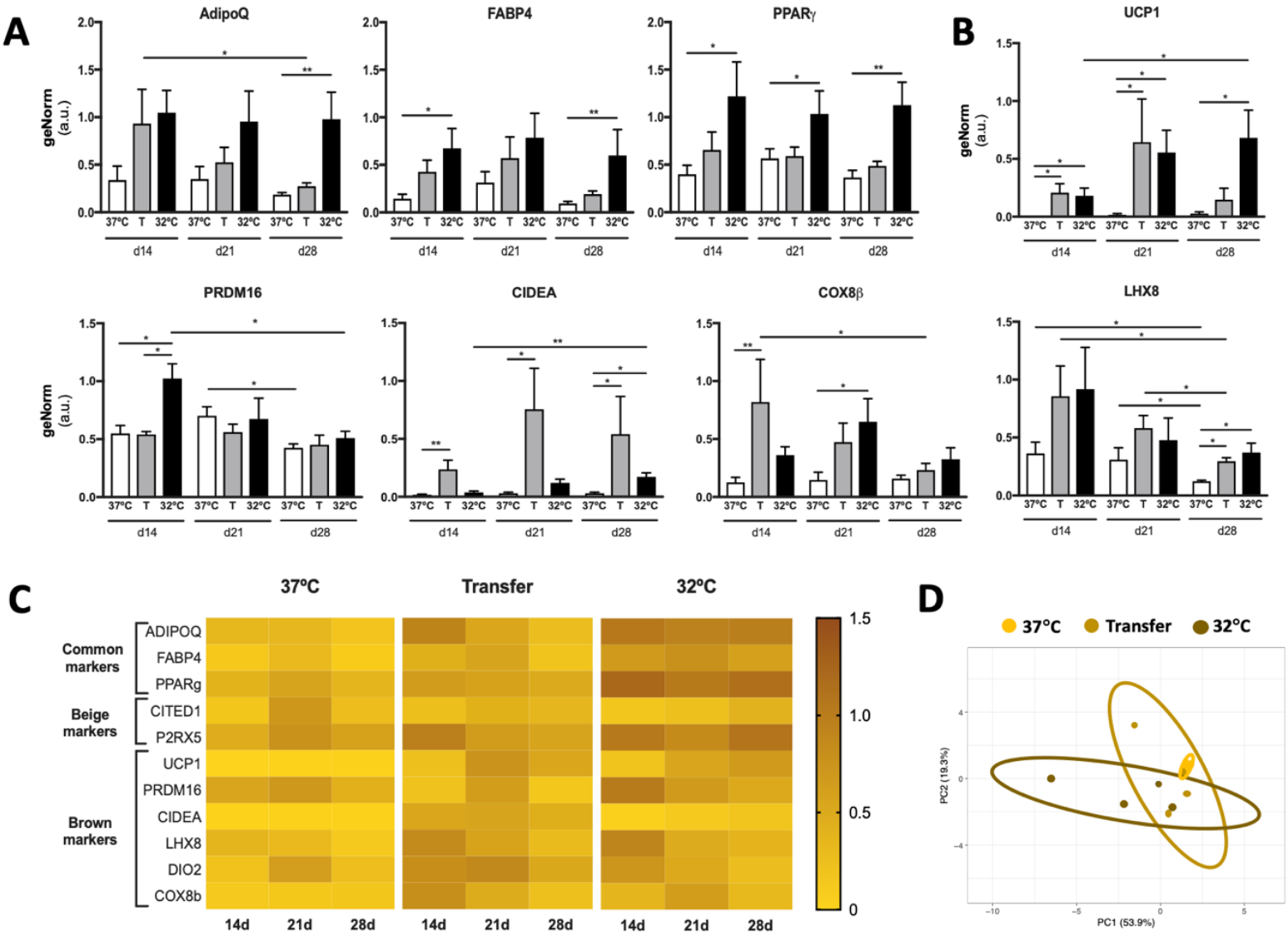

A
AdipoQ
FABP4
PPARγ
B
UCP1
PRDM16
CIDEA
COX8β
LHX8
geNorm (a.u.)
37°C T 32°C
d14 d21 d28
C
37°C
Transfer
32°C
Common markers
Beige markers
Brown markers
ADIPOQ
FABP4
PPARg
CITED1
P2RX5
UCP1
PRDM16
CIDEA
LHX8
DIO2
COX8b
14d 21d 28d
D
37°C Transfer 32°C
PC1 (53.9%)
PC2 (19.3%)

Figure 4.5. The effect of incubation temperature on gene expression patterns as determined by hierarchical clustering (HCA) and principal component analysis (PCA). (A) Expression levels of common adipogenic markers: Adiponectin, FABP4 and PPARγ. (B) Expression level of brown adipogenic markers: UCP1, PRDM16, CIDEA, COX8b, and LHX8. (C) Heatmaps of the GeNorm normalization on expression levels of common adipogenic markers: Adiponectin, FABP4 and PPARγ, beige adipogenic markers: CITED1 and P2RX5, and brown adipogenic markers: UCP1, PRDM16, CIDEA, LHX8, DIO2 and COX8b. Each row represents a gene while each column symbolises a timepoint at 14, 21 and 28 days -brown = high (1.5), yellow = low (0)-. (D) Scatter plots of the two principal components containing 73.2% of total variance for day 28. n = 4 individual experiments per timepoint. Data represent the mean of four replicas ± SEM. Statistical significance was set at $p < 0.05$. *p<0.05, **p<0.01, ***p<0.001.

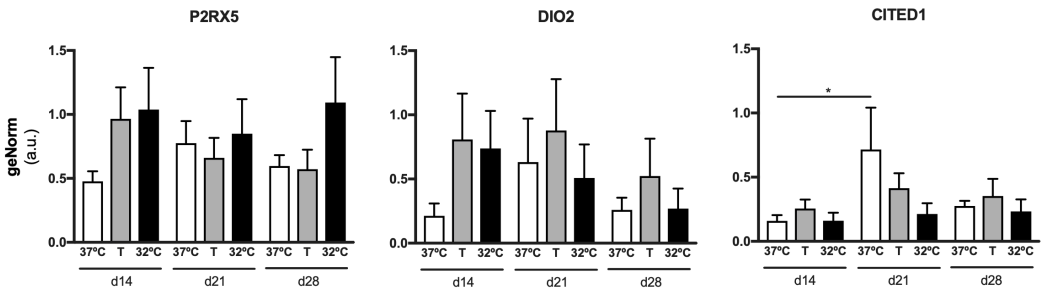


Figure 4.6. Changes in gene expression between normal, Transfer and hypothermic treatments of adipogenic MSC cultures at day 14, 21 and 28.

Expression of brown and beige adipogenic markers P2RX5, DIO2 and CITED1. All data was normalised using GeNorm. Data are shown as mean ± SEM. *p<0.05, **p<0.001, ***p<0.0001.

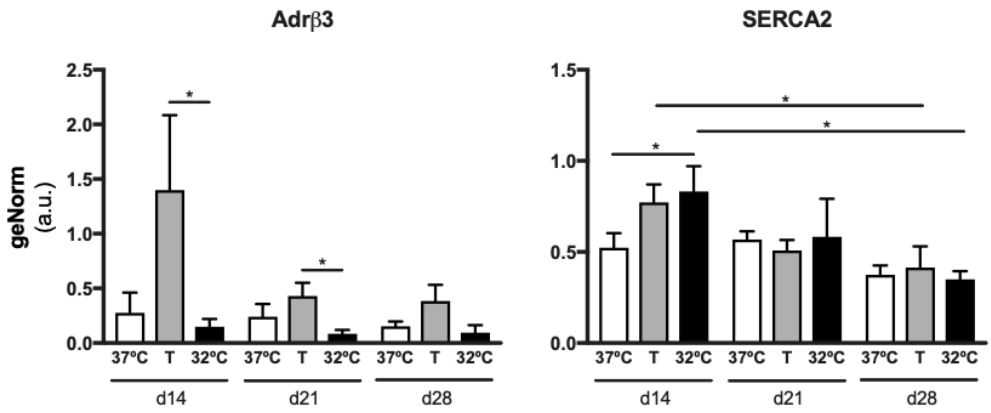


Figure 4.7. Changes in gene expression between normal, Transfer and hypothermic treatments of adipogenic MSC cultures at day 14, 21 and 28.

Expression of brown and beige adipogenic markers β3-AR and SERCA2. All data was normalised using GeNorm. Data are shown as mean ± SEM. *p<0.05, **p<0.001, ***p<0.0001.

To further explore the temperature responsiveness of Transfer adipocytes, expression of thermotransient receptor potential (TRPV) ion channels 1, 2 and 4 were evaluated. At day 14, *TRPV1* expression was significantly increased in Transfer cells and hypothermal conditions compared to normal 37°C conditions, and while *TRPV2* maintained a similar trend over the whole time-course, *TRPV4* only showed the same trend at day 28 (Fig. 4.8A). In order to detect if Transfer cells could be using both *UCP1*-dependent and independent thermogenesis, evaluation of intracellular calcium was done in all timepoints. Calcium measurements in Transfer and hypothermal differentiated cells showed higher intensity than cells differentiated under normal culture conditions (Fig. 4.8B), images of calcium staining corroborate fluorescent measurements (Fig. 4.8C and Fig.4.9). An overview of changes in *TRPV* expression pattern under the different treatments can be observed in Fig. 4.8D.

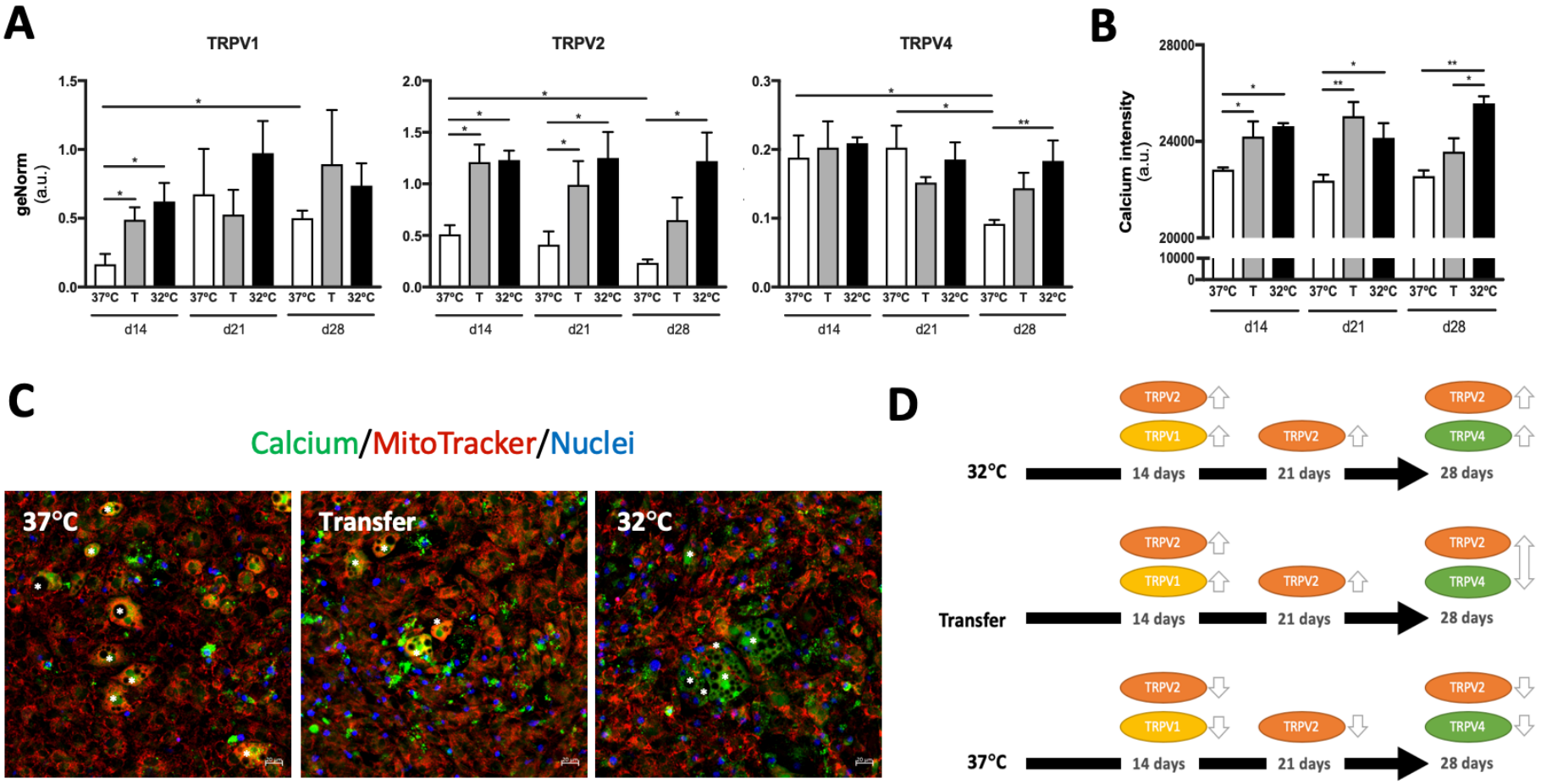

A
TRPV1
TRPV2
TRPV4
geNorm (a.u.)
37°C T 32°C
d14
d21
d28
B
Calcium intensity (a.u.)
C
Calcium/MitoTracker/Nuclei
37°C
Transfer
32°C
D
TRPV2
TRPV1
TRPV4
32°C
Transfer
37°C
14 days
21 days
28 days

Figure 4.8. Gene expression comparison of thermotransient receptor potential ion channels at same time-points by real time PCR.

(A) TRPV1, TRPV2 and TRPV4. All data was normalised using GeNorm. Data represent the mean of four replicas ± SEM. Statistical significance was set at $p < 0.05$. (B) Calcium intensity measurements 494/516. Data represent the mean of three replicas ± SEM. Statistical significance was set at $p < 0.05$. (C) Representative images of calcium staining (Fluo-4 - green) at day 28. Asterisks indicate differentiated cells showing calcium staining. Scale bar: 20 μm. (D) Summary of changes in TRPV expression pattern under the different treatments. Arrow pointing up and down means no significance between 37°C and 32°C treatments.

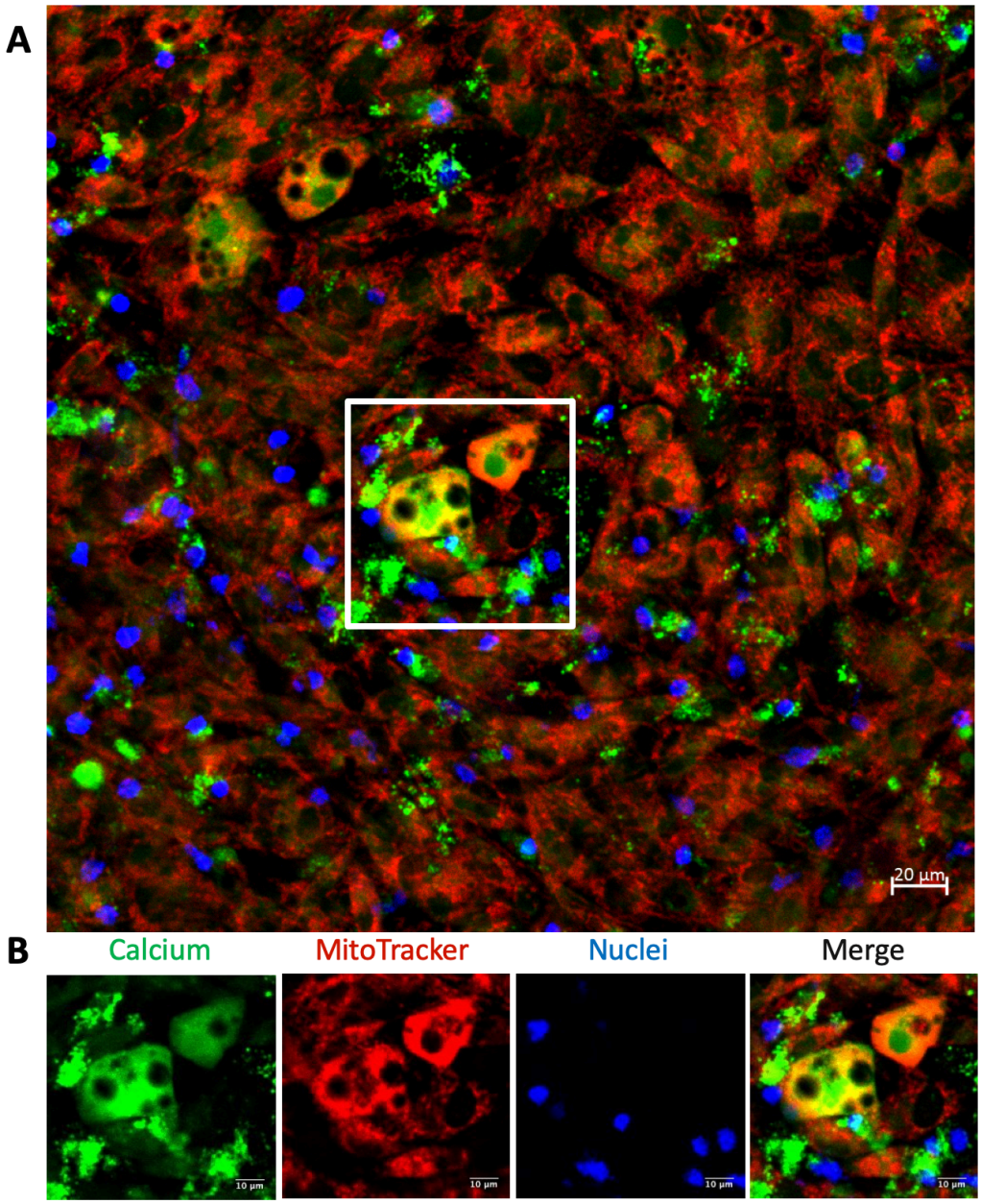


Figure 4.9. Zoom image of Figure 4.8D Transfer. Live staining showing calcium staining in Transfer cells at day 28.

(a) Representative image showing the prevalence of calcium staining (Fluo-4 Direct in green), MitoTracker (red), Hoechst 33258 was used to identify nuclei (blue). The dashed square highlights difference in staining between two adjacent adipocytes. Scale bar: 20 µm. (b) Enlarged view of the square area, with individual and merged images showing adipocytes positive for both calcium (green) and MitoTracker (red). Scale bars: 10µm. n = 3 individual experiments.

4.4.3 Metabolic function of cold-induced adipocytes is modified when returned to a thermoneutral environment

Metabolic function was analysed by a Seahorse XF96 flux analyser (Chapter 2.4.2 Seahorse assay, p. 50). OCR and ECAR readings were taken over time under basal conditions and after the addition of mitochondrial inhibitors (2.5 μM oligomycin, 0.5μM FCCP and 1μM rotenone/antimycin). The higher rate of oxygen consumption in cells maintained at 32°C was not sustained when these cells had been transferred to 37°C (Fig 4.10A). Transfer cells were however able to upregulate glycolysis to meet the requirement for ATP when upon FCCP stimulation (Fig 4.10B), reflecting an intermediary bioenergetic status in these cells, in which glycolysis rather than mitochondrial respiration was enhanced. No differences were observed when analysing basal respiration, ATP production, proton leak and non-mitochondrial oxygen consumption when Transfer cells were compared to normothermic conditions.

The bioenergetic status of Transfer cells was characterised by an intermediary profile, showing a maximal respiration and spare capacity higher than cells differentiated at 37°C, but significantly lower than cells differentiated at 32°C. Additionally, coupling efficiency of Transfer cells showed no significant difference between hypothermal 32°C cultures when compared to constant 37°C condition (Fig 4.10C). When plotting basal ECAR against OCR, Transfer adipocytes showed increased glycolysis and mitochondrial respiration reflecting more metabolically active cells following their acclimatisation to normal culture conditions (Fig 4.10D).

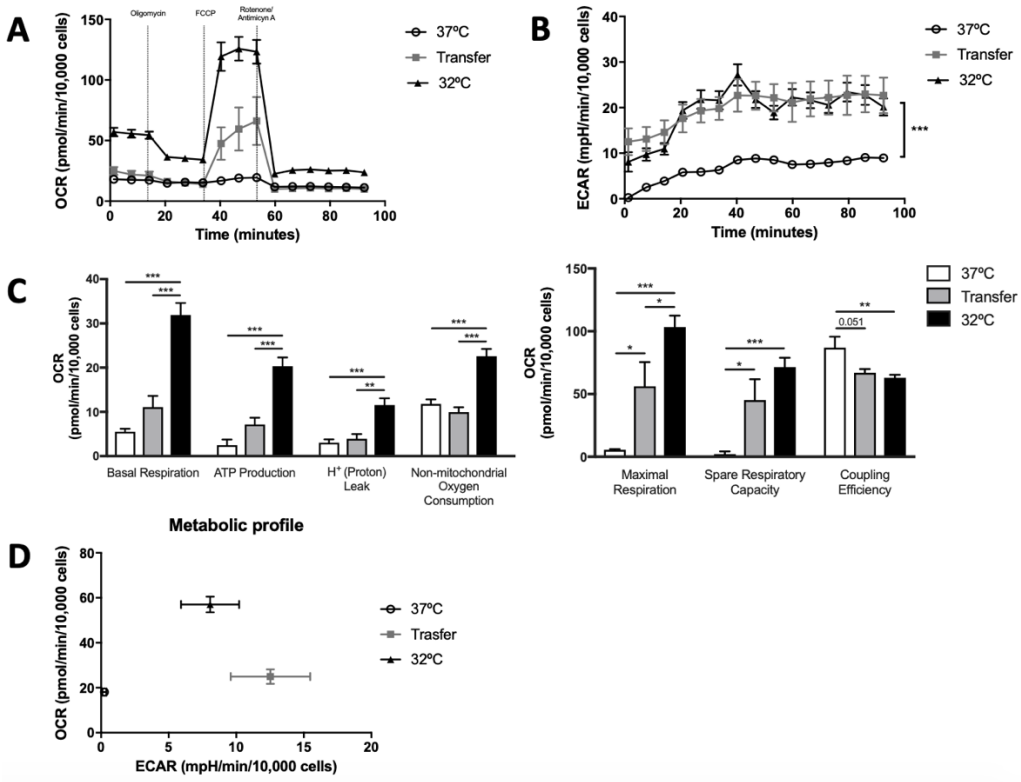


Figure 4.10. Effect of incubation temperature on the bioenergetics status of adipogenic MSC cultures after 28 days.

(A) Oxygen consumption rate (OCR), (B) Extracellular acidification rate (ECAR), (C) mitochondrial function calculated from the bioenergetics profile (basal respiration, ATP-linked respiration, proton leak, non-mitochondrial respiration, maximal respiration, spare respiratory capacity and coupling efficiency) and (D) metabolic profile. Data shown as mean ± SEM, n = 6 individual experiments. *p<0.05, **p<0.01, ***p<0.001.

4.5 Discussion

Mesenchymal stem cells can form adipocytes, and exposure to hypothermic conditions has been shown to trigger the induction of brown-like properties, including morphological, biometabolic and molecular traits[92,144].

It was hypothesised that cold mMSCs derived adipocytes are able to maintain beige like properties after 21 days of being transferred to normal culture conditions (37°C). Therefore, the present study investigated whether these brown-like cells produced *in vitro* at 32°C were able to adapt to environmental changes, and whether their acquired traits may be reversible over time. To this end, adipocytes differentiated from MSCs at 32°C following an established protocol[92] were then transferred to normal 37°C culture conditions, and their capacity to maintain brown features was analysed over 3 weeks of subsequent culture.

4.5.1 The bioenergetics benefits are retained

Mitochondria evaluation in Transfer adipocytes showed a significant decrease overtime when compared to adipocytes differentiated in hypothermic conditions. Nonetheless, *UCP1* protein expression was maintained over the course of the treatment as well as in 32°C adipocytes. These results paired with *COX8b* mRNA reduction[209] suggest a decline in mitochondrial content once the browning stimulus is removed, possibly as a step towards whitening[157]. Although the presence of T3 in the differentiation medium[69,101] was not by itself sufficient to trigger an increased bioenergetics capacity nor mRNA

UCP1 expression in MSC-derived adipocytes when maintained under normal 37°C conditions, an increase in UCP1 protein expression overtime was observed. However, it would be interesting to show if T3 is a key player on the rewarming conditions or if temperature by itself is enough to maintain this brown signature.

The bioenergetic analysis further showed that Transfer adipocytes could be activated when the mitochondrial uncoupler FCCP[210] was added, displaying higher OCR, ECAR, maximal respiration, spare capacity and metabolic profile than adipocytes differentiated at 37°C, which reflect a transitional bioenergetic status in which glycolysis rather than mitochondrial respiration was enhanced. Glycolysis has been confirmed to support full adipocyte thermogenesis in BAT by providing pyruvate formation and other intermediates for metabolic pathways as well as maintaining oxygen consumption rates[211] alongside *in vivo* evidence shows that intracellular glycolysis acts by controlling short-term nonshivering thermogenesis[212]. These results suggest that Transfer cells maintain a high glycolytic rate in order to replenish ATP when uncoupled oxidative phosphorylation and thermogenic activation is occurring[211]. Altogether with the mitochondrial measurements and increased UCP1 protein expression[213], show that Transfer cells are metabolically activated by enhancing lipolysis and fatty acid oxidation, agreeing with a previous report done in 3T3-L1 adipocytes treated with FCCP[210]. These observations also suggest that beige MSC-derived adipocytes have a distinctive bioenergetic response, as these cells can both store lipids and produce heat when stimulated[65], adding to previous *in vitro*[92,144] and *in vivo*[99,214] reports to highlight MSCs as a source of adipocytes that can be used to study brown/beige adipogenesis.

4.5.2 The induced brown-like phenotype is not fully reversible

When evaluating the phenotype of Transfer culture treatment, cultures exhibited an intermediary amount of lipid content, morphology and percentage of differentiated cells more similar to that of cells kept at 32°C than that of cells differentiated under normothermic culture conditions. This is in accord with the two main processes of brown adipocyte generation, i.e. *de novo* and trans- differentiation[79]. Additionally, lipogenesis and lipolysis, two key mechanisms in brown adipocytes, are required for *UCP1* proton transport[215,216] which could explain why adipocytes that were differentiated in hypothermal and in Transfer conditions contained more lipid content and differentiated cells over the course of the treatment. Even though Transfer cells possessed significantly less mitochondria than hypothermic differentiated adipocytes, their ability to retain *UCP1* protein could be due to the capacity to maintain a brown/beige morphology with multilocular LDs, which provided more substrate availability than possessing larger or unilocular LDs.

4.5.3 Beige-brown marker expression

Following the discovery that human BAT may be essentially comprised by beige adipocytes[184], a recent interest on beige adipocyte gene expression maintenance has been investigated, however this process remains unclear. This study showed that expression of common adipogenic genes was followed by cell morphological changes, lipid content and percentage of differentiation, with Transfer adipocytes acquiring a transitional pattern for mRNA expression. A decrease in *AdipoQ* mRNA was observed, a marker which has been directly related

with obesity[217], however maintenance of *FABP4* and *PPARγ* suggested a persistence in brown signature as these two genes play an important role in brown adipocyte physiology and functioning[218,219].

One of the objectives to achieve was to examine the brown/beige molecular signature of Transfer adipocytes, in order to do this evaluation several markers were selected. Is widely known that *UCP1* expression is present in brown and beige adipocytes, to uncouple respiration and consume energy in the form of heat[145,158,220–222], however recent studies reports beige transition to white occurs after 15 days of stimuli withdrawal, in which these cells lose their brown characteristics, specifically *UCP1* mRNA and protein signature[144,157]. Here, Transfer differentiated cells showed a similar *UCP1* mRNA and protein expression to 32°C differentiated adipocytes after 3 weeks of acclimation, demonstrating the ability of these cells to retain their uncoupling capacity after being returned to warm conditions. The intermediary *COX8b* mRNA expression of Transfer cells could be indicative of their response to stress under conditions of increase energy demand, since *COX8b* is involved in respiratory electron transport and has been recently described to mark beigeing in mouse WAT[60]. Calcium levels observed in Transfer adipocytes in addition with high *β3-AR* mRNA expression and SERCA2 mRNA intermediate expression at day 14 could suggest a regulation of SERCA2 by intracellular calcium[223], since cold exposure could activate *β3-AR* and lead to increase intracellular calcium by activating SERCA2 in beige adipocytes[163]. However, a decrease of *UCP1* and *COX8b* after 3 weeks paired with an intermediate bioenergetic profile, enhanced glycolysis and high intracellular calcium intensity of Transfer cells could suggest

a shared mechanism of calcium mediated *UCP1*-independent thermogenesis[163].

Furthermore, high expression of the classical beige and brown adipogenic markers *CIDEA*[60] and *LHX8*[224–226] was detected on Transfer cells. *CIDEA* plays a major role in controlling lipid storage, lipid droplet fusion[227,228] and uncoupling *UCP1* activity in BAT upon cold exposure[60]. Here, its high expression could be involved in maintaining the intermediate morphology seen in Transfer adipocytes[229], by mediating the growth of LDs upon acclimatisation to normal culture conditions and controlling lipogenesis and lipolysis[228]. Moreover, the substantial increase in *CIDEA* in Transfer cells agrees with previous data showing that besides *UCP1* and *LHX8*, *CIDEA* represents the best marker to evaluate the beige-ing of WAT during cold treatment[60].

The persistence of brown-like properties under changing conditions might hint at epigenetics mechanisms controlling the adipogenic response in MSCs[230,231]. In particular, cold exposure has been reported to promote chromatin remodelling triggered by JMJD1A (histone H3 lysine 9 (H3K9) demethylase) phosphorylation[231,232]. Based on the above results it is suggested that the molecular signature of Transfer adipocytes is somewhat distinct from that of cells differentiated under constant 37°C or 32°C conditions. Our results align to an extent with that reported by Altshuller-Keylin and colleagues, who described that a full transition of beige to white adipocytes lasted 15 to 20 days[157]. Here an intermediate beige molecular signature was still present 3 weeks after transferring adipocytes back to standard 37°C temperature, highlighting the plasticity of MSCs to generate and preserve *de novo* beige adipocytes.

4.5.4 Temperature sensing channels

This study revealed a complex interaction between *TRPV1*, 2 and 4 over the course of the differentiation treatments. *TRPV1* has already been described to increase when cold stimulation is applied to adipocytes[92,144], and its activation at a pre-adipocyte stage could be clinically beneficial by increasing intracellular calcium levels and preventing adipogenesis[161]. Furthermore, *TRPV2* mRNA expression is known to augment in differentiated mouse brown adipocytes[165,233]. Here, it could be that a cascade of *TRPV* channels is necessary to retain the bioenergetics response, starting with the activation of *TRPV1*, maintenance of *TRPV2* and finally the activation of *TRPV4*. Sun and colleagues showed that *TRPV2* not only is the highest expressed thermoreceptor channel member but is also essential in brown adipocytes thermogenic function[164,165,233]. Taking into account calcium importance in *UCP1*-dependent[234] and *UCP1*-independent adipocyte thermogenesis[155,163,234], it is possible that *TRPV2* is one of the main regulators for beigeing maintenance and/or temperature sensing mechanism of cells[233]. Although the role of *TRPV4* has been diversely reported[200,235], Transfer cells display a similar pattern to 32°C adipocytes in *TRPV4* and UCP1 mRNA expression by day 28. These results together with bioenergetics response could indicate a positive correlation with *TRPV4* intermediate expression and browning, this observation support it as one of the main regulator of BAT oxidative metabolism[162]. Further investigations on *in vivo* activation of TRPVs could be used as an approach to modulate obesity and related disorders.

Finally, the second objective of this investigation was achieved, it was possible to evaluate T3 and cold exposure in mMSCs as pro-adipogenic *in vitro* regulator and environmental stimuli, respectively. Overall, these results suggest that MSCs differentiated under Transfer conditions may retain some brown-like features rather than completely reverting to a white phenotype, even after extended incubation in normal temperature culture conditions over 3 weeks. This indicate a type of cellular memory reflecting prior environmental culture conditions. It could thus be useful to monitor the epigenetic status of differentiating MSCs upon change in temperature conditions, and to evaluate potential overlap with genes involved in obesity. These results also underline MSCs as an accessible cell source to model the differentiation and maintenance of beige adipocytes.

Chapter 5. Isolation and media optimisation of hUCT MSCs

5.1 Main findings

- hUCT-MSCs can be isolated with an enzymatic method using Collagenase B.
- MSCs isolated from hUCT are able to successfully grow in a medium containing human platelet lysate.
- hUCT-MSCs co-express CD90 and CD105, as well as CD73 and CD105.
- MSCs derived from hUCT can differentiate into adipocytes.

5.2 Introduction

MSCs are plastic adherent cells with specific surface antigen expression; such as cluster of differentiation (CD) 73, CD90 and CD105 positive expression and negative expression of CD11b, CD14, CD19, CD34, CD45, CD79α and HLA class II[5]. MSCs have become an attractive therapeutic tool because their distinctive characteristics to differentiate into several cell types including osteoblast, adipocytes, chondroblast and myoblast[5,7]. MSCs are easily isolated from different tissues such as bone marrow[186,236], adipose tissue[236], dental pulp[237], placenta[112], umbilical cord blood and umbilical cord tissue[111,238]. Umbilical cord tissue (UCT) is a rich source of mesenchymal stem cells (MSCs) and is known to possess higher amount of MSCs than cord blood[111]. MSCs are multipotent cells with high self-renew capacity and immune modulation properties.

Also, hUCT is an alternative source of MSCs from a disposable tissue after delivery and its collection is non-invasive. Moreover, it has been reported that cells isolated from fresh or frozen tissue have the same ability to grow, differentiate and express same MSC markers[113]. For these reasons, hUCT appears to be an ideal source of MSCs which make them attractive for research and clinical application, such as graft-versus-host disease, and diabetes mellitus types 1 and 2 and many others[171,186,239].

Although many efforts to standardize the isolation and culture of MSCs from hUCT have been done, literature on how to isolate and culture these cells is not consistent. Currently there are several techniques used which makes its standardization difficult. Firstly, some authors consider the isolation of whole UCT[240–243], Wharton's jelly region[244–247],

or hUCT vessels[248], using different isolation methods: enzymatic and explant protocols. Non-enzymatic isolation involves cutting the UCT into small pieces, explants of approximately 10 mm, and making incisions on the inner matrix to expose more tissue to contact with the culture medium[170,249,250]. Enzymatic disaggregation can be done by mincing the tissue manually or using a Miltenyi GentleMACS Dissociator (#130-093-235) with different enzymes varying from collagenase type I[250,251], type IV[252], a mixture of collagenase/hyaluronidase/trypsin[170] and/or collagenase B[253]. Secondly, the ability of the cells isolated from the hUCT has been questioned, as some report that these cells lack the multilineage ability to differentiate[254,255], while others claim only certain cell populations found in hUCT are able to differentiate[110,256], others report an easy multilineage differentiation capacity[240,241,257]. Thirdly, different types of media have been used to culture and expand hUCT-MSCs. Media types vary with respect of the amount of serum and other supplements[258,259] included. Some use FBS (foetal bovine serum), or FCS (foetal calf serum) and others hPL (human platelet lysate) or HS (human serum), and it has also been described that serum free media can be used for MSCs culture and expansion[260]. FBS is the most extensively used serum supplement for *in vitro* culture of MSCs due to its relatively easy production and rich content of growth factors and hormones that stimulate cellular proliferation, differentiation and maintenance[258]. On the other hand, several alternatives have been evaluated numerous studies describing the preparation and efficient use of hPL have been done[259]. Different recipes show DMEM with high glucose (4.5 g/l), supplemented with 10% FBS or HS[261]; or DMEM low glucose (1 g/l) supplemented with 10% FBS[170]; DMEM F12

supplemented with 10% FCS[110]; DMEM low glucose supplemented with L-glutamine and 10% hPL[172], all media containing 1% of penicillin and streptomycin (P/S). One of the main goals is to use a xenogeny-free medium, that provides robust expansion of MSCs and be suitable for clinical manufacturing[172].

This chapter evaluates two different isolation methods, three growth media and two adipogenic recipes in order to find which technique and media are suitable for culturing hUCT-MS cells. Results showed hUCT-MSCs can be obtained from both enzymatic, using Collagenase B, and explant methods cultured in DMEM low glucose supplemented with L-glutamine, hPL and P/S with a doubling time of 22.8 ± 4 h. Furthermore, MSCs isolated from hUCT showed plastic adherence, fibroblastic-like shape and co-expression of CD73 with CD105 and CD90 with CD105. Finally, cells are able to differentiate into adipocytes using a different medium from the one they were grown, containing DMEM F12, 10% FBS and 1% P/S supplemented with 10μg/ml insulin, 1 μM rosiglitazone, 500μM IBMX and 1 μM dexamethasone.

5.3 Methods

For the optimization of the isolation method one hUCT (#851-Chapter 2. Table 2.1, p. 46) was collected from the Anthony Nolan centre, 24 cm long approximately, tissue was cut in half. The isolation of MSCs from hUCT two protocols were tested, as described in Chapter 2.3.2 hUCT isolation, p.44 (Figure 2.1, p. 46).

The first protocol was performed in the first half of the hUCT using the tissue explants technique, no problems were encountered when processing the tissue, it was a straightforward method and easy to follow (Fig. 5.1). For the second protocol, the other half of the hUCT was minced (Fig. 5.2) and then the enzymatic method with Collagenase B was implemented, a technical problem was faced in the filtration step, as disaggregated hUCT became very thick and unable to easily be filtered. For this reason, the remaining unfiltered tissue was seeded immediately after the neutralisation step in each of the mediums described before. For the unfiltered tissue, remaining from non-digested tissue, approximately 5 mm, could be seen when seeded into the flasks. This tissue was carefully kept during the medium changes until cells reached 60-70% confluency. In summary, three isolation protocols were evaluated parallel with three culture media (Figure 2.1, 2.3.2 hUCT isolation, p. 44)

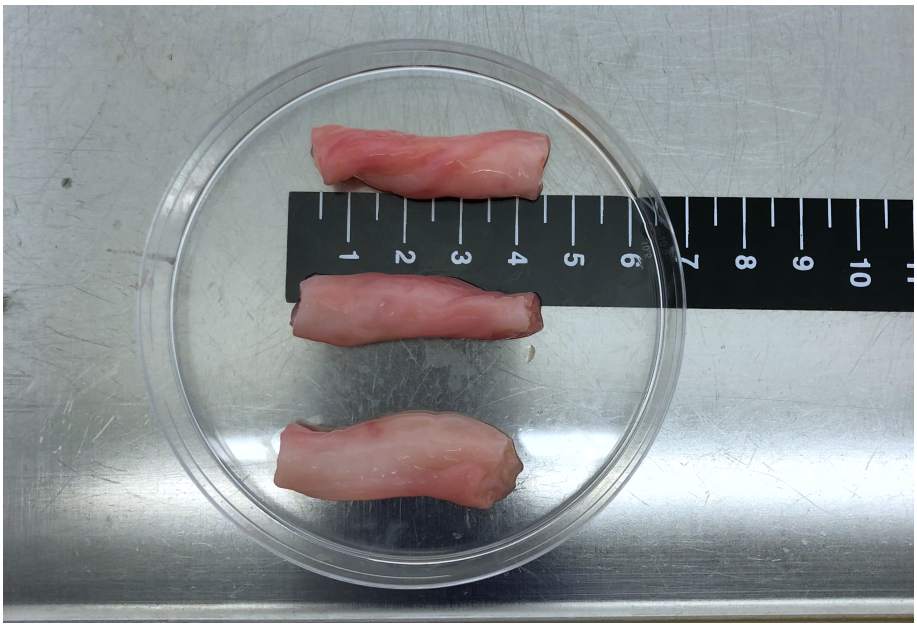


Figure 5.1. Picture of the first half of the hUCT before processing for explants. Each piece was cut in four 10 mm pieces.

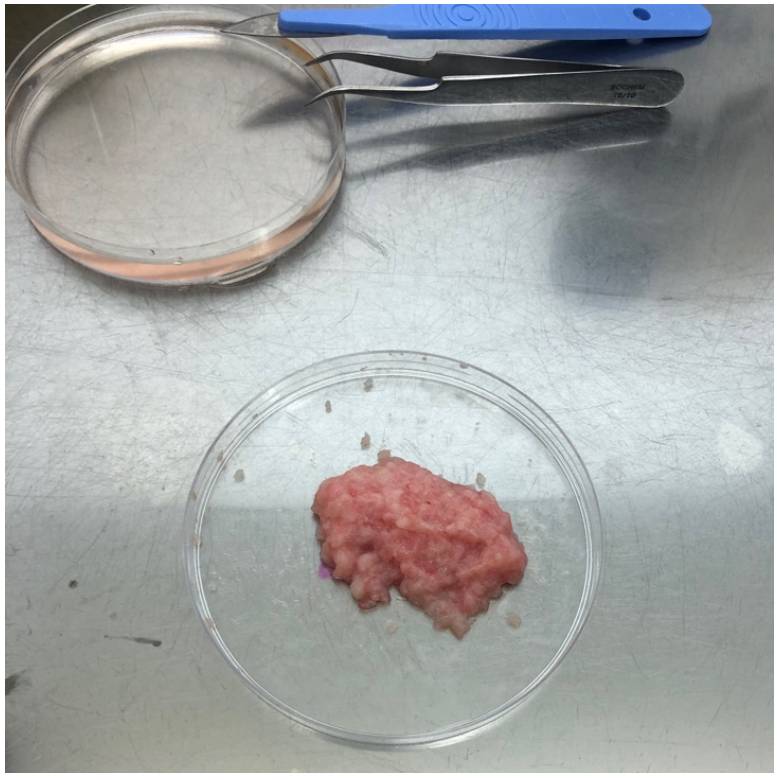


Figure 5.2. Picture of the second half of the hUCT after the mincing process and before the collagenase step.

5.4 Results

5.4.1 Media evaluation for hUCT MSCs expansion

Three different MSC media were evaluated in order to determine with one provided a heathy status and rapid growing time on hUCT MS cells (Chapter 2.3.4 hUCT-MSCs culture, p. 47).

Results showed the explants method was not successful with medium one and two, while explants from medium number three managed to grow some MSC-like cells (Table 5.1 - Explants). When the enzymatic method with filtering was evaluated, no cells were observed in the flasks from method number two. Regarding the other two mediums (one and three), due to the small number of cells isolated with this method, they were not able to proliferate successfully and reach confluency. Table 5.1 shows number of cells obtained per passage from the third method, variation of the enzymatic method (unfiltered tissue), which resulted in the best of the three methods evaluated. With this method, each medium managed to grow MSC-like cells, the doubling time was 36.66± 0.5 h, 47.68 h and 22.8 ± 4 h for medium one, two and three, respectively (Table 5.1). To confirm these results, a second DT was performed only on cells grown in medium three, giving an average of 26.65 h over ten passages (Fig. 5.3). Moreover, hUCT MS-like cells from every media exhibited an elongated healthy morphology, forming colonies and attaching to plastic in each passage (Figure 5.4).

As shown in Figure 5.4 cells cultured in medium one and two exhibited a similar morphology when compared to cells cultured in medium three. However, cells cultured in medium three appeared to have a smaller size which could be the reason of harvesting more cells from medium three in each passage. Finally, it was determined that the enzymatic method (Collagenase B) without filtration step accompanied by medium number three were the best methods to isolate and grow hUCT MS-like cells, respectively.

Table 5.1. Cell number according to MSC medium used from different passages and doubling time (DT) calculation.

MEDIUM	P0	P1	P2	P3	DT
1	4.12 x 10^5 cells/T75 flask 04.04 (412,000 cells seeded)	1.3 x 10^6 cells/T75 Total frozen: 2.6 x 10^6 09.04 (330,000 cells seeded)	8.25 x 10^5 cells/T75 Total frozen: 1.6 x 10^6 11.04 (110,000 cells seeded)	2.150 x 10^6 cells/T75 Total frozen: 2.150 x 10^6 17.04	36.66 ± 0.5 h
2	4.5 x 10^5 cells/T75 flask 07.04: (450,000 cells seeded)	1.725 x 10^6 cells/T75 Total frozen: 3.3 x 10^6 14.04: (333,000 cells seeded)	2.587 x 10^6 cells/T75 Total frozen: 5.1 x 10^6 18.04: (630,000 cells seeded)	1.950 x 10^6 cells/T75 Total frozen: 5.85 x 10^6 21.04	47.68 h
3	1.3 x 10^6 cells/T75 flask 07.04: (216,000 cells seeded)	2.737 x 10^6 cells/T75 Total frozen: 14.415 x 10^6 11.04: (456,000 cells seeded)	3.075 x 10^6 cells/T75 Total frozen: 6 x 10^6 14.04: (566,000 cells seeded)	3.338 x 10^6 cells/T75 Total frozen: 10 x 10^6 16.04	22.8 ± 4 h
Explants	4.7 x 10^5 cells/T75 flask	2.3 x 10^6 cells/T75 Total frozen: 4.6 x 10^6			

A

Passage	Initial cell number	Final cell number	Time (h)	DT (h)
0	Thawed 1x10^6		72	-
1	-	945,000	48	-
2	157,500	887,500	48	28.86
3	221,875	1,075,000	48	21.08
4	268,750	1,012,000	48	25.08
5	253,125	1,506,250	48	18.65
6	376,562.5	1,068,750	48	31.89
7	267,187.5	746,000	48	32.40
8	186,500	789,473	48	23.06
9	197,368	1,065,789	48	29.59
10	266,447	828,947		29.31

B

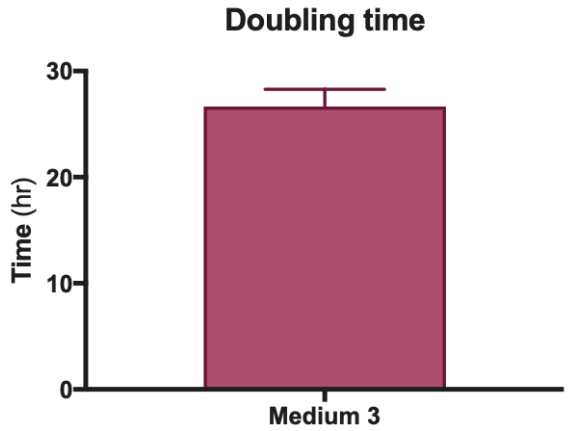


Figure 5.3. Doubling time of hUCT-MSCs cultured in medium three.

Cells were thawed at passage 0 and passaged ten times, in each passage cells were counted twice manually with a haemocytometer to calculate doubling time. (A) shows initial cell seeded number, final cell number after 72 or 48 h and doubling time calculated. (B) shows average doubling time of 26.65 h. Data are shown as mean ± SEM of the nine doubling times calculated.

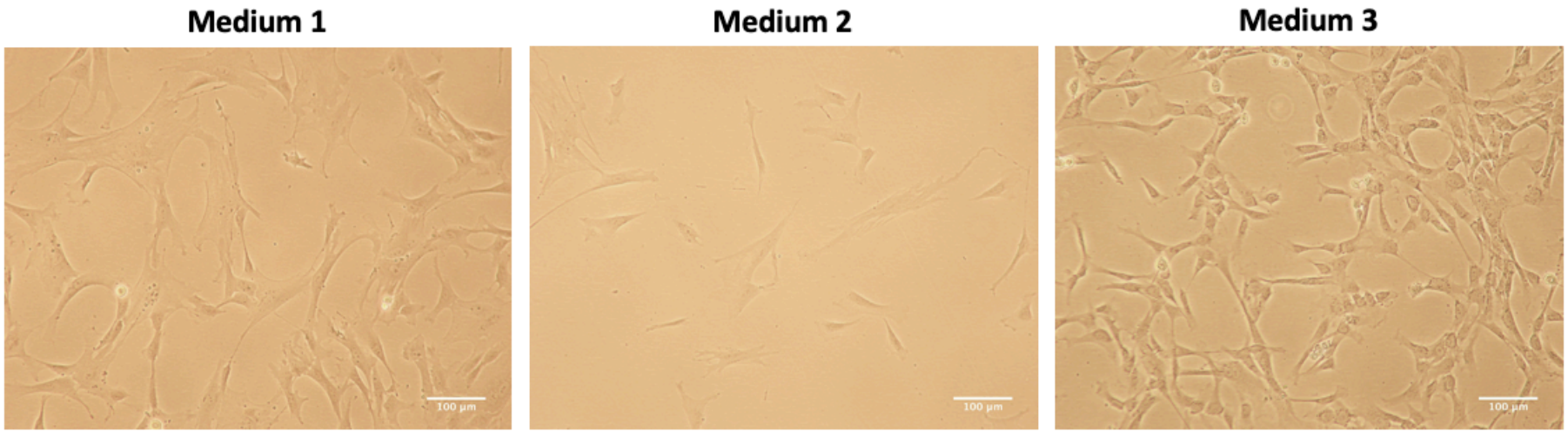


Figure 5.4. hUCT MSC-like isolated with the collagenase method without filtration from donor 851 in medium one, two and three. Representative images were taken from each flask at same passage (P2). Scale bar 100 µm.

According to Dominici et al, minimal criteria to define human MSCs should be followed. First, MSCS should be plastic adherent when maintained in standard culture conditions. Second, MSCs must express certain markers such as: CD73, CD90, CD105, and lack expression of CD11b, CD14, CD34, CD45 or CD79α and HLA-DR membrane markers. Third, MSCs must differentiate into osteoblast, adipocytes and chondroblast *in vitro*[5].

5.4.2 Immunofluorescence characterization of hUCT-MSCs

Here, cells isolated from donor 851 were stained for positive CD73, CD90 and CD105 individual markers. Fig. 5.5 shows the majority of the stained cells positive for each individual marker.

To further investigate if the isolated hUCT-MSCs cells positively co-express two out of the three CD73, CD90 and CD105 markers, cells were immunostained for each marker. Fig. 5.6 shows many cells have positive co-expression of the two membrane markers.

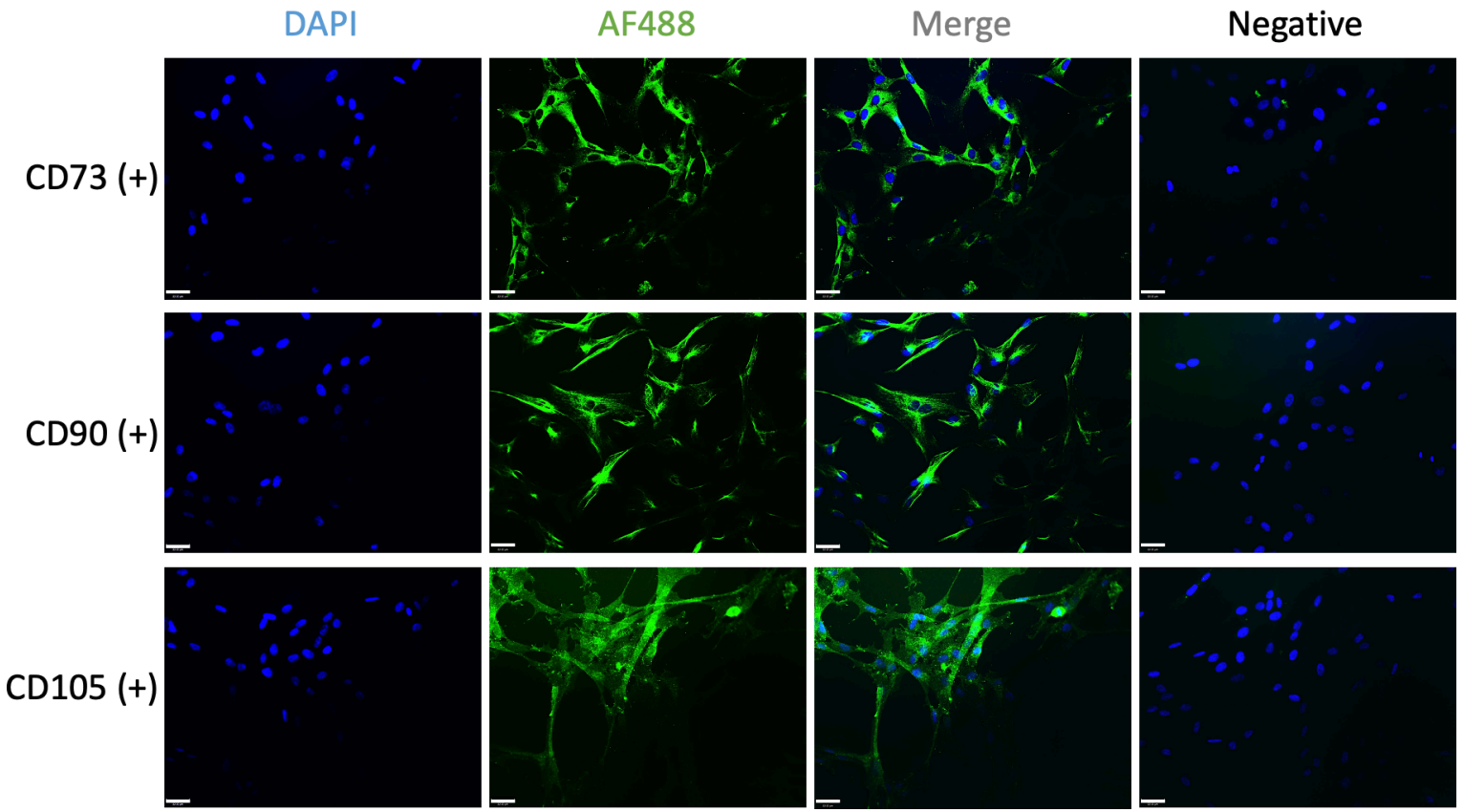


Figure 5.5. hUCT-MSCs stained individually for CD73, CD90 and CD105.
Nuclei is stained in blue (DAPI), primary antibodies were coupled with Alexa Fluor 488 (green). Representative images were selected. Cells were stained at passages 1 and 2. Scale bar: 32 μm.

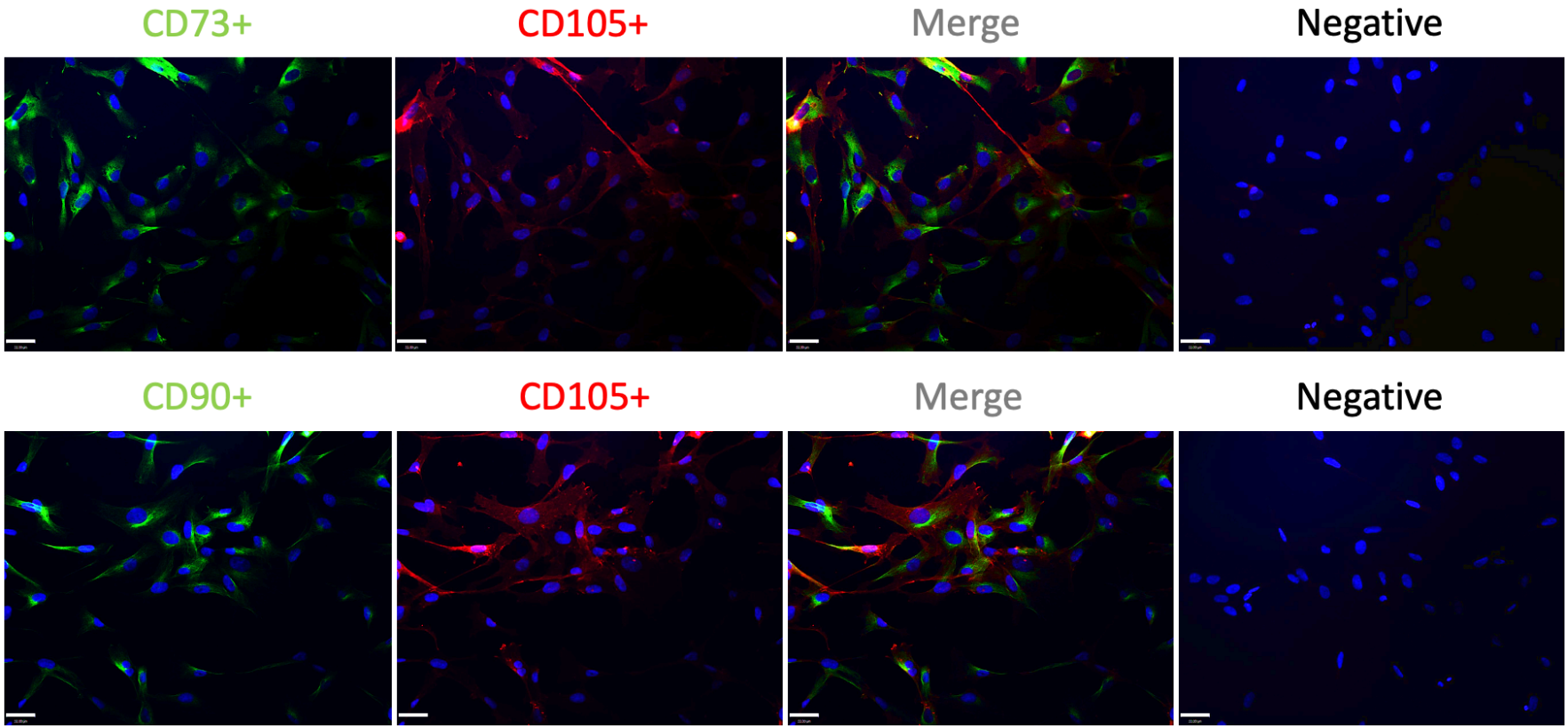


Figure 5.6 hUCT-MSCs co-stained for CD73 with CD105 and CD90 with CD105.

Nuclei is stained in blue (Hoechst 33258), primary antibodies were coupled with Alexa Fluor 488 (green) for CD73 and CD90, and Alexa Fluor 594 (red) for CD105. Representative images were selected. Cells were stained at passages 1 and 2. Scale bar: 32 μm.

5.4.3 Adipogenic medium evaluation for hUCT MSCs

To continue with the medium optimization two different adipogenic cocktails were tested as described in Chapter 2.3.7 hUCT-MSCs adipogenic differentiation, p. 48. Both adipogenic recipes were prepared using each cells' growth medium: one, two or three described previously (Chapter 2.3.4 hUCT-MSCs culture, p. 47), supplemented with the corresponding molecules (Figure 5.7).

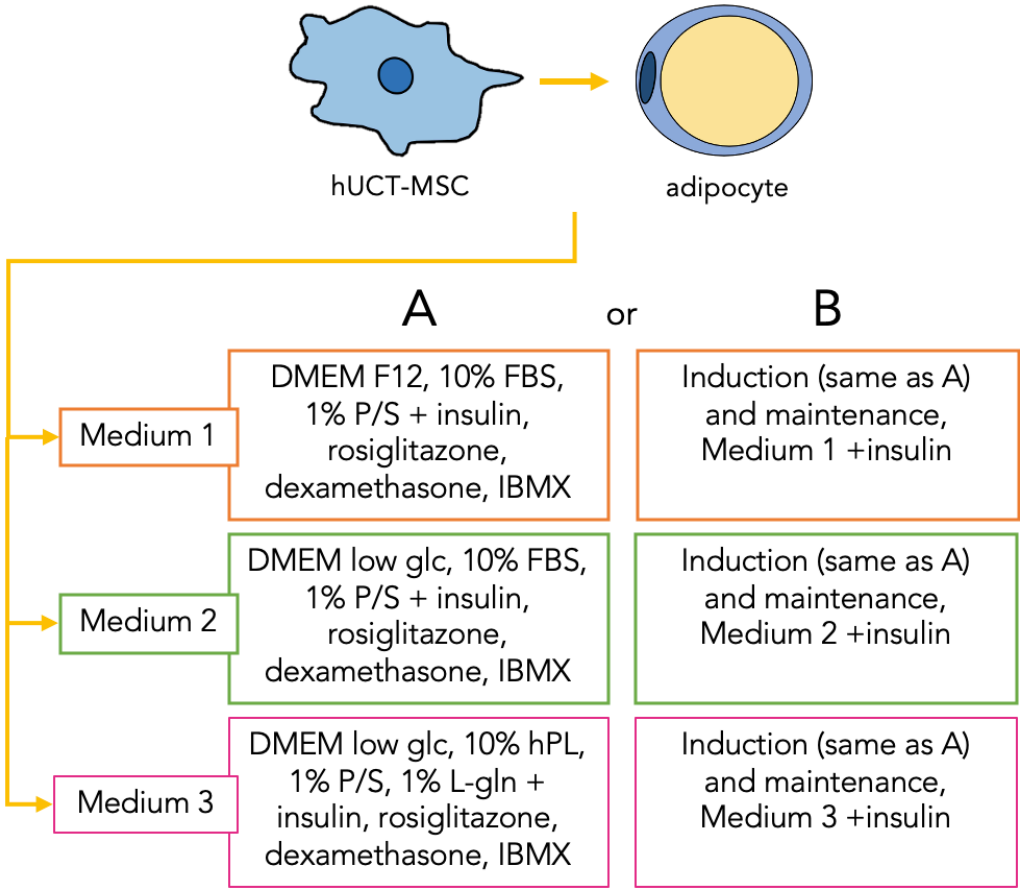


Figure 5.7. Adipogenic differentiation of hUCT-MSC.

Schematic figure displaying different mediums used for adipogenic media evaluation, three media were used with two variations A and B. Detailed methods are described in Chapter 2.3.7. hUCT-MSC adipogenic differentiation.

Results showed that cells, from Medium 1A and B, were able to differentiate equally. Medium 2A and 2B were unsuccessful. Furthermore, cells from Medium 3A were able to differentiate contrary to cells differentiated in Medium 3B which were not able to be maintained and peeled off before the end of the treatment (Fig. 5.8A). Lipid content evaluation was done for each adipogenic differentiation (Figure 5.8B), results showed that cells treated with medium 2A and 2B did not give a significant increase in lipid content quantification. On the other hand, cells differentiated on Medium 1A and 3A showed a significant increase in lipid content when compared to their control. Untreated control cultures, which were grown in regular medium without adipogenic differentiation stimuli, from medium two and three exhibited varying degrees of spontaneous lipid droplet formation, as shown in Figure 5.8A- Control.

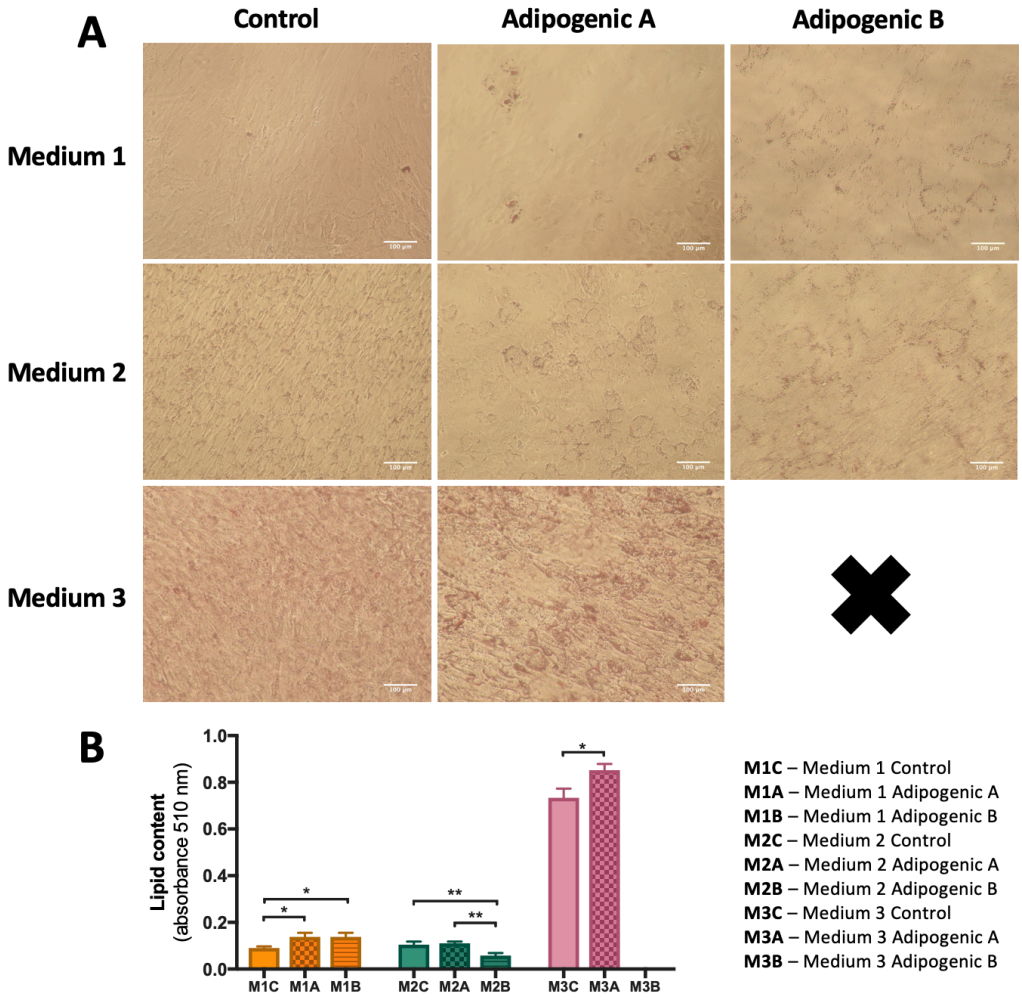


Figure 5.8. Evaluation of adipogenic differentiation with three different growth media and two adipogenic differentiation medium in hUCT MSC-like.

(A) Oil Red O images of cells isolated and grown in their corresponding medium, cells were differentiated into adipocytes with two different cocktails (A and B). Scale bar 100 μm. (B) Lipid content measured by Oil Red O staining in adipogenic cultures of hUCT-MSCs with cells grew and differentiated in their corresponding adipogenic medium. Data are shown as mean ± SEM. *p<0.05, **p<0.01, ***p<0.001.

After evaluating the three different mediums with the two different adipogenic recipes, it was thought that cells grown with medium three could develop a better adipogenic differentiation response with adipogenic A mix prepared in growth medium one (Medium 1A). Results from this adipogenic differentiation showed that cells grown in medium three, had an improved adipogenic response with medium one than with its own differentiation medium (Medium 3A), showing no differentiation in control cells treated with Medium 1A compared with control cells from Medium 3A (Fig. 5.9A). After evaluating lipid content, a significant increase was detected in both adipogenic mediums, however, cells in Medium 1A showed a clear pattern of differentiation when compared to its control (Fig 5.9B).

To confirm these results, three biological replicas (passages 1, 3 and 5) using Medium 1A in hUCT-MSC grown in medium three were assessed. Results showed that adipogenic differentiation on cells grown in medium three and differentiated in Medium 1A could be maintained throughout passages (Fig. 5.9C). Concluding that cells grown in medium three and differentiated with medium 1A had a higher lipid content accumulation and hence a better response.

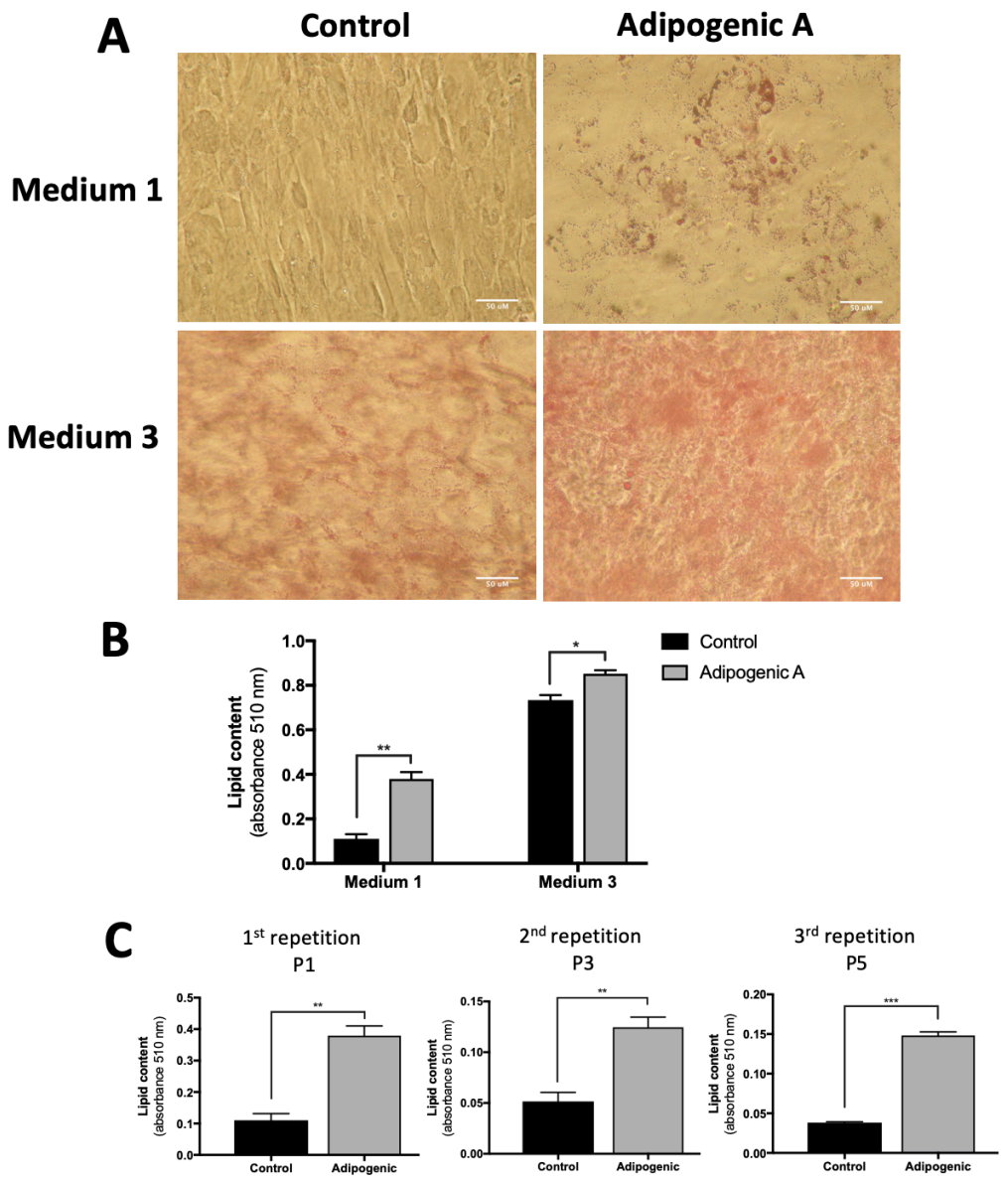


Figure 5.9. Oil Red O staining and quantification of hUCT MSC-like passage 1 grown in medium three.

(A) representative images of hUCT-MSCs stained with Oil Red O after adipogenic differentiation. Cells were grown in medium three and differentiated with adipogenic A prepared with medium one and three. Scale bar 50 μm. (B) Lipid content measured by Oil Red O staining in adipogenic cultures of hUCT-MSCs growth in medium three and differentiated with adipogenic A in medium one and three. (C) Cells grown in medium three were differentiated at passage 1, 3 and 5 with Medium 1A. Data are shown as mean ± SEM. *p<0.05, **p<0.01, ***p<0.001.

5.4.4 Osteogenic evaluation of hUCT MSCs

To further test hUCT-MSC ability to differentiate into different lineages, osteogenic response was tested (Chapter 2.3.8 hUCT-MSCs osteogenic differentiation, p. 49). After 28 days of osteogenic treatment, viability of the cells was evaluated, Fig. 5.10A shows a higher metabolic activity in cells under osteogenic treatment when compared with control. In order to evaluate extracellular calcium deposits, cells were then stained with Alizarin Red (AR). Even though AR quantification showed higher values in osteogenic differentiated cells (Fig. 5.10B) it can be seen in Fig. 5.10C the lack of the characterised red staining which suggest that hUCT-MSC were not successfully differentiated into osteoblast. Osteogenic cultures exhibited varying degrees of lipid droplets formation after the 28 days of cultivation, this could be due to the dexamethasone concentration used in the differentiation cocktail (100 nM). Dexamethasone is an anti-inflammatory steroid molecule that promotes both adipogenesis and osteogenesis upon time[262], cell and concentration dependent exposure, it has been previously reported that dexamethasone can directly stimulate MSCs differentiation into adipocytes and inhibit their osteogenic differentiation[125].

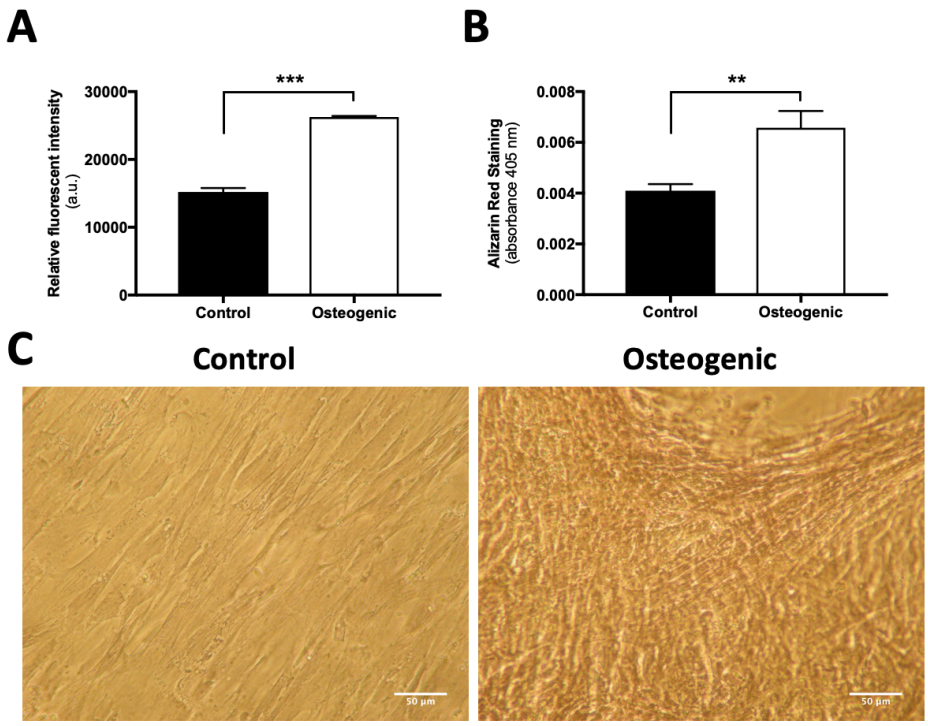


Figure 5.10. Alizarin red staining and quantification of hUCT MSC.

(A) Viability assay with Presto Blue at day 28. (B) Alizarin Red quantification in osteogenic cultures. Data are shown as mean ± SEM of two biological replicas (passage 1 and 2), each replicate was done in triplicates. *p<0.05, **p<0.01, ***p<0.001. (C) representative images of hUCT-MSCs stained with Alizarin Red after osteogenic differentiation. Scale bar 50 μm.

5.5 Discussion

The first objective of this chapter was to isolate, characterise primary MSCs derived from healthy and gestational diabetes conditions. Due to the extensive literature found in isolation and culture of hUCT MSC, it was decided to evaluate two different isolation methods: explants and enzymatic. The second objective of this chapter was to grow and differentiate the isolated hUCT-MSCs into adipocytes. In order to achieve this objective three types of media and two adipogenic differentiation cocktails were evaluated with the aim of ensuring a healthy growth of the primary cells obtained from hUCT.

5.5.1 Explant culture versus enzymatic isolation

In order to achieve the first objective of this chapter two different isolation methods were evaluated. The explant method is considered to be one of the best isolation techniques used[170], as reducing the size of the tissue improves the diffusion of gases and nutrients towards the cells[263]. It has been reported that higher number of cells can be obtained due to their migration capacity from tissue to plastic, so these cells present a more homogeneous populations with high proliferation rates and cells viability[253,264]. On the other hand, several enzymatic mixtures have been tested, collagenase B, collagenase type 2, trypsin, and mixtures of the aforementioned[170,250–253,265]. Several groups have reported that certain enzymatic methods could damage extra cellular matrix resulting in low yield[244] and double the time for cell adherence[265]. Here, results showed that enzymatic method with collagenase B previously minced without filtration is an efficient and rapid way to disaggregate hMSCs. Although little pieces of non-

disaggregated tissue were observed in the cultured flasks, it is believed that they may boost MSC migration, attachment and cell division. These results match to an extent with what Han and colleagues previously reported, using the tissue explant method had a lower yield of primary cells compared with the enzyme digestion method[265]. It was hypothesised that an enzymatic method will be the best isolation technique to isolate hUCT-MSCs. This theory is further supported with the results described above.

5.5.2 Human Platelet lysate (hPL) medium provides the best growth

For the growth of hMSCs, several media have been reported. So far, the majority of the standard media contains FBS, which contains high concentration of cell growth and attachment factors, as well as nutritional and physicochemical compounds essential for cell maintenance, while hPL contains growth promoting properties and its use helps differentiation, therapeutic and immunomodulatory potential maintenance. Both are used at a concentration of 10-20% (v/v)[263]. These results agree with previous reports[172,266–269] that human platelet lysate (hPL) added to the growth medium gives a higher growth rate, smallest and viable cells[172]. Moreover, hPL cultured cells grow faster and recover from the cryopreservation process rapidly. It has been shown that hPL enriched medium could be produced in a good manufacturing practice, compliant format[270] and could produce good expansion of MSCs[258,259] by the release of cytokines and growth factors[258,259]. Also, identifying the dangers of xeno-immunization against bovine genes, transmission pathogens, ethical issues and possible availability restrictions, suggest the need for human

alternatives for the production of clinical cell therapeutic products[266,271].

5.5.3 Adipogenic differentiation medium differs from growth medium

Several groups around the world use different adipogenic cocktails to induce MSC differentiation into adipocytes[119]. There are different molecules known as the main inducers of adipogenesis, such as insulin, indomethacin, dexamethasone and IBMX; with the variation of adding rosiglitazone and T3. For this reason and in order to achieve the second objective of this chapter, two different adipogenic regimens were evaluated, one with the same induction cocktail throughout the treatment and the second with an induction and maintenance medium.

It has been demonstrated that MSCs from bone marrow cultured with hPL or FBS showed similar adipogenic differentiation. Furthermore, there are literature reporting the trilineage differentiation of MSCs derived from hUCT, many experiments also report variability between source material. For example, mixed cord, Wharton Jelly and artery showed a consistent differentiation for all the tested mesenchymal lineages[110]. However, these results show a clear difference with cells cultured with FBS compared with hPL with regards of adipogenic potential, showing that cells isolated and cultured with hPL have better response to the adipogenic cocktail and some of them spontaneously differentiate in their control medium. These results indicate that although cell proliferation was enhanced, the use of hPL could alter the expression of some hMSCs surface markers resulting not only in the immunosuppressive capacity decrease[272] but also in a differentiation

potential reduction. Therefore, after completing the evaluation of the adipogenic potential of the isolated hUCT-MSCs with different media it was feasible to achieve the second objective of this chapter, to differentiate hUCT-MSCs into adipocytes.

5.5.4 MSCs potential and membrane markers

Several guidelines have been reported for the characterisation of hMSCs[5]. Here, isolated cells from hUCT showed positive co-expression of CD73 and CD105 as well as CD90 and CD105. These paired with their capacity of plastic attachment and their ability to differentiate into adipocytes shows the potentiality of these cells. It has been reported that hUCT cells isolated from vein were better differentiated towards adipogenesis but consistently poor with regards of osteogenesis[110], and due to the UCT isolation was done with the whole cord it could be that cells from this depot took over the rest. Moreover, the variability of certain molecules, such as dexamethasone[125], in the medium could play a major role for a successful differentiation, also it has been discussed that the type of the expansion medium used determined the stem cell character[273]. Overall, it is possible that an osteogenic medium optimisation is needed as well as the adipogenic optimisation done.

To conclude, results shown here indicate that hUCT- MSCs present a somehow heterogenic population and multipotency. This study aimed to standardize the best isolation method, culture and differentiation medium for cells isolated from hUCT. Here, cells minced and then digested with Collagenase B gave the best doubling time of 22.8 ± 4 h, showed plastic adherence and co-expressed CD73 or CD90 together with CD105. Furthermore, hUCT MSCs were able to

differentiate into adipocytes. Extensive characterization of these cells adding some negative markers such as CD34 and CD45 as well as the positive markers already mentioned, is needed, preferably by flow cytometry in order to have a full profile of these cells. Additional osteogenic and chondrogenic differentiation studies are required to complete their multilineage potential. Furthermore, it would be of interest to replicate the enzymatic and explant isolation protocols with a greater sample number to establish optimized and standardized procedures. Finally, hUCT-MSCs possess several advantages, such as rapid availability, no hazard for the donor, small risk of rejection and large isolation cell numbers[274]. Developments in precise isolation and growth could facilitate their clinical application.

Chapter 6. Cold temperature exposure of hUCTs MSCs from healthy and diabetic backgrounds

6.1 Main findings

- hUCT-MSCs from healthy and diabetic backgrounds are able to differentiate into adipocytes at 37°C and 32°C.
- Healthy adipocytes displayed higher lipid content when differentiated at normal culture conditions than 32°C adipocytes.
- Healthy hUCT-MSCs derived adipocytes showed high UCP1 protein expression at hypothermal culture conditions.
- Diabetic hUCT-MSCs derived adipocytes displayed high *β3-AR* mRNA expression at both temperatures.

6.2 Introduction

Gestational diabetes (GD) is defined as any glucose intolerance, characterised by insulin resistance and β-cell disfunction[275]. Since the discovery that exposure to an altered GD in utero environment is associated with high birth weight, obesity, type 2 diabetes mellitus (T2DM), and the metabolic syndrome among other diseases to the offspring[276–282], several groups have tried to explain the molecular mechanisms through which GD exposure translate into the high predisposition of several diseases[173,283–285]. Despite these efforts, the diabetic exposure link is still not well understood.

Both umbilical cord blood (UCB) and tissue (UCT) are potential sources of MSCs. Their collection is completely safe, non-invasive, painless and risk-free from both the mother and new-born[242]. But, isolation of MSCs from UCB is lower than UCT isolations which requires longer culture periods[111].

As previously described, UCT possess mesenchymal stem cells (MSCs) which have distinct characteristics such as their potential to differentiate into adipocytes and their different types: white, brown and beige. Apart of their differentiation capacity, these cells express defined membrane markers, such as CD73, CD90 and CD105.

One study suggests that commitment of MSCs into pre-adipocytes could occur at an early developmental stage, hence if the foetus was exposed to an GD environment this might affect the adipogenic determination process[286] such as their ability to differentiate into brown adipocytes. Another study showed that MSCs from GD-UCT had lower cell proliferation, stem cell like properties, differentiation potential, higher cell oxidative stress, rapid aging and deleterious

mitochondrial function when compared to healthy cells, even though when GD was controlled by insulin or diet. These results suggest GD UCT-derived cells may not be able to become brown due to their mitochondrial damage[283,284]. Nonetheless, the browning capacity of MSCs from different backgrounds is still under research. A recent study analysed the white and brown differentiation potential of UCB in comparison with adipose tissue derived MSCs (ADMSCs). It showed limited adipogenic differentiation in UCB-MSCs when compared to ADMSCs adipocytes, which implies MSCs from UCB are not an appropriate stem cell to use for browning evaluation and/or regenerative medicine[109]. However, the differentiation potential of UCT-MSCs into brown adipocytes has not been reported.

Following the development of a cell culture model of differentiation under hypothermic conditions, this chapter evaluates the adipogenic potential of umbilical cord tissue-derived mesenchymal stem cells (UCT-MSCs) into brown adipocytes by cold temperature exposure in order to characterize their potency according to their background. MSCs were isolated from three healthy (H) and three gestational diabetic (GD) UCT samples and two different temperatures were assessed in order to better understand the mechanisms involved in the predisposition of GD cells to differentiate into brown adipocytes compared with healthy MSCs. Metabolic activity was measured in differentiated adipocytes, then they were stained with Oil Red O and lipid content was measured in both backgrounds at both temperatures. The uncoupling protein 1 (*UCP1*) abundance in adipocytes differentiated at 32ºC was investigated by immunofluorescence. Previously these cells, showed an expression of mesenchymal stem

cells markers (CD73+ with CD105+, and CD90+ with CD105+). Oil Red O staining demonstrated that differentiated adipocytes obtained from UCT-MSCs were able to successfully differentiate under normal and hypothermal culture conditions (37°C and 32°C), showing higher lipid content in their differentiated status. Lipid droplets (LDs) were smaller at hypothermal conditions when compared to 37°C differentiated adipocytes in both backgrounds. Fluorescence microscope analysis indicated strong *UCP1* protein signal in UCT-MSCs healthy-derived adipocytes differentiated at 32°C, whereas GD adipocytes displayed a decreased *UCP1* protein expression. Furthermore, molecular analysis showed high *β3-AR* mRNA expression in GD differentiated cells at both temperatures and decreased *PRDM16* expression in 37°C derived adipocytes, while healthy adipocytes showed increased *AdipoQ* and *Glut4* at normal culture conditions, and high *PPARγ* expression at both culture temperatures.

Overall healthy and GD UCT-MSCs are able to go under adipogenic differentiation at normal and hypothermal culture conditions. While the data is preliminary, due to a relatively small sample size and gender, the current study has identified an elevation of *β3-AR* mRNA associated with GD at both culture temperatures which could play an important role in regulating browning, while healthy 32°C differentiated adipocytes showed some brown traits which could highlight them as a suitable stem cell type for new therapeutic approach for obesity and its related diseases.

6.3 Methods

As previously described, three tissues from each background (H and GD) were collected (Chapter 2, table 2.1, p. 42), hMS cells were isolated and tested negative for mycoplasma. Shortly, the modified collagenase B method was used in all UCT for MSC isolation, MSCs were grown in DMEM low glucose supplemented with 10% hPL, 1% L-glutamine and 1% P/S, finally adipogenic differentiation was done by using DMEM F12 supplemented with 10% FBS, 1% P/S adding insulin, rosiglitazone, dexamethasone and IBMX (Chapter 2.3.7 hUCT-MSCs adipogenic differentiation, p. 48).

It has been demonstrated that animal models display a sex difference. Current literature show that males exhibit more pronounced disease phenotypes than females, and male rodents present better metabolic disease when compared to females[287]. Although, estrogen cycle in female mice involves estradiol, progesterone, gonadotrophins and other hormones fluctuation[288] which may increase variability in gene expression including epigenetic changes[289–291], testosterone levels in mice male could also rise discrepancies in phenotype[292]. Hence, females have been less used because a known sex difference which could be seen as an opportunity to comprehend metabolic disease in a more prone model[287]. However, females have been used less than men although is it recognised they present as much variability as males[293]. In this study only males were selected due to the role of estrogen in diabetes prevention[294].

6.4 Results

6.4.1 Metabolic activity and lipid content

Several researches have point out that weight of the babies can be affected by the mother's health status[295]. It has been reported that obese and gestational diabetic mothers have overweight new-borns[295]. However, number of samples collected in this study were not enough to have a representative overview of the population.

With the aim to evaluate the adipogenic response of the hUCT-MSCs isolated from either a healthy or GD background. Browning induction by hypothermic conditions was assessed by metabolic activity, morphologic and molecular signature besides UCP1 protein expression at an endpoint of 28 days at both 37°C and 32°C (Fig. 6.1). From each tissue, two repeats were done at two different passages.

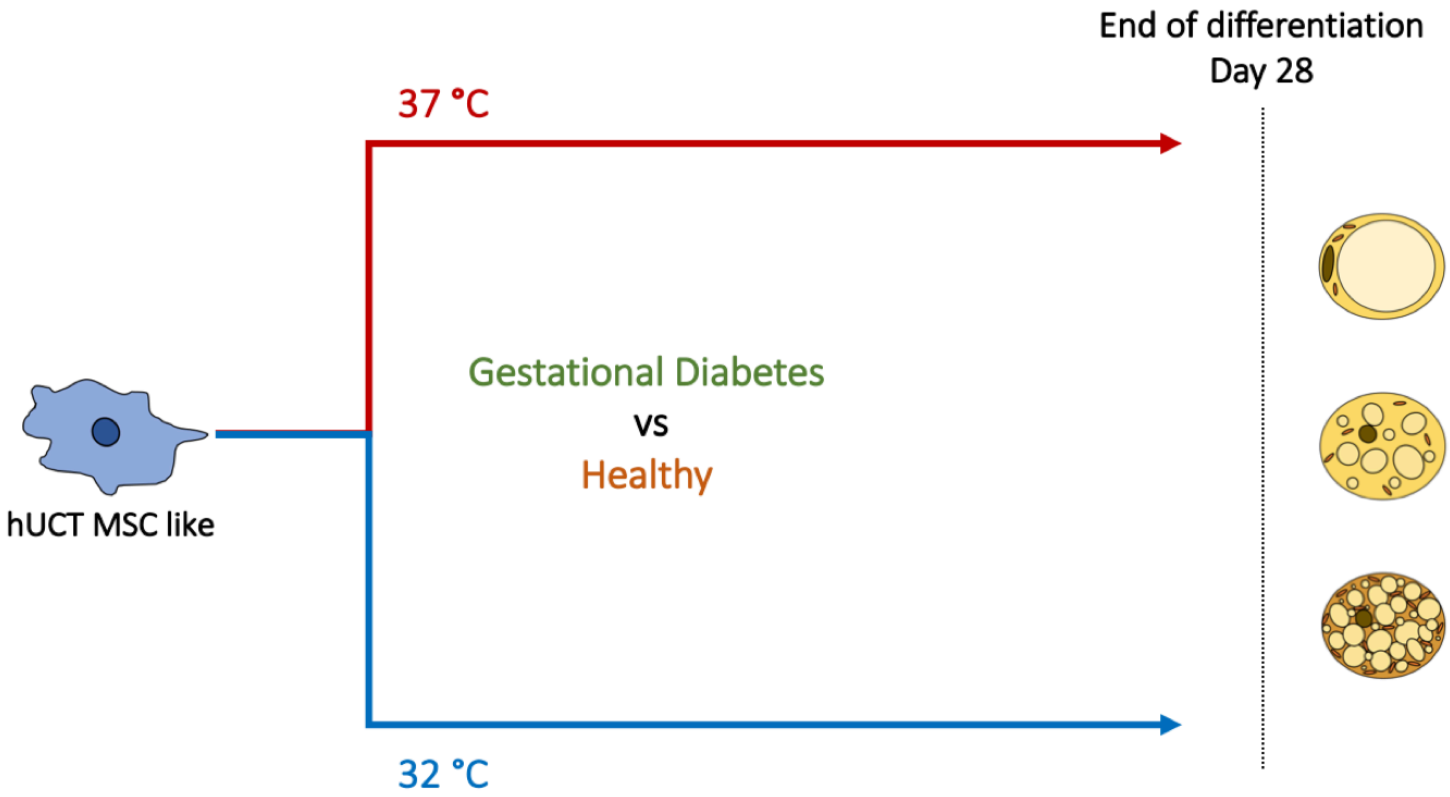


Figure 6.1. Schematic diagram of hUCT-MSCs adipogenesis treatments.

MSCs were cultured in adipogenic medium at 37°C or 32°C for 28 days and then analysed for metabolic activity, lipid content, lipid droplet size, molecular signature and UCP1 protein expression.

To evaluate the metabolic response of the cells at both culture conditions, Presto Blue assay was undertaken. Almost all conditions in both backgrounds showed higher metabolic activity at day 28 in control cells, except GD-derived adipocytes at 32ºC which exhibited no change when compared to its control and less metabolic activity when compared to GD-derived adipocytes differentiated at normal culture conditions (Fig. 6.2A).

To further evaluate the adipogenic response of all cells, ORO staining was done. In contrast with metabolic activity, lipid content increased in nearly all adipogenic differentiated cells (Fig 6.2B). Results showed healthy cells differentiated under hypothermic conditions showed less lipid content when compared to 37ºC healthy adipocytes while GD cells displayed same amount of lipid content in both temperatures (Fig. 6.2B). Variations in adipogenic response between different donors was observed, GD 272 presented higher adipogenic response in both passages when compared to the other two GD tissues, but when data was combined no significant differences were observed between healthy and GD lipid content (Fig. 6.2B).

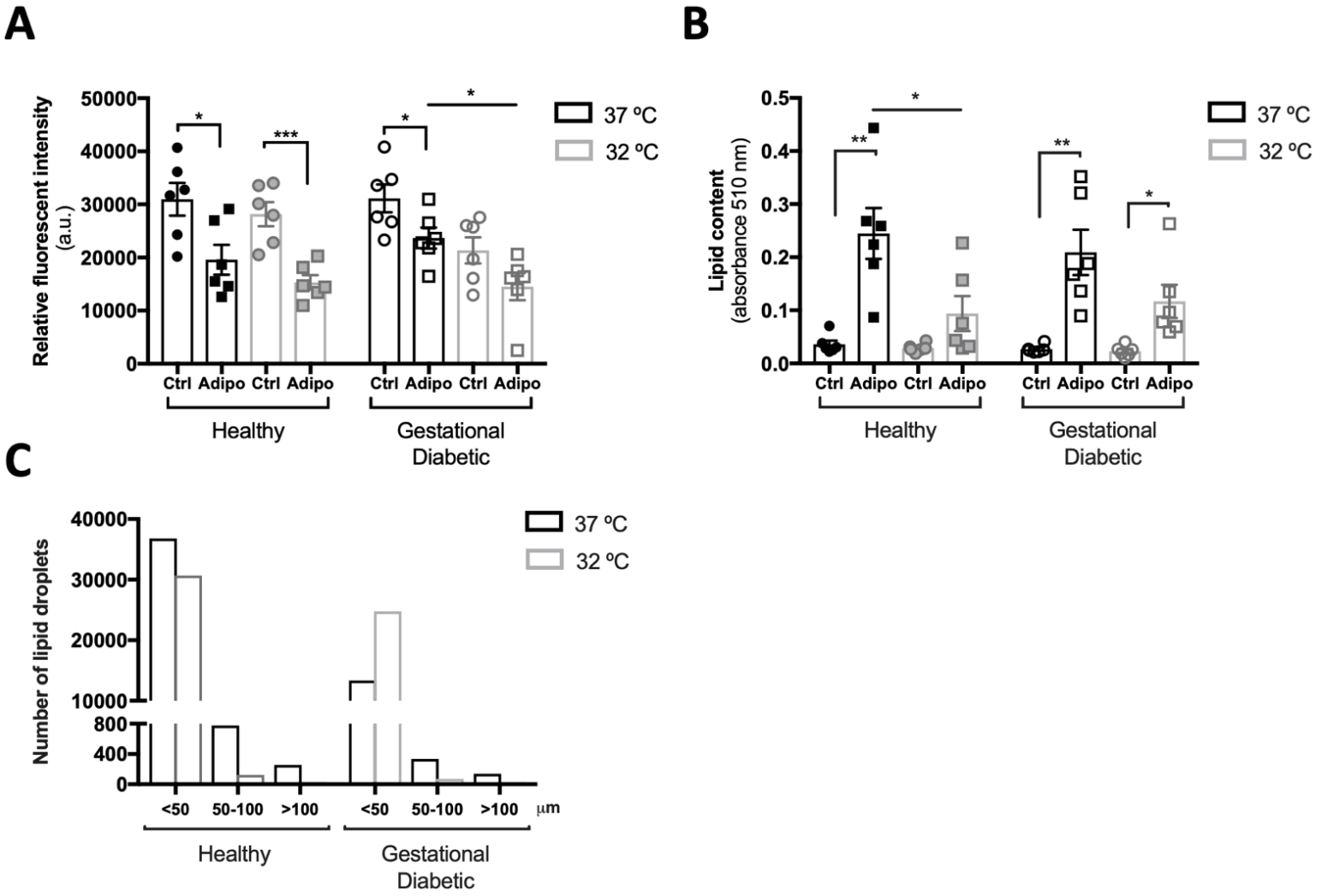

A
Relative fluorescent intensity (a.u.)
50000
40000
30000
20000
10000
0
*
***
*
*
37 ºC
32 ºC
Ctrl Adipo Ctrl Adipo Ctrl Adipo Ctrl Adipo
Healthy
Gestational Diabetic
B
Lipid content (absorbance 510 nm)
0.5
0.4
0.3
0.2
0.1
0.0
**
*
**
*
37 ºC
32 ºC
Ctrl Adipo Ctrl Adipo Ctrl Adipo Ctrl Adipo
Healthy
Gestational Diabetic
C
Number of lipid droplets
40000
30000
20000
10000
800
400
0
37 ºC
32 ºC
<50 50-100 >100 <50 50-100 >100 µm
Healthy
Gestational Diabetic

Figure 6.2.Cellular and morphological response of adipogenic hMSCs differentiated under normal and hypothermic conditions at 28 days.

(A) Metabolic activity measurements in control and adipogenic cultures. (B) Lipid content measured by Oil Red O staining in control and adipogenic cultures. Data represent two biological replicates at passages 1 and 2 of each donor. (C) Lipid droplet size measured for each condition, less than 20 lipid droplets >100 μm were detected at 32°C in both conditions. Data are shown as mean ± SEM. *p<0.05, **p<0.01, ***p<0.001.

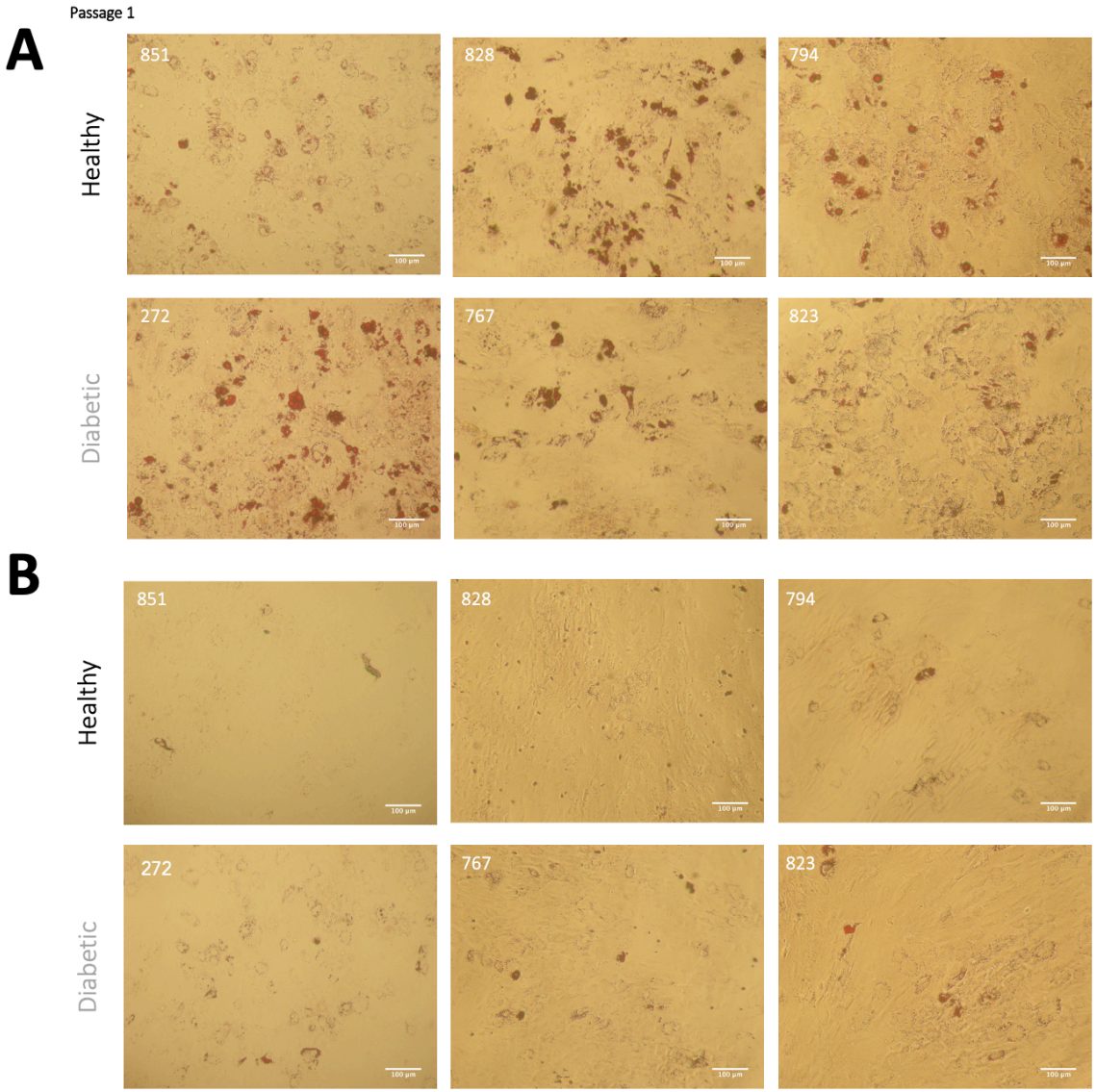


Figure 6.3. Oil Red O staining of healthy and gestational diabetic hUCT MSC-like passage 1 at day 28.

Representative images of hUCT-MSCs stained with Oil Red O after adipogenic differentiation at (A) 37°C and (B) 32°C. Cells were grown in medium three and differentiated with adipogenic A prepared in medium one. Scale bar 100 μm.

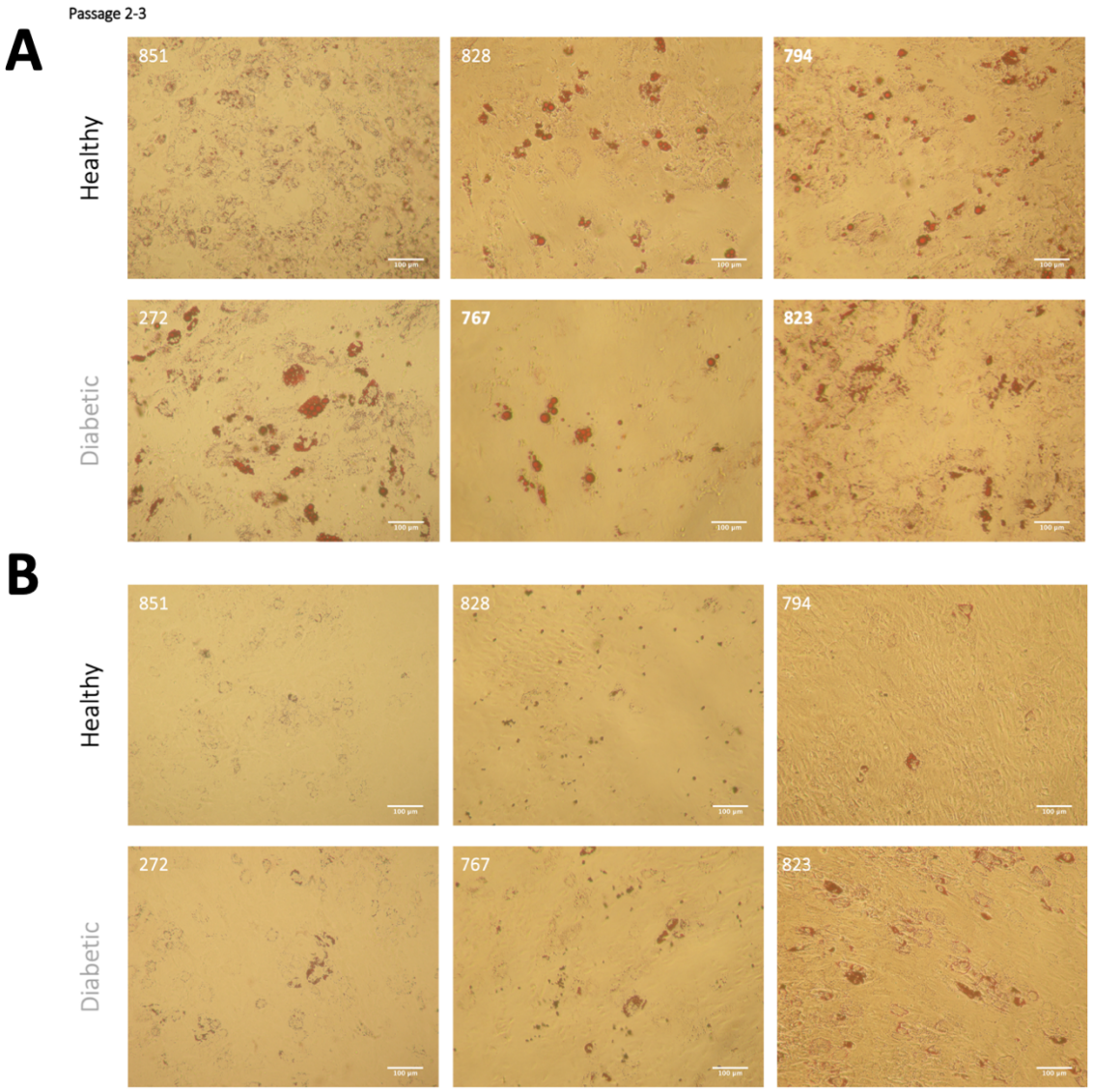


Figure 6.4. Oil Red O staining of healthy and gestational diabetic hUCT MSC-like passage 2 or 3 at day 28. Representative images of hUCT-MSCs stained with Oil Red O after adipogenic differentiation at (A) 37°C and (B) 32°C. Cells were grown in medium three and differentiated with adipogenic A prepared in medium one. Scale bar 100 μm.

Lipid content matched with the number of lipid droplets measured in all conditions (Fig. 6.2C). Moreover, healthy and GD hUCT-adipocytes differentiated under hypothermic conditions showed smaller intracytoplasmic lipid droplets, similar to hADSCs described in Chapter 3, than of adipocytes differentiated at normal culture conditions (Fig. 6.2C). On the other hand, at normal culture conditions healthy adipocytes displayed higher number of lipid droplets (LDs) >50 μm than of GD adipocytes.

ORO microscopic images of UCT differentiated adipocytes at both temperatures are presented in Fig. 6.3 and Fig 6.4. Cells at higher passages showed a better response under adipogenic differentiation than cells at passage one (Fig 6.3 and 6.4) at both temperatures. This could indicate contamination of other cell types in MSCs at earlier passages. As passage number increase cells may become more homogeneous with less cell contamination[296]. Overall the changes in lipid content corresponded with the adipogenic response, cells differentiated at normal culture conditions showed larger LDs while adipocytes at hypothermic conditions were mostly multilocular with smaller LDs.

6.4.2 Gene expression at hypothermal and normal culture conditions

To continue with the evaluation of hUCT-derived adipocytes and the effect of temperature in both healthy and GD conditions, mRNA expression was evaluated with real-time PCR. Healthy cells at normal culture conditions (37°C) showed enhanced response in common adipogenic markers *AdipoQ*, *PPARγ* and *Glut4*. On the other hand, healthy cells differentiated at 32°C and GD at 37°C displayed only *PPARγ* mRNA increased expression (Fig. 6.5). No significant differences were detected in leptin and *InsR*.

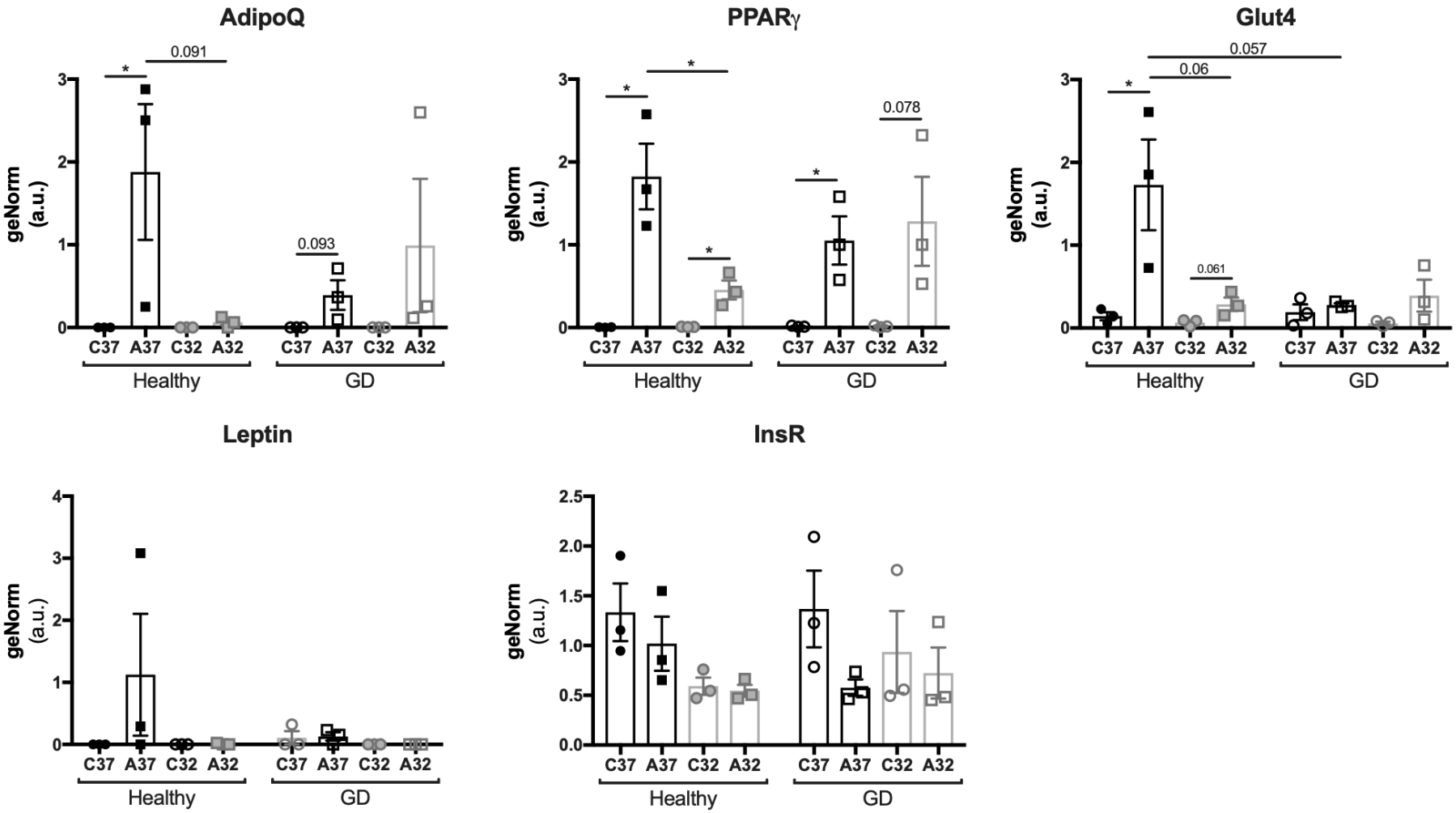

AdipoQ
PPARγ
Glut4
Leptin
InsR
geNorm (a.u.)
C37 A37 C32 A32
Healthy
GD
*
0.091
0.093
0.078
0.057
0.06
0.061

Figure 6.5. Expression levels of common adipogenic markers: Adiponectin, PPARγ, Glut4, Leptin and Insulin receptor at day 28.
n = 3 individual experiments per condition. Data represent the mean of three replicas ± SEM. Statistical significance was set at $p < 0.05$. *p<0.05, **p<0.01, ***p<0.001.

To determine if hypothermic culture conditions could generate adipocytes that exhibit brown/beige features in both healthy and GD cells, brown markers were evaluated. For these markers, only few changes were detected. First, GD cells showed a decreased *PRDM16* expression when differentiated under normal conditions. Then, *β3-AR* was increased in GD cells differentiated at both temperatures, while changes in *PGC1α, CIDEA*, *DIO2* and *FGF21* were not detected (Fig. 6.6).

Finally, to complete the marker expression two more markers, *UCP1* and *Res*, were done but unfortunately no mRNA detection was observed after 40 cycles.

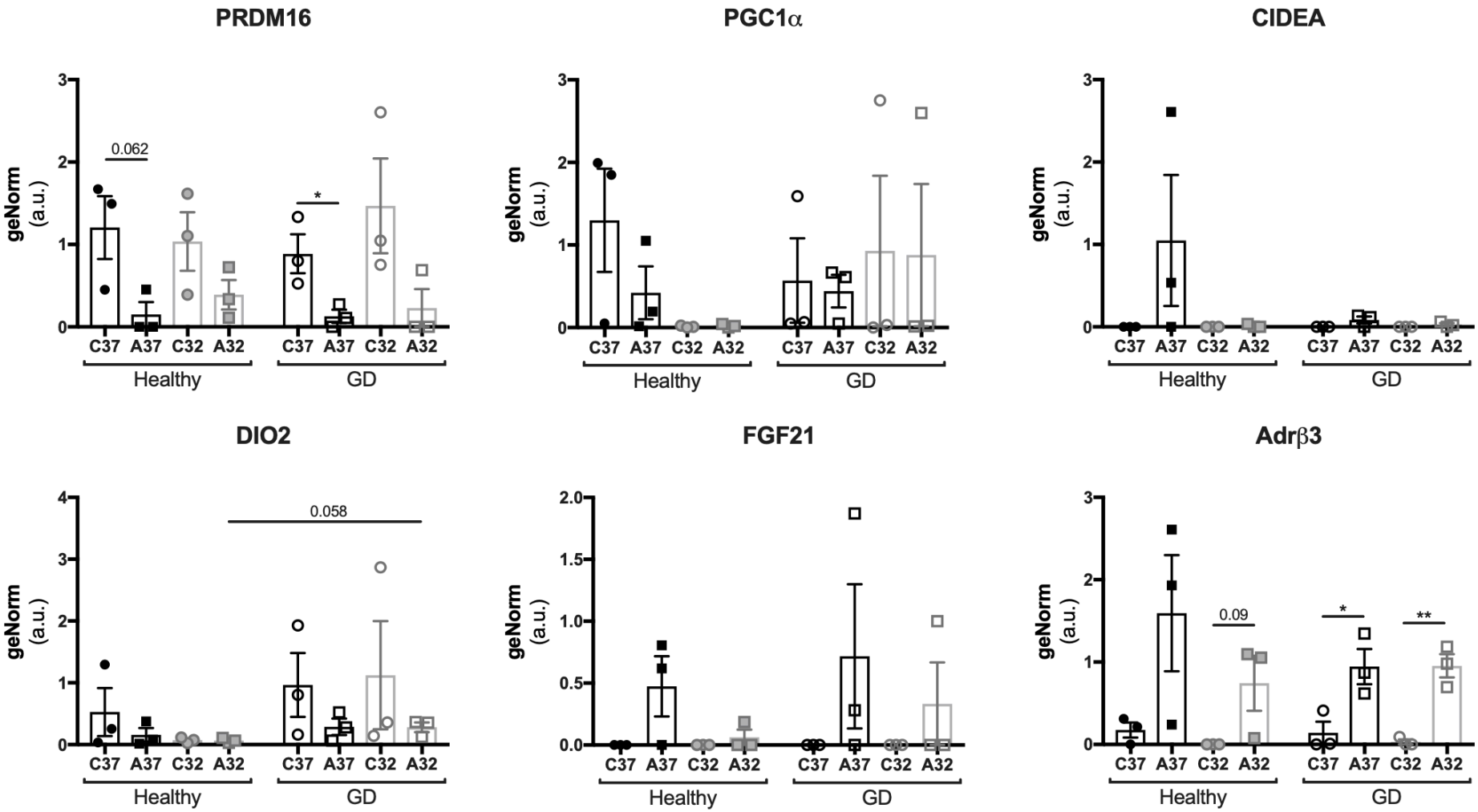

PRDM16
PGC1α
CIDEA
DIO2
FGF21
Adrβ3
geNorm (a.u.)
0.062
*
0.058
0.09
**
C37 A37 C32 A32
Healthy
GD

Figure 6.6. Expression level of brown adipogenic markers: PRDM16, PGC1α, CIDEA, DIO2, FGF21, and *β3-AR* at day 28.
n = 3 individual experiments per condition. Data represent the mean of three replicas ± SEM. Statistical significance was set at $p < 0.05$. *p<0.05, **p<0.01, ***p<0.001.

6.4.3 Molecular signature overview

To continue with the gene expression analysis, hierarchical clustering analysis (HCA) and principal component analysis (PCA) of all genes were performed (Fig. 6.7). For PCA, different arranges were done, temperatures were compared against both conditions and vice versa. Then all conditions were graph together (Fig. 6.7E). For HCA, datasets were grouped per gene and the three replicas were presented for each temperature and condition. (Fig. 6.7F) Both analyses confirmed heterogeneity of the samples at different temperatures.

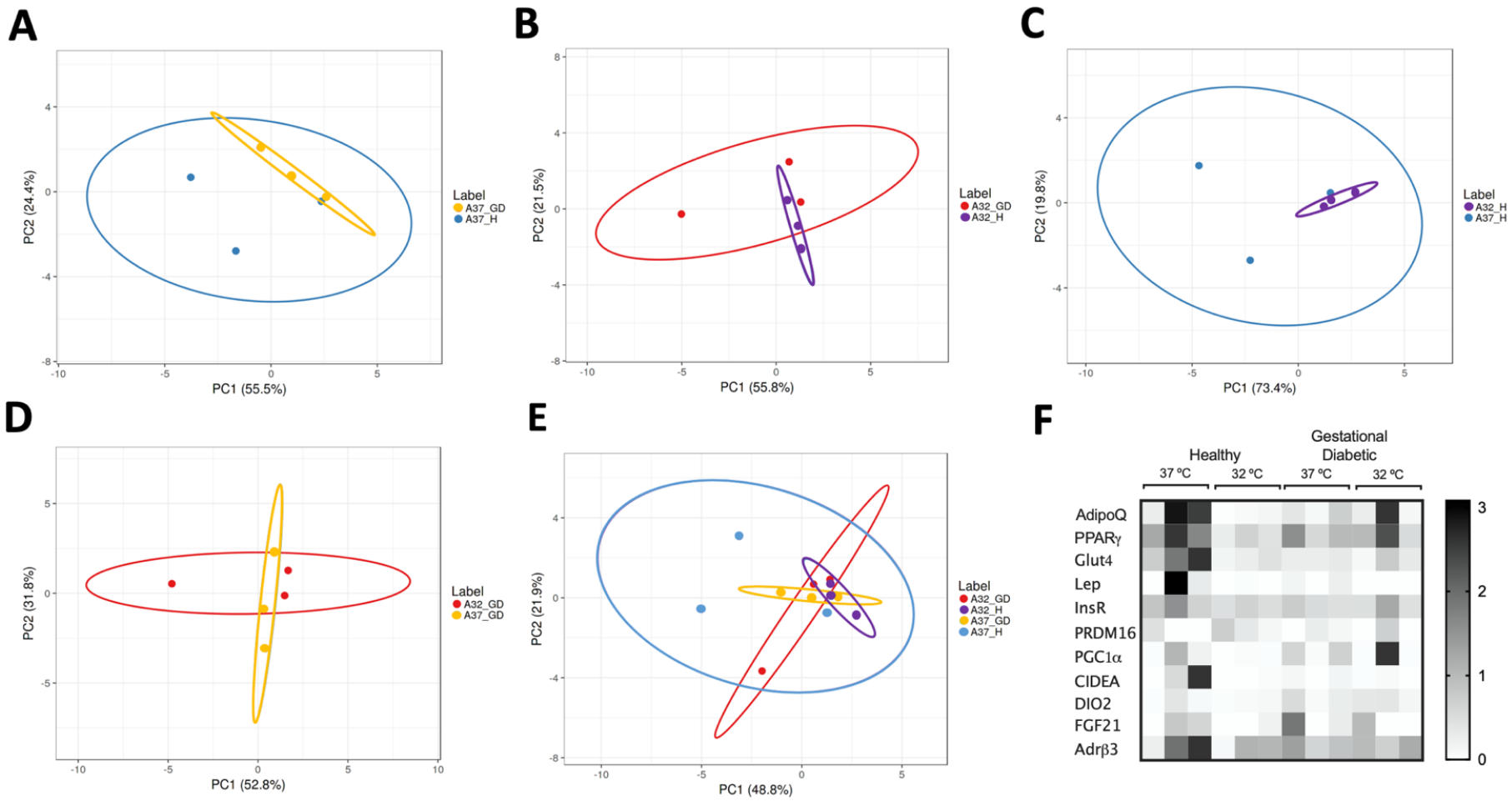

A
PC2 (24.4%)
PC1 (55.5%)
Label
A37_GD
A37_H
B
PC2 (21.5%)
PC1 (55.8%)
Label
A32_GD
A32_H
C
PC2 (19.8%)
PC1 (73.4%)
Label
A32_H
A37_H
D
PC2 (31.8%)
PC1 (52.8%)
Label
A32_GD
A37_GD
E
PC2 (21.9%)
PC1 (48.8%)
Label
A32_GD
A32_H
A37_GD
A37_H
F
Healthy
Gestational Diabetic
37 °C
32 °C
37 °C
32 °C
AdipoQ
PPARγ
Glut4
Lep
InsR
PRDM16
PGC1α
CIDEA
DIO2
FGF21
Adrβ3
3
2
1
0

Figure 6.7. The effect of incubation temperature on gene expression patterns as determined by hierarchical clustering (HCA) and principal component analysis (PCA). Scatter plots of the two principal components containing (A) 79.9%, (B) 77.3%, (C) 93.2%, (D) 84.6%, (E) 70.7% of total variance at day 28 for GD vs Healthy at 37°C and 32°C, and 32°C vs 37°C of Healthy and GD, respectively. Blue=Healthy 37°C, Purple= Healthy 32°C, Yellow= GD 37°C and Red= GD 32°C. (F) Heatmap of the GeNorm normalization on expression levels of common adipogenic markers: Adiponectin, PPARγ, Glut4, Leptin (Lep), Insulin Receptor (InsR) and brown adipogenic markers: PRDM16, PGC1α, CIDEA, DIO2, FGF21 and Adrenoreceptor β3 (β3-AR) at 28 days - black = high (3), white = low (0)-. n = 3 individual experiments.

6.4.4 UCP1 protein expression is enhanced in healthy cells at hypothermal conditions

The *UCP1* expression is normally used as a recognized biomarker of brown adipocytes. In this study, *UCP1* protein was measured by quantifying relative immunofluorescence intensity (Fig 6.8). Healthy and GD adipocytes at normal culture conditions exhibited the same amount of *UCP1* protein (Fig. 6.8A). Even though hypothermic healthy adipocytes showed less lipid content when compared to healthy adipocytes differentiated at normal conditions, this might be explained due to a mild increment in *UCP1* protein expression after 28 days (Fig. 6.8B). However, no significant increase in UCP1 protein expression was detected between these two culture conditions. On the other hand, hypothermic differentiated adipocytes from healthy background, showed raised *UCP1* protein expression when compared to GD cold-derived adipocytes (Fig. 6.8C).

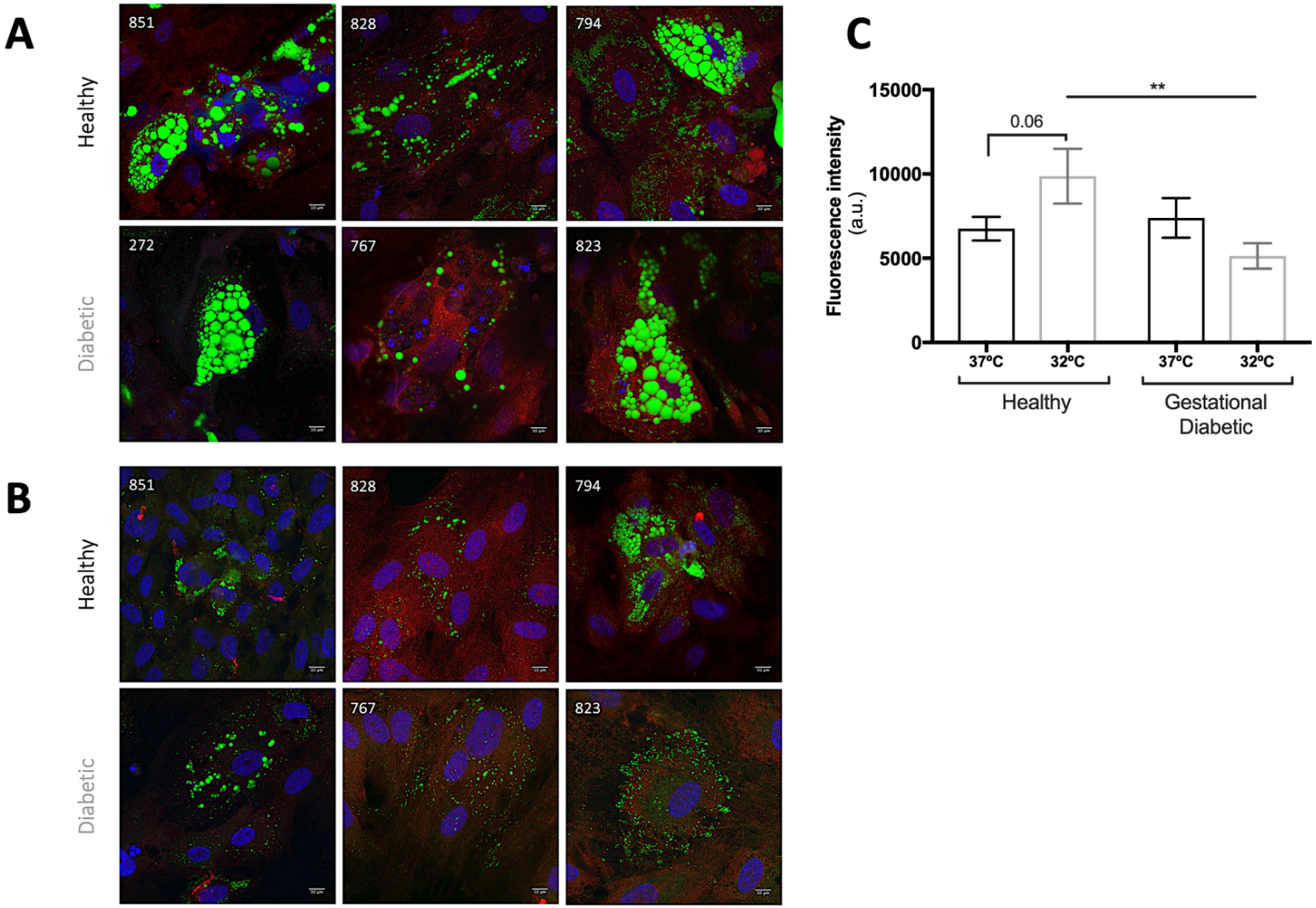

A
Healthy
Diabetic
851
828
794
272
767
823
B
Healthy
Diabetic
851
828
794
767
823
C
Fluorescence intensity
(a.u.)
15000
10000
5000
0
0.06
**
37°C
32°C
37°C
32°C
Healthy
Gestational
Diabetic

Figure 6.8. Effect of culture temperature on the abundance of uncoupling protein (UCP)1 in hUCT-MSCs at 28 days.

Representative images of UCP1 shown in red at (A) 37°C and (B) 32°C, with Hoechst 33258 nuclear counterstain in blue, and Bodipy in green. Scale bar = 10 μM. (C) Relative fluorescence intensity of UCP1 staining measured in 30 randomly selected micrographs of 3 independent experiments. *p<0.05, **p<0.01, ***p<0.001.

6.5 Discussion

6.5.1 Obesity and GD evidence in early development

There is evidence that implies that an altered intrauterine metabolic environment produced by hyperglycaemia in pregnant mothers could increase the risk of obesity and diabetes in the new-born[281,297-301]. A high interest in the hypothesis that metabolic diseases could be influenced by early life events, such as early stages of development, has been raised. Moreover, numerous studies have reported that exposure to elevated glucose during pregnancy increase the risk to develop T2DM and obesity later in life[281,297,298]. Here, the number of samples were insufficient to be able to detect a difference. However, it has been reported that although no significant differences in birth weight between healthy and GD new-borns was identified, an increased fat mass and body fat in the infants of the GD mothers was observed when compared with the healthy ones[302]. Moreover, the HAPO (Hyperglycaemia and Adverse Pregnancy Outcome) study has validated a constant relationship between maternal hyperglycaemia and perinatal adiposity[303,304].

Following the above evidence, the objective of this chapter involved studying the effect of gestational diabetes on the adipogenic differentiation of the previously isolated hUCT-MSCs, specifically towards browning using hypothermal culture conditions.

6.5.2 hUCT-MSCs potentiality towards adipogenesis

Pierdomenico and colleagues, previously reported no differences of the proliferative rates when comparing healthy versus GD cells[173]. Here,

although no comparison was done, cells from both backgrounds showed similar morphological features as well as growth ratio. It has been reported that maternal obesity and gestational diabetes could enhance MSCs potentiality towards adipogenic differentiation[173]. However, in this study the weight of the mother was unfortunately not known. There was only one GD sample (272) that meet this claim, which was reported to have a gestational diabetic background plus hereditary T2DM (Table 2.1, p. 42). Nevertheless, when all samples were pooled for comparison, no differences regarding lipid content were seen when GD was compared with healthy adipocytes at normal temperature (37°C). Kim and colleagues reported that GD-MSCs have a reduced adipogenic differentiation potential[283]. This claim is not in line with results reported here, UCT-MScs from both backgrounds are able to go under adipogenesis at both temperatures. These results could be related with the development of gestational diabetes at early or late pregnancy stages, it has been reported that differentiation of MSCs from diabetic patients is influenced by hyperglycaemic microenvironment[305], it will thus be of interest to determine the period of stem cell niche of GD-MSCs. Here, adipocytes displayed multilocular cytoplasmic LDs at 32°C while at 37°C LDs were bigger as described before[92].

6.5.3 Adipogenic response of GD MSCs

When GD cells were evaluated, adipocytes differentiated under normal culture conditions exhibited small multilocular LDs, similar to healthy adipocytes. These cells also showed similar metabolic activity and UCP1 protein expression than healthy adipocytes. However, when GD-MSCs were differentiated at 32°C, adipocytes displayed lower

metabolic activity as well as decreased *UCP1* protein than of 37°C GD-adipocytes. Metabolic activity results contrast with hypothermal mMSCs-derived adipocytes, nonetheless its possible than a more refined method is required, such as Seahorse, as well as cell number normalisation. Previously, it was reported that high levels of glucose lead to mitochondria dysfunction[283,284]. Here, GD-MSCs differentiated at 32°C, showed decreased *UCP1* protein expression when compared to hypothermic healthy adipocytes at the end of the treatment. It would thus be crucial to compare and analyse mitochondrial amount and function, respectively.

Moreover, GD cells displayed an interesting molecular signature, cells differentiated at normal culture temperatures showed increased *PPARγ* and decreased *PRDM16* when compared to undifferentiated cells. *PRDM16* is found in mesenchymal progenitors with the ability to differentiate into brown adipocytes both *in vitro* and *in vivo*[3], additionally *PRMD16* activates the transcriptional activity of *PPARγ*[63,224]. These results could indicate that GD cells have the potential to differentiate towards a kind of brown/beige adipocytes, these cells might not express *UCP1*, but their thermogenic capacity could be linked to a *UCP1*-independent pathway. It has been reported that stimulation of *β3-AR* induces lipolysis through the futile cycle[306], thus increased *β3-AR* in both temperatures could indicate a possible adrenergic stimulation which might contribute to increased energy expenditure independently of *UCP1*-mediated thermogenesis[234,306–308]. However, functionality of these membrane receptors should be tested. Furthermore, activation of PRDM16 expression promote beige adipocyte differentiation[309]. In the absence of *UCP1*, the beige adipocytes response to cold exposure might be linked to NE binding

to *β3-AR* and increasing intracellular Ca^{2+} by activating SERCA2b[163]. To confirm either of these hypotheses more studies are needed in order to evaluate the energy expenditure and glycolysis capacity as well as *PRDM16* mRNA expression in early adipogenic stages in both healthy and GD cells.

Glut4 is one of the genes involved in the insulin signalling pathway stimulating glucose entry in adipocytes also known to be downregulated in both humans and rodents with obesity or T2DM[310,311] and in a GD rat model[312]. Here low *Glut4* expression in GD cells is in line with studies showing hyperglycaemic conditions[313,314] and low differentiation could be a consequence of a compromised insulin pathway. Besides FFA, glucose is the second most important substrate for browning[315], altogether this could indicate adipogenic impairment to go towards browning.

Although no differences were detected when *AdipoQ*, *InsR* and *leptin* were evaluated in GD adipocytes, several genetic alterations have been reported in different GD populations, specifically polymorphisms[316,317], which would be interesting to evaluate in control MSCs from both backgrounds.

6.5.4 Adipogenic response of healthy MSCs

Adipogenic response of healthy MSCs at normal culture conditions displayed increased *AdipoQ*, *PPARγ* and *Glut4* mRNA. *AdipoQ* and *PPARγ* are known to stimulate adipocyte differentiation, insulin sensitivity and lipid accumulation[318,319], while *Glut4* is also upregulated as adipocytes differentiate[320,321]. These results indicated a normal adipogenic differentiation process in healthy cells.

Despite no *UCP1* mRNA detection from healthy donors was detected, this could be due to the differences between the half-life of *UCP1* protein (2-20 days) and UCP1 mRNA (3 h)[322,323]. Moreover, the small size of LDs observed in hypothermic differentiated healthy adipocytes, are in accordance with brown morphology characteristics. However, low lipid content could be explained by increased lipolysis due to the high *UCP1* protein and *PPARγ* mRNA, that are known to occur with BAT activation during cold exposure. Increased *PPARγ* in BAT could supply an essential link between fuel availability and the process of energy consumption with high rate of fatty acid oxidation, specially triglycerides[306,315,324]. Still, it would be important to analyse the bioenergetic response of these cells in order to have a better understanding of their thermogenic capacity due to the lack of brown molecular response at hypothermic conditions.

6.5.5 Heterogeneity of the hUCT-MSCs

Heterogeneity in MSCs has been widely recognised, and such variations are related to biological origin, donor differences or *in vitro* manipulation[325,326]. Lee et al. reported metabolic heterogeneity in activated beige adipocytes from iWAT under adrenergic activation. It was unknown if this feature reflected developmental plasticity or the capacity of cells to adjust between phenotypes[327]. Here, results showed molecular variations when samples were analysed as groups. Is possible that heterogeneity among UCT is due to patient-to-patient variability, an increased sample number and grouping the samples per early or late GD detection could have a major effect on minimising these high variations[328].

6.5.6 hUCT-MSCs as a therapeutic option

In this study limited information about the mothers was available. It would be of interest to evaluate the disease condition of the diabetic mothers, as well as their weight and co-relate if the GD adipocytes were also from obese pregnant women. Moreover, this study only evaluated male new-borns; however, it would be useful to evaluate both sexes, male and female.

It was hypothesised that hUCT-MSCs from a gestational diabetic background will display a higher adipogenic potential at normal culture conditions than healthy cells while at hypothermal culture conditions these cells would be impaired to differentiate towards this lineage. This theory was not achieved, GD cells displayed same amount of lipid content than healthy differentiated cells under both culture conditions and LDs size was similar between both backgrounds.

Regarding GD cells impairment to differentiate towards adipocytes and healthy cells expressing beige molecular signature at hypothermic conditions, this hypothesis was not fully confirmed. Firstly, significant differences were found in protein expression, starting with increased *UCP1* protein expression at 32ºC and small multilocular LDs in healthy adipocytes when compared to GD adipocytes. Secondly, no differences were found in any of the browning genes for both healthy and GD cells. Thirdly, *β3-AR* mRNA increase at both temperatures was the only change detected in GD adipocytes. Activation of BAT through *β3-AR* has been investigated for a potential anti-obesity therapeutic treatment[329]. Here, *β3-AR* agonist such as CL-316,243[330] or mirabegron[331], could be tested in healthy and GD cells in order to evaluate their thermogenic stimulation in addition to cold exposure.

Lastly, it could be interesting to evaluate the behaviour of cells from females deliveries in cold culture conditions, as it has been reported that females may possess higher amounts of brown fat and are more sensitive to BAT activation than men[179,332–335], which could suggest greater potential of female MSCs to go towards brown adipogenic differentiation.

As mentioned before, MSCs from UCT have increased interest due to their functional properties and that these cells come from a "waste" tissue[242]. Although these cells could be used as a therapeutic potential, it has been reported that UCT-MSCs from obese/diabetic mothers are unsuitable for cell therapy clinical protocols[336]. In order to use these cells as a potential alternative for stem cell therapies, both sexes should be studied to have a better understanding of biological sex differences from genes to hormones, hence detailed analyses are needed in order to elucidate if MSCs from different disease backgrounds could potentially be beneficial for other therapies.

Overall, although preliminary these results show that healthy and GD MSCs derived from UCT are able to differentiate into adipocytes at two different temperatures. Further studies are now required to elucidate functionality of adipocytes from both backgrounds.

Chapter 7. Final conclusions

The global rise in obesity has focused research interest in brown fat and its activation to counteract metabolic disorders. Recent evidence demonstrate that adult humans possess *UCP1*-positive brown fat in the supraclavicular and neck region[149,179,180]. Studies indicate that brown cells developing in WAT are a different type known as beige adipocytes[63]. Beige adipocytes relevance in humans has been described, with Wu and colleagues showing that adult human BAT displays beige molecular markers rather than classical brown fat signature in *UCP1*-positive cells. These results emphasise the previously unknown molecular identity of BAT signature in humans[337].

As previously mentioned, adipocytes arise from a mesenchymal progenitor[4,6,83,338]. The ability of MSCs to be used as cellular transplantation of modified cells or to elucidate new mechanisms regulating beige adipogenesis and its activation is still under research.

This study aimed to highlight the potential of MSCs and mechanisms governing browning differentiation during cold exposure. First of all, the browning potential of MSCs was tested to undergo adipogenic differentiation at normal (37ºC) and hypothermic culture conditions (32ºC) (Chapter 3, p. 71). Secondly, the ability of these cold-differentiated adipocytes was tested in order to evaluate their capacity to maintain browning traits obtained at 32ºC (Chapter 4, p. 106).

To continue, two different isolation methods and three culture media were tested to select the best growth approach for hUCT-MSCs (Chapter 5, p. 136). Thirdly, hUCT from healthy and gestational diabetic background were used in order to determine if the *in vitro* model of differentiation under hypothermic culture condition was translatable to primary MSCs (Chapter 6, p. 164).

7.1 MSC-derived adipocytes

During the differentiation of MSCs at two different culture conditions (37ºC and 32ºC), the most striking feature detected was the dual *UCP1*/leptin expressing phenotype in adipocytes differentiated at normal culture conditions which indicates their functional potential to develop into both white and brown like adipocytes[92,339–341] (Fig. 3.1, p. 79). The morphological and molecular changes of adipocytes differentiated at hypothermic conditions showed signs of browning, expressing upregulation of *COX8b*, *UCP1*, *P2RX5*, *CITED1* (Fig. 3.11, p. 98). These cells also displayed an increased adipocyte differentiation and *UCP1* protein expression. Moreover, cold differentiated cells expressed enhanced uncoupled respiration and metabolic adaptation (Fig. 3.7, p. 91). Beige adipocytes exhibited a leptin translocation into the cells nuclei, which could indicate a possible role for leptin in the MSC-browning process[189,339,340] (Fig. 3.3, p.84 and Fig. 3.4, p. 85).

Recently it has been discussed that leptin is not a thermogenic hormone, but it effect resides in temperature regulation[342]. Moreover, evidence suggest that *TRPV1* and leptin might interact in adipose tissue[200]. Since adipocytes differentiated at cold temperatures expressed high mRNA and protein *TRPV1* staining (Fig. 3.11, p. 98), nuclear detection of leptin and *UCP1* protein expression could suggest leptin's involvement in fatty acid oxidation and *UCP1* activation[192].

Moreover, hADSC and primary mMSCs displayed the same morphological traits, with high *UCP1* and leptin expression (Fig. 3.5, p. 87) indicating the ability of these cells to acquire browning phenotype under hypothermic culture conditions.

Further research is now required to provide experimental evidence and a more detailed role of leptin involvement during adipogenic browning at cold culture conditions. Some data suggest that *TRPV1* might mediate leptin effect in neurons[343]. Moreover, mice lacking *TRPV1* showed an obese and insulin resistance phenotype[344], it would thus be of interest to investigate the mechanism in which leptin acts in adipocytes and *TRPV1* involvement. A graphical abstract of the main findings of Chapter 3 is detailed in Fig.7.1.

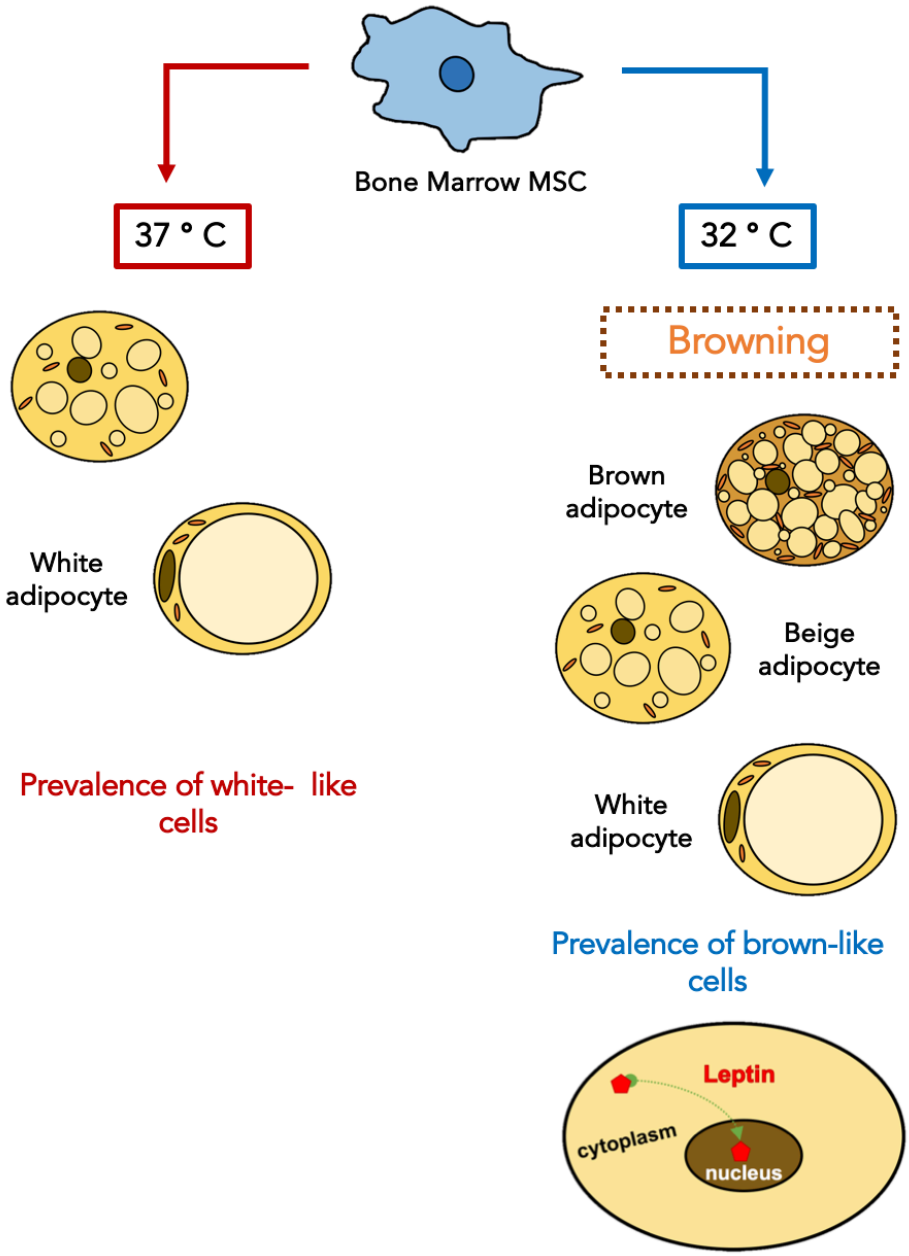


Figure 7.1. Cold temperature exposure induces browning of MSC-derived adipocytes. Schematic figure displaying an overview of bone marrow MSC differentiation under 37°C and 32°C culture conditions. Cells differentiated at normal culture conditions displayed a prevalence of white-like cells while MSCs differentiated under hypothermal culture conditions showed a prevalence of brown-like cells with a leptin translocation from the cytoplasm to the nucleus of the adipocytes.

7.2 Brown features maintenance

One of the major questions on browning is the maintenance of these acquired traits after the stimuli is removed, in this case cold exposure. Brown adipocytes differentiated at hypothermic culture conditions are able to maintain their morphological and molecular traits after 21 days of being transferred to warm conditions (Fig. 4.4, p. 118 and Fig. 4.5, p. 122).

UCP1-independent thermogenesis has been proposed as recent evidence suggests that beige adipocytes require SERCA2b mediated Ca^{2+} cycling for beige fat thermogenesis both *in vivo* and *in vitro*[163,345]. Taken together, these results indicated that MSCs-derived adipocytes at cold culture conditions express a higher Ca^{2+} signal than in normal cultured adipocytes, while rewarmed adipocytes expressed an intermediate signal (Fig. 4.8, p. 125) suggesting a shared *UCP1*-dependent and independent mechanism. Moreover, a complex interplay between *TRPV1*, 2 and 4 was recognised , suggesting *TRPV2* as one of the main regulator in beigeing maintenance[233] (Fig. 4.8, p. 125).

Overall the collected evidence indicates these cells are not only able to differentiate into brown adipocytes at 32°C but also to retain this brown signature, specially *UCP1* protein expression (Fig. 4.2, p. 114)

and an increased bioenergetic response (Fig. 4.10, p. 128). However, further research is needed in order to investigate *in vivo* beigeing maintenance. A summary of the key findings of Chapter 4 can be observed in Fig. 7.2.

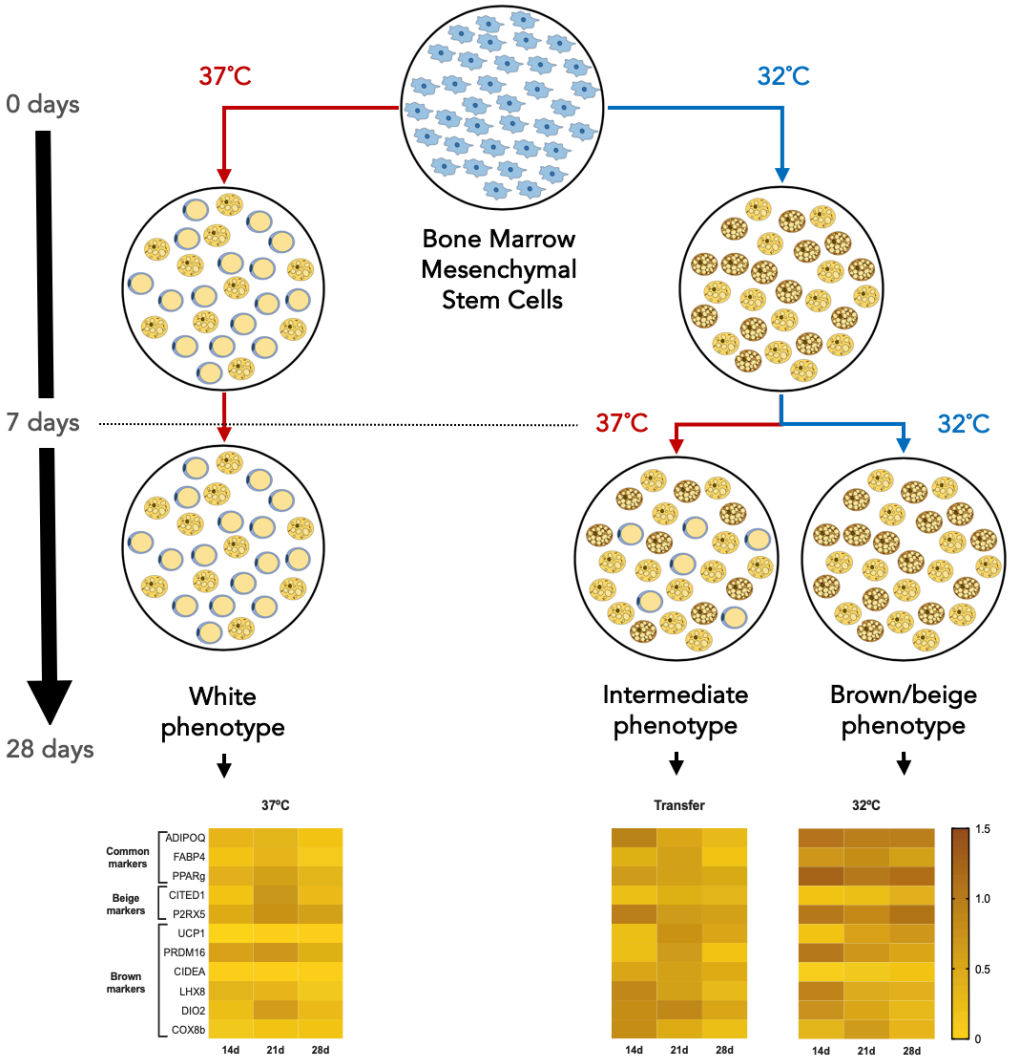


Figure 7.2. Cold induced browning of MSC-derived adipocytes is not fully reversible after return to normal culture conditions.

Schematic figure displaying an overview of bone marrow MSC differentiation at 37°C and 32°C. Hypothermal differentiated cells were transferred after 7 days of cold exposure (Transfer), normal and cold cultured adipocytes were differentiated in parallel for comparison. Cells differentiated at 37°C and 32°C showed a white and brown/beige phenotype, respectively while Transfer cells displayed an intermediate phenotype after 21 days of being transferred from cold to normal conditions.

7.3 MSC human isolation

Primary MSCs are widely used to validate and compare findings made in rodent cell lines. Here, a healthy UCT was used to optimise the best isolation protocol, growth and adipogenic differentiation medium.

One of the earliest techniques of cell isolation is the explant culture. However, the enzymatic method seems to yield shorter DT[250,263], which was in accordance with results reported here (DT=22.8± 4h; Fig. 5.4, p. 148). hPL is known to stimulate MSC proliferation and expansion, and used in different cell types that have been used in clinical trials with no reported side effects[258,259,267,346]. Therefore, cells isolated from hUCT were able to successfully grow in a medium containing DMEM low glucose (1 g/L), 10% hPL, 1% L-gln and 1% P/S, these cells showed plastic adherence (Fig. 5.5, p. 150) and positive CD73, CD90 and CD105 staining[5] (Fig. 5.6, p.151 and 5.7, p. 152). Although, MSCs were able to undergo adipogenic differentiation, the medium used was different from the growth medium containing DMEM-F12, 10% FBS and 1% P/S supplemented with insulin, dexamethasone, rosiglitazone and IBMX[110] (Fig. 5.9, p. 156). However several studies have reported using two different mediums for growth and MSCs potency testing[112,256,347].

Taken together, the data obtained gave a suitable isolation method, growth and differentiation media for hUCT-MSCs. It would be of importance to validate each method selected in order to corroborate these results with a greater sample size and to test a different osteogenic recipe which in these results failed to meet the MSCs induction requirements (Fig. 5.10, p. 158). Fig. 7.3 shows a concise summary of the best protocol and media used in Chapter 5.

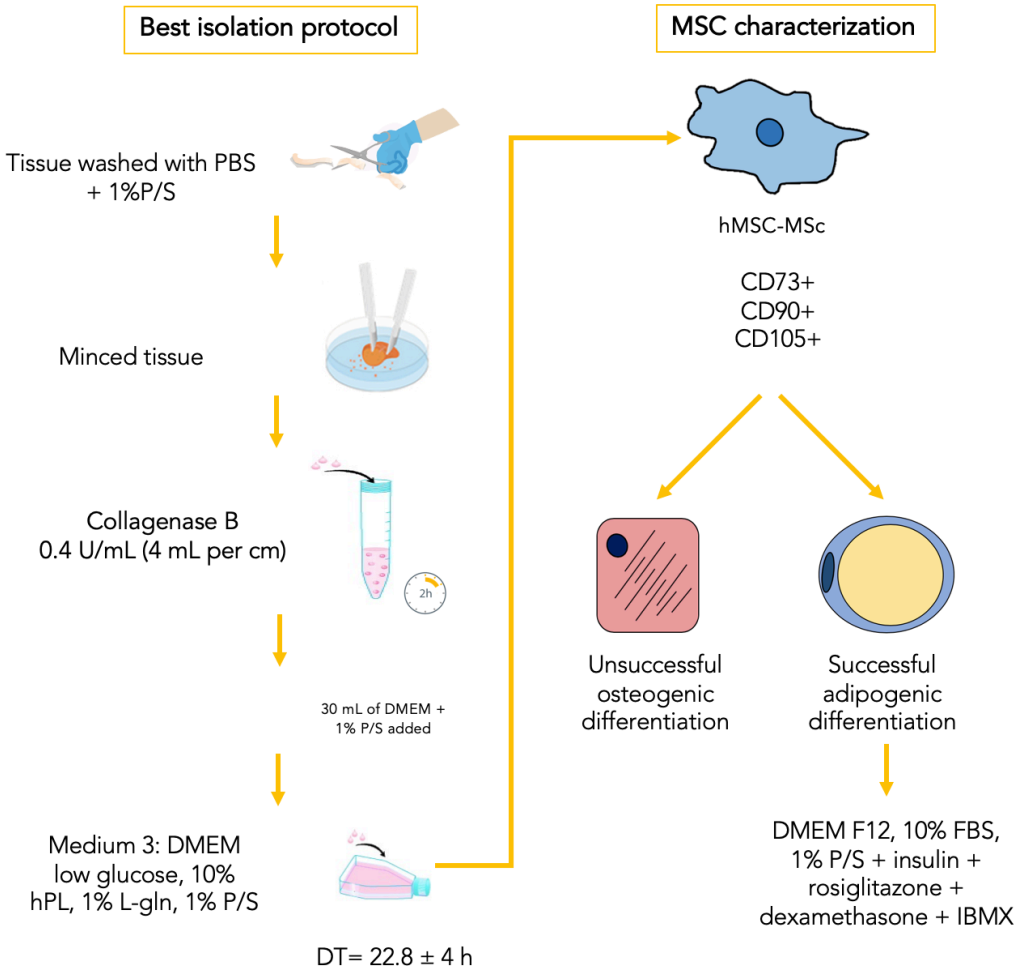


Figure 7.3. hUCT-MSC isolation and characterization.

Schematic figure displaying the best isolation protocol which involved mincing the human umbilical cord tissue (hUCT), disaggregating it with collagenase B and seeding it with a medium containing human platelet lysate (hPL). MSC characterization showed positive co-staining of CD73+, CD90+ and CD105+. hUCT-MSCs differentiation into osteoblast was not successful while adipogenic differentiation was achieved with a medium containing DMEM-F12, FBS, P/S supplemented with an adipogenic cocktail.

7.4 Browning of healthy and GD hUCT-MSCs

Metabolic diseases, such as diabetes, are one of the main concerns for impairing brown fat development[348-351]. The analysis of healthy and GD MSCs derived from hUCT highlighted the ability of healthy cells to differentiate into adipocytes exhibiting common white features (Fig. 6.5 p. 180) at normal culture conditions while at 32ºC these cells showed high UCP1 protein expression (Fig. 6.8 p.186). It was previously reported that hUCB-MSCs were an inappropriate cell type to be differentiated into brown adipocytes[109], these results agree to an extent due to the lack of other brown molecular markers in cells at 32ºC (Fig. 6.6 p. 182). However, a more detailed analysis on the bioenergetics of healthy MSCs would indicate their normal thermogenic functionality. On the other hand, GD-MSCs showed browning impairment at 32ºC while at 37ºC these cells appear to achieve adipogenic differentiation (Fig. 6.3 p. 175). Taken together these results showed that GD cells cannot be differentiated towards brown adipocytes, hence these cells are also unsuitable for therapeutic options[173].

Further research is now required to elucidate the bioenergetic of both of these backgrounds, and to identify their potential to respond to *β3-AR* agonists. Summary of the key finding for Chapter 6 can be observed in Fig. 7.4.

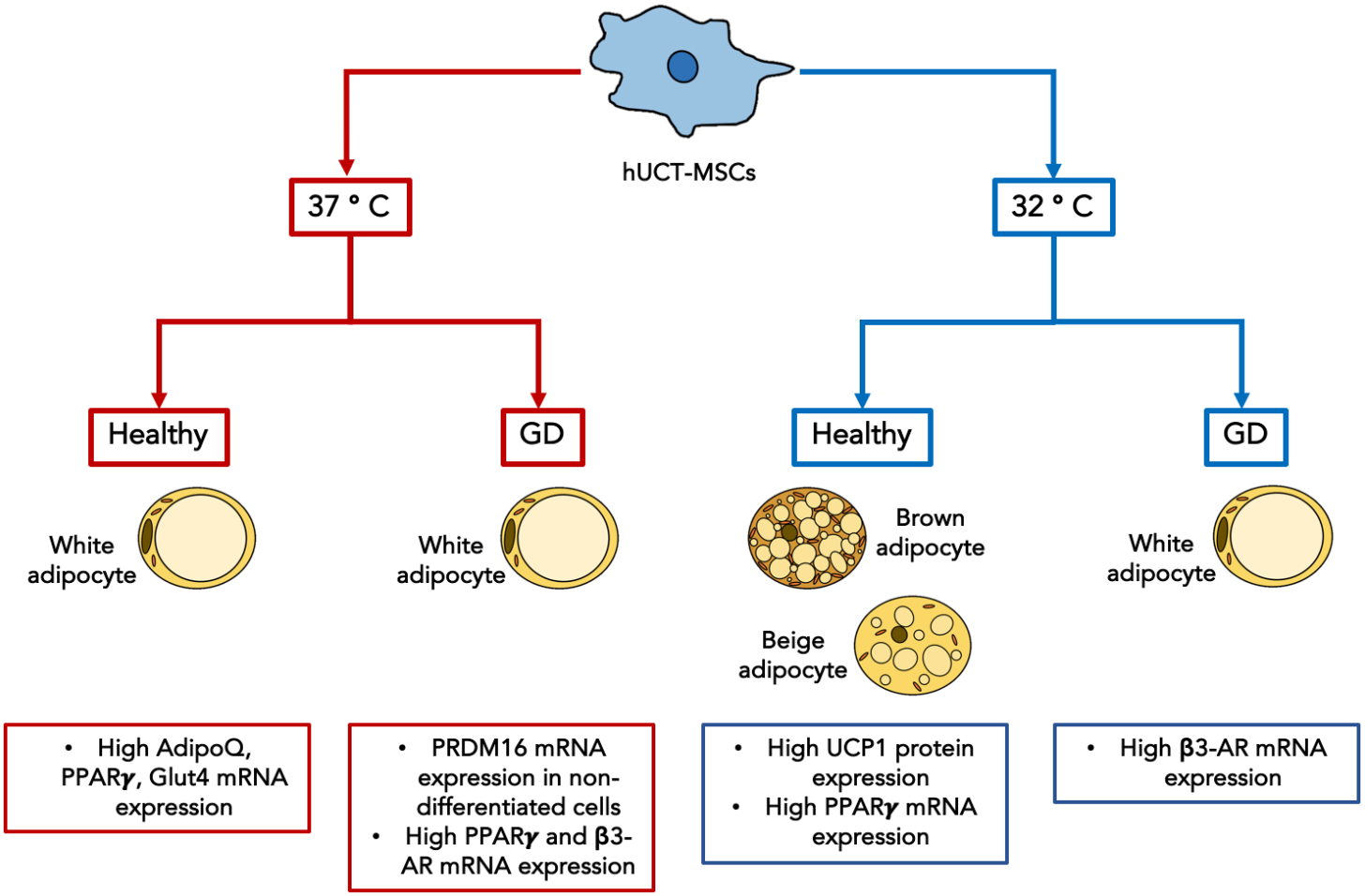


Figure 7.4. hUCT MSCs-derived adipocytes are able to differentiate under normal and hypothermal culture conditions. Schematic figure displaying the main features related to healthy and Gestational diabetic (GD) MSCs-derived adipocytes at both culture conditions. Healthy adipocytes showed normal adipogenic markers at 37°C while 32°C differentiated cells displayed browning traits with high UCP1 protein expression. GD cells showed high β3-AR mRNA at both 37°C and 32°C conditions.

7.5 Final remarks

In this study human and mouse MSCs were used in order to evaluate their browning potential when a cold temperature stimulus was applied during their differentiation. These results showed four main conclusions: first, MSCs differentiated under hypothermic conditions acquire brown morphology and molecular signature. Second, cold MSCs-derived adipocytes display an increased bioenergetics response and are able to maintain it after 21 days of being transferred to warm conditions. Third, cold derived adipocytes may share a *UCP1*-dependent and independent thermogenesis through the SERCA2b Ca^{2+} increased mechanism. Finally, GD-MSCs are unable to differentiate into brown adipocytes under cold culture conditions.

Chapter 3 described an adipogenic differentiation method in which only cold temperature is used in order to enhance beigeing traits in fully differentiated adipocytes. One of the main differences found in the gene expression was the increased TRPV1 mRNA in cold differentiated adipocytes when compared to those in normal culture conditions. A study found a 40% reduction in glucose metabolism in WAT and BAT TRPV1 knockout mice exposed to high fat diet when compared to wild type which highlights the importance of TRPV1 in energy expenditure[200]. It would be interesting to investigate the role of UCP1 in TRPV1 knockout MSCs during adipogenesis, this could help to elucidate a possible feedback between these two genes, and if the absence of TRPV1 could trigger another TRPs channels such as TRPV2 and TRPV4, as described in Chapter 4.

Another interesting subject to explore is the analysis of the MSC population able to differentiate. As described before, only 30-40% of MSCs were differentiated into adipocytes, therefore a more homogeneous population could provide a higher beige/brown profile in MS cells. For this reason, the main markers to use for an early commitment detection are PRDM16, PGC1α, CD137 and Myf5[60,66,352–354]. Interestingly, the bioenergetic of the hypothermic differentiated cells was higher than of cells differentiated under normal culture conditions. Although the percentage of differentiation in adipocytes at 37°C might be increased to same levels as 32°C derived adipocytes, OCR and ECAR could not reach the same values of those observed in the hypothermic conditions, which highlights the importance of cold stimulus applied in this research. In addition, fully differentiated adipocytes could be also targeted via TRPV1/UCP1 co-expression to perform single-cell analysis.

As described in Chapter 4, hypothermic differentiated adipocytes are still metabolically active after 28 days of being transferred into warm conditions. The next step would be to calculate the amount of energy these cells can consume and how this energy could relate to obesity management. The adaptability observed in cold differentiated adipocytes, as well as their molecular and bioenergetic profile could provide a possible therapeutic option not only for obesity but for other related diseases. Moreover, further research is needed in order to know the length of time these cells are bioenergetically active and if they could be continuously activated through the TRPs channels.

Regarding UCT MSCs from healthy and GD backgrounds, more studies and a high number of samples are needed in order to continue the evaluation of these cells and their adipogenic potential. Additionally,

their rapid availability, large number of cells obtained and low risk of rejection makes them an excellent candidate for cellular therapy[274]. Furthermore, the exposure of a high glucose niche in GD cells could open up the possibility to evaluate their pathway behaviour after a browning stimulus is applied, such as cold exposure. This could help to elucidate if the same molecules used in obese individuals can equally work in diabetic patients.

Additionally, understanding beige commitment could help to comprehend the adaptability of the different adipose depots throughout climate change. Several studies suggest that individuals exposed to cold temperatures possess higher amounts of BAT than those exposed to warmer conditions[147,149,355]. However, there are still some questions to be answered, how much time does a person need to reduce a significant amount of weight after the activation or transplant of beige / brown adipocytes? Does cold temperature play a major role in the maintenance of these cells? How much BAT does an individual need?

In conclusion, there are two potential therapies that could benefit patients with obesity and related metabolic diseases. It is known that a percentage of BM-MSCs travel to different adipose depots[50,356], for this reason one possible application would be to target MSCs derived from the bone marrow. This could be done by using a molecule, either a drug or a natural compound, which can modulate TRPV1 channel activity as a possible treatment for obesity and its related diseases, such as diabetes[357]. As an example, it has been previously described that capsaicin ingestion benefits controlling food intake and obesity. TRPV1 is activated by several stimuli and molecules, such as cold exposure and capsaicin, respectively[358]. Capsaicin has been widely studied due

to its ability to decrease body temperature in different species, including human[359]. A study revealed that volunteers ingesting capsaicin capsules displayed increased satiety and energy expenditure[360]. Moreover, capsaicin consumption also helped to maintain body weight in obese subjects[361]. Altogether, these data could suggest a role of TRPV1 in the control of diabetes, insulin resistance and obesity[357].

The second potential translational application of MSCs could be using the already differentiated brown/beige adipocytes as cellular therapy[354]. The cell therapy could be based with MSCs isolated from UCT treated with factors that either enhance or promote beige/brow differentiation, e.g. cold stimuli, then these cells could be transplanted into individuals to allow *in vivo* expansion to generate functional brown adipocytes and help lose undesired fat. This is potentially beneficial to individuals prone to obesity or with physical limitations. However, additional research is needed to ensure cell engraftment, as well as clinical trials, and to assess and improve the efficacy of these two possible approaches.

Finally, further research will now be necessary to elucidate the exact regulatory characteristics of which these newly derived adipocytes regulate energy expenditure and if the *UCP1*/TRPVs link could play a major role in temperature regulation, browning activation and maintenance. Overall, the work presented highlight MSCs potentiality towards beigeing. This could facilitate future studies on how to recruit and conserve these cells by targeting specific pathways in obese individuals and to control other metabolic diseases.

References

1. Lobstein, T., Brinsden, H., Gill, T., Kumanyika, S. & Swinburn, B. Comment: obesity as a disease – some implications for the World Obesity Federation's advocacy and public health activities. *Obes. Rev.* **18**, 724–726 (2017).
2. Bray, G. A., Kim, K. K. & Wilding, J. P. H. Obesity: a chronic relapsing progressive disease process. A position statement of the World Obesity Federation. *Obes. Rev.* **18**, 715–723 (2017).
3. Seale, P., Kajimura, S. & Spiegelman, B. M. Transcriptional control of brown adipocyte development and thermogenesis. *Genes Dev.* 788–797 (2009). doi:10.1038/ijo.2010.178
4. Park, A. Distinction of white, beige and brown adipocytes derived from mesenchymal stem cells. *World J. Stem Cells* **6**, 33 (2014).
5. Dominici, M. *et al.* Minimal criteria for defining multipotent mesenchymal stromal cells. The International Society for Cellular Therapy position statement. *Cytotherapy* **8**, 315–317 (2006).
6. Caplan, A. I. Mesenchymal Stem Cells *. *J. Orthop. Res.* 641–650 (1991).
7. Pittenger, M. F. *et al.* Multilineage potential of adult human mesenchymal stem cells. *Science (80-.).* **284**, 143–147 (1999).
8. Beranger, G. E. *et al.* In vitro brown and 'brite'/"beige" adipogenesis: Human cellular models and molecular aspects. *Biochim. Biophys. Acta - Mol. Cell Biol. Lipids* **1831**, 905–914 (2013).
9. Galic, S., Oakhill, J. S. & Steinberg, G. R. Molecular and Cellular Endocrinology : Adipose tissue as an endocrine organ. *Mol. Cell. Endocrinol.* **316**, 129–139 (2010).
10. Cinti, S. The adipose organ. *Prostaglandins Leukot. Essent. Fat. Acids* **73**, 9–15 (2005).
11. Freedland, E. S. Role of a critical visceral adipose tissue threshold (CVATT) in metabolic syndrome: implications for controlling dietary carbohydrates: a review. *Nutr. Metab. (Lond).* **1**, 12 (2004).
12. Frontini, A. & Cinti, S. Distribution and Development of Brown Adipocytes in the Murine and Human Adipose Organ. *Cell Metab.* **11**, 253–256 (2010).
13. Cristancho, A. G. & Lazar, M. A. Forming functional fat: a growing understanding of adipocyte differentiation. *Nat. Rev. Mol. Cell Biol.* **12**, 722–34 (2011).
14. Alexander, C. M. *et al.* Dermal white adipose tissue: A new component of the thermogenic response. *J. Lipid Res.* **56**, 2061–2069 (2015).
15. Kasza, I. *et al.* Syndecan-1 Is Required to Maintain Intradermal Fat and Prevent Cold Stress. *PLoS Genet.* **10**, (2014).
16. Schoettl, T., Fischer, I. P. & Ussar, S. Heterogeneity of adipose tissue in development and metabolic function. *J. Exp. Biol.* **121**, (2018).
17. Sanchez-Gurmaches, J., Hung, C. M. & Guertin, D. A. Emerging Complexities in Adipocyte Origins and Identity. *Trends Cell Biol.* **26**, 313–326 (2016).
18. Gesta, S., Tseng, Y. H. & Kahn, C. R. Developmental Origin of Fat: Tracking

Obesity to Its Source. *Cell* **131**, 242–256 (2007).

19. Andersson, D. P., Arner, E., Hogling, D. E., Rydén, M. & Arner, P. Abdominal subcutaneous adipose tissue cellularity in men and women. *Int. J. Obes.* **41**, 1564–1569 (2017).

20. Edens, N. K., Fried, S. K., Kral, J. G., Hirsch, J. & Leibel, R. L. In vitro lipid synthesis in human adipose tissue from three abdominal sites. *Am. J. Physiol. Metab.* **265**, E374–E379 (1993).

21. Fried, S. K., Leibel, R. L., Edens, N. K. & Kral, J. G. Lipolysis in Intraabdorninal Adipose Tissues of Obese Women and Men. *Obes. Res.* **1**, 443–448 (1993).

22. Tchkonia, T. *et al.* Identification of depot-specific human fat cell progenitors through distinct expression profiles and developmental gene patterns. *Am. J. Physiol. - Endocrinol. Metab.* **292**, 298–307 (2007).

23. Chau, Y.-Y. *et al.* Visceral and subcutaneous fat have different origins and evidence supports a mesothelial source. *Nat. Cell Biol.* **16**, 367–375 (2014).

24. Driskell, R. R., Jahoda, C. A. B., Chuong, C. M., Watt, F. M. & Horsley, V. Defining dermal adipose tissue. *Exp. Dermatol.* **23**, 629–631 (2014).

25. Zwick, R. K., Guerrero-Juarez, C. F., Horsley, V. & Plikus, M. V. Anatomical, Physiological, and Functional Diversity of Adipose Tissue. *Cell Metab.* **27**, 68–83 (2018).

26. Gasperoni, C. & Salgarello, M. Rationale of subdermal superficial liposuction related to the anatomy of subcutaneous fat and the superficial fascial system. *Aesthetic Plast. Surg.* **19**, 13–20 (1995).

27. Smith, S. R. *et al.* Contributions of total body fat, abdominal subcutaneous adipose tissue compartments, and visceral adipose tissue to the metabolic complications of obesity. *Metabolism* **50**, 425–435 (2001).

28. Walker, G. E. *et al.* Deep subcutaneous adipose tissue: A distinct abdominal adipose depot. *Obesity* **15**, 1933–1943 (2007).

29. Chase, H. B., Montagna, W. & Malone, J. D. Changes in the skin in relation to the hair growth cycle. *Anat. Rec.* **116**, 75–81 (1953).

30. Wojciechowicz, K., Gledhill, K., Ambler, C. A., Manning, C. B. & Jahoda, C. A. B. Development of the Mouse Dermal Adipose Layer Occurs Independently of Subcutaneous Adipose Tissue and Is Marked by Restricted Early Expression of FABP4. *PLoS One* **8**, 1–15 (2013).

31. Wojciechowicz, K., Markiewicz, E. & Jahoda, C. A. B. C/EBP**α** identifies differentiating preadipocytes around hair follicles in foetal and neonatal rat and mouse skin. *Exp. Dermatol.* **17**, 675–680 (2008).

32. Festa, E. *et al.* Adipocyte Lineage Cells Contribute to the Skin Stem Cell Niche to Drive Hair Cycling. *Cell* **146**, 761–771 (2011).

33. Rodeheffer, M. S., Birsoy, K. & Friedman, J. M. Identification of White Adipocyte Progenitor Cells In Vivo. *Cell* **135**, 240–249 (2008).

34. Frank, S., Stallmeyer, B., Kämpfer, H., Kolb, N. & Pfeilschifter, J. Leptin enhances wound re-epithelialization and constitutes a direct function of leptin in skin repair. *J. Clin. Invest.* **106**, 501–509 (2000).

35. Ring, B. *et al.* Systemically and topically administered leptin both accelerate wound healing in diabetic ob/ob mice. *Endocrinology* **141**, 446–449 (2000).

36. Sierra-Honigmann, M. R. *et al.* Biological Action of Leptin as an Angiogenic Factor. *Science (80-.).* **281**, 1683 LP – 1686 (1998).

37. Salathia, N. S., Shi, J., Zhang, J. & Glynne, R. J. An in vivo screen of secreted proteins identifies adiponectin as a regulator of murine cutaneous wound healing. *J. Invest. Dermatol.* **133**, 812–821 (2013).

38. Shibata, S. *et al.* Adiponectin Regulates Cutaneous Wound Healing by Promoting Keratinocyte Proliferation and Migration via the ERK Signaling Pathway. *J. Immunol.* **189**, 3231–3241 (2012).

39. Jin, C. E., Xiao, L., Ge, Z. H., Zhan, X. B. & Zhou, H. X. Role of adiponectin in adipose tissue wound healing. *Genet. Mol. Res.* **14**, 8883–8891 (2015).

40. Draghi, F., Ferrozzi, G., Urciuoli, L., Bortolotto, C. & Bianchi, S. Hoffa's fat pad abnormalities, knee pain and magnetic resonance imaging in daily practice. *Insights Imaging* **7**, 373–383 (2016).

41. Distel, E. *et al.* The infrapatellar fat pad in knee osteoarthritis: An important source of interleukin-6 and its soluble receptor. *Arthritis Rheum.* **60**, 3374–3377 (2009).

42. Gandhi, R. *et al.* Microarray analysis of the infrapatellar fat pad in knee osteoarthritis: Relationship with joint inflammation. *J. Rheumatol.* **38**, 1966–1972 (2011).

43. Hui, W. *et al.* Leptin produced by joint white adipose tissue induces cartilage degradation via upregulation and activation of matrix metalloproteinases. *Ann. Rheum. Dis.* **71**, 455 LP – 462 (2012).

44. Iacobellis, G. Epicardial and pericardial fat: Close, but very different. *Obesity* **17**, 625 (2009).

45. Iacobellis, G. Local and systemic effects of the multifaceted epicardial adipose tissue depot. *Nat. Rev. Endocrinol.* **11**, 363–371 (2015).

46. Sacks, H. S. *et al.* Uncoupling Protein-1 and Related Messenger Ribonucleic Acids in Human Epicardial and Other Adipose Tissues: Epicardial Fat Functioning as Brown Fat. *J. Clin. Endocrinol. Metab.* **94**, 3611–3615 (2009).

47. Yudkin, J. S., Eringa, E. & Stehouwer, C. D. A. "Vasocrine" signalling from perivascular fat: a mechanism linking insulin resistance to vascular disease. *Lancet* **365**, 1817–1820 (2005).

48. Mazurek, T. *et al.* Human Epicardial Adipose Tissue Is a Source of Inflammatory Mediators. *Circulation* **108**, 2460–2466 (2003).

49. Sacks, H. & Symonds, M. E. Anatomical locations of human brown adipose tissue: Functional relevance and implications in obesity and type 2 diabetes. *Diabetes* **62**, 1783–1790 (2013).

50. Horowitz, M. C. *et al.* Bone marrow adipocytes. *Adipocyte* **6**, 193–204 (2017).

51. Ambrosi, T. H. *et al.* Adipocyte Accumulation in the Bone Marrow during Obesity and Aging Impairs Stem Cell-Based Hematopoietic and Bone Regeneration. *Cell Stem Cell* **20**, 771-784.e6 (2017).

52. Naveiras, O. *et al.* Bone-marrow adipocytes as negative regulators of the haematopoietic microenvironment. *Nature* **460**, 259–263 (2009).

53. Fazeli, P. K. *et al.* Marrow fat and bone--new perspectives. *J. Clin. Endocrinol. Metab.* **98**, 935–945 (2013).

54. Menagh, P. J. *et al.* Growth hormone regulates the balance between bone formation and bone marrow adiposity. *J. Bone Miner. Res.* **25**, 757–768 (2010).

55. Cawthorn, W. P. *et al.* Bone marrow adipose tissue is an endocrine organ that contributes to increased circulating adiponectin during caloric restriction. *Cell Metab.* **20**, 368–375 (2014).

56. Scheller, E. L. *et al.* Region-specific variation in the properties of skeletal adipocytes reveals regulated and constitutive marrow adipose tissues. *Nat. Commun.* **6**, (2015).

57. Zhou, B. O. *et al.* Bone marrow adipocytes promote the regeneration of stem cells and haematopoiesis by secreting SCF. *Nat. Cell Biol.* **19**, 891–903 (2017).

58. Jong, J. M. A. de, Larsson, O., Cannon, B. & Nedergaard, J. A stringent validation of mouse adipose tissue markers. *Am. J. Physiol. Endocrinol Metab* E1085–E1105 (2015).

59. Wang, W. & Seale, P. Control of brown and beige fat development. *Nat. Rev. Mol. Cell Biol.* **17**, 691–702 (2016).

60. Garcia, R. A., Roemmich, J. N. & Claycombe, K. J. Evaluation of markers of beige adipocytes in white adipose tissue of the mouse. *Nutr. Metab. (Lond).* **13**, 24 (2016).

61. Carrière, A. *et al.* Browning of white adipose cells by intermediate metabolites: An adaptive mechanism to alleviate redox pressure. *Diabetes* **63**, 3253–3265 (2014).

62. Carobbio, S., Rosen, B. & Vidal-Puig, A. Adipogenesis: New insights into brown adipose tissue differentiation. *J. Mol. Endocrinol.* **51**, (2013).

63. Seale, P. *et al.* PRDM16 controls a brown fat/skeletal muscle switch. *Nature* **454**, 961–7 (2008).

64. Kajimura, S., Seale, P. & Spiegelman, B. M. Transcriptional Control of Brown Fat Development. *Cell Metab.* **11**, 257–262 (2010).

65. Wu, J. *et al.* Beige Adipocytes are a Distinct Type of Thermogenic Fat Cell in Mouse and Human. *Cell* **150**, 366–376 (2012).

66. Ussar, S. *et al.* Asc-1, PAT2 and P2RX5 are novel cell surface markers for white, beige and brown adipocytes. **6**, 882–886 (2014).

67. Rosenwald, M., Perdikari, A., Rülicke, T. & Wolfrum, C. Bi-directional interconversion of brite and white adipocytes. *Nat. Cell Biol.* **15**, 659–667 (2013).

68. Juffroy, O. *et al.* Subcutaneous graft of D1 mouse mesenchymal stem cells leads to the formation of a bone-like structure. *Differentiation* **78**, 223–231 (2009).

69. Asano, H. *et al.* Induction of beige-like adipocytes in 3T3-L1 cells. *J. Vet. Med. Sci.* **76**, 57–64 (2014).

70. Boon, M. R. *et al.* BMP7 Activates Brown Adipose Tissue and Reduces Diet-Induced Obesity Only at Subthermoneutrality. *PLoS One* **8**, (2013).

71. Tseng, Y. *et al.* New role of bone morphogenetic protein 7 in brown adipogenesis and energy expenditure. *Nature* **454**, 1000–1004 (2008).

72. Whittle, A. J. *et al.* BMP8B increases brown adipose tissue thermogenesis through both central and peripheral actions. *Cell* **149**, 871–885 (2012).

73. Pellegrinelli, V. *et al.* Adipocyte-secreted BMP8b mediates adrenergic-induced

remodeling of the neuro-vascular network in adipose tissue. *Nat. Commun.* **9**, 1–18 (2018).

74. Elsen, M. *et al.* BMP4 and BMP7 induce the white-to-brown transition of primary human adipose stem cells. *Am. J. Physiol. Cell Physiol.* **306**, C431-40 (2014).

75. Townsend, K. & Tseng, Y.-H. Brown adipose tissue: Recent insights into development, metabolic function and therapeutic potential. *Adipocyte* **1**, 13–24 (2012).

76. Schulz, T. J. *et al.* Identification of inducible brown adipocyte progenitors residing in skeletal muscle and white fat. *Proc. Natl. Acad. Sci. U. S. A.* **108**, 143–148 (2011).

77. Koppen, A. & Kalkhoven, E. Brown vs white adipocytes: The PPAR?? coregulator story. *FEBS Lett.* **584**, 3250–3259 (2010).

78. Hu, J. *et al.* Short-chain fatty acid acetate stimulates adipogenesis and mitochondrial biogenesis via GPR43 in brown adipocytes. *Endocrinology* **157**, 1881–1894 (2016).

79. Barbatelli, G. *et al.* The emergence of cold-induced brown adipocytes in mouse white fat depots is determined predominantly by white to brown adipocyte transdifferentiation. *Am. J. Physiol. Metab.* **298**, E1244–E1253 (2010).

80. Petrovic, N. *et al.* Chronic peroxisome proliferator-activated receptor **γ** (PPAR**γ**) activation of epididymally derived white adipocyte cultures reveals a population of thermogenically competent, UCP1-containing adipocytes molecularly distinct from classic brown adipocytes. *J. Biol. Chem.* **285**, 7153–7164 (2010).

81. Guerra, C., Koza, R. A., Yamashita, H., Walsh, K. & Kozak, L. P. Emergence of brown adipocytes in white fat in mice is under genetic control effects on body weight and adiposity. *J. Clin. Invest.* **102**, 412–420 (1998).

82. Yoshimura, K. *et al.* Characterization of Freshly Isolated and Cultured Cells Derived From the Fatty and Fluid Portions of Liposuction Aspirates. *J. Cell. Physiol.* **208**, 64–76 (2006).

83. Moreno-Navarrete, J. M. & Fernández-Real, J. M. Adipose tissue biology. in *Adipose Tissue Biology* (ed. Symonds, M. E.) 1–413 (2012). doi:10.1007/978-1-4614-0965-6

84. Diduch, D. R., Coe, M. R. & Joyner, C. Cell from Osteogenic That Differ in Terms of Collagen Synthesis , and Matrix Characteristics , Mineralization * CB8-. *J. bone Jt. surgery.* **75-A**, 92–105 (1993).

85. Cui, Q., Wang, G. J. & Balian, G. Steroid-induced adipogenesis in a pluripotential cell line from bone marrow. *J. Bone Joint Surg. Am.* **79**, 1054–1063 (1997).

86. Fernandez, N. *et al.* Mouse Mesenchymal Progenitor Cells Expressing Adipogenic and Osteogenic Transcription Factors Suppress the Macrophage Inflammatory Response. *Stem Cells Int.* **2017**, (2017).

87. Spiegelman, B. M., Hu, E., Kim, J. B. & Brun, R. PPARg and the control of adipogenesis. *Biochimie* **79**, 111–112 (1997).

88. Carbonare, L. D., Innamorati, G. & Valenti, M. T. Transcription Factor Runx2 and its Application to Bone Tissue Engineering. *Stem Cell Rev. Reports* **8**, 891–897 (2012).

89. Park, S. B. *et al.* SOX2 has a crucial role in the lineage determination and proliferation of mesenchymal stem cells through Dickkopf-1 and c-MYC. *Cell Death Differ.* **19**, 534–545 (2012).

90. Wang, D., Haile, A. & Jones, L. Rosiglitazone Induced Adipogenesis in a Bone Marrow Mesenchymal Stem Cell Line. *Poster No. 1756 • ORS 2011 Annu. Meet.* (2011).

91. Contador, D. *et al.* Dexamethasone and rosiglitazone are sufficient and necessary for producing functional adipocytes from mesenchymal stem cells. *Exp. Biol. Med.* **240**, 1235–46 (2015).

92. Velickovic, K. *et al.* Low temperature exposure induces browning of bone marrow stem cell derived adipocytes in vitro. *Sci. Rep.* **8**, 1–12 (2018).

93. Velickovic, K. *et al.* Caffeine exposure induces browning features in adipose tissue in vitro and in vivo. *Sci. Rep.* **9**, 1–11 (2019).

94. Klein, J., Fasshauer, M., Klein, H. H., Benito, M. & Kahn, C. R. Novel adipocyte lines from brown fat: a model system for the study of differentiation, energy metabolism, and insulin action. *BioEssays* **24**, 382–388 (2002).

95. Zilberfarb, V. *et al.* Human immortalized brown adipocytes express functional beta3-adrenoceptor coupled to lipolysis. *J. Cell Sci.* **110**, 801–807 (1997).

96. Shamsi, F. & Tseng, Y. Protocols for generation of immortalized human brown and white preadipocyte cell lines. *Methods Mol Biol.* **1566**, 77–85 (2017).

97. Tiraby, C. *et al.* Acquirement of brown fat cell features by human white adipocytes. *J. Biol. Chem.* **278**, 33370–33376 (2003).

98. Jo, S. J. *et al.* Temporary increase of PPAR-**γ** and transient expression of UCP-1 in stromal vascular fraction isolated human adipocyte derived stem cells during adipogenesis. *Lipids* **46**, 487–494 (2011).

99. Cinti, S. Transdifferentiation properties of adipocytes in the adipose organ. *Am. J. Physiol. Metab.* **297**, E977–E986 (2009).

100. Lee, P., Swarbrick, M. M., Zhao, J. T. & Ho, K. K. Y. Inducible brown adipogenesis of supraclavicular fat in adult humans. *Endocrinology* **152**, 3597–3602 (2011).

101. Lee, J.-Y. *et al.* Triiodothyronine induces UCP-1 expression and mitochondrial biogenesis in human adipocytes. *Am. J. Physiol. Cell Physiol.* **302**, C463-72 (2012).

102. Lee, Y.-H., Petkova, A. P., Mottillo, E. P. & Granneman, J. G. In vivo identification of bipotential adipocyte progenitors recruited by **β**3-adrenoceptor activation and high fat feeding. *Cell Metab.* **15**, 480–491 (2012).

103. Di Franco, A. *et al.* Searching for classical brown fat in humans: Development of a novel human fetal brown stem cell model. *Stem Cells* 1–18 (2016). doi:10.1002/stem.

104. Huang, P.-I. *et al.* PGC-1**α** Mediates Differentiation of Mesenchymal Stem Cells to Brown Adipose Cells. *J. Atheroscler. Thromb.* **18**, 966–980 (2011).

105. Collins, S., Yehuda-Shnaidman, E. & Wang, H. Positive and negative control of Ucp1 gene transcription and the role of **β**-adrenergic signaling networks. *Int. J. Obes.* **34**, S28–S33 (2010).

106. Fernandez-Marcos, P. & Auwerx, J. Regulation of PGC-1a, a nodal regulator of mitochondrial biogenesis. *Am J Clin Nutr* **93**, 884S–90S (2011).

107. Morganstein, D. L. *et al.* Human fetal mesenchymal stem cells differentiate into brown and white adipocytes: a role for ERRα in human UCP1 expression. *Cell Res.* **20**, 434–444 (2010).

108. Crisan, M. *et al.* A Reservoir of Brown Adipocyte Progenitors in Human Skeletal Muscle. *Stem Cells* **26**, 2425–2433 (2008).

109. Rashnonejad, A., Ercan, G., Gunduz, C., Akdemir, A. & Tiftikcioglu, Y. O. Comparative analysis of human UCB and adipose tissue derived mesenchymal stem cells for their differentiation potential into brown and white adipocytes. *Mol. Biol. Rep.* **45**, 233–244 (2018).

110. Mennan, C. *et al.* Isolation and characterisation of mesenchymal stem cells from different regions of the human umbilical cord. *Biomed Res. Int.* **2013**, (2013).

111. Secco, M. *et al.* Multipotent stem cells from umbilical cord: cord is richer than blood! *Stem Cells* **26**, 146–150 (2008).

112. Shaer, A., Azarpira, N., Aghdaie, M. H. & Esfandiari, E. Isolation and characterization of human mesenchymal stromal cells derived from placental decidua basalis; umbilical cord wharton's jelly and amniotic membrane. *Pakistan J. Med. Sci.* **30**, 1022–1026 (2014).

113. Choudhery, M. S., Badowski, M., Muise, A. & Harris, D. T. Comparison of human mesenchymal stem cells derived from adipose and cord tissue. *Cytotherapy* **15**, 330–343 (2013).

114. Saben, J. *et al.* Distinct adipogenic differentiation phenotypes of human umbilical cord mesenchymal cells dependent on adipogenic conditions. *Exp. Biol. Med. (Maywood).* **239**, 1340–1351 (2014).

115. Kern, S., Eichler, H., Stoeve, J., Klüter, H. & Bieback, K. Comparative analysis of mesenchymal stem cells from bone marrow, umbilical cord blood, or adipose tissue. *Stem Cells* **24**, 1294–1301 (2006).

116. Wagner, W. *et al.* Comparative characteristics of mesenchymal stem cells from human bone marrow, adipose tissue, and umbilical cord blood. *Exp. Hematol.* **33**, 1402–1416 (2005).

117. Ahfeldt, T. *et al.* Programming human pluripotent stem cells into white and brown adipocytes. *Nat. Cell Biol.* **14**, 209–219 (2012).

118. Hafner, A.-L. *et al.* Brown-like adipose progenitors derived from human induced pluripotent stem cells: Identification of critical pathways governing their adipogenic capacity. *Sci. Rep.* **6**, 32490 (2016).

119. Scott, M. A., Nguyen, V. T., Levi, B. & James, A. W. Current methods of adipogenic differentiation of mesenchymal stem cells. *Stem Cells Dev.* **20**, 1793–804 (2011).

120. Sarjeant, K. & Stephens, J. M. Adipogenesis. *Cold Spring Harb. Perspect. Biol.* (2012). doi:10.1016/B978-0-12-378630-2.00089-X

121. Chen, Q. *et al.* Fate decision of mesenchymal stem cells: adipocytes or osteoblasts? *Cell Death Differ.* **23**, 1128–1139 (2016).

122. Klemm, D. J. *et al.* Insulin-induced adipocyte differentiation: Activation of CREB rescues adipogenesis from the arrest caused by inhibition of prenylation. *J. Biol. Chem.* **276**, 28430–28435 (2001).

123. Cignarelli, A. *et al.* Insulin and insulin receptors in adipose tissue development.

Int. J. Mol. Sci. **20**, 1–20 (2019).

124. Zhang, H. H. *et al.* Insulin stimulates adipogenesis through the Akt-TSC2-mTORC1 pathway. *PLoS One* **4**, (2009).

125. Li, Y., Yue-bai, L. & Yi-sheng, W. Dexamethasone-induced adipogenesis in primary marrow stromal cell cultures: mechanism of steroid-induced osteonecrosis. *Chin. Med. J. (Engl).* **119**, 581–588 (2006).

126. Hung, S. H. *et al.* Pioglitazone and dexamethasone induce adipogenesis in D1 bone marrow stromal cell line, but not through the peroxisome proliferator-activated receptor-**γ** pathway. *Life Sci.* **82**, 561–569 (2008).

127. Park, Y.-K. & Ge, K. Glucocorticoid Receptor Accelerates, but Is Dispensable for, Adipogenesis. *Mol. Cell. Biol.* **37**, 1–14 (2017).

128. Kodama, H. -A, Amagai, Y., Koyama, H. & Kasai, S. Hormonal responsiveness of a preadipose cell line derived from newborn mouse calvaria. *J. Cell. Physiol.* **112**, 83–88 (1982).

129. Ding, J., Nagai, K. & Woo, J. Insulin-Dependent Adipogenesis in Stromal ST2 Cells Derived from Murine Bone Marrow. *Biosci. Biotechnol. Biochem.* **67**, 314–321 (2003).

130. Camp, H. S. *et al.* Differential activation of peroxisome proliferator-activated receptor-**γ** by troglitazone and rosiglitazone. *Diabetes* **49**, 539–547 (2000).

131. Lorenzo, M. Rosiglitazone up-regulates lipoprotein lipase and uncoupling protein-1 , and down-regulates insulin-induced fatty acid synthase gene expression in brown adipocytes of Wistar rats. *Diabetologia* **48**, 1180–1188 (2005).

132. Obregon, M.-J. Adipose tissues and thyroid hormones. *Front. Physiol.* **5**, 1–12 (2014).

133. Oliveira, M. de *et al.* Triiodothyronine Increases mRNA and Protein Leptin Levels in Short Time in 3T3-L1 Adipocytes by PI3K Pathway Activation. *PLoS One* **8**, 1–7 (2013).

134. Davis, P. J., Shih, A., Lin, H. Y., Martino, L. J. & Davis, F. B. Thyroxine promotes association of mitogen-activated protein kinase and nuclear thyroid hormone receptor (TR) and causes serine phosphorylation of TR. *J. Biol. Chem.* **275**, 38032–38039 (2000).

135. Moeller, L. C. & Broecker-Preuss, M. Transcriptional regulation by nonclassical action of thyroid hormone. *Thyroid Res.* **4**, S6 (2011).

136. Moeller, L. C., Dumitrescu, A. M. & Refetoff, S. Cytosolic action of thyroid hormone leads to induction of hypoxia-inducible factor-1**α** and glycolytic genes. *Mol. Endocrinol.* **19**, 2955–2963 (2005).

137. Obregon, M.-J. Thyroid hormone and adipocyte differentiation. *Thyroid* **18**, 185–195 (2008).

138. Bianco, A. C. & McAninch, E. A. The role of thyroid hormone and brown adipose tissue in energy homoeostasis. *Lancet Diabetes Endocrinol.* **1**, 1–23 (2013).

139. Choi, K. M. *et al.* Effect of ascorbic acid on bone marrow-derived mesenchymal stem cell proliferation and differentiation. *J. Biosci. Bioeng.* **105**, 586–594 (2008).

140. Neubauer, M. *et al.* Basic fibroblast growth factor enhances PPAR**γ** ligand-induced adipogenesis of mesenchymal stem cells. *FEBS Lett.* **577**, 277–283

(2004).

141. Kakudo, N., Shimotsuma, A. & Kusumoto, K. Fibroblast growth factor-2 stimulates adipogenic differentiation of human adipose-derived stem cells. *Biochem. Biophys. Res. Commun.* **359**, 239–244 (2007).

142. Klaus, S., Seivert, A. & Boeuf, S. Effect of the b3-adrenergic agonist Cl316,243 on functional differentiation of of white and brown adipocytes in primary cell culture. *Biochim. Biophys. Acta* **1539**, 85–92 (2001).

143. Himms-Hagen, J. *et al.* Multilocular fat cells in WAT of CL-316243-treated rats derive directly from white adipocytes. *Am. J. Physiol. Physiol.* **279**, C670–C681 (2017).

144. Ye, L. *et al.* Fat cells directly sense temperature to activate thermogenesis. *Proc. Natl. Acad. Sci.* **110**, 12480–12485 (2013).

145. Cannon, B. & Nedergaard, J. Brown Adipose Tissue : Function and Physiological Significance. *Physiol Rev* **84**, 277–359 (2004).

146. Davis, T. R. A. Chamber cold acclimatization in man. *J. Appl. Physiol.* **16**, 1011–1015 (1961).

147. Van Der Lans, A. A. J. J. *et al.* Cold acclimation recruits human brown fat and increases nonshivering thermogenesis. *J. Clin. Invest.* **123**, 3395–3403 (2013).

148. Langeveld, M. *et al.* Mild cold effects on hunger, food intake, satiety and skin temperature in humans. *Endocr. Connect.* **5**, 65–73 (2016).

149. van Marken Lichtenbelt, W. D. *et al.* Cold-Activated Brown Adipose Tissue in Healthy Men. *N. Engl. J. Med.* **360**, 1500–1508 (2009).

150. Hanssen, M. J. W. *et al.* Short-term Cold Acclimation Recruits Brown Adipose Tissue in Obese Humans. *Diabetes* **65**, 1179–1189 (2016).

151. Blondin, D. P. *et al.* Increased brown adipose tissue oxidative capacity in cold-acclimated humans. *J. Clin. Endocrinol. Metab.* **99**, 438–446 (2014).

152. Blondin, D. P. *et al.* Contributions of white and brown adipose tissues and skeletal muscles to acute cold-induced metabolic responses in healthy men. *J. Physiol.* **593**, 701–714 (2015).

153. Blondin, D. P. *et al.* Four-week cold acclimation in adult humans shifts uncoupling thermogenesis from skeletal muscles to brown adipose tissue. *J. Physiol.* **595**, 2099–2113 (2017).

154. Shore, A. M. *et al.* Cold-Induced Changes in Gene Expression in Brown Adipose Tissue , White Adipose Tissue and Liver. *PLoS One* **8**, 1–9 (2013).

155. Ukropec, J., Anunciado, R. P., Ravussin, Y., Hulver, M. W. & Kozak, L. P. UCP1-independent Thermogenesis in White Adipose Tissue of Cold-acclimated Ucp1-/- Mice*. *J. Biol. Chem.* **281**, 31894–31908 (2006).

156. Wang, T., Liu, C., Wang, A. & Sun, Q. Intermittent cold exposure improves glucose homeostasis associated with brown and white adipose tissues in mice. *Life Sci.* **139**, 153–159 (2015).

157. Altshuler-Keylin, S. *et al.* Beige Adipocyte Maintenance Is Regulated by Article Beige Adipocyte Maintenance Is Regulated by Autophagy-Induced Mitochondrial Clearance. *Cell Metab.* **24**, 402–419 (2016).

158. Ikeda, K., Maretich, P. & Kajimura, S. The Common and Distinct Features of

Brown and Beige Adipocytes. *Trends Endocrinol. Metab.* **29**, 191–200 (2018).

159. Uchida, K., Sun, W., Yamazaki, J. & Tominaga, M. Role of thermo-sensitive transient receptor potential channels in brown adipose tissue. *Biol. Pharm. Bull.* **41**, 1135–1144 (2018).

160. Zheng, J. Molecular mechanism of TRP channels. *Compr. Physiol.* **3**, 221–242 (2013).

161. Bishnoi, M., Kondepudi, K. K., Gupta, A., Karmase, A. & Boparai, R. K. Expression of multiple Transient Receptor Potential channel genes in murine 3T3-L1 cell lines and adipose tissue. *Pharmacol. Reports* **65**, 751–755 (2013).

162. Ye, L. *et al.* TRPV4 is a regulator of adipose oxidative metabolism, inflammation and energy homeostasis. *Cell* **151**, 96–110 (2012).

163. Ikeda, K. *et al.* UCP1-independent signaling involving SERCA2b-mediated calcium cycling regulates beige fat thermogenesis and systemic glucose homeostasis. *Nat. Med.* **23**, 1454–1465 (2017).

164. Sun, W. *et al.* Activation of TRPV2 negatively regulates the differentiation of mouse brown adipocytes. *Eur. J. Physiol.* **468**, 1527–1540 (2016).

165. Sun, W. *et al.* Lack of TRPV 2 impairs thermogenesis in mouse brown adipose tissue. *EMBO Rep.* **17**, 383–399 (2016).

166. Lieder, B. *et al.* The alkamide trans-pellitorine targets PPARγ via TRPV1 and TRPA1 to reduce lipid accumulation in developing 3T3-L1 adipocytes. *Front. Pharmacol.* **8**, 1–11 (2017).

167. Ma, S. *et al.* Activation of the cold-sensing TRPM8 channel triggers UCP1-dependent thermogenesis and prevents obesity. *J. Mol. Cell Biol.* **4**, 88–96 (2012).

168. Jiang, C. *et al.* Dietary menthol-induced TRPM8 activation enhances WAT 1C 'browning 1D' and ameliorates diet-induced obesity. *Oncotarget* **8**, 75114–75126 (2017).

169. Rossato, M. *et al.* Human white adipocytes express the cold receptor TRPM8 which activation induces UCP1 expression, mitochondrial activation and heat production. *Mol. Cell. Endocrinol.* **383**, 137–146 (2014).

170. Hua, J. *et al.* Comparison of different methods for the isolation of mesenchymal stem cells from umbilical cord matrix: Proliferation and multilineage differentiation as compared to mesenchymal stem cells from umbilical cord blood and bone marrow. *Cell Biol. Int.* **38**, 198–210 (2014).

171. Van Pham, P. *et al.* Isolation and proliferation of umbilical cord tissue derived mesenchymal stem cells for clinical applications. *Cell Tissue Bank.* **17**, 289–302 (2016).

172. Smith, J. R. *et al.* Standardizing Umbilical Cord Mesenchymal Stromal Cells for Translation to Clinical Use: Selection of GMP-Compliant Medium and a Simplified Isolation Method. *Stem Cells Int.* **2016**, (2016).

173. Pierdomenico, L. *et al.* Diabetes Mellitus During Pregnancy Interferes with the Biological Characteristics of Wharton's Jelly Mesenchymal Stem Cells. *Open Tissue Eng Regen Med J* **4**, 103–111 (2011).

174. Jaiswal, N., Haynesworth, S. E., Caplan, A. I. & Bruder, S. P. Osteogenic differentiation of purified, culture-expanded human mesenchymal stem cells in

vitro. *J. Cell. Biochem.* **64**, 295–312 (1997).

175. Sonnaert, M., Papantoniou, I., Luyten, F. P. & Schrooten, J. Quantitative Validation of the Presto Blue™ Metabolic Assay for Online Monitoring of Cell Proliferation in a 3D Perfusion Bioreactor System. *Tissue Eng. Part C Methods* **21**, 519–529 (2015).

176. Miller, C. N. *et al.* Isoproterenol increases uncoupling, glycolysis, and markers of beiging in mature 3T3-L1 adipocytes. *PLoS One* **10**, 1–14 (2015).

177. Papadimitriou, E. & Lelkes, P. I. Measurement of cell numbers in microtiter culture plates using the fluorescent dye Hoechst 33258. *J. Immunol. Methods* **162**, 41–45 (1993).

178. Rizzatti, V. *et al.* Lipid droplets characterization in adipocyte differentiated 3T3-L1 cells: Size and optical density distribution. *Eur. J. Histochem.* **57**, 159–162 (2013).

179. Cypess, A. M. *et al.* Identification and Importance of Brown Adipose Tissue in Adult Humans. *N Engl J Med* **360**, 1509–1526 (2009).

180. Virtanen, K. A. *et al.* Functional Brown Adipose Tissue in Healthy Adults. *N. Engl. J. Med.* **360**, 1518–1525 (2009).

181. de Jong, J. M. A. *et al.* The β3-adrenergic receptor is dispensable for browning of adipose tissues. *Am. J. Physiol. - Endocrinol. Metab.* **312**, E508–E518 (2017).

182. Ishibashi, J. & Seale, P. Beige can be slimming. *Science (80-.).* **328**, 1113–1114 (2010).

183. Bartelt, A. & Heeren, J. Adipose tissue browning and metabolic health. *Nat. Publ. Gr.* **10**, 24–36 (2013).

184. Sharp, L. Z. *et al.* Human BAT Possesses Molecular Signatures That Resemble Beige/Brite Cells. *PLoS One* **7**, (2012).

185. Villanueva, C. J. *et al.* Adipose subtype–selective recruitment of TLE3 or Prdm16 by PPARγ specifies lipid-storage versus thermogenic gene programs. *Cell Metab.* **17**, 423–435 (2013).

186. Pontikoglou, C., Deschaseaux, F., Sensebé, L. & Papadaki, H. A. Bone Marrow Mesenchymal Stem Cells : Biological Properties and Their Role in Hematopoiesis and Hematopoietic Stem Cell Transplantation. *Stem Cell Rev. Reports* 569–589 (2011). doi:10.1007/s12015-011-9228-8

187. Klingenspor, M. Cold-induced recruitment of brown adipose tissue thermogenesis. *Exp. Physiol.* **88**, 141–148 (2003).

188. Puigserver, P. & Spiegelman, B. M. Peroxisome proliferator-activated receptor-γ coactivator 1α (PGC-1α): Transcriptional coactivator and metabolic regulator. *Endocr. Rev.* **24**, 78–90 (2003).

189. Dessolin, S., Schalling, M., Lonnqvist, F., Ailhaud, G. & Ricquier, D. Leptin gene is expressed in Rat Brown Adipose Tissue at birth. **11**, 382–387 (1997).

190. Davis, P. J., Tillmann, H. C., Davis, F. B. & Wehling, M. Comparison of the mechanisms of nongenomic actions of thyroid hormone and steroid hormones. *J. Endocrinol. Invest.* **25**, 377–388 (2002).

191. Al-Shibli, S. M., Amjad, N. M., Al-Kubaisi, M. K. & Mizan, S. Subcellular localization of leptin and leptin receptor in breast cancer detected in an electron microscopic study. *Biochem. Biophys. Res. Commun.* **482**, 1102–1106 (2017).

192. Suzuki, A. *et al.* Leptin Stimulates Fatty Acid Oxidation and Peroxisome Proliferator-Activated Receptor Gene Expression in Mouse C2C12 Myoblasts by Changing the Subcellular Localization of the 2 Form of AMP-Activated Protein Kinase. *Mol. Cell. Biol.* **27**, 4317–4327 (2007).

193. Laharrague, P. *et al.* High expression of leptin by human bone marrow adipocytes in primary culture. *FASEB J. Off. Publ. Fed. Am. Soc. Exp. Biol.* **12**, 747–752 (1998).

194. Cancello, R., Zingaretti, M. C., Sarzani, R. & Cinti, S. Leptin and UCP1 Genes Are Reciprocally Regulated in Brown Adipose Tissue. *Endocrinology* **139**, 4747–4750 (1998).

195. Flier, J. S. & Maratos-Flier, E. Leptin's Physiologic Role: Does the Emperor of Energy Balance Have No Clothes? *Cell Metab.* **26**, 24–26 (2017).

196. Cinti, S., Zingaretti, M. C., Cancello, R., Ceresi, E. & Ferrara, P. *Morphologic techniques for the study of brown adipose tissue and white adipose tissue. Methods in molecular biology (Clifton, N.J.)* **155**, (2001).

197. Drehmer, D. L. *et al.* Metabolic switches during the first steps of adipogenic stem cells differentiation. *Stem Cell Res.* **17**, 413–421 (2016).

198. Xing Xian, Y. U., Lewin, D. A., Forrest, W. & Adams, S. H. Cold elicits the simultaneous induction of fatty acid synthesis and β-oxidation in murine brown adipose tissue: Prediction from differential gene expression and confirmation in vivo. *FASEB J.* **16**, 155–168 (2002).

199. Nedergaard, J. & Cannon, B. UCP1 mRNA does not produce heat. *Biochim. Biophys. Acta - Mol. Cell Biol. Lipids* **1831**, 943–949 (2013).

200. Lee, E. *et al.* Transient receptor potential vanilloid type-1 channel regulates diet-induced obesity, insulin resistance, and leptin resistance. *FASEB J.* **29**, 3182–3192 (2015).

201. Ihnat, M. A. *et al.* Reactive oxygen species mediate a cellular 'memory' of high glucose stress signalling. *Diabetologia* **50**, 1523–1531 (2007).

202. Rosenwald, M. & Wolfrum, C. The origin and definition of brite versus white and classical brown adipocytes. *Adipocyte* **3**, 4–9 (2014).

203. Nicholls, D. G. The physiological regulation of uncoupling proteins. *Biochim. Biophys. Acta* **1757**, 459–466 (2006).

204. Lu, X. *et al.* Mitophagy controls beige adipocyte maintenance through a Parkin-dependent and UCP1-independent mechanism. *Sci. Signal.* **8526**, 1–10 (2018).

205. Bianco, A. C. & Silva, J. E. Nuclear 3,5,3'-Triiodothyronine (T3) in Brown AdiposeTissue: Receptor Occupancy and Sources of T3 as Determined by in Vivo Techniques*. *Endocrinology* **120**, 55–62 (2016).

206. Klaus, S., Ely, M., Encke, D. & Heldmaier, G. Functional assessment of white and brown adipocyte development and energy metabolism in cell culture. *J. Cell Sci.* **4008**, 3171–3180 (1995).

207. Guerra, C., Roncero, C., Porras, A., Fernández, M. & Benito, M. Triiodothyronine induces the transcription of the uncoupling protein gene and stabilizes its mRNA in fetal rat brown adipocyte primary cultures. *J. Biol. Chem.* **271**, 2076–2081 (1996).

208. Lafontan, M. *et al.* Adrenergic regulation of adipocyte metabolism. *Eur. Soc.*

Hum. Reprod. Embryol. **12**, 6–20 (1997).

209. Uldry, M. *et al.* Complementary action of the PGC-1 coactivators in mitochondrial biogenesis and brown fat differentiation. *Cell Metab.* **3**, 333–341 (2006).

210. Tejerina, S. *et al.* Mild mitochondrial uncoupling induces 3T3-L1 adipocyte de-differentiation by a PPAR -independent mechanism, whereas TNF -induced de-differentiation is PPAR dependent. *J. Cell Sci.* **122**, 145–155 (2009).

211. Winther, S. *et al.* Restricting glycolysis impairs brown adipocyte glucose and oxygen consumption. *Am. J. Physiol. - Endocrinol. Metab.* **314**, E214–E223 (2018).

212. Jeong, J. H., Chang, J. S. & Jo, Y. H. Intracellular glycolysis in brown adipose tissue is essential for optogenetically induced nonshivering thermogenesis in mice. *Sci. Rep.* **8**, 1–14 (2018).

213. Rafael, J., Fesser, W. & Nicholls, D. G. Cold adaptation in guinea pig at level of isolated brown adipocyte a. *Am. Physiol. Soc.* 228–235 (1986).

214. Rosell, M. *et al.* Brown and white adipose tissues: intrinsic differences in gene expression and response to cold exposure in mice. *AJP Endocrinol. Metab.* **306**, E945–E964 (2014).

215. Divakaruni, A. S., Humphrey, D. M. & Brand, M. D. Fatty acids change the conformation of uncoupling protein 1 (UCP1). *J. Biol. Chem.* **287**, 36845–36853 (2012).

216. Fedorenko, A., Lishko, P. V. & Kirichok, Y. Mechanism of Fatty-Acid-Dependent UCP1 Uncoupling in Brown Fat Mitochondria. *Cell* **185**, 974–981 (2013).

217. Viengchareun, S., Zennaro, M. C., Tallec, L. P. Le & Lombes, M. Brown adipocytes are novel sites of expression and regulation of adiponectin and resistin. *FEBS Lett.* **532**, 345–350 (2002).

218. Shan, T., Liu, W. & Kuang, S. Fatty acid binding protein 4 expression marks a population of adipocyte progenitors in white and brown adipose tissues. *FASEB J.* **27**, 277–287 (2013).

219. Ahmadian, M. *et al.* PPARgamma signaling and metabolism: the good, the bad and the future. *Nat Med* **19**, 557–566 (2013).

220. Kalinovich, A. V, de Jong, J. M. A., Cannon, B. & Nedergaard, J. UCP1 in adipose tissues : two steps to full browning. *Biochimie* **134**, 127–137 (2017).

221. Shabalina, I. *et al.* UCP1 in Brite/Beige adipose tissue mitochondria is functionally thermogenic. *Cell Rep.* **5**, 1196–1203 (2013).

222. Zingaretti, M. C. *et al.* The presence of UCP1 demonstrates that metabolically active adipose tissue in the neck of adult humans truly represents brown adipose tissue. *FASEB J.* **23**, 3113–3120 (2018).

223. Hong, C. Y. *et al.* Sarcoplasmic reticulum Ca2+ ATPase 2 (SERCA2) reduces the migratory capacity of CCL21-treated monocyte-derived dendritic cells. *Exp. Mol. Med.* **48**, (2016).

224. Seale, P. *et al.* Transcriptional Control of Brown Fat Determination by PRDM16. *Cell Metab.* **6**, 38–54 (2007).

225. Waldén, T. B., Hansen, I. R., Timmons, J. A., Cannon, B. & Nedergaard, J. Recruited vs. nonrecruited molecular signatures of brown, "brite," and white adipose tissues. *Am. J. Physiol. Metab.* **302**, E19–E31 (2011).

226. Cypess, A. M. *et al.* Anatomical Localization, Gene Expression Profiling, and Functional Characterization of Adult Human Neck Brown Fat. *Nat. Med.* **118**, 6072–6078 (2016).

227. Wu, L. Z. *et al.* Cidea controls lipid droplet fusion and lipid storage in brown and white adipose tissue. *Sci. China Life Sci.* **57**, 107–116 (2014).

228. Barneda, D. *et al.* The brown adipocyte protein CIDEA promotes lipid droplet fusion via a phosphatidic acid-binding amphipathic helix. *Elife* **4**, 1–24 (2015).

229. Zhou, Z. *et al.* Cidea-deficient mice have lean phenotype and are resistant to obesity. *Nat. Genet.* **35**, 49–56 (2003).

230. Matsumura, Y. *et al.* H3K4/H3K9me3 Bivalent Chromatin Domains Targeted by Lineage-Specific DNA Methylation Pauses Adipocyte Differentiation. *Mol. Cell* **60**, 584–596 (2015).

231. Inagaki, T., Sakai, J. & Kajimura, S. Transcriptional and epigenetic control of brown and beige adipose cell fate and function. *Nat. Rev. Mol. Cell Biol.* **17**, 480–495 (2016).

232. Abe, Y. *et al.* Histone demethylase JMJD1A coordinates acute and chronic adaptation to cold stress via thermogenic phospho-switch. *Nat. Commun.* **9**, (2018).

233. Sun, W., Uchida, K. & Tominaga, M. TRPV2 regulates BAT thermogenesis and differentiation. *Channels* **11**, 94–96 (2017).

234. Chang, S.-H. H., Song, N.-J. J., Choi, J. H., Yun, U. J. & Park, K. W. Mechanisms underlying UCP1 dependent and independent adipocyte thermogenesis. *Obes. Rev.* **20**, 241–251 (2019).

235. O'Conor, C. J., Griffin, T. M., Liedtke, W. & Guilak, F. Increased susceptibility of Trpv4-deficient mice to obesity and obesity-induced osteoarthritis with very high-fat diet. *Ann. Rheum. Dis.* **72**, 300–304 (2013).

236. Schäffler, A. & Büchler, C. Concise review: adipose tissue-derived stromal cells-basic and clinical implications for novel cell-based therapies. *Stem Cells* **25**, 818–827 (2007).

237. Rojewski, M. T., Weber, B. M. & Schrezenmeier, H. Phenotypic characterization of mesenchymal stem cells from various tissues. *Transfus. Med. Hemotherapy* **35**, 168–184 (2008).

238. Reddy, N., Vemuri, M. & Pallu, R. Isolation of stem cells from human umbilical cord blood. *Methods Mol. Biol.* **407**, 149–63 (2007).

239. Zhao, Y. & Mazzone, T. Human cord blood stem cells and the journey to a cure for type 1 diabetes. *Autoimmun. Rev.* **10**, 103–107 (2010).

240. De Lima Prata, K. *et al.* Cryopreservation of umbilical cord mesenchymal cells in xenofree conditions. *Cytotherapy* **14**, 694–700 (2012).

241. Marmotti, A. *et al.* Minced umbilical cord fragments as a source of cells for orthopaedic tissue engineering: An in vitro study. *Stem Cells Int.* **2012**, (2012).

242. Choudhery, M., Badowski, M., Muise, A. & Harris, D. Utility of Cryopreserved Umbilical Cord Tissue for Regenerative Medicine. *Curr. Stem Cell Res. Ther.* **8**, 370–380 (2013).

243. Badowski, M., Muise, A. & Harris, D. T. Mixed effects of long-term frozen storage on cord tissue stem cells. *Cytotherapy* **16**, 1313–1321 (2014).

244. Karahuseyinoglu, S. *et al.* Biology of Stem Cells in Human Umbilical Cord Stroma: In Situ and In Vitro Surveys. *Stem Cells* **25**, 319–331 (2007).

245. Koliakos, I., Tsagias, N. & Karagiannis, V. Mesenchymal cells isolation from Wharton's jelly, in perspective to clinical applications. *J. Biol. Res.* **16**, 194–201 (2011).

246. Roy, S., Arora, S., Kumari, P. & Ta, M. A simple and serum-free protocol for cryopreservation of human umbilical cord as source of Wharton's jelly mesenchymal stem cells. *Cryobiology* **68**, 467–472 (2014).

247. Chatzistamatiou, T. K. *et al.* Optimizing isolation culture and freezing methods to preserve Wharton's jelly's mesenchymal stem cell (MSC) properties: An MSC banking protocol validation for the Hellenic Cord Blood Bank. *Transfusion* **54**, 3108–3120 (2014).

248. Polchow, B. *et al.* Cryopreservation of human vascular umbilical cord cells under good manufacturing practice conditions for future cell banks. *J. Transl. Med.* **10**, 1–17 (2012).

249. Qiao, C. *et al.* Human mesenchymal stem cells isolated from the umbilical cord. *Cell Biol. Int.* **32**, 8–15 (2008).

250. Paladino, F. V., Peixoto-Cruz, J. S., Santacruz-Perez, C. & Goldberg, A. C. Comparison between isolation protocols highlights intrinsic variability of human umbilical cord mesenchymal cells. *Cell Tissue Bank.* **17**, 123–136 (2016).

251. Kim, J. W. *et al.* Mesenchymal progenitor cells in the human umbilical cord. *Ann. Hematol.* **83**, 733–738 (2004).

252. Romanov, Y. A., Svintsitskaya, V. A. & Smirnov, V. N. Searching for Alternative Sources of Postnatal Human Mesenchymal Stem Cells: Candidate MSC-Like Cells from Umbilical Cord. *Stem Cells. Rapid Commun.* 105–110 (2003).

253. Salehinejad, P. *et al.* Comparison of different methods for the isolation of mesenchymal stem cells from human umbilical cord Wharton's jelly. *Vitr. Cell. Dev. Biol. - Anim.* **48**, 75–83 (2012).

254. Bosch, J. *et al.* Distinct differentiation potential of 'mSC' derived from cord blood and umbilical cord: Are cord-derived cells true mesenchymal stromal cells? *Stem Cells Dev.* **21**, 1977–1988 (2012).

255. Zeddou, M. Umbilical cord fibroblasts: Could they be considered as mesenchymal stem cells? *World J. Stem Cells* **6**, 367 (2014).

256. Ishige, I. *et al.* Comparison of mesenchymal stem cells derived from arterial, venous, and Wharton's jelly explants of human umbilical cord. *Int. J. Hematol.* **90**, 261–269 (2009).

257. Cheng, H. *et al.* Replicative senescence of human bone marrow and umbilical cord derived mesenchymal stem cells and their differentiation to adipocytes and osteoblasts. *Mol. Biol. Rep.* **38**, 5161–5168 (2011).

258. Hemeda, H., Giebel, B. & Wagner, W. Evaluation of human platelet lysate versus fetal bovine serum for culture of mesenchymal stromal cells. *Cytotherapy* **16**, 170–180 (2014).

259. Burnouf, T., Strunk, D., Koh, M. B. C. & Schallmoser, K. Human platelet lysate: Replacing fetal bovine serum as a gold standard for human cell propagation? *Biomaterials* **76**, 371–387 (2016).

260. Chase, L. G., Lakshmipathy, U., Solchaga, L. A., Rao, M. S. & Vemuri, M. C. A novel serum-free medium for the expansion of human mesenchymal stem cells. *Stem Cell Res. Ther.* **1**, 1–11 (2010).

261. Dulugiac, M., Moldovan, L. & Zarnescu, O. Comparative studies of mesenchymal stem cells derived from different cord tissue compartments - The influence of cryopreservation and growth media. *Placenta* **36**, 1192–1203 (2015).

262. Zhang, Y., Khan, D., Delling, J. & Tobiasch, E. Mechanisms underlying the osteo- and adipo-differentiation of human mesenchymal stem cells. *Sci. World J.* **2012**, (2012).

263. Mushahary, D., Spittler, A., Kasper, C., Weber, V. & Charwat, V. Isolation, cultivation, and characterization of human mesenchymal stem cells. *Cytom. Part A* **93**, 19–31 (2018).

264. Yoon, J. H. *et al.* Comparison of Explant-Derived and Enzymatic Digestion-Derived MSCs and the Growth Factors from Wharton's Jelly. *Biomed Res. Int.* **2013: 4287**, (2013).

265. Han, Y. F. *et al.* Optimization of human umbilical cord mesenchymal stem cell isolation and culture methods. *Cytotechnology* **65**, 819–827 (2013).

266. Schallmoser, K. *et al.* Human platelet lysate can replace fetal bovine serum for clinical-scale expansion of functional mesenchymal stromal cells. *Transfusion* **47**, 1436–1446 (2007).

267. Rauch, C. *et al.* Alternatives to the use of fetal bovine serum: platelet lysates as serum replacement in cell and tissue culture. *ALTEX* **25**, 2008 (2008).

268. Gottipamula, S., Sharma, A., Krishnamurthy, S., Majumdar, A. Sen & Seetharam, R. N. Human platelet lysate is an alternative to fetal bovine serum for large-scale expansion of bone marrow-derived mesenchymal stromal cells. *Biotechnol. Lett.* **34**, 1367–1374 (2012).

269. Capelli, C. *et al.* Minimally manipulated whole human umbilical cord is a rich source of clinical-grade human mesenchymal stromal cells expanded in human platelet lysate. *Cytotherapy* **13**, 786–801 (2011).

270. Castiglia, S. *et al.* Inactivated human platelet lysate with psoralen: A new perspective for mesenchymal stromal cell production in good manufacturing practice conditions. *Cytotherapy* **16**, 750–763 (2014).

271. Bieback, K., Kern, S., Klüter, H. & Eichler, H. Critical parameters for the isolation of mesenchymal stem cells from umbilical cord blood. *Stem Cells* **22**, 625–634 (2004).

272. Abdelrazik, H., Spaggiari, G. M., Chiossone, L. & Moretta, L. Mesenchymal stem cells expanded in human platelet lysate display a decreased inhibitory capacity on T- and NK-cell proliferation and function. *Eur. J. Immunol.* **41**, 3281–3290 (2011).

273. Apel, A. *et al.* Suitability of human mesenchymal stem cells for gene therapy depends on the expansion medium. *Exp. Cell Res.* **315**, 498–507 (2009).

274. Fan, C. G., Zhang, Q. jun & Zhou, J. ru. Therapeutic Potentials of Mesenchymal Stem Cells Derived from Human Umbilical Cord. *Stem Cell Rev. Reports* **7**, 195–207 (2011).

275. Jovanovic, L. & Pettitt, D. J. Gestational diabetes mellitus. *JAMA* **286**, 2016–2018

(2001).

276. Lawlor, D. A., Lichtenstein, P. & Långström, N. Association of maternal diabetes mellitus in pregnancy with offspring adiposity into early adulthood: Sibling study in a prospective cohort of 280 866 men from 248 293 families. *Circulation* **123**, 258–265 (2011).

277. Crume, T. L. *et al.* The impact of in utero exposure to diabetes on childhood body mass index growth trajectories: The EPOCH study. *J. Pediatr.* **158**, 941–946 (2011).

278. Dabelea, D. *et al.* Association of intrauterine exposure to maternal diabetes and obesity with type 2 diabetes in youth: The SEARCH case-control study. *Diabetes Care* **31**, 1422–1426 (2008).

279. Pettitt, D. J., Baird, H. R., Aleck, K. A., Bennett, P. H. & Knowler, W. C. Excessive Obesity in Offspring of Pima Indian Women with Diabetes during Pregnancy. *N. Engl. J. Med.* **308**, 242–245 (1983).

280. Bunt, J. C., Tataranni, A. & Salbe, A. D. Intrauterine Exposure to Diabetes Is a Determinant of Hemoglobin A1 c and Systolic Blood Pressure in Pima Indian Children. *J Clin Endocrinol Metab.* **90**, 3225–3229 (2005).

281. Dabelea, D. & Pettitt, D. Intrauterine Diabetic Environment Confers Risks for Type 2 Diabetes Mellitus and Obesity in the Offspring, in Addition to Genetic Susceptibility. *Journal of Pediatric Endocrinology and Metabolism* **14**, 1085–1092 (2016).

282. Boney, C. M., Verma, A., Tucker, R. & Vohr, B. R. Metabolic syndrome in childhood: Association with birth weight, maternal obesity, and gestational diabetes mellitus. *Pediatrics* **115**, (2005).

283. Kim, J. *et al.* Umbilical Cord Mesenchymal Stromal Cells Affected by Gestational Diabetes Mellitus Display Premature Aging and Mitochondrial Dysfunction. *Stem Cells Dev.* **24**, 575–586 (2015).

284. Kong, C. M. *et al.* Changes in Stemness Properties, Differentiation Potential, Oxidative Stress, Senescence and Mitochondrial Function in Wharton's Jelly Stem Cells of Umbilical Cords of Mothers with Gestational Diabetes Mellitus. *Stem Cell Rev. Reports* **15**, 415–426 (2019).

285. Nomura, Y. *et al.* Global methylation in the placenta and umbilical cord blood from pregnancies with maternal gestational diabetes, preeclampsia, and obesity. *Reprod. Sci.* **21**, 131–137 (2014).

286. Tang, W. *et al.* White fat progenitors reside in the adipose vasculature. *Science (80-.).* **322**, 583–586 (2008).

287. Mauvais-Jarvis, F., Arnold, A. P. & Reue, K. A Guide for the Design of Pre-clinical Studies on Sex Differences in Metabolism. *Cell Metab.* **25**, 1216–1230 (2017).

288. Caligioni, C. Assessing Reproductive Status/Stages in Mice Claudia. *Curr Protoc Neurosci* 1–11 (2009). doi:10.1002/0471142301.nsa04is48.Assessing

289. Kubarek, Kozłowska, A., Przybylski, M., Lianeri, M. & Jagodzinski, P. P. Down-regulation of CXCR4 expression by tamoxifen is associated with DNA methyltransferase 3B up-regulation in MCF-7 breast cancer cells. *Biomed. Pharmacother.* **63**, 586–591 (2009).

290. Schwarz, J. M., Nugent, B. M. & McCarthy, M. M. Developmental and hormone-

induced epigenetic changes to estrogen and progesterone receptor genes in brain are dynamic across the life span. *Endocrinology* **151**, 4871–4881 (2010).

291. Nugent, B. M., Schwarz, J. M. & McCarthy, M. M. Hormonally mediated epigenetic changes to steroid receptors in the developing brain: Implications for sexual differentiation. *Horm. Behav.* **59**, 338–344 (2011).

292. Machida, T., Yonezawa, Y. & Noumura, T. Age-associated changes in plasma testosterone levels in male mice and their relation to social dominance or subordinance. *Horm. Behav.* **15**, 238–245 (1981).

293. Itoh, Y. & Arnold, A. P. Are females more variable than males in gene expression? Meta-analysis of microarray datasets. *Biol. Sex Differ.* **6**, 1–9 (2015).

294. Mauvais-Jarvis, F., Clegg, D. J. & Hevener, A. L. The role of estrogens in control of energy balance and glucose homeostasis. *Endocr. Rev.* **34**, 309–338 (2013).

295. O'Reilly, J. R. & Reynolds, R. M. The risk of maternal obesity to the long-term health of the offspring. *Clin. Endocrinol. (Oxf).* **78**, 9–16 (2013).

296. Baustian, C., Hanley, S. & Ceredig, R. Isolation, selection and culture methods to enhance clonogenicity of mouse bone marrow derived mesenchymal stromal cell precursors. *Stem Cell Res. Ther.* **6**, 1–13 (2015).

297. Gillman, M. W., Rifas-Shiman, S., Berkey, C. S., Field, A. E. & Colditz, G. A. Maternal gestational diabetes, birth weight, and adolescent obesity. *Pediatrics* **111**, (2003).

298. Clausen, T. D. *et al.* High Prevalence of Type 2 Diabetes and Pre-Diabetes in Adult Offspring of Women With Gestational Diabetes Mellitus or Type 1 Diabetes: The role of intrauterine hyperglycemia. *Diabetes Care* **31**, 340–346 (2008).

299. Boyle, K. E. *et al.* Mesenchymal stem cells from infants born to obese mothers exhibit greater potential for adipogenesis: The healthy start babybump project. *Diabetes* **65**, 647–659 (2016).

300. Baker, P. R. *et al.* Maternal obesity and increased neonatal adiposity correspond with altered infant mesenchymal stem cell metabolism. *JCI Insight* **2**, 1–15 (2017).

301. Baker, P. R. *et al.* Altered gene expression and metabolism in fetal umbilical cord mesenchymal stem cells correspond with differences in 5-month-old infant adiposity gain. *Sci. Rep.* **7**, 1–10 (2017).

302. Catalano, P. M., Thomas, A., Huston-Presley, L. & Amini, S. B. Phenotype of infants of mothers with gestational diabetes. *Diabetes Care* **30**, 156–160 (2007).

303. Lowe, L. P. *et al.* Hyperglycemia and Adverse Pregnancy Outcome (HAPO) Study: Associations of maternal A1C and glucose with pregnancy outcomes. *Diabetes Care* **35**, 574–580 (2012).

304. Metzger, B. E. *et al.* Hyperglycemia and adverse pregnancy outcome (HAPO) study: Associations with neonatal anthropometrics. *Diabetes* **58**, 453–459 (2009).

305. Phadnis, S. M., Ghaskadbi, S. M., Hardikar, A. A. & Bhonde, R. R. Mesenchymal stem cells derived from bone marrow of diabetic patients portrait unique markers influenced by the diabetic microenvironment. *Rev. Diabet. Stud.* **6**, 260–270 (2009).

306. Mottillo, E. P. *et al.* Coupling of lipolysis and de novo lipogenesis in brown, beige, and white adipose tissues during chronic β3-adrenergic receptor

activation. *J. Lipid Res.* **55**, 2276–2286 (2014).

307. Granneman, J. G., Burnazi, M., Zhu, Z. & Schwamb, L. A. White adipose tissue contributes to UCP1-independent thermogenesis. *Am. J. Physiol. - Endocrinol. Metab.* **285**, 1230–1236 (2003).

308. Ukropec, J., Anunciado, R. P., Ravussin, Y., Hulver, M. W. & Kozak, L. P. UCP1-independent thermogenesis in white adipose tissue of cold-acclimated Ucp1-/- mice. *J. Biol. Chem.* **281**, 31894–31908 (2006).

309. Seale, P. *et al.* Prdm16 determines the thermogenic program of subcutaneous white adipose tissue in mice. *J Clin Invest* **121**, 53–56 (2011).

310. Shepherd, P. R. & Kahn, B. B. Glucose Transporters and Insulin Action — Implications for Insulin Resistance and Diabetes Mellitus. *N. Engl. J. Med.* **341**, 248–257 (1999).

311. Carvalho, E., Jansson, P.-A., Nagaev, I., Wenthzel, A.-M. & Smith, U. L. F. Insulin resistance with low cellular IRS-1 expression is also associated with low GLUT4 expression and impaired insulin-stimulated glucose transport. *FASEB J.* **15**, 1101–1103 (2001).

312. Aziz, S. H. A. *et al.* Animal Model of Gestational Diabetes Mellitus with Pathophysiological Resemblance to the Human Condition Induced by Multiple Factors (Nutritional, Pharmacological, and Stress) in Rats. *Biomed Res. Int.* **2016**, (2016).

313. Stenbit, A. E. *et al.* GLUT4 heterozygous knockout mice develop muscle insulin resistance and diabetes. *Nat. Med.* **3**, 1096–1101 (1997).

314. Gaster, M., Staehr, P., Beck-Nielsen, H., Schrøder, H. D. & Handberg, A. GLUT4 is reduced in slow muscle fibers of type 2 diabetic patients: Is insulin resistance in type 2 diabetes a slow, type 1 fiber disease? *Diabetes* **50**, 1324–1329 (2001).

315. Townsend, K. L. & Tseng, Y. Brown fat fuel utilization and thermogenesis. *Trends Endocrinol. Metab.* **25**, 168–177 (2014).

316. Fallucca, F. *et al.* Polymorphisms of insulin receptor substrate 1 and β3-adrenergic receptor genes in gestational diabetes and normal pregnancy. *Metabolism.* **55**, 1451–1456 (2006).

317. Robitaille, J. & Grant, A. M. The genetics of gestational diabetes mellitus: Evidence for relationship with type 2 diabetes mellitus. *Genet. Med.* **10**, 240–250 (2008).

318. Fu, Y., Luo, N., Klein, R. L. & Timothy Garvey, W. Adiponectin promotes adipocyte differentiation, insulin sensitivity, and lipid accumulation. *J. Lipid Res.* **46**, 1369–1379 (2005).

319. Rosen, E. D. *et al.* C/EBPa induces adipogenesis through PPARg: a unified pathway. *Genes Dev.* 22–26 (2002). doi:10.1101/gad.948702.nuclear

320. Jackson, R. M., Griesel, B. A., Gurley, J. M., Szweda, L. I. & Olson, A. L. Glucose availability controls adipogenesis in mouse 3T3-L1 adipocytes via up-regulation of nicotinamide metabolism. *J. Biol. Chem.* **292**, 18556–18564 (2017).

321. Govers, R. Molecular mechanisms of GLUT4 regulation in adipocytes. *Diabetes Metab.* **40**, 400–410 (2014).

322. Patel, H. V, Freeman, K. B. & Desautels, M. Selective loss of uncoupling protein mRNA in brown adipose tissue on deacclimation of cold-acclimated mice.

Biochem. Cell Biol. **65**, 955–959 (1987).

323. Jacobsson, A., Cannon, B. & Nedergaard, J. Physiological activation of brown adipose tissue destabilizes thermogenin mRNA. *FEBS Lett.* **224**, 353–356 (1987).

324. Bartelt, A. *et al.* Brown adipose tissue activity controls triglyceride clearance. *Nat. Med.* **17**, 200–206 (2011).

325. Christodoulou, I., Kolisis, F. N., Papaevangeliou, D. & Zoumpourlis, V. Comparative evaluation of human mesenchymal stem cells of fetal (Wharton's Jelly) and adult (adipose tissue) origin during prolonged in vitro expansion: Considerations for cytotherapy. *Stem Cells Int.* **2013**, (2013).

326. Sen, A. *et al.* Adipogenic Potential of Human Adipose Derived Stromal Cells From Multiple Donors is Heterogeneous. *J. Cell. Biochem.* **81**, 312–319 (2001).

327. Lee, Y., Kim, S., Kwon, H. & Granneman, J. G. Metabolic heterogeneity of activated beige/brite adipocytes in inguinal adipose tissue. *Sci. Rep.* **7**, 1–11 (2017).

328. Fenn Buderer, N. M. Statistical methodology: incorporating the prevalence of disease into the sample size calculation for sensitivity and specificity. *Acad. Emerg. Med.* **3**, 895–900 (1996).

329. Zhang, J. K. *et al.* β3-Adrenergic Activation Improves Maternal and Offspring Perinatal Outcomes in Diet-Induced Prepregnancy Obesity in Mice. *Obesity* **27**, 1482–1493 (2019).

330. Granneman, J. G., Li, P., Zhu, Z. & Lu, Y. Metabolic and cellular plasticity in white adipose tissue I: Effects of β3-adrenergic receptor activation. *Am. J. Physiol. - Endocrinol. Metab.* **289**, 608–616 (2005).

331. Cypess, A. M. *et al.* Activation of Human Brown Adipose Tissue by a β3-Adrenergic Receptor Agonist. *Cell Metab.* **21**, 33–38 (2015).

332. Mauvais-Jarvis, F. Sex differences in metabolic homeostasis, diabetes, and obesity. *Biol. Sex Differ.* **6**, 1–9 (2015).

333. Lee, P., Greenfield, J. R., Ho, K. K. Y. & Fulham, M. J. A critical appraisal of the prevalence and metabolic significance of brown adipose tissue in adult humans. *Am. J. Physiol. - Endocrinol. Metab.* **299**, 601–606 (2010).

334. Pfannenberg, C. *et al.* Impact of age on the relationships of brown adipose tissue with sex and adiposity in humans. *Diabetes* **59**, 1789–1793 (2010).

335. Au-Yong, I. T. H., Thorn, N., Ganatra, R., Perkins, A. C. & Symonds, M. E. Brown adipose tissue and seasonal variation in humans. *Diabetes* **58**, 2583–2587 (2009).

336. Montanucci, P. *et al.* Functional Profiles of Human Umbilical Cord-Derived Adult Mesenchymal Stem Cells in Obese/Diabetic Versus Healthy Women. *Curr. Diabetes Rev.* **14**, 24–35 (2017).

337. Wu, J. *et al.* Beige adipocytes are a distinct type of thermogenic fat cell in mouse and human. *Cell* **150**, 366–376 (2012).

338. Farmer, S. R. Transcriptional control of adipocyte formation. *Cell Metab.* **4**, 263–273 (2006).

339. Commins, S. P., Watson, P. M., Frampton, I. C. & Gettys, T. W. Leptin selectively reduces white adipose tissue in mice via a UCP1-dependent mechanism in brown adipose tissue. *Am J Physiol Endocrinol Metab* **280**, 372–377 (2001).

340. Ukropec, J., Anunciado, R. V. P., Ravussin, Y. & Kozak, L. P. Leptin is required for uncoupling protein-1-independent thermogenesis during cold stress. *Endocrinology* **147**, 2468–2480 (2006).

341. Cancello, R., Zingaretti, M. C., Sarzani, R., Ricquier, D. & Cinti, S. Leptin and UCP1 genes are reciprocally regulated in brown adipose tissue. *Endocrinology* **139**, 4747–4750 (1998).

342. Fischer, A. W., Cannon, B. & Nedergaard, J. Leptin – is it thermogenic? Alexander. *Endocr. Rev.* **bnz016**, (2019).

343. Zsombok, A. *et al.* Regulation of leptin receptor-expressing neurons in the brainstem by TRPV1. *Physiol. Rep.* **2**, 1–10 (2014).

344. Lee, E. *et al.* Transient receptor potential vanilloid type-1 channel regulates diet-induced obesity, insulin resistance, and leptin resistance. *FASEB J.* **29**, 3182–3192 (2015).

345. Antonacci, M. A. *et al.* Direct detection of brown adipose tissue thermogenesis in UCP1−/− mice by hyperpolarized 129Xe MR thermometry. *Sci. Rep.* **9**, 1–12 (2019).

346. Smith, J. R. *et al.* Standardizing Umbilical Cord Mesenchymal Stromal Cells for Translation to Clinical Use: Selection of GMP-Compliant Medium and a Simplified Isolation Method. *Stem Cells Int.* **2016**, (2016).

347. Stanko, P., Kaiserova, K., Altanerova, V. & Altaner, C. Comparison of human mesenchymal stem cells derived from dental pulp, bone marrow, adipose tissue, and umbilical cord tissue by gene expression. *Biomed. Pap.* **158**, 373–377 (2014).

348. Choo, H. J. *et al.* Mitochondria are impaired in the adipocytes of type 2 diabetic mice. *Diabetologia* **49**, 784–791 (2006).

349. Boucher, J. *et al.* Impaired thermogenesis and adipose tissue development in mice with fat-specific disruption of insulin and IGF-1 signalling. *Nat. Commun.* **3**, (2012).

350. Krings, A. *et al.* Bone marrow fat has brown adipose tissue characteristics, which are attenuated with aging and diabetes. *Bone* **50**, 546–552 (2012).

351. Lapa, C. *et al.* Whitening and Impaired Glucose Utilization of Brown Adipose Tissue in a Rat Model of Type 2 Diabetes Mellitus. *Sci. Rep.* **7**, 5–10 (2017).

352. Wang, Y. L., Lin, S. P., Hsieh, P. C. H. & Hung, S. C. Concomitant beige adipocyte differentiation upon induction of mesenchymal stem cells into brown adipocytes. *Biochem. Biophys. Res. Commun.* **478**, 689–695 (2016).

353. Jong, J. M. A. De, Larsson, O., Cannon, B. & Nedergaard, J. A stringent validation of mouse adipose tissue identity markers. *J. Physiol. Metab.* **308**, 1085–1105 (2015).

354. Tseng, Y.-H., Cypess, A. M. & Kahn, C. R. Cellular Bioenergetics as a Target for Obesity Therapy. *Nat Rev Drug Discov* **9**, 465–482 (2010).

355. Saito, M. *et al.* High incidence of metabolically active brown adipose tissue in healthy adult humans: Effects of cold exposure and adiposity. *Diabetes* **58**, 1526–1531 (2009).

356. Hardouin, P., Rharass, T. & Lucas, S. Bone Marrow Adipose Tissue: To Be or Not To Be a Typical Adipose Tissue? *Front. Endocrinol. (Lausanne).* **7**, 1–11 (2016).

357. Brito, R., Sheth, S., Mukherjea, D., Rybak, L. & Ramkumar, V. TRPV1: A Potential

Drug Target for Treating Various Diseases. *Cells* **3**, 517–545 (2014).

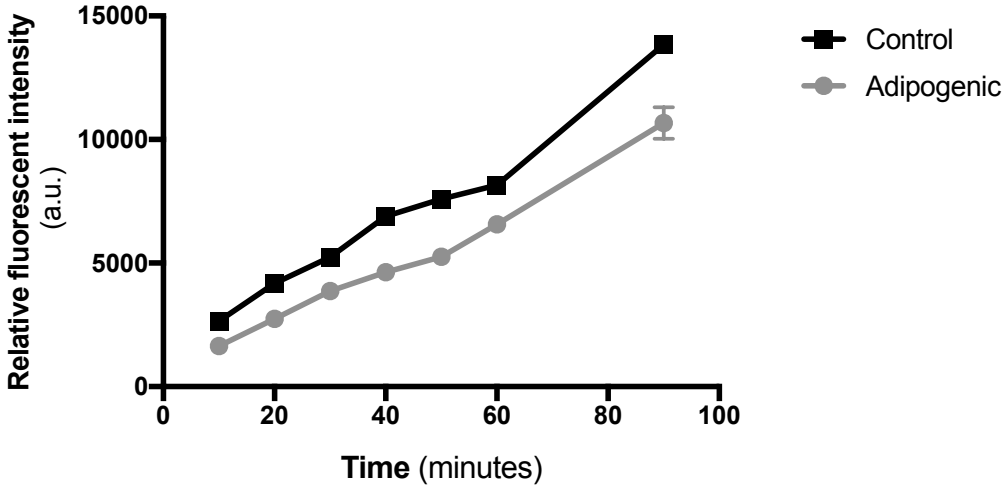
358. Caterina, M. J. *et al*. The capsaicin receptor: a heat-activated ion channel in the pain pathway. *Nature* **389**, 816–824 (1997).

359. Hori, T. Capsaicin and central control of thermoregulation. *Pharmacol. Ther.* **26**, 389–416 (1984).

360. Westerterp-Plantenga, M. S., Smeets, A. & Lejeune, M. P. G. Sensory and gastrointestinal satiety effects of capsaicin on food intake. *Int. J. Obes.* **29**, 682–688 (2005).

361. Belza, A., Frandsen, E. & Kondrup, J. Body fat loss achieved by stimulation of thermogenesis by a combination of bioactive food ingredients: A placebo-controlled, double-blind 8-week intervention in obese subjects. *Int. J. Obes.* **31**, 121–130 (2007).

Appendix



Appendix Figure 1. Metabolic activity (Presto Blue) standard curve in mMSCs D1 undifferentiated (control) and differentiated (adipogenic).

Every time point was done in triplicates. Data are shown as mean ± SEM.

Equipment

EQUIPMENT	IDENTIFIER
Cell culture laboratory	
Class II MSC	Walker Safety Cabinets Limited
Class II microbiological safety cabinets	Biomat 2
Incubator Hera Cell 150	Thermo Electron Corporation
Beads Bath	Fisher Scientific
Centrifuge	Sigma 3-16
Microscope Nikon Elipse TS100	Nikon
Microscope	Leica DMIL
Incubator safe cell UV	Panasonic
Microscope Evos XL core	AMG
Plate reader infinite M200	Life Sciences Tecan
pH meter	Ion Epsilon
Seahorse XFe96 Extracellular Flux Analyser	Agilent
Plate hotter M186	GenLab
Molecular laboratory	
Real-Time PCR system Step One Plus	Applied Biosystems Thermo Fisher Scientific
Fuji-LAS 3000 imager	Fujifilm
BioRad Power Pac 300	BioRad
Mini plate spinner MPS 1000	Labnet
Touchgene gradient	Techne Scientific Lab Supplies
Mini Spin centrifuge	Eppendorf Scientific Lab Supplies
Balance PS-200	FisherBrand
Micro Centaur Microcentrifuge	MSE Scientific Lab Supplies
PV-1 Vortex mixer	Grant bio
Centrifuge 5810R	Eppendorf

Reagents

REAGENT or RESOURCE	SOURCE	IDENTIFIER
Antibodies		
Rabbit polyclonal Anti-UCP1	Abcam	Cat# ab10983; RRID: AB_2241462
Goat polyclonal Anti-UCP1	Novus Biologicals	Cat# NB100-2828; RRID: AB_792527
Rabbit polyclonal Anti-Ob	Santa Cruz	Cat# sc-843; RRID: AB_2136068
Rabbit polyclonal Anti-CD137	Abcam	Cat# ab203391
Rabbit polyclonal Anti-TMEM26	Novus Biologicals	Cat# NBP2-27334
Secondary antibodies		
Goat Anti-rabbit IgG Alexa 594	Thermo Fisher Scientific	Cat# R37117; RRID: AB_2556545
Goat Anti-rabbit IgG Alexa 488	Thermo Fisher Scientific	Cat# A11008; RRID: AB_143165
Goat Anti-goat IgG Alexa 647	Thermo Fisher Scientific	Cat# A21244; RRID: AB_2535812
Donkey Anti-goat IgG Alexa 647	Thermo Fisher Scientific	Cat# A21447; RRID: AB_2535864
Donkey Anti-goat IgG Alexa 488	Abcam	Cat# ab150129; RRID: AB_2687506
HRP Goat Anti-Rabbit IgG Antibody	Vector Laboratories	Cat# PI-100
Chemicals, Peptides, and Recombinant Proteins		
DMEM, Low Glucose, Pyruvate	Thermo Fisher Scientific	Cat# 31885-023
DMEM/F-12 (1:1) 1X, (-) L-Glutamine	Thermo Fisher Scientific	Cat#21331-020
FBS	Thermo Fisher Scientific	Cat# 10500-064
Human Platelet Lysate	Stem Cell Technologies	Cat#06961
L-Glutamine (100X)	Thermo Fisher Scientific	Cat# 25030-024
Pen/Strep	Thermo Fisher Scientific	Cat# 15140-122

MEM NEAA (100X)	Thermo Fisher Scientific	Cat# 11140-035
Sodium Pyruvate 100 mM (100X)	Thermo Fisher Scientific	Cat#11360-039
Collagenase B	Roche	Cat#11088815001
Insulin solution human	Sigma Aldrich	Cat# I9278
Rosiglitazone	Cayman Chemical	Cat# 71740
Dexamethasone	Cayman Chemical	Cat# 11015
3-Isobutyl-1-methylxanthine	Sigma Aldrich	Cat# I5879
0.05% Trypsin-EDTA (1X)	Thermo Fisher Scientific	Cat# 25300-054
PBS (Dulbecco A)	Thermo Fisher Scientific	Cat# BR0014G
Paraformaldehyde	Sigma Aldrich	Cat # P-6148
TRI reagent	Sigma Aldrich	Cat# T9424
Hoechst 33258	Thermo Fisher Scientific	Cat# H3569
Bodipy 493/503	Thermo Fisher Scientific	Cat# D3922
MitoTrackerR Orange CM-H2TMRos	Thermo Fisher Scientific	Cat# M7511
Hydrogen Peroxide Solution	Sigma Aldrich	Cat# H1009
ImmPact DAB	Vector Laboratories	Cat# SK-4105
Hematoxylin QS	Vector Laboratories	Cat# H-3404
Vectashield mounting medium with DAPI	Vector Laboratories	Cat# H-1200
DPX Mountant for histology	Sigma Aldrich	Cat # 06522
Tween 20	Sigma Aldrich	Cat# P1379
Trito X-100	Sigma Aldrich	Cat# T9284
Ethidium Bromide Solution	Sigma Aldrich	Cat# E1510
Optical adhesive covers for PCR	Thermo Fisher Scientific	Cat#4360954
MicroAmp® Fast 96-well reaction plate (0.1mL)	Thermo Fisher Scientific	Cat#4346907
Nuclease free water	Qiagen	Cat# 129114

High performance cover glasses 1 ½, 18 mm x 18 mm (0.17± 0.005 mm)	Zeiss	Cat# 10474379
Oil Red O	Sigma Aldrich	Cat# O0625
Presto Blue	Thermo Fisher Scientific	Cat# A13262
Propanol-2-ol	Fisher Scientific	Cat# 10315720
Ethanol	Fisher Scientific	Cat# 10284580
Cellular models		
mMSCs D1 (D1 ORL UVA [D1])	ATCC	Cat# CRL-12424
hADSCs (StemPro™ Human Adipose-Derived Stem Cells)	Thermo Fisher Scientific	Cat# R7788-115
Critical commercial Assays		
XFe96 Extracellular Flux Analyser	SeaHorse Bioscience	http://www.agilent.com/en/promotions/seahorse-xf-technology
Rneasy micro kit	QIAGEN	Cat# 74004
Quick-load 100 bp DNA ladder	New England BioLabs	N0467L
EZ-PCR Mycoplasma test kit	Biological Industries	Cat#20-700-20
High capacity RNA to cDNA kit	Thermo Fisher Scientific	Cat# 4387406
QIAquick Gel Extraction Kit	QIAGEN	Cat# 28704
OneTaq HS Quick Load 2X MM with standard buffer	New England BioLabs	M04885
Fast SYBR Green Master Mix	Thermo Fisher Scientific	Cat# 4385612
iTaq Universal Probes Supermix	BIORAD	Cat# 1725134
Oligonucleotides		
Mouse qRT-PCR Primer Sequences	Different Sources	See Molecular Biology Chapter 2.6.5
Software and Algorithms		
GraphPad Prism 7	GraphPad Software	https://www.graphpad.com
ImageJ Software	ImageJ	https://imagej.net/